PONTIFÍCIA UNIVERSIDADE CATÓLICA
DO RIO DE JANEIRO

Fernanda de Andrade Salgado

Assessment on Mix Design and Flexural Performance of Reinforced Concrete Short Beams Made with Mixed Recycled Coarse Aggregate

Tese de Doutorado

Thesis presented to the Programa de Pós-Graduação em Engenharia Civil of PUC-Rio in partial fulfillment of the requirements for the degree of Doutor em Ciências – Engenharia Civil.

Advisor: Prof. Flávio de Andrade Silva

Rio de Janeiro
April 2023

PONTIFÍCIA UNIVERSIDADE CATÓLICA
DO RIO DE JANEIRO

Fernanda de Andrade Salgado

Assessment on Mix Design and Flexural Performance of Reinforced Concrete Short Beams Made with Mixed Recycled Coarse Aggregate

Thesis presented to the Programa de Pós-Graduação em Engenharia Civil of PUC-Rio in partial fulfillment of the requirements for the degree of Doutor em Ciências – Engenharia Civil. Approved by the Examination Committee:

Prof. Flávio de Andrade Silva
Advisor
Departamento de Engenharia Civil e Ambiental – PUC-Rio

Prof. Daniel Carlos Taissum Cardoso
Departamento de Engenharia Civil e Ambiental – PUC-Rio

Prof. Conrado de Souza Rodrigues
CEFET-MG

Prof. Ederli Marangon
Universidade Federal do Pampa

Profa. Marlova Piva Kulakowski
UniSinos

Rio de Janeiro, April 24th, 2023

Fernanda de Andrade Salgado

Bachelor of Civil Engineering at Pontifícia Universidade Católica do Rio de Janeiro in 2008, and Master of Civil Engineering at Pontifícia Universidade Católica do Rio de Janeiro in 2010. The area of interest encompasses recycled aggregates, non-conventional materials, and sustainability.

Bibliographic data

Salgado, Fernanda de Andrade

Assessment on mix design and flexural performance of reinforced concrete short beams made with mixed recycled coarse aggregate / Fernanda de Andrade Salgado ; advisor: Flávio de Andrade Silva. – 2023.
209 f.: il. color.; 30 cm.

Tese (doutorado)–Pontifícia Universidade Católica do Rio de Janeiro, Departamento de Engenharia Civil e Ambiental, 2023.
Inclui bibliografia

1. Engenharia Civil e Ambiental - Teses. 2. Agregado reciclado. 3. Concreto reciclado. 4. Dosagem. 5. Desempenho à flexão. 6. Vigas curtas. I. Silva, Flávio de Andrade. II. Pontifícia Universidade Católica do Rio de Janeiro. Departamento de Engenharia Civil e Ambiental. III. Título.

CDD: 624

Acknowledgments

Finishing this doctoral thesis while working full-time and facing a pandemic was undoubtedly the most challenging task of my life. Moreover, getting here was only possible because I had many people by my side who supported and encouraged me endlessly, even in the most stressful moments when I seriously thought about giving up. I will be forever grateful to everyone.

I thank my love and partner, Felipe, for understanding that our weekends and leisure hours would be compromised. Thank you for never questioning, criticizing, or pressuring me. Thank you for sharing with me not only the achievements but also the difficulties during this journey. Having you by my side brought me lightness and peace. Thank you for believing in me and for not letting me give up. I love you.

To my family, my parents, Ronald and Cláudia, my brother Guilherme, my sister-in-law Carol, and my nephews, Gustavo and Giulia, thank you for understanding my absence in so many moments. Papy and mommy, thank you for giving me all the bases needed to get here. You are my life.

To my grandparents, Luiz Carlos and Maria América, and to my second mother, Cidinha, all in memoriam. I will take you with me forever. I know you are still cheering at every achievement I make.

I also thank my lifelong friends, Flávia, Marcela, and Aline, who, even distant, always cheered for me and gave me precious injections of encouragement.

To my friends at PUC, Kissila, Tathi, Victor Nogueira, Rebecca, Thiago Carnavale, Felipe Rodrigues, João Marcelo, Lourdes, Filipe Sá, Vitor Monteiro and Isabel. Thanks for sharing so many emotions over these years, for helping me with doubts and valuable tips, but mostly for being a source of fun and strength when I needed it the most. Kissila and Thati, thank you for the (often virtual) coffees, the endless text revisions, the laughs, and the unconditional support.

To all the friends at Casagrande Engenharia, mainly Leonardo, Casagrande, Amanda, Nathalia, Marcelo, Caio, Armando, Arthur, and Matheus, thank you for the partnership and support so I could be able to finalize this research.

To my advisor, professor Flávio de Andrade Silva, I thank you for all the available resources, for the support granted from the beginning to the end of this work, and for understanding my unconventional routine.

To the laboratory technicians, Euclides, José Nilson, Rogério, and Jhansen, for all their assistance in the elaboration and execution of the tests in the Laboratory of Structures and Materials of PUC-Rio. Without you, this research could not have been carried out.

I would also like to thank engineer Rafael Vieira from IBRATA company and Kléber Rodrigues from Reciclax company for donating the natural aggregate and recycled aggregate used in this research. To the Votorantim company for donating the Portland cement CP-II-F32. To CNPq, CAPES, and FAPERJ for the financial support that indirectly made this work possible.

Finally, I would like to thank all the other professors, technicians, employees, and colleagues at PUC-Rio, who supported me until the end of this journey. PUC-Rio is also my home.

This study was financed in part by the Coordenação de Aperfeiçoamento de Pessoal de Nível Superior - Brasil (CAPES) - Finance Code 001.

Agradecimentos

Finalizar o doutorado, dividindo o tempo com as demandas de trabalho, e ainda passando por uma pandemia no meio do caminho, foi com certeza a tarefa mais difícil da minha vida. E chegar até aqui só foi possível pois tive ao meu lado uma quantidade enorme de pessoas que me apoiaram e me incentivaram infinitamente, mesmo nos momentos mais confusos, quando pensei seriamente em desistir. Serei eternamente grata a todos.

Agradeço ao meu amor e companheiro Felipe, por entender que nossos fins de semana e horas de lazer estariam comprometidos. Obrigada por jamais me questionar, criticar ou pressionar. Obrigada por dividir comigo não só as conquistas, mas também as dificuldades dessa etapa. Ter você ao meu lado me trouxe leveza e paz. Obrigada por acreditar em mim e não me deixar desistir. Te amo.

À minha família, meus pais, Ronald e Cláudia, meu irmão Guilherme, minha cunhada-irmã Carol, e aos meus sobrinhos, Gustavo e Giulia, obrigada por compreenderem minha ausência em tantos momentos. Papy e mommy, obrigada por terem me dado todas as bases necessárias para chegar até aqui. Vocês são a minha vida.

Aos meus avós, Luiz Carlos e Maria América, e à minha segunda mãe, Cidinha, todos in memoriam. Levarei vocês comigo sempre, por toda a vida. Sei que vocês ainda vibram comigo em cada conquista.

Agradeço também às minhas amigas de uma vida inteira, Flávia, Marcela e Aline, que mesmo à distância sempre torceram por mim e me deram injeções preciosas de ânimo.

Aos amigos da PUC, Kissila, Tathi, Victor Nogueira, Rebecca, Thiago Carnavale, Felipe Rodrigues, João Marcelo, Lourdes, Filipe Sá, Vitor Monteiro and Isabel. Obrigada por compartilharem comigo tantas emoções ao longo desses anos, por me ajudarem com dúvidas e dicas valiosas, mas principalmente por serem fonte de diversão e força quando eu mais precisava. Kissila e Thati, obrigada pelos cafés (muitas vezes virtuais), as infinitas revisões de texto, as risadas e o apoio incondicional.

A todos os amigos da Casagrande Engenharia, principalmente Leonardo, Casagrande, Amanda, Nathalia, Marcelo, Caio, Armando, Arthur e Matheus, agradeço a parceria e o suporte para que eu pudesse efetivamente ser capaz de finalizar essa pesquisa.

Ao meu orientador, professor Flávio de Andrade Silva, por todos os recursos disponibilizados, pelo apoio concedido do início ao fim deste trabalho e pela compreensão com relação à minha rotina não convencional.

Aos técnicos do laboratório, Euclides, José Nilson, Rogério e Jhansen, por todo o auxílio prestado na elaboração e execução dos ensaios no Laboratório de Estruturas e Materiais da PUC-Rio. Sem vocês, essa pesquisa não poderia ser realizada.

Agradeço também ao engenheiro Rafael Vieira, da empresa IBRATA, e ao engenheiro Kléber Rodrigues, da empresa Reciclax, pela doação do agregado natural e do agregado reciclado utilizados nesta pesquisa. À empresa Votorantim, pela doação do cimento Portland CP-II-F32. À CNPq, CAPES e FAPERJ pelo apoio financeiro que, de forma indireta, tornou possível esse trabalho.

Por fim, agradeço a todos os demais professores, técnicos, funcionários e colegas da PUC-Rio, que me deram suporte até o fim dessa jornada. A PUC-Rio é também a minha casa.

O presente trabalho foi realizado com apoio da Coordenação de Aperfeiçoamento de Pessoal de Nível Superior – Brasil (CAPES) – Código de Financiamento 001.

Abstract

Salgado, Fernanda de Andrade; Silva, Flávio de Andrade (Advisor). **Assessment on Mix Design and Flexural Performance of Reinforced Concrete Short Beams Made with Mixed Recycled Coarse Aggregate**. Rio de Janeiro, 2023. 209p. Tese de Doutorado – Departamento de Engenharia Civil e Ambiental, Pontifícia Universidade Católica do Rio de Janeiro.

In the last decades, the construction sector has tried to mitigate the adverse effects of its activity by developing new formulations for more sustainable materials. Several studies have analyzed the feasibility of using recycled aggregate from construction and demolition waste in concrete to replace natural aggregate. International standards restrict the use of recycled aggregates in structural concrete, usually limiting to recycled aggregates composed only of cement-based fragments. However, using recycled aggregate with a certain content of ceramic fragments would simplify the separation process before recycling, making it more feasible and cheaper. In this work, it was observed that even replacing 100% of the natural aggregate with mixed recycled aggregate did not cause a significant impact on fresh and hardened concrete properties. The experimental results also showed that the Compressible Packing Model could be successfully applied for the mix design of mixed recycled aggregate concrete up to strength class C50. Finally, the results regarding the flexural behavior of short reinforced concrete beams showed that the prescriptions of the Brazilian standard ABNT NBR 6118:2014 for the bending behavior of conventional concrete beams could also be applied to beams made with concrete with mixed recycled aggregate up to 15% of ceramic fragments.

Keywords

Recycled aggregate; Recycled concrete; Mix design; Flexural performance; Short beams.

Resumo

Salgado, Fernanda de Andrade; Silva, Flávio de Andrade (Orientador). **Avaliação da Dosagem e Desempenho à Flexão de Vigas Curtas de Concreto Armado Produzidas com Agregado Graúdo Reciclado Misto.** Rio de Janeiro, 2023. 209p. Tese de Doutorado – Departamento de Engenharia Civil e Ambiental, Pontifícia Universidade Católica do Rio de Janeiro.

Nas últimas décadas, o setor da construção tem procurado mitigar os efeitos da sua atividade desenvolvendo novas formulações de materiais mais sustentáveis. Diversos estudos têm analisado a viabilidade do uso de agregado reciclado a partir de resíduos de construção e demolição, em substituição ao agregado natural. As normas internacionais restringem o uso de agregados reciclados em concreto estrutural, geralmente limitando-se a agregados reciclados compostos apenas por fragmentos cimentícios. Entretanto, a utilização de agregado reciclado com certo teor de fragmentos cerâmicos simplificaria o processo de separação antes da reciclagem, tornando-a mais viável e barata. Neste trabalho, observou-se que mesmo a substituição de 100% do agregado natural por agregado reciclado misto não causou impacto significativo nas propriedades do concreto fresco e endurecido. Os resultados experimentais também mostraram que o Modelo do Empacotamento Compressível pode ser aplicado com sucesso para a dosagem de concretos produzidos com agregado reciclado misto até a classe de resistência C50. Por fim, os resultados à flexão de vigas curtas de concreto armado mostraram que as prescrições da norma brasileira ABNT NBR 6118:2014 para concretos convencionais também podem ser aplicadas a vigas de concreto com agregado reciclado misto com até 15% de fragmentos cerâmicos.

Palavras-chave

Agregado reciclado; Concreto reciclado; Dosagem; Desempenho à flexão; Vigas Curtas.

Table of contents

List of figures

List of tables

1. Introduction

The construction sector is responsible for approximately 6 billion tons of CO_2 emissions, which means 23% of global emissions [1]. Furthermore, in the period 1970 to 2019, global extraction of sand gravel and crushed rock for construction increased by 425% [2]. For example, during 2019, only China was responsible for the extraction of approximately 14 billion tons of sand gravel and crushed rock for construction, while Brazil is responsible for 700 million tons/year in Brazil [3]. Besides, at the end of the construction chain, constructing new buildings and demolishing and maintaining existing structures generate excessive waste. Construction and Demolition Waste, commonly called CDW, covers many materials, such as concrete, tiles, ceramics, plastic, wood, glass, bituminous mixtures, metals, and even soil.

On a global scale, CDW accounts for 36% by weight of the total waste produced on Earth [4]. In the USA, CDW discarded increased from 50 million tons in 1980 to 548 million tons in 2015 [5]. In China, the annual CDW production exceeds 1.5 billion tons [6]; meanwhile, in European Union countries, it reaches about 850 million tons per year, representing 31% of the total waste generation in the EU [7]. In 2020, Brazilian municipalities produced around 45 million tons of CDW, equivalent to approximately 124 thousand tons/day [8].

Therefore, improper CDW disposal is a huge problem faced by many countries. Irregular disposal in open dumps has the potential for environmental contamination, causing flooding and landscape damage, and is also harming human health as it enables disease proliferation. Thus, many countries, such as the USA and European Union members, created waste management plans, looking for waste reduction, the prohibition of uncontrolled disposal, and an increase in the CDW recycling rate [9].

According to the USA Code of Federal Regulation 40 CFR Section 258.2, all construction and demolition waste must be sent to special landfills [9]; meanwhile, the EU members follow the Council Directive 2000/532/EC, which states that members should draw up waste management plans, looking for waste

reduction and prohibition of uncontrolled discharge [10]. In Brazil, in 2010, Federal Law Nº. 12.305 established the guidelines to reduce waste generation, increase recycling, promote eco-efficiency and sustainable development, and encourage appropriate waste disposal.

Some countries are applying charges for landfill dumping. For example, a $10/ton charge in New Zealand was introduced in 2008 as landfill sites became scarce yearly [11]. In France, by federal law, illegal CDW dumping or incineration on site is punishable with two years' imprisonment plus a 76000 € fine [12]. As another recycling incentive, nowadays, buildings under construction or significant renovations can earn one to two points in the LEED Certification process when their non-hazardous construction and demolition wastes are recycled or reused [13].

In countries lacking natural resources and landfills, such as Japan, CDW recycling is about 85% [14]. However, although recycling and reuse are good alternatives to waste disposal, in the USA and considering the average of European countries, only 30% of the total CDW volume is consigned to recycling [15]. This rate is even lower in some countries, such as China (5%) [6] and Portugal (9%) [16]. In Brazil, about 60% of municipalities dispose of their waste inappropriately in open dumps [17], recycling plants work on average with only 35% of their capacity, and only 18% of CDW is recycled [18].

Despite the inexpressive number of CDW recycling, this process can generate a material known as "recycled aggregate". Using recycled aggregate to replace natural coarse aggregate in concrete can be considered an environment-friendly solution to the increasing landfill requirement for CDW disposal and the scarcity of natural resources since aggregates represent about 70% of the total volume of concrete [19].

However, since CDW is usually very heterogeneous and its composition can be affected by several factors, such as the raw materials and the construction and demolition procedures, the basic physical and mechanical properties of recycled aggregates (shape and texture, specific gravity, absorption, moisture content, permeability, and strength) will vary considerably.

CDW is frequently composed of concrete rubble and crushed clay bricks from partitioning walls and cladding. For example, 70% of the recycling plants in Brazil claim to receive predominantly mixed material [20] since wall portioning in most

reinforced concrete buildings in Brazil have masonry, and CDW collection is disorganized [21].

Because of this heterogeneity, recycled aggregates are classified as Recycled Concrete Aggregate (RCA) when it is composed mainly of cement-based fragments and natural rocks and as Mixed Recycled Aggregate (MRA) when it is composed of a mixture of ceramic debris, bricks, cladding, concrete blocks, and mortar.

The use of Recycled Concrete Aggregate (RCA) as a replacement for natural coarse aggregate has been extensively studied since the 90s. Most research works have observed that an RCA replacement ratio smaller than 30% does not induce expressive variations in the mechanical properties and durability aspects of the resulting concrete [22]–[27]. The feasibility of using RCA in structural concrete has also been verified [28]–[31].

Nevertheless, regarding the use of Mixed Recycled Aggregate (MRA), because of its significantly variable composition, most researches focused only on road construction and non-structural applications [32]–[37]. However, Yang, Du, and Bao [38] analyzed the influence of using MRA from a British recycling plant containing different levels of ceramic debris and verified that it was still possible to produce quality concrete with MRA containing up to 20% of ceramic. In Brazil, although similar results were obtained with MRA from the southeast region [39], MRA is employed only as a road sub-base in Brazil.

Since aggregates represent about 70% of the total volume of concrete [19], concrete properties are directly dependent on aggregates' physical and mechanical properties. Therefore, international standards limit the use of recycled aggregate in structural concrete depending on the desired concrete strength class and the characteristics of the recycled aggregate. For example, Spanish, British, and Portuguese standards limit the use of RCA to a 20% replacement ratio in structural concretes up to C40 while not mentioning the use of MRA [40]–[42]. German and Italian standards only allow the use of MRA in non-structural concretes [43], [44]. Meanwhile, the Australian standard allows using 100% MRA in structural concrete C25 if its ceramic content is limited to 30% [45]. In Brazil, the use of recycled aggregates in structural concrete, regardless of strength class, is limited to 20% RCA by the Brazilian standard NBR 15116:2021 [46].

1.1. Research significance

Despite all the environmental benefits and the growth potential of the CDW recycling sector, some barriers still hamper the use of recycled aggregates on a larger scale. It is necessary, for example, to ensure that recycling plants can guarantee a consistent supply of high-quality recycled aggregates [47].

Usually, the ordinary recycling process comprehends different crushing, screening, and separation stages to remove contaminants like reinforcement bars, plastic, and glass. Different recycled methods can be applied depending on the maximum size and the desired composition of the final output [48], [49].

The removal of contaminants can occur during construction/demolition, optimizing the crushing time in the recycling plant and increasing the quality of the recycled aggregate. However, pre-crushing separation demands more elaborate waste management plans and an organized CDW collection, being more expensive and time-consuming for the contractors. As a second option, CDW can be stockpiled according to significant constituents in the recycling plant, and separation can be done only after crushing (post-crushing separation) [50].

In the case of post-crushing separation, when it is necessary to separate the ceramic and the concrete-based fragments, further advanced sorting techniques are used, such as gravity concentration in the presence of water or air [51]. However, in addition to being very expensive, these advanced techniques do not guarantee a complete separation between the ceramic and the concrete-based fractions [52].

Regarding structural elements, most research focuses on recycled concrete aggregate [53]–[66], and most of them use recycled aggregate produced in the laboratory, that is, with known characteristics and high technological control. On the other hand, little is known in terms of the structural performance of concrete produced with mixed recycled aggregate, that is, with a certain amount of ceramic fragments, since research with this type of material is limited to the study of the behavior of the concrete itself ([23], [34], [35], [67]–[70]), without reaching the structural scale. Finally, most of the concrete produced in the world is manufactured in mixing centers, that is, one way to promote the use of recycled aggregate in concrete would be to develop or use standard mix design processes.

A better comprehension of Mixed Recycled Aggregate (MRA) properties and their impact on structural concrete would increase market demand for this material

as this initiative can decrease recycling costs and make the recycling process more feasible. Consequently, the CDW recycling rate would increase, generating numerous environmental benefits and improving the recycling sector economically.

1.2. Objectives

To move towards more sustainable building practices, the present work seeks to assess the mix design and flexural performance of reinforced concrete beams made with mixed recycled aggregate (with a certain amount of ceramic fragments) to replace natural coarse aggregate. It is important to note that the mixed recycled aggregate to be used in this research comes from a Brazilian recycling plant.

Thus, to achieve this main objective, three steps were defined. First, the physical and mechanical properties of the recycled coarse aggregates with different contents of ceramic fragments will be investigated. The results will be compared with the physical and mechanical properties of a natural granitic coarse aggregate. For each material, the experimental analysis will be carried out regarding pulverulent content, grain-size distribution, shape index, density, porosity, water absorption, strength, and packing density. Understanding the impact of the content of ceramic fraction on the characteristics of the recycled coarse aggregate would instigate the use of this material since recycling costs will decrease based on the non-necessity of separating the ceramic fraction. This will also make the recycling process more feasible, increases market demand for this material, and makes the material more attractive for large-scale use.

Secondly, the compressive strength of predetermined concrete mixtures will be estimated using the software BétonLab Pro 3, which is based on the Compressible Packing Model (CPM) and was developed by the *Institut français des sciences et technologies des transports, de l'aménagement et des réseaux* (IFSTTAR). This software relies on a raw materials database to estimate concrete properties in fresh and hardened states and allows the simulation of different materials mixtures to select the one that best meets the concrete's desired properties. At this stage of the research, two concrete strength classes will be analyzed concerning compressive strength at 28 days: concrete class of 30 MPa and 50 MPa. The concretes will be designed with 20%, 50%, and 100% mixed recycled coarse aggregate to compare with the reference concretes (0% mixed recycled coarse

aggregate). The theoretical results of compressive strength at 28 days will be compared with the experimental values, to verify the accuracy of the concrete mix design based on the Compressible Packing Model (CPM). In addition, the experimental values of tensile strength and modulus of elasticity will be analyzed, comparing them with the theoretical values provided by the Brazilian standard ABNT NBR 6118:2014 [71].

Finally, the third stage of this research investigates the flexural behavior of short reinforced concrete beams manufactured with mixed recycled aggregate when subjected to short-term loading. Beams will be produced with concretes of strength classes C30 and C50, and different contents of mixed recycled aggregate. Some beams will be designed according to the Brazilian standard ABNT NBR 6118:2014 [71], considering a ductile failure, which means that reinforcement yields before concrete failure. Some other beams will be designed with an over-reinforced section to present a brittle failure (characterized by the crushing of concrete before the rebar yields). The beams will be subjected to a four-point bending load and, through instrumentation with LDVTs and strain gauges, analysis will be made regarding the moment-strain diagram of the beams. In addition, using the Digital Image Correlation (DIC) technique, the cracking pattern and crack opening will be evaluated. In this stage, pull-out tests will also be executed to investigate the bond behavior between the steel rebar and the different concretes. Finally, to investigate the applicability of the Brazilian standard ABNT NBR 6118:2014 [71] to beams made with mixed recycled aggregate, the experimental results will be compared to theoretical equations, mainly concerning the cracking moment and crack opening.

1.3. Work Organization

Chapter 1: *Introduction*

This chapter describes the research's significance and objectives.

Chapter 2: *Literature Review*

This chapter presents a literature review on 1) CDW characterization; 2) the recycling process; 3) the influence of recycled coarse aggregates in concrete; 4) methods to improve the physical properties of recycled aggregates, 5) mix design methods, and 5) structural applications.

Chapter 3: *Investigation of Physical and Mechanical Properties of Recycled and Natural Coarse Aggregate*

This chapter describes an experimental investigation of recycled coarse aggregates' physical and mechanical properties compared with a natural coarse aggregate. This investigation encompassed three types of recycled coarse aggregate (mixed recycled aggregate - MRA, recycled concrete aggregate - RCA, and recycled masonry aggregate - RMA). Each of these recycled coarse aggregates has a different content of ceramic debris.

Chapter 4: *Mix Design for Mixed Recycled Aggregate Concrete through the Compressible Packing Model (CPM)*

This chapter discusses the concrete mix design method based on the Compressible Packing Model (CPM) principles, using the software Bétonlab Pro 3, which relies on data from the constituent materials to forecasting specific concrete properties. At the end of this chapter, the theoretical compressive strengths of predetermined concrete mixtures were compared with the experimental compressive strength to verify the accuracy of the concrete mix design based on the Compressible Packing Model (CPM).

Chapter 5: *Flexural Behavior of Short Reinforced Concrete Beams Made with Mixed Recycled Aggregate*

This chapter investigates the flexural behavior of short reinforced concrete beams made with mixed recycled aggregate compared to the behavior of natural aggregate concrete beams under short-term loading. Consequently, it evaluates the possibility of using mixed recycled aggregate concrete beams in structural concrete elements. It also evaluates the bond behavior between the steel rebar and the different concretes through the results of pull-out tests.

Chapter 6: *General Conclusions*

This chapter presents a general briefing on the issues discussed in the thesis.

Chapter 7: *Suggestions for Future Research*

This chapter addresses some suggestions for future research to complement the results of the present work.

Chapter 8: *Published Articles*

This chapter presents the details regarding the publication of articles based on the results of this doctoral thesis.

2. Literature Review

2.1. Introduction

This chapter presents a literature review on recycled coarse aggregate replacing natural coarse aggregate in concrete. The paper selection was carried out concerning the following selected keywords: "recycled aggregate" and "concrete", plus one of the following: "mechanical properties", "enhancement treatment", and "structural performance". The survey was restricted to titles, abstracts, and keywords of scientific papers, conference papers, and book chapters. Moreover, the selected studies must have been published in English after 2000. The search for eligible studies was conducted using Engineering Village, Science Direct, and SciELO databases.

This literature review covers the characterization of Construction and Demolition Waste (CDW) and the recycling process. Then, it shows how recycled aggregates influence the characteristics of concrete and describes different methods capable of improving the physical properties of recycled aggregates. Finally, it presents different mix design methods and examples of structural applications of recycled aggregate concrete.

The literature review shows that using recycled aggregate from construction and demolition waste in structural concrete elements is feasible and can help solve the excessive environmental impact caused by the construction industry worldwide.

2.2. Characterization of CDW

CDW composition can be affected by several factors, such as architectural techniques, raw materials, and construction/demolition procedures. Nevertheless, concrete, mortar, and red ceramics are the main components of CDW, reaching above 70% by weight [72]. **Figure 2-1** shows a CDW pile and concrete waste from construction and demolition at Reciclax Recycling Plant in Ribeirão Preto, Brazil.

(a) (b)

Figure 2-1. (a) CDW pile and (b) Concrete waste stocked at Reciclax Recycling Plant (Ribeirão Preto, Brazil) before being processed through the Ordinary Recycling Process.

In 2002, CONAMA (Brazilian National Council for the Environment) published Resolution nº 307 [73] classifying CDW as:

- Class A: brick, tile, flooring board, mortar, and concrete;
- Class B: plastic, glass, cardboard, paper, wood, and metal;
- Class C: materials with no economically feasible recycling techniques (e.g., gypsum);
- Class D: hazardous waste (e.g., solvent, oil, paint, and materials that contain asbestos).

In the USA, the CDW classification includes the materials mentioned above and salvaged building components (e.g., doors, windows, and plumbing), soil, and rocks from clearing sites [74].

Nevertheless, crushed concrete and masonry are the primary CDW material that can be transformed into different types of recycled aggregate. Technical standards from different countries present different nomenclatures and classifications for recycled aggregate produced from construction and demolition waste. For example, the British Standard BS 8500-2:2015 [75] classifies:

- Recycled Concrete Aggregate (RCA): consisting of a minimum of 90% by weight of Portland cement-based fragments;
- Recycled Masonry Aggregate (RMA): consisting of a minimum of 90% by weight of ceramic bricks, roofing tiles, and mortar rendering;
- Mixed Recycled Aggregate (MRA) consists of masonry-based materials and Portland cement-based fragments, the latter being up to 90% by weight.

On the other hand, the Brazilian standard ABNT NBR 15116:2021 [47] does not have a nomenclature for recycled aggregates with a composition of primarily ceramic materials. This standard considers three classifications, as described below:

- Concrete Recycled Aggregate (ARCO): consisting only of different cement-based fragments, such as concrete, mortar, and precast concrete blocks;
- Cementitious Recycled Aggregate (ARCI): consisting predominantly of cement-based fragments; however, it may include up to 10% by weight of ceramic materials such as ceramic blocks, tiles, and bricks;
- Mixed Recycled Aggregate (ARM): consisting of a mixture of cement-based fragments (up to 60% by weight) and ceramic materials (up to 40% by weight).

In addition to concrete and ceramic materials, glass and plastic can replace sand. A filler effect occurs when glass particles are smaller than 38 μm and used in a replacement ratio of up to 30%. This filler effect improves the compressive strength of the concrete and some long-term properties, such as permeability and resistance to chloride ion penetration. If the glass can be ground even finer, pozzolanic activity is expected to improve remarkably [76]–[78].

When plastic aggregates are used in concrete, mechanical properties decline as the replacement ratio increases due to a weak bond between plastic aggregates and cement paste and because plastic aggregates present low strength and low modulus of elasticity [79], [80]. Nevertheless, concrete with plastic substituting fine aggregates can be used as sub-bases for highway pavements and low-strength applications. Moreover, due to the increase in water absorption, recycled fine aggregates can be used in sports courts and pavements where there is a need for proper water drainage [81].

Nevertheless, when processing recycled aggregate, every effort should be made to reduce as far as possible the percentage of embedded items (e.g., wood, plastic, and glass). The weak bonding between these components and cementitious matrices can lead to lower-strength concrete and more susceptibility to hazardous materials that reduce durability [69], [82].

2.3. Recycling Process

The recycling process transforms the construction and demolition waste into a smaller-sized fraction in mobile or fixed recycling plants [15]. The number of

recycling stages and different types of crushing influence recycled aggregate characteristics. Due to collision and peeling-off effects, the recycling process also improves the shape of aggregates leading to rounder and less sharp particles [75], [83], [84]. In this mechanical grinding process, a high-speed rotating eccentric gear causes a rolling vibration effect that pulverizes the adhered mortar [85]. Different recycled methods can be applied depending on the maximum size and the desired quality of the final output.

The "Ordinary Recycling Process" (ORP) comprehends different crushing, screening, and sorting stages to remove contaminants like reinforcement bars, plastic, and glass. In this method, CDW passes through a primary crusher in a jaw crusher, which can handle residual reinforcement bars and large pieces of concrete. Then iron scraps are removed using a magnetic separator, and the remaining material passes through sieves. Thus, particles larger than 20 mm are crushed again in a secondary crusher, such as an impact or rotary crusher. Secondary crushing can be repeated if necessary [11], [14], [86], [87]. A schematic representation of the "Ordinary Recycling Process" can be seen in **Figure 2-2**.

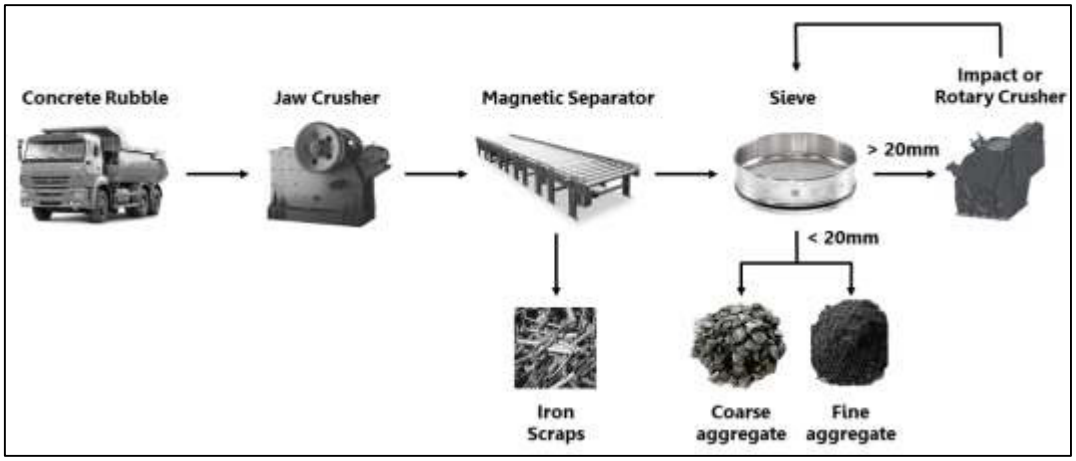

Figure 2-2. Schematic representation of the Ordinary Recycling Process (ORP).

Nevertheless, other mechanical methods allow higher-quality recycled aggregates with similar characteristics to conventional ones. In these methods, the impact or rotary crusher is substituted by an eccentric rotor, a screw crusher, or an improved jaw crusher [49]. During this more complex mechanical method, the input material is better processed, removing the adhered mortar and reducing the size of the aggregates by continuous friction between them.

Besides the mechanical grinding, it is also possible to heat the recycled aggregate, weakening the adhered mortar. The high temperature during the thermal

process generates cracks in the adhered mortar, decreasing its mechanical strength, thus becoming easily removable from the original aggregate surface. For example, the Heating and Sorting (HS-RK) method produces recycled aggregates with only 2% of adhered mortar after thermal treatment up to 700ºC in a rotary kiln [88]. In 2005, a method known as Heating and Rubbing (HR-F) was introduced. In this procedure, rough-crushed concrete pieces (smaller than 40 mm) are first heated to approximately 300ºC in a kerosene furnace during 40-60 min and then crushed and rubbed in a tube mill [89].

This process was improved in 2011, using an impact crusher and a special microwave oven instead of a kerosene furnace [90]. In this new technique, the material is heated for only 2 min, reducing energy consumption. Microwave weakening pre-treatment is effective irrespective of the nature of the aggregates used in concrete and even when the material is exposed to a shallow microwave heating energy [91]. Generally, the adhered mortar is easily removed at a higher temperature; however, the properties of RCA may be degraded when it exceeds 500ºC. Besides the good results of thermal grinding, it consumes a lot of energy and produces additional carbon dioxide emissions. **Figure 2-3** shows a schematic representation of the recycling processes involving heat.

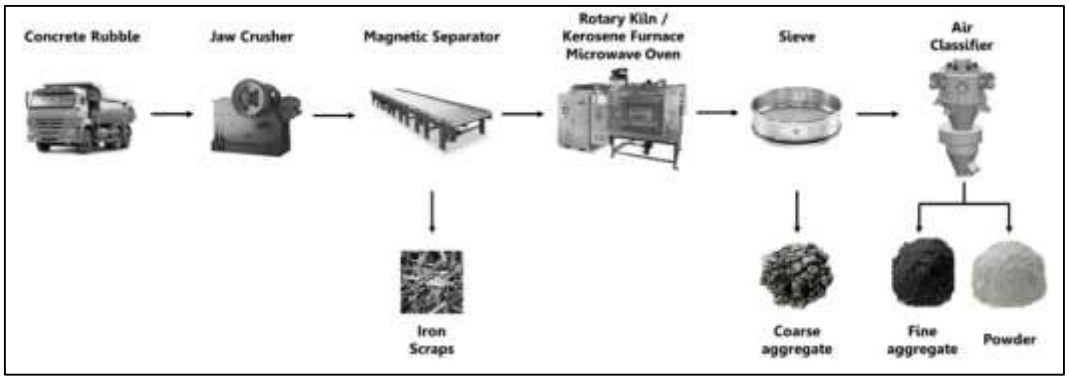

Figure 2-3. Schematic representation of recycling processes involving heat.

Regarding water use, thermal expansion is an advanced wet recycling technique. CDW is immersed in water for two hours to saturate the adhered mortar thoroughly. After that, samples are dried at about 500ºC for two hours and then submerged in cold water. While heating induces the formation of water vapor in the saturated adhered mortar, the immediate cooling causes stress and, consequently, cracks in the adhered mortar, which can be easily removed afterward [92].

Wet techniques also include autogenous cleaning, where recycled aggregate particles collide against each other in a rotating mill drum. Then the material is cleaned with water and dried to remove all the remaining fines and impurities [93]. However, although these wet recycling methods effectively remove the adhered mortar, they have a significant water demand, making the process more complex, expensive, and, in some way, impacting its sustainability.

2.4. Influence of Recycled Coarse Aggregates on the Concrete

2.4.1. Fresh State and Workability

The coarse aggregate grains' shape directly influences the concrete's quality as it changes its workability and, consequently, its mechanical strength. For the same workability, concrete made with rounded aggregates requires less mixing water than concrete made with angular-shaped aggregates. Therefore, spherical aggregates are more advantageous as the water/cement ratio highly affects the compressive strength of concretes. Also, irregular, elongated, and lamellar grains have a larger specific surface. They can get stuck between the steel bars of the reinforced concrete, resulting in the formation of voids during concrete pouring, a phenomenon highly harmful to the performance of structural concrete elements. On the other hand, aggregates with an angular shape offer higher adhesion to the mortar and increase interlocking. Thus, using angular aggregates for the same w/c ratio and guaranteeing proper casting and compaction leads to concretes with higher strength.

There are, therefore, two characteristics regarding the shape of coarse aggregates: the rounded shape, facilitating workability and worsening adherence; and the angular shape, worsening workability but enhancing the bond between aggregates and mortar. Recycled aggregates are usually flatter and elongated than natural aggregates, exhibiting a higher shape index [23].

Another important consideration is that recycled aggregates have a higher water absorption capacity; thus, they absorb water from the cement paste, resulting in concrete with poor workability and reduced control of the effective w/c ratio in the cement paste [94]. For Recycled Concrete Aggregate (RCA), this higher water absorption capacity can be explained by the presence of an adhered mortar characterized by micro-cracks and pores [95], [96]. Likewise, as ceramic materials are naturally more porous than natural rocks, Recycled Masonry Aggregate (RMA)

and Mixed Recycled Aggregate (MRA) also absorb more water than conventional aggregate [97]. Therefore, when recycled aggregates are saturated before mixing, it improves hardened concrete's workability and compressive strength [98].

The slump value of concretes made with recycled aggregates is influenced by their moisture states, shape, and replacement ratio [95]. As the replacement ratio increases, concrete loses cohesion, affecting the fresh concrete's homogeneity during casting. Thus, the mechanical and durability properties of hardened concrete can be modified.

2.4.2. Hardened Recycled Aggregate Concrete

2.4.2.1. Microstructure and Interfacial Transition Zone (ITZ)

Conventional concrete is a two-phase composite with an interfacial transition zone (ITZ) between aggregate and cement matrix. The ITZ serves as a bridge between the aggregate and mortar matrix. Moreover, when the individual components have high stiffness, the stiffness of the concrete may be low because of the voids and micro-cracks in the ITZ, which do not permit stress to be transferred [99]. **Figure 2-4** shows an optical micrograph of recycled aggregate concrete made with 50% mixed recycled aggregate (MRA) where it is possible to observe a natural aggregate, a recycled ceramic aggregate, and the interfacial transition zone between the cement mortar and the two types of aggregates. This optical micrograph was taken using a stereomicroscope at the Structures and Materials Laboratory at PUC-Rio.

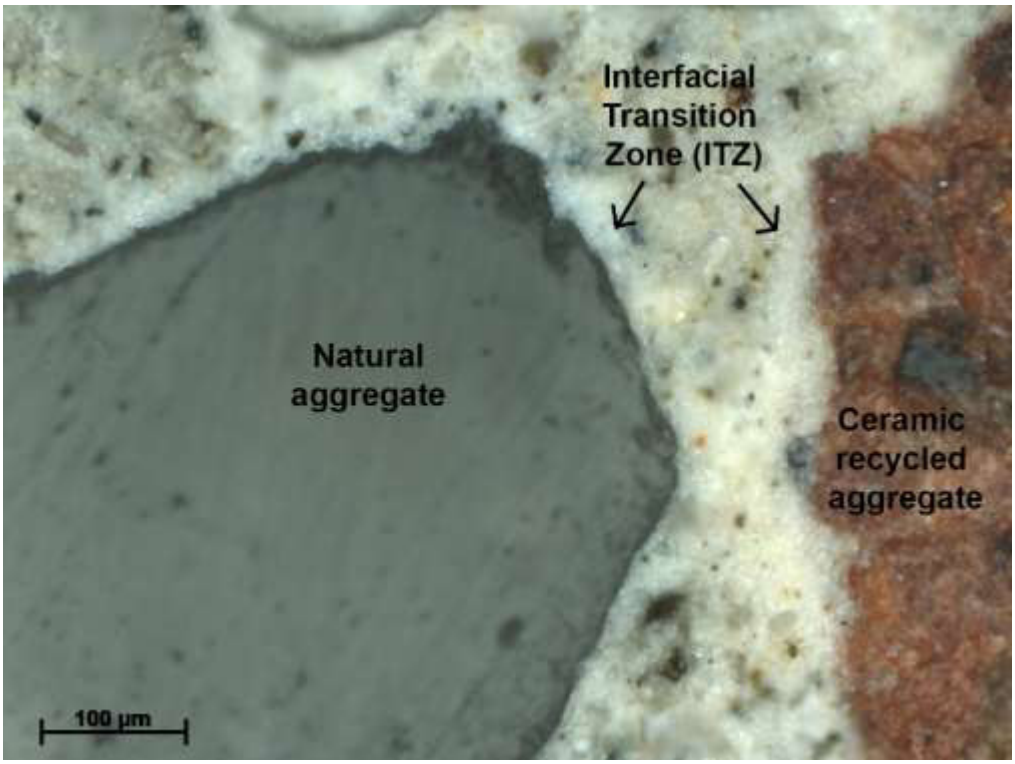

Figure 2-4. Optical micrograph of concrete made with Mixed Recycled Aggregate (MRA).

Concrete made with recycled concrete aggregate (RCA) differs from conventional concrete by the presence of two ITZs: an old one between the conventional coarse aggregate and the adhered (old) mortar; and a new one between adhered (old) mortar and new cement matrix (**Figure 2-5**). Through nanoindentation, the thickness of the old ITZ was measured between 40–50 µm, while for the new ITZ, it ranges from 55–65 µm [100].

Therefore, in this case, the microstructure of recycled aggregate concrete is much more complicated than conventional concrete. The old ITZ represents a weak region because it is more porous and has pre-existing cracks. Thus, this old ITZ has a more significant potential to initiate cracks and, consequently, affects the mechanical behavior of the recycled aggregate concrete [101]. The mechanical tests have shown that failure happens, in general, through the old ITZ, meaning that the old mortar has a higher tendency to crack when compared with new mortar [25], [102], [103]. Nevertheless, the presence of the old mortar does not affect the bond strength between recycled aggregate and new cement mortar [104].

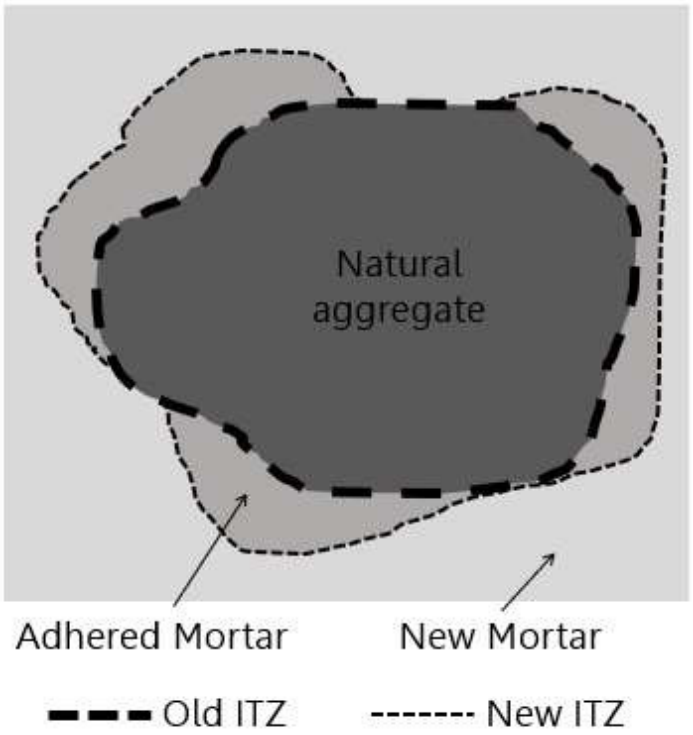

Figure 2-5. Schematic diagram of old and new ITZ.

2.4.2.2. Porosity and Pore Structure

Concrete is a compulsorily porous material regardless of the aggregate used. The voids in concrete can appear because of excess water used to obtain suitable workability, a decrease in absolute volume from the hydration of cement constituents, air incorporated during the mixing process, and cracks of different origins. These voids are usually interconnected, so concrete is customarily permeable to liquids and gases. Consequently, it is crucial to understand the permeability of concrete, not only for its use in submerged constructions but also when aggressive agents can threaten concrete durability.

Different methods can be used to evaluate the permeability of cement-based materials [105]. Mercury intrusion porosimetry (MIP), water vapor adsorption, and nitrogen adsorption are typical techniques. However, these methods assume that the pore geometry is regular, interconnected pores and that water loss does not affect pore size distribution during drying. Thus, as a single technique cannot sufficiently characterize the cement-based materials' pore structure, Abell et al. [106] suggested a combination of mercury intrusion porosimetry (MIP) and microscopy with backscattered electron images (BSE).

The higher porosity of recycled aggregate concrete acts as a presumable channel for water transport. On average, recycled aggregate concrete absorbs 25% more water than conventional concrete, independently of the type and quantity of binder [96], [107]. This higher water absorption capacity affects the actual w/c ratio of concrete as concrete made with recycled coarse aggregates typically needs more water than conventional concrete to obtain the same workability; it also affects the cement hydration process and the homogeneity of the fresh concrete during casting, reducing the mechanical strength and the durability of concrete. Besides, the literature does not specifically discuss different curing methods for recycling aggregates. Like conventional concrete, recycled aggregate concretes are kept under curing conditions, usually in a humid chamber, for 28 days.

The higher water absorption of recycled aggregates also affects the concrete drying shrinkage. In conventional concrete, the drying shrinkage is mainly influenced by the cement mortar; meanwhile, coarse aggregates play an inhibitory effect on the shrinkage of cement mortar. However, because of the higher water absorption of recycled aggregates, drying shrinkage increases with the recycled aggregate replacement ratio [26], [83], [108], [109]. This effect is due to the higher deformability of recycled aggregate concretes, caused mainly by the adhered mortar on the recycled aggregate surface, generating a weaker interfacial transition zone (ITZ), resulting in less aggregate-restrained shrinkage.

Since density is the ratio between the mass and volume of the material, because of its higher porosity, recycled aggregate concrete also presents a lower density than conventional concretes for all different strengths and curing ages [83], [107]. The existing voids in the concrete facilitate the propagation of cracks, reducing the strength of the hardened concrete. The higher permeability of recycled aggregate concrete also makes it more susceptible to aggression by external agents such as chloride ions, reducing its durability [110].

This pore structure also interferes with the mechanical strength of the aggregate itself. Regarding its strength to crushing and degradation, recycled aggregate has a higher aggregate crushing value, higher Los Angeles abrasion index, and lower “10% fine” value [83], [95], [96], [109]. As an example, **Table 2-1** compares some properties of recycled concrete aggregate (RCA) with natural granitic coarse aggregate (NAT) [111].

Table 2-1. Properties of recycled concrete aggregate (RCA) and natural granitic coarse aggregate (NAT) [111].

Properties	NAT	RCA
Oven-dry Density (kg/m^3)	2570	2253
Bulk Density (kg/m^3)	1424	1315
Apparent Porosity (%)	3.1	14.4
Water Absorption (%)	1.2	6.4
Shape Index	1.87	1.97
Aggregate Crushing Value (ACV)	30.5	32.5

However, this influence on porosity is less critical at higher ages because of the continuation of the hydration process, increasingly generating calcium silicate hydrates (C–S–H). Kwan *et al*. [112] showed that microstructure becomes denser at later ages and capillary spaces narrow. Moreover, after Ultrasonic Pulse Velocity Test (UPV), it was observed that although UPV values decreased for a higher recycled aggregate replacement ratio (indicating a higher number of cracks and voids), the UPV values were still acceptable for all samples. Thus, these results suggested that recycled aggregate concretes do not contain large voids or cracks directly affecting their structural integrity.

2.4.2.3. Mechanical Behavior

The impact on concrete mechanical behavior when using recycled aggregate to replace natural coarse aggregate has been extensively studied. Like conventional concrete, the compressive strength increases over the age of recycled aggregate concrete. However, as the recycled aggregate replacement ratio increases, the compressive strength at a given age usually decreases.

Nonetheless, the results vary considerably among the several published studies on the compressive strength of concrete produced with recycled aggregate. Two main reasons can explain this significant variability. First, the same recycled aggregate can cause different impacts on concrete depending on the quality of the mechanical properties of the natural aggregate to be replaced. Second, different studies usually adopt different strategies: concretes with the same water/cement ratio, the same effective water/cement ratio, or the same workability (which leads to a different water/cement ratio). Furthermore, the conclusions also depend on the recycled aggregates' shape, size, composition, and mechanical properties [113].

Several studies have shown that tensile strength also decreases when the replacement ratio of recycled aggregate increases. This reduction can reach 13% for higher replacement ratios [107], [114]–[119]. This reduction in tensile strength directly impacts the use of recycled aggregates in structural elements. It reduces the shear strength and the flexural cracking load of recycled reinforced concrete beams compared to beams made with conventional concrete.

Bravo et al. [23] analyzed the mechanical performance of concretes made with recycled aggregate from different locations in Portugal and obtained the worst results with aggregates with a higher amount of clay. The clay covers the recycled aggregate grains and restrains the bond between aggregate and cement paste. Moreover, as it absorbs the mixing water, it is necessary to increase the water-cement ratio to obtain the same slump. Regarding the use of recycled concrete aggregate (RCA), the mechanical behavior is directly proportional to the strength value of the original concrete because recycled aggregate from high-performance concrete has a relatively dense ITZ, while recycled aggregate from normal-strength concrete has a porous ITZ [120], [121]. Concerning the moisture state of recycled aggregates, De Oliveira and Vazquez [122] observed that using semi-saturated aggregates presents better results regarding concrete compressive and flexural strength.

Figure 2-6 presents the relationship between the compressive strength and recycled aggregate replacement ratio for different concrete grades based on the results published by several authors [23], [24], [26], [38], [67], [68], [83], [95], [107], [108], [112], [115], [116], [118]–[120], [123]–[167]. The results present a preeminent variation for higher concrete grades and especially for higher recycled aggregate ratios. For C35-C40, C45-C50, and C55-C60 over 50% recycled aggregate, the results present a more significant variation, profoundly increasing for RA/NA ratio equal to 100%. This expressive variation does not occur for the C25-C30 concrete grade: the results vary approximately constantly, regardless of the recycled aggregate ratio.

For all types of concrete, it is possible to observe a reduction in compressive strength as the recycled aggregate ratio increases. However, this reduction is much more expressive for higher concrete grades (C45-C50 and C55-C60). The failure planes could explain this. Butler et al. [140] observed that failure planes for a concrete C30 occurred around the aggregate, indicating that the interfacial

transition zone (ITZ) was the limiting strength factor. However, for a concrete C50, the failure plane occurred mainly through the aggregates, indicating that the strength of the coarse aggregate itself was the limiting strength factor. Thus, it is possible to assume that, for higher concrete grades, where ITZ is stronger, the concrete strength reduces more expressively when the recycled aggregate ratio increases. On the other hand, for lower concrete grades, depending on the properties of the recycled aggregate, the ITZ can be more limiting for the strength, and the increase in recycled aggregate ratio could not cause a significant impact on the concrete strength.

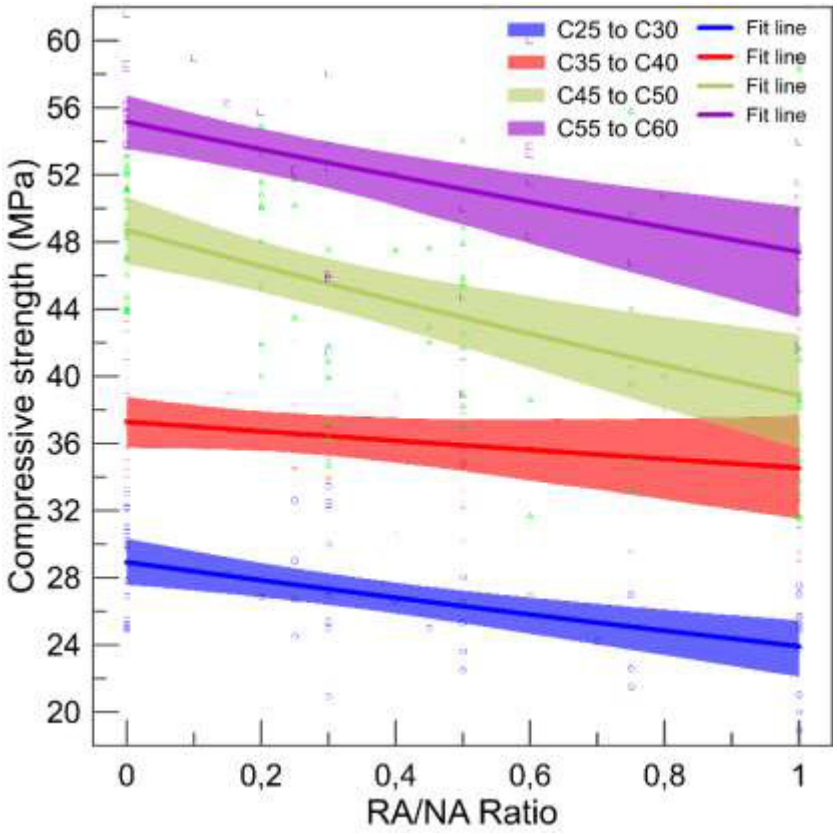

Figure 2-6. Compressive Strength *versus* Recycled/Natural aggregate (RA/NA) ratio for different concrete grades, based on the results published by several authors [23], [24], [26], [38], [67], [68], [83], [95], [107], [108], [112], [115], [116], [118]–[120], [123]–[167].

Different studies have also shown that the concrete modulus of elasticity reduces as the content of recycled aggregate in concrete increases [23], [24], [38], [83], [107], [108], [118], [119], [123]–[139], [167]. However, this decrease is more noticeable when recycled aggregate has more adhered mortar [83]. The modulus of elasticity is an important parameter to be observed because it directly affects the behavior of reinforced concrete structural elements. For example, the higher the modulus, the lower the deflection of beams and slabs.

Some authors have suggested different equations that correlate the modulus of elasticity and the compressive strength of recycled aggregate concrete. Some of these equations are in **Table 2-2**.

Table 2-2. Correlation between modulus of elasticity and compressive strength of recycled aggregate concrete (Ec in GPa and fc in MPa).

Reference	Equation
Cabral *et al.* [72]	$Ec = 2.58 * fc^{0.63}$
Lovato [168]	$Ec = 5.74 * fc^{0.5} - 13.39$
Ravindrarajah and Tam [169]	$Ec = 4.63 * fc^{0.5}$

Each of these authors analyzed only their experimental results to define their equation. Thus, to increase sampling in this study, the experimental results obtained for the compressive strength and modulus of elasticity of several studies were compiled in a single graphic curve, namely "Experimental Data" in **Figure 2-7**. Then, using the equations above and the compressive strength obtained experimentally, the theoretical modulus of elasticity was calculated using the three equations in **Table 2-2.** Therefore, **Figure 2-7** presents these three theoretical curves and the original "Experimental data" curve for four different concrete grades (C25-C30, C35-C40, C45-C50, and C55-C60).

Figure 2-7 shows that the modulus of elasticity reduces as the content of recycled aggregates in concrete increases. This effect is attributed to the two interfacial transition zones (ITZ). This second (old) ITZ tends to be weaker than the paste-aggregate matrix of conventional concretes and consequently reduces the concrete strength, leading to higher deformability of recycled concretes compared with conventional concretes.

It is also possible to observe from **Figure 2-7** that regardless of the concrete grade and the recycled aggregate ratio, there is a large discrepancy between the results obtained experimentally and those obtained through the theoretical curves proposed by the three authors in **Table 2-2**. This divergence occurs mainly because the recycled aggregates are very heterogeneous, and the theoretical curves use only compressive strength as a parameter. Thus, for better estimation, probably more parameters should be considered, such as recycled aggregate density or water absorption.

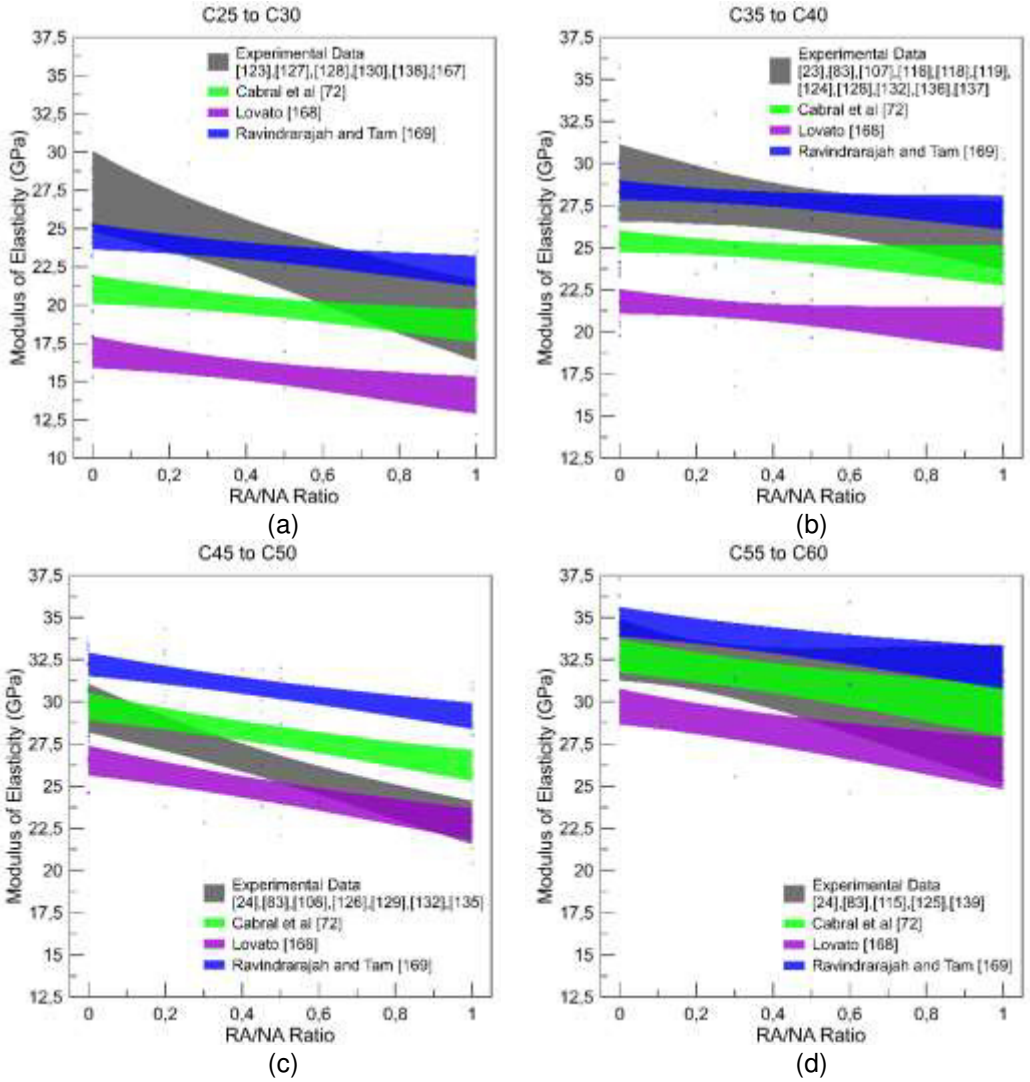

Figure 2-7. Correlation between modulus of elasticity and Recycled/Natural aggregate (RA/NA) ratio for different concrete grades: (a) C25-C30, (b) C35-C40, (c) C45-C50, and (d) C55-C60.

Because of this considerable heterogeneity of recycled aggregates, different parameters should also be considered for mix design. As will be seen later, several authors proposed different approaches for the mix design of recycled aggregate concretes and the prediction of their compressive strength, considering the peculiar characteristics of recycled aggregates.

2.5. Methods to Improve the Recycled Aggregates Physical Properties

In addition to mix design methods, some strategies are used to improve the physical properties of recycled aggregates and minimize the gap performance between natural and recycled aggregate concrete mixtures, such as pre-soaking in acid, two-stage mixing approach (TSMA), the addition of pozzolanic micro-

powders, use of polymer emulsion, microbial carbonate bio-deposition, and carbonation.

Modifying the materials' mixing sequence can be enough to change concrete properties when using recycled aggregates. For example, some authors have adopted the "Two-Stage Mixing Approach (TSMA)." In this method, the required water is split into two equal parts, and each part is added to the mixture at two different times, as shown in **Figure 2-8**. By doing that, researchers have observed a layer of cement slurry on the surface of recycled aggregate [170]–[172]. Also, the total volume of voids and CH crystals in the new ITZ decreased [158].

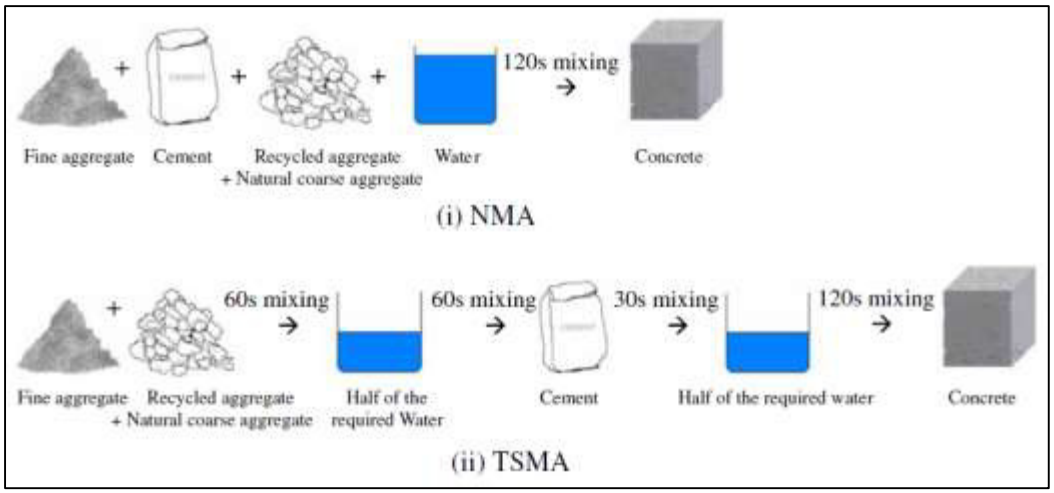

Figure 2-8. NMA (Normal Mixing Approach) and TSMA (Two-Stage Mixing Approach) [158].

Pre-soaking in acid, for example, can be used to remove the adhered mortar and enhance the quality of recycled concrete aggregate (RCA), as the hydration products of cement in the hardened paste are dissolved, reducing porosity and water absorption capacity [73],[134]–[136]. However, using acids in higher concentrations threatens the workers' safety and adds detrimental ions, such as Cl^- and SO_4^{2-}, to the recycled concrete aggregates, which can cause durability issues in recycled concrete. Therefore, there is a need for a massive amount of water to wash treated recycled concrete aggregates. Moreover, the disposal of this washing water and the residual of this treatment create new environmental problems. To compensate for these drawbacks, Wang et al. [176] used acid acetic as a treatment solution in their studies because it is safer, cleaner, and lower cost than HCl or H_2SO_4.

On the other hand, some methods were developed to seal the pores of recycled aggregates. The addition of pozzolanic micro-powders, polymer emulsion, microbial carbonate bio-deposition, and carbonation are some examples.

Polymer emulsions have adhesive properties and can solidify in a short period. As they are water-repellent, polymer emulsions reduce the water absorption capacity of porous materials, such as recycled aggregates [166], [177]–[181]. This treatment can usually be done by two methods: dispersion of the polymer emulsion into fresh concrete during the fabrication process or coating treatment, where the surface of the concrete is coated by polymer emulsion. Both methods can improve the durability of recycled aggregate concrete. However, the coating treatment is more effective because it can achieve a more considerable impregnation depth [182].

Regarding the addition of pozzolanic micro-powders, modification of ITZ microstructure can be achieved through physical or chemical mechanisms. The first is characterized by mineral admixtures' ability as micro-filler, filling ITZ micro-pores. Meanwhile, the chemical mechanism relates to the pozzolanic reaction in water presence [152]. When mineral admixture is added to the concrete, a denser ITZ, as well as better workability and mechanical, are observed because: (a) the relatively lower water-to-binder ratio of coating slurry promotes a higher strength of the recycled aggregate concrete; (b) the pozzolanic coating layer forms a barrier to inner bleeding of water, which improves the workability and, consequently, strengthen the traditional weak ITZ; (c) pozzolanic material results in consumption of calcium hydroxide accumulated in the pores and on the surface of the adhered mortar to form new hydration products, resulting in a denser calcium silicate hydrate (C-S-H) structure and C_3A, capable of chemically binding chloride ions and improve the bond between the recycled aggregate and cement paste [183].

Microbial carbonate bio-deposition has already been widely studied to protect and consolidate the surface of stones and concretes. It is based on the ability of some bacteria to induce calcium carbonate crystal precipitation through various physiological activities. These physiological activities form a continuous waterproof layer on the surface and fill the pores, working as a barrier to prevent water penetration and other corrosive substances. This dense surface and decreased permeability improve the mechanical behavior and durability of the concrete [184]–[187].

In another innovative method, known as “carbonation”, the CO_2 reacts with $Ca(OH)_2$ and hydrated calcium silicate (C-S-H), which are the main cement hydration products in the old cement mortar, to form $CaCO_3$ and silica gel, which fill the pores of the adhered cement mortar. Overall, this method decreases porosity, strengthening the weak surface and lowering the water absorption of the porous cement mortar, which is usually accompanied by a strengthening effect [188].

Therefore, carbonation treatment is efficient and environmentally friendly as it can capture CO_2 emitted from industrial processes. However, the time needed is much longer than other methods. Also, the concentration of CO_2 and humidity influence efficiency. The method can be helpful in non-reinforced structures; however, reinforcement steel bars, used in reinforced concretes, lose their passivity and becomes vulnerable to corrosion, as the carbonation causes a reduction in the pH of the cement paste [188]–[192].

Sometimes, a combination of methods is used. For example, some authors proposed pre-soaking in acid and impregnation with a solution of calcium metasilicate [125] or silica fume [175]. In the same way, in some studies, the Two-stage Mixing Approach (TSMA) was used in addition to impregnation with different pozzolanic micro-powders, such as fly ash, silica fume, and blast furnace, improving, even more, the characteristics of the recycled aggregate concrete [193], [194].

Ultimately, all methods can improve the durability and mechanical characteristics of concrete made with recycled aggregate. **Table 2-3** summarizes different techniques and the results obtained by various authors.

Table 2-3. Different techniques to improve the durability and mechanical characteristics of recycled aggregate concrete.

Method	Results	References
Pre-soaking in acid	• Acid solution dissolves the hydration products of the adhered mortar in RA • ITZ becomes less porous and cracked; water absorption decreases while specific density increases • However, it increases the chloride and sulfate ratio in recycled aggregate concrete • HCl concentration up to 0.5mol improve RA microstructure; higher HCl concentration induces a corrosive effect on RA • The use of acid acetic is safer, cleaner, and has a lower cost than HCl or H_2SO_4. • It is possible to combine impregnation with different pozzolanic micro-powders	[125], [173]–[176]
Two-Stage Mixing Approach (TSMA)	• Mixing required water is divided into two equal parts and added to the mixture at two different moments • Develops a stronger ITZ by filling the cracks and pores in RA • Improves the mechanical properties and durability performance of recycled aggregate concrete • It is possible to combine impregnation with different pozzolanic micro-powders	[158], [170]–[172]
Addition of pozzolanic micro-powders	• Consumption of calcium hydroxide results in a denser calcium silicate hydrate (C-S-H) structure, reducing porosity • Improves mechanical performance and increases compactness of recycled aggregate concrete • Contributions to the performance of recycled aggregate concrete are higher than that to natural aggregate concrete • Efficiency depends on particle size and amount of calcium hydroxide in the adhered mortar • Incorporation of silica fume reduces porosity and, consequently, increases resistance to chloride ions attack; however, treated recycled aggregate concrete presents less resistance towards carbonation • Incorporation of fly ash decreases water absorption and improves the flowability of concrete. In advanced ages, it significantly reduces concrete permeability and increases compressive strength because of its delayed binder property when compared to Portland cement • Incorporation of ground bagasse ash (GBA) and granulated blast furnace slag (GGBS) reduces RAC water permeability and porosity; also increases resistance to chloride ion penetration and reduces the expansion by sulfate attack.	[126], [152], [159], [195]–[203]

Table 2-3. Different techniques to improve the durability and mechanical characteristics of recycled aggregate concrete. (cont.)

Use of polymer emulsion	• When RA is immersed in a polymer emulsion, it fills the adhered mortar pores, sealing the RA surface. 10% PVA solution is proposed as an optimal concentration for impregnation • Treatment significantly decreases RA water absorption while increasing crushing value and density • Treated RAC presents a lower drying shrinkage and a higher resistance to chloride ion penetration and carbonation • However, compatibility between the polymer and the concrete paste is a concern: reactive silanol groups can make RA surface hydrophobic, deaccelerating cement hydration and leading to a mechanical strength loss	[166], [177]–[182]
Microbial carbonate bio-deposition	• Bacteria Physiological activity causes $CaCO_3$ crystal precipitation, creating a continuous water-proof layer on the RA surface • Permeability of recycled aggregate concrete reduces, improving mechanical behavior and durability properties • Efficiency depends on pH, temperature, amount of calcium, and bacteria concentration • Microbial carbonate precipitation peaks at pH 9.5 and decreases sharply for higher pH values • Enzyme activity and rate of urea hydrolysis are enhanced at higher temperatures. Thus, this method has great potential in a tropical climate with a hot and humid environment throughout the year • Higher bacteria concentration and amount of calcium (> 15 g/L of CaCl) increase $CaCO_3$ precipitation • Bacteria solution can be applied by spraying or immersion: spraying is more readily applicable and efficient.	[184]–[187]
Carbonation	• CO_2 reacts with $Ca(OH)_2$ and hydrated calcium silicate (C-S-H), generating $CaCO_3$ and silica gel, which fill RA pores • Decreases porosity and water absorption while increasing density • It is an environmentally friendly method as it can capture CO_2 emitted from industrial processes • Optimum results are obtained with 24h immersion in a 100% CO_2 environment • Concrete made with treated RA presents a lower drying shrinkage and improved mechanical properties • Carbonation improves the original and new ITZ • However, the time needed for carbonation is much longer than for other treatments. • It should not be applied to reinforced concrete as the reinforcement steel bars, when subjected to carbonation, lose their passivity and become vulnerable to corrosion.	[188]–[192]

2.6. Mix Design Methods

As seen in Section 2.5, the proposed methodologies to improve recycled aggregates' physical properties include strategies to remove the adhered mortar or seal the pores of recycled aggregates, consequently reducing their water absorption capacity. Unfortunately, they are usually expensive, create pollutants, and increase energy consumption, enhancing the cost of producing recycled aggregate concrete and creating barriers to application on construction sites.

Thus, while trying to better understand the impact of using recycled aggregate as a substitute for natural coarse aggregate, some authors concluded that two key parameters need to be overseen: the initial moisture conditions of the aggregates and the mixing procedure [98], [204]–[206].

However, although ACI-555R [207], for example, provides some guidelines for proportioning concrete mixes made with recycled concrete aggregate, neither it nor any other source gives a specific mix design method for achieving targeted fresh and hardened properties for recycled aggregate concrete. However, because of the higher porosity and water absorption of recycled aggregates, the mix design procedures available in the literature for conventional concrete cannot be directly applied in the case of recycled aggregate concrete [208].

Thus, in 1990, Bairagi et al. [209] developed an empirical relation to modifying the aggregate-to-cement ratio obtained by the ACI method, making it possible to design recycled aggregate concrete for a required strength between 15 and 30 MPa. After that, Topcu and Sengel [210] obtained recycled aggregate concretes with compressive strength equal to the associated conventional concretes by direct weight, replacing the natural aggregates with recycled aggregates and adjusting the w/c ratio. Still, their study has not reported equal or higher modulus of elasticity for recycled aggregate concrete. The compressive strength in concrete mostly depends on the mortars' strength and interfacial transition zone, while the modulus of elasticity is a function of the volume fractions and the modulus of elasticity of the aggregate and the mortar. Generally, recycled aggregate concrete's lower modulus of elasticity is attributed to residual mortar in recycled aggregate.

For this reason, Fathifazl et al. [211] believed that knowledge of the actual residual mortar content in recycled aggregates is essential for proper mix design. Therefore, based on the assumption that recycled aggregate is composed of mortar

and natural aggregate, they proposed a mix design method where the amount of each phase is considered, and the coarse aggregate and cementitious paste content are adjusted to achieve the same mortar volume of a mixture entirely made with natural coarse aggregates. This method was called “Equivalent Mortar Volume (EMV)”. Applying the proposed EMV method, the recycled aggregate concrete's cement and fine aggregate content can be significantly reduced without jeopardizing its fresh and hardened properties compared to conventional concrete.

Later, a different concept was developed by Gupta et al. [212] for mixing recycled aggregate concrete, namely “Equivalent Coarse Aggregate Mass (ECAM)”. The central concept in the ECAM method is that an equivalent mass of the original virgin coarse aggregate from recycled aggregate replaces the mass of coarse aggregate in conventional concrete. In other words, the total quantity of coarse aggregate in the recycled concrete mix equals the sum of the mass of natural coarse aggregate and the mass of original virgin aggregate. Thus, the authors could design recycled concrete up to a nominal replacement ratio of 50% with fresh or hardened state characteristics like conventional concrete.

Usually, replacing natural aggregate with recycled aggregate is done without considering particle sizes. However, within a sample of coarse aggregates, natural or recycled, there are distinct fractions of different sizes. So, in 2017, Bui et al. [131] improved the mechanical properties of recycled aggregate concrete by replacing only small-size particles of natural aggregate with recycled aggregate. With the new combination method, they made concrete with 50% recycled aggregate with significant improvement in the modulus of elasticity and no major reductions in compressive strength.

Some authors have also proposed methods to predict the compressive strength of recycled aggregate concrete. While Deshpande et al. [213] used the Artificial Neural Network technique, Pepe [214] proposed a conceptual model where recycled aggregate's high porosity influences the free water available for the mixture and, consequently, the time evolution of the compressive strength.

Cement-based materials, including recycled aggregate concrete, are composed of a granular system, whereas the size (coarse or fine), shape (rounded or angular), and type of parent rock of the aggregate significantly affect their performance. The fresh and hardened properties of concrete are significantly affected by the packing density of the solid ingredients. Therefore, the proper

estimation of the proportion of aggregates is essential. The "Particle Packing Method (PPM)" method involves determining the proportion of coarse aggregate and fine aggregate mixture to obtain maximum packing density.

In this optimization process, smaller particles fill up the voids between large particles. With a smaller volume of voids at the fresh state, the volume of voids remaining to be filled by cement hydration products at the hardened state would also be smaller, leading to a more compact micro-structure of the recycled aggregate concrete. This compact micro-structure makes the concrete stronger (higher strength), stiffer (larger modulus), and tougher (higher toughness). Moreover, the increase in packing density leads to a reduction in the binder and water content. Therefore, the two important steps in the PPM mix design are determining aggregate fractions packing density and the paste content. There are different discrete Particle Packing Models to calculate the concrete packing density, such as the Furnas Model, Aim Model, Modified Toufar Model, Strovall Model, Dewar model, Linear Packing Model (LPM), Solid Suspension Model (SSM), Compressible Packing Model (CPM), and 3-Parameter Model. [215], [216]. Pradhan et al. [217] used a Particle Packing Method and observed that recycled concrete aggregate could be effectively used at 100% replacement level without deteriorating compressive strength, tensile strength, and modulus of elasticity of recycled aggregate concrete.

2.7. Structural Applications

Although studies on recycled aggregates have been done for many years, their current applications are almost exclusively in low utilities, such as landscaping and pavements [218]. This situation can be explained by the inconsistent supply of recycled materials, limited standards or specifications, lack of in-service evidence, insufficient financial incentives and government support, and the general perception that recycled aggregate concrete is inferior to conventional concrete [219], [220].

As seen before, international standards restrict the use of recycled aggregates in structural concretes. The acceptable content of recycled aggregates in concrete depends on the desired concrete strength class and the characteristics of

the recycled aggregate, such as composition, dry density, water absorption, and the content of contaminants.

In Brazil, for example, until 2020, recycled aggregates were limited to non-structural applications. However, a revision of the Brazilian standard ABNT NBR 15116:2021 [46], published in 2021, allowed up to 20% of recycled aggregate in structural concrete of any strength class. Nevertheless, the recycled aggregates must have specific characteristics such as water absorption up to 7%, a content of SO_4 and Cl smaller than 0.1%, contaminants smaller than 1%, and, most importantly, be composed of only cement-based fragments.

Table 2-4 summarizes standards governing recycled aggregates' use in different countries. The increase in the recycled aggregate's allowed content is usually accompanied by a reduction in the allowed water absorption capacity and percentage of contaminants, as in the German standards [221], [43]. For recycled concrete aggregate from concrete waste, the use of up to 90% of recycled aggregate is allowed if water absorption is at most equal to 10% and the content of contaminants up to 0.2%; meanwhile, for recycled concrete aggregate from demolition waste, the content of recycled aggregate is limited to 70%, while the limits for water absorption capacity and percentage of contaminants increase to 15% and 0.5%, respectively. A similar situation occurred in Portugal [42] and Australia [45]. On the other hand, in Italy [44] the limitation occurs only for concrete strength class and type of recycled aggregate: RCA (recycled concrete aggregate) can replace up to 30% of natural coarse aggregate for concrete with strength class up to C30/37.

Table 2-4. Comparison of international standards for recycled aggregate.

Country	Standard	Type of recycled coarse aggregate	Concrete Specifications	% of RA allowed	Recycled aggregate characteristics							
					Concrete fraction (%)	Ceramic fraction (%)	Dry Density (km/m^3)	Water absorp. (%)	SO_4 (%)	CI (%)	Contaminants non-minerals (%)	Sieve 75µm passing (%)
Brazil	NBR 15116 [46]	ARCO	Structural concrete	20%	100	-	n.a.	≤ 7	≤ 0.1	≤ 0.1	≤ 1	≤ 12
		ARCI	Non-structural concrete	100%	> 90	< 10		≤ 12		≤ 0.2		
		ARM	Non-structural concrete		> 60	< 40						
Portugal	LNEC E471 [42]	RCA 1	C 35/45	25%	> 90	≤ 10	≥ 2200	≤ 7	≤ 0.8	n.a.	< 0.2	n.a.
		RCA 2	C 40/50	20%	> 70	≤ 30					< 0.5	
		RMA	n.a.	n.a.	≤ 10	> 90	≥ 2000				< 1	
Germany	DIN 4226-100 [221] DIN 12620 [43]	RCA (concrete waste)	Structural concrete	90%	> 90	< 10	≥ 2000	≤ 10	n.a.	≤ 0.04	≤ 0.2	n.a.
		RCA (demolition waste)		70%	> 70	< 30		≤ 15			≤ 0.5	
		RBA (brick rubble)	Non-structural concrete	20%	< 20	> 80	≥ 1800	≤ 20				
		RMA (mixed material)		n.a.	-	> 80 *	≥ 1500	n.a.		≤ 0.15	≤ 1	
Italy	NTC - 2008 [44]	RCA	C 30/37	30%	n.a.	n.a.	n.a.	n.a.	n.a.	n.a.	n.a.	n.a.
Netherlands	NEN 5905 [222]	RCA	C 45/55	20%	n.a.	n.a.	≥ 2100	n.a.	≤ 1	≤ 1	≤ 1	n.a.
		RMA	Non-structural concrete	n.a.			≥ 2000					
United Kingdom	BS 8500-2 [40]	RCA	C 20/25 & C 40/50	20%	> 95	< 5	n.a.	n.a.	≤ 1	n.a.	≤ 0.5	≤ 5
		RA	C 16/20	100%	-	< 100			n.a.		≤ 1	≤ 3
RILEM [223]		RCA 1	C 50/50	100%	n.a.	n.a.	≥ 2000	≤ 10	≤ 1	n.a.	n.a.	n.a.
		RCA 2	C 16/20				≥ 1500	≤ 20				
		RMA	No limit	20%			≥ 2400	≤ 3				
Japan	JIS A 5021 [224]	RCA	C 45/55	n.a.	n.a.	< 2	≥ 2500	≤ 3	n.a.	≤ 0.04	≤ 1	≤ 1
China	DG/TJ 07/008 [29], [225]	RCA	n.a.	n.a.	≥ 95	< 5	n.a.	< 10	< 1	< 0.25	< 1	< 2
		RMA			≤ 90	> 10		n.a.	n.a.	n.a.	n.a.	n.a.
Australia	HB 155:2002 [45]	RCA (Class 1A)	C 40	30%	< 100	-	≥ 2100	≤ 6	n.a.	n.a.	< 1	n.a.
		RCA (Class 1B)	C 25	100%	< 70	> 30	≥ 1800	≤ 8			< 2	n.a.

* 20% bituminous materials and others

Many authors have investigated the structural performance of reinforced concrete beams with different contents of recycled concrete aggregate instead of natural aggregates to assess the applicability of recycled aggregates on a structural scale.

The literature review [54]–[59], [61], [63] demonstrates, for example, that when structural beams made with recycled concrete aggregate are designed to present a ductile failure (reinforcement yields before concrete failure), bending moments and deflections at serviceability are not significantly affected even with higher content of recycled concrete aggregate, as concrete properties have low influence on the flexural behavior of beams. In the same way, the yielding moment and ultimate moment of beams made with concrete with recycled concrete aggregate are similar to conventional beams. However, the authors also observed that beams made with concrete with recycled concrete aggregate usually present a more significant and earlier cracking than conventional beams, attributed to the lower angularity of recycled aggregates, the pre-existing cracks at the old ITZ, and the lower tensile strength of recycled aggregate concretes.

As the content of recycled concrete aggregate increases, beams present a substantially lower ductility ratio [54], [55] because of the lower interfacial bond and interlocking between the recycled aggregate and mortar [226], [227], which can affect the mechanical bond strength between concrete and steel.

Bai and Sun [187] observed a similarity between recycled aggregate concrete beams and conventional concrete beams regarding crack patterns. When subject to four-point bending tests, both recycled and conventional concrete beams show similar crack behavior: crack progression began with flexural cracks in the maximum moment region, then additional flexural cracks emerged between the load and support regions. Some inclined flexure-shear cracks appear as load increases, although most flexural cracks are developed vertically. Similar behavior was observed by other authors [54]–[56], [58], [59]. **Figure 2-9** shows a conventional concrete beam (CC) and a 100% recycled aggregate concrete beam (RCA) after a four-point flexural test.

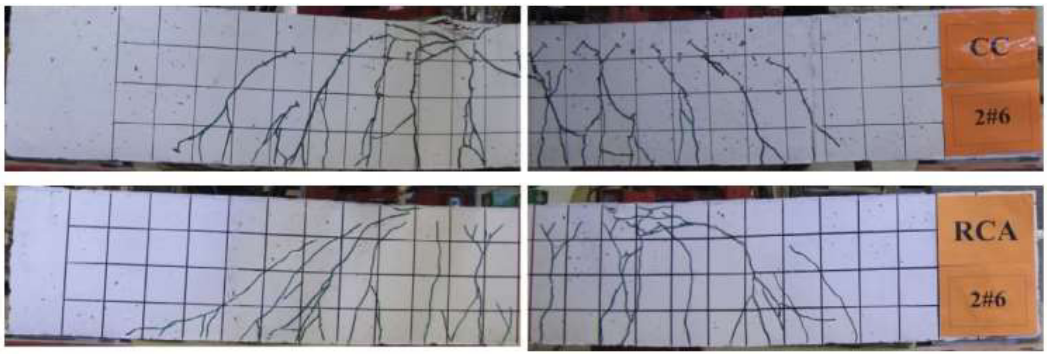

Figure 2-9. Crack pattern of a conventional concrete beam (CC) and a 100% recycled aggregate concrete beam (RCA) at flexural failure, adapted from Arezoumandi et al. [59].

Ignjatovic et al. [63] and Kang et al. [54] verified that the cracking pattern of recycled aggregate concrete beams is similar to the reference beams, even for a recycled aggregate replacement rate of over 50%. Meanwhile, Seara-Paz et al. [58], Arezoumandi et al. [184], Pradhan et al. [55], and Fathifazl et at. [53] observed a decrease in cracking spacing and an increase in crack width in beams with a higher content of recycled aggregate. The difference in the cracking spacing and width may be related to the reinforcement rate adopted by each author in their studies. In this way, it can be considered that the existing flexural analysis method can quite well predict the recycled aggregate concrete beams' flexural behavior, but some attention must be paid to cracking spacing and width.

Table 2-5 summarizes beams' properties, ultimate flexural strength, and ultimate deflection of beams submitted to four-point bending tests by different authors.

Table 2-5. Summary on the flexural behavior of recycled aggregate concrete beams.

Authors	RA Content (%)	w/c	Reinforcement ratio (%)	fc28 (MPa)	Size (mm) L x B x H	P_{ult} (kN) / M_{ult} (kN.m)	δ_{ult} (mm)
Kang et al. [54]	0	0.45	0.5	38.6	3030 x 135 x 270	35.3 / 15.9	70
	15			32.7		32.8 / 14.8	31
	30			31.7		32.7 / 14.7	32
	50			29.0		30.3 / 13.6	17
	0	0.45	1.0	38.6	3030 x 135 x 270	62.7 / 28.2	37
	15			32.7		60.5 / 27.2	27
	30			31.7		58.4 / 26.3	18
	50			29.0		54.2 / 24.4	16
	0	0.45	1.5	38.6	3030 x 135 x 270	81.9 / 36.9	36
	15			32.7		79.5 / 35.8	25
	30			31.7		78.5 / 35.3	19
	50			29.0		72.9 / 32.8	15
	0	0.45	1.8	38.6	3030 x 135 x 270	117.4 / 52,8	26
	15			32.7		114.7 / 51.6	20
	30			31.7		111.6 / 50.2	24
	50			29.0		112.2 / 50.5	20
Pradhan et al. [55]	0	0.45	0.42	42.75	2400 x 200 x 300	67.04 / -	20.56
	100			42.82		65.05 / -	16.45
	0	0.45	0.75	42.75	2400 x 200 x 300	115.33 / -	25.56
	100			42.82		114.77 / -	25.74
	0	0.45	1.31	42.75	2400 x 200 x 300	173.00 / -	25.91
	100			42.82		165.04 / -	14.56
	0	0.45	1.61	42.75	2400 x 200 x 300	171.10 / -	18.85
	100			42.82		161.97 / -	12.48
Zhao and Sun [56]	0	0.5	1.4	43.5	2000 x 120 x 200	191.6 / -	-
	30			41.2		186.6 / -	-
	75			29.4		183.6 / -	-
Bai and Sun [57]	0	0.56	0.68	41,9	2100 x 150 x 300	- / 34.3	-
	50	0.49	0.68	42.3		- / 34.0	-
	70	0.46	0.68	43.7		- / 35.5	-
	100	0.42	0.68	43.5		- / 34.0	-
	100	0.56	0.89	43.5		- / 40.4	-
	100	0.56	1.13	43.5		- / 48.4	-
Seara-Paz et al. [58]	0	0.5	0.76	60.7	3600 x 200 x 300	- / 55.71	95.16
	20			53.5		- / 58.89	96.14
	50			51.8		- / 56.32	98.29
	100			42.9		- / 52.93	96.40
	0	0.65	0.81	46.9	3600 x 200 x 300	- / 58.51	93.31
	20			46.7		- / 58.27	96.65
	50			42.2		- / 60.21	81.36
	100			32.4		- / 60.83	96.41
Arezoumandi et al. [59]	0	0.37	0.47	37.2	3300 x 300 x 460	- / 154.1	34.0
	100	0.40		30.5		- / 149.6	34.3
	0	0.37	0.64	37.2	3300 x 300 x 460	- / 170.7	29.5
	100	0.40		30.5		- / 172.6	35.6
Ignjatovic et al. [63]	0	0.52	0.28	43.7	3500 x 200 x 300	28.4 / -	75.4
	50	0.52		44.2		27.0 / -	97.9
	100	0.51		42.5		26.8 / -	92.6
	0	0.52	1.46	43.7	3500 x 200 x 300	108.6 / -	45.8
	50	0.52		44.2		110.6 / -	46.2
	100	0.51		42.5		105.4 / -	38.9
	0	0.52	2.54	43.7	3500 x 200 x 300	137.6 / -	28.5
	50	0.52		44.2		160.4 / -	34.5
	100	0.51		42.5		142.6 / -	30.4

Regarding the shear behavior of recycled aggerate concrete beams, the authors observed that the crack pattern is similar to conventional concrete, although shear strength is lower because of the lower tensile strength of the recycled concrete and the lower strength of the recycled aggregates itself, thus reducing the contribution of the interlock mechanism of the aggregates [65], [228]–[233]. Moreover, an analysis at the macroscopic scale showed that shear failures in recycled concrete beams occurred through the recycled aggregates and not at the interface between mortar and aggregates, as usually happens for conventional concrete [234].

Tošic et al. [235] compiled 217 experimental results, creating a database on flexural and shear strength of reinforced recycled aggregate concrete beams and evaluating the applicability to Eurocode 2 provisions. As a result, they observed that Eurocode 2 predictions of flexural strength are precise, but predictions of shear strength for beams with stirrups are not. However, most studies considered the minimum transverse reinforcement ratios in recycled aggregate concrete beams. Thus, Tošic et al. [235] proposed more experiments on recycled aggregate concrete beams with higher transverse reinforcement ratios. Similar results were obtained by Pacheco et al. [236].

Despite some uncertainties, it is also possible to find references to recycled aggregate concrete elements in real applications. In 2004, the "Shanghai Ecological Building" was constructed using 388m^3 of concrete made with 100% recycled concrete aggregate. This building was the first to incorporate a large amount of this material, and the results for mechanical and durability properties of randomly selected samples indicated that recycled aggregate concrete generally meets the existing requirements for conventional concrete [29].

Based on the lack of good quality local natural aggregate and the increasing demand for infrastructure projects for World Cup 2020, the Qatar government has developed a laboratory program and a full-scale building trial to assess the suitability of recycled aggregate concrete in structural applications [237]. The excellent results enabled changes in the 2014 edition of Qatar Construction Specification (QCS) to allow a maximum recycled aggregate replacement ratio of 20% in structural concretes up to C30 strength. Finally, in 2014, Zhang and Zhao [31] used strain gages to monitor beams made of recycled aggregate concrete in a recently built building in China. The beams had not cracked, and the strain

development trend showed that they would probably be kept safe for the long term, indicating the feasibility of using recycled aggregate concrete in actual engineering projects.

2.8. Conclusions

Compared to natural aggregates, recycled aggregates are more porous and have a more complex microstructure. This higher porosity acts as a presumable canal for water transport and aggressive agents such as chloride ions, affecting the material's durability. Because of the higher water absorption, recycled coarse aggregates typically need more water than conventional concrete to obtain the same workability; it also affects the homogeneity of the fresh concrete during casting, reducing the mechanical strength of the concrete. Despite that, the literature has no specific discussion regarding special curing procedures for recycled aggregate concretes.

The analysis of the results obtained by several authors showed that the concrete compressive strength decreases as the recycled aggregate ratio increases, regardless of the concrete grade. However, for higher concrete grades, such as C45-C50 and C55-C60, the ITZ is stronger, and the strength of the coarse aggregate itself becomes the limiting strength factor. Thus, the greater the amount of recycled aggregate, the greater the reduction in compressive strength.

The literature also shows that the modulus of elasticity reduces as the content of recycled aggregates in concrete increases, and this is attributed to the presence of two different interfacial transition zones (ITZ). As the second (old) ITZ tends to be weaker than the paste-aggregate matrix of conventional concretes, the concrete strength reduces, leading to higher deformability of recycled concretes when compared to conventional concretes. The analysis of different literature results also shows a large discrepancy between the results obtained experimentally and those obtained through the theoretical curves, which use only compressive strength as a parameter. For better estimation, more parameters should probably be considered, such as recycled aggregate density, water absorption, or cement composition.

Authors have tried different treatments on recycled aggregates to improve the recycled aggregate concrete's mechanical behavior and long-term properties,

allowing a higher replacement ratio. The most widespread methods in the literature are the addition of pozzolanic micro-powders and polymer emulsions and pre-soaking in acid, microbial carbonate bio-deposition, and carbonation. The results obtained with these methods are relevant, and in many cases, the properties of the recycled concrete were very close to those obtained for the conventional concrete.

There are still some barriers to using recycled aggregate in structural concrete. For example, there is no consensus regarding the mix design method that best suits the significant heterogeneity of recycled aggregates and their specificities. In addition, although there are positive results in the literature regarding the existing models for strength prediction, there are still some doubts about the recycled aggregate concrete flexural and shear behavior and the integrity of the structural elements throughout their useful life. Therefore, most standards and specifications worldwide limit the recycled aggregate replacement ratio to approximately 30% in structural elements. The content of ceramic fragments in the composition of recycled aggregate is also limited.

Although there are still uncertainties, recycled aggregate from Construction and Demolition Waste is one of the sustainable solutions for the growing waste disposal crisis and depletion of natural aggregate sources caused by the construction sector. However, recycled aggregates are mostly used in low-value applications such as pavement bases, and non-structural concretes.

Thus, to promote energy savings and environmental preservation, it is essential to advance studies about the feasibility of using higher percentages of recycled aggregate on structural concretes. Also, it would be convenient to develop technical specifications and guidelines for the production and quality control of structural recycled aggregate concrete, improving contractors' and users' general perception of this material.

3. Investigation of Physical and Mechanical Properties of Recycled and Natural Coarse Aggregates

3.1. Introduction

Using recycled coarse aggregate from construction and demolition waste (CDW) has become a trend in many countries to solve the high depletion of natural resources and huge waste generated by the construction industry. Crushed concrete and crushed masonry (ceramic materials) are the main components of CDW, and depending on the content of each of these fractions, the recycled aggregate receives a different classification. Generally, the standards define the allowed content of ceramic material in recycled aggregate and determine its possible applications.

As presented in Chapter 2, recycled aggregate mainly composed of concrete debris has been widely studied over the last decades. The use of this material in structural concrete, up to 30%, is now well-accepted in most countries. However, when it comes to recycled aggregate with some levels of ceramic material, its use is limited to sub-base material for paving and non-structural applications.

It is possible to separate the crushed concrete and the crushed masonry before or after crushing during the CDW recycling process. Post-crushing separation demands advanced sorting techniques and does not guarantee a complete separation. On the other hand, pre-crushing separation is expensive and time-consuming for the contractors because it requires more elaborate waste management plans, as concrete and masonry must be accurately separated on the construction site. Because of these, there are still obstacles to using recycled aggregates on a larger scale, mostly in Brazil, where the recycling culture is still poorly disseminated.

A better understanding of recycled aggregates with higher content of ceramic material – and, consequently, their impact on structural concrete – would instigate the use of this material and make the recycling process cheaper and more attractive for large-scale use. Therefore, this chapter presents an experimental investigation of the physical and mechanical properties of recycled coarse aggregates with different ceramic debris contents compared with a natural coarse aggregate.

3.2. Experimental Program

For this research, mixed recycled aggregates (MRA) were obtained from a Brazilian recycling plant. After receiving the material, a certain amount of this MRA sample was manually separated into two other samples of recycled coarse aggregate: (i) recycled concrete aggregate (RCA), composed only of cement-based fragments, and (ii) recycled masonry aggregate (RMA), composed only of ceramic debris, bricks, and roof tiles. Thus, in this study, four types of coarse aggregate were used: mixed recycled aggregate (MRA), recycled concrete aggregate (RCA), recycled masonry aggregate (RMA), and a natural granitic coarse aggregate (NAT), as reference. **Figure 3-1** illustrates the experimental program for investigating the material's physical and mechanical properties.

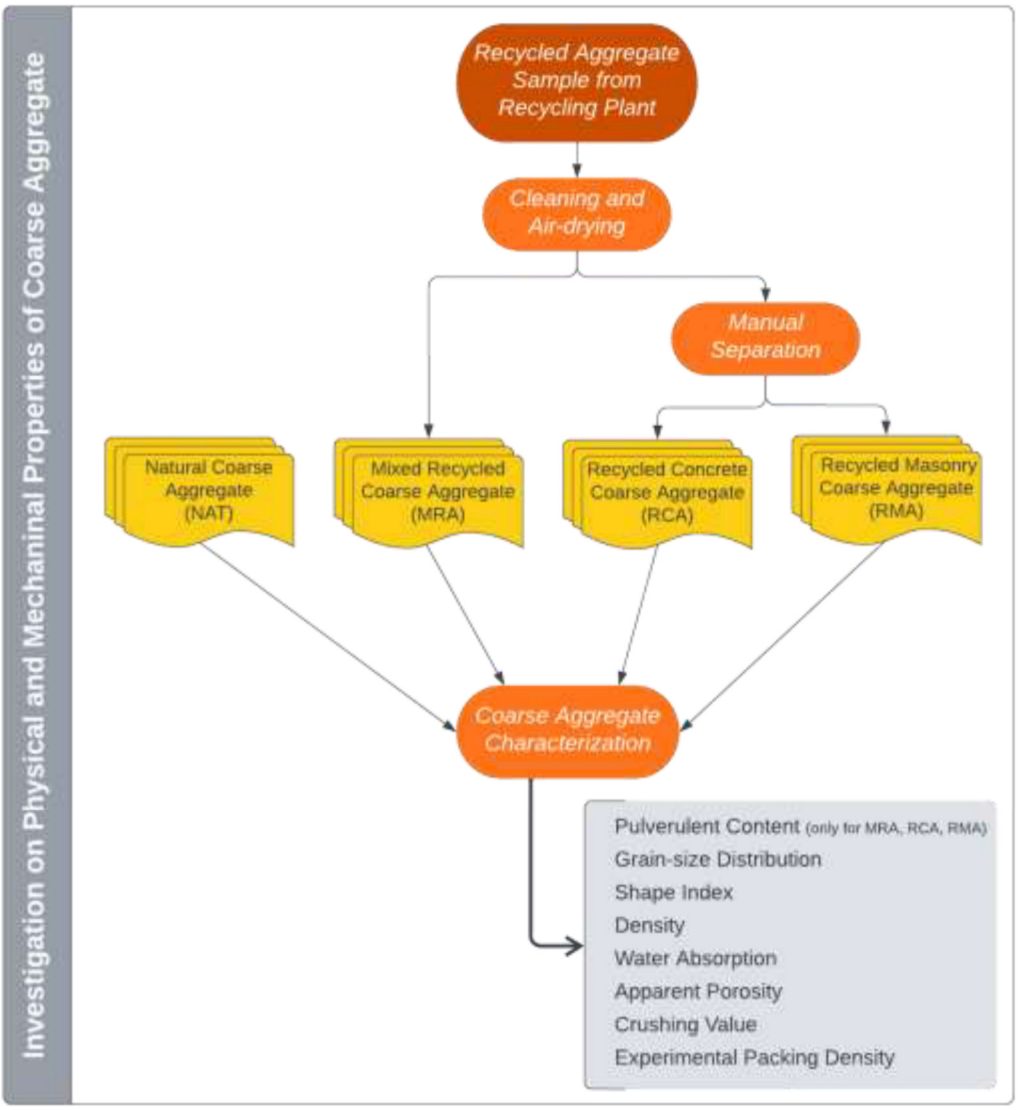

Figure 3-1. Experimental Program – Investigation of physical and mechanical properties of coarse aggregate.

3.2.1. Preparation of Recycled Aggregate Samples

The recycled aggregate was obtained from a recycling plant called Reciclax, located in Ribeirão Preto, São Paulo. The material was delivered in five metallic containers, each with 200 kg, and kept inside the Structures and Materials Laboratory at PUC-Rio, protected from moisture and organic contamination.

Since the recycled aggregate had a large amount of adhered fine material, a standard washing and drying procedure has been adopted regularly. Samples were washed with running water using a 2.36 mm mesh sieve (**Figure 3-2**). After washing, the samples were air-dried for five days (**Figure 3-3**).

Figure 3-2. Recycled aggregate cleaning process with running water.

Figure 3-3. Recycled aggregate air-drying process.

The recycled aggregate composition was determined through visual analysis, as defined in Annex A of the Brazilian standard ABNT NBR 15116:2021 [46]. Three samples of 10 kg of recycled aggregate were oven-dried for three days at 105ºC. Then, the samples were cooled to room temperature for 4 h, and the total mass (M_t) was measured. Subsequently, for each one of the three samples, fragments were manually separated according to the following criteria (**Figure 3-4**):

- Group 1: cementitious material composed of cement-based fragments;
- Group 2: ceramic materials, composed of ceramic debris, bricks, and roof tiles;
- Group 3: contaminants and impurities, such as wood, plastic, bitumen, foam, glass, plaster, and metal.

Each group was weighed, and masses of M_{g1}, M_{g2}, and M_{g3}, representing groups 1, 2, and 3, were obtained. Finally, the percentages of each group were obtained by dividing the values of M_{g1}, M_{g2}, and M_{g3} by M_t (**Table 3-1**).

Table 3-1. Composition of recycled aggregate.

Type of material	Sample 1	Sample 2	Sample 3	%
Cementitious material (kg)	8.442	8.759	8.717	**86.4**
Ceramic material (kg)	1.507	1.210	1.249	**13.2**
Contaminants and impurities (kg)	0.051	0.031	0.034	**0.4**

Figure 3-4. Sample of recycled aggregate separated into three groups: contaminants and impurities, ceramic material, and cementitious material.

Table 3-1 shows that recycled aggregate comprises 86.4% of cementitious materials. Thus it can be confirmed that the material received from the recycling plant is classified as Mixed Recycled Aggregates, according to the Brazilian standard ABNT NBR 15116:2021 [46]. Contaminants and impurities represented 0.4%, therefore being within the limit (< 1%) also established by the Brazilian standard ABNT NBR 15116:2021 [46] for recycled aggregates to be used in concrete. Similar results were obtained by Salles [221].

After that, 300 kg of recycled aggregate was manually separated into the same three groups described above to continue the experimental program. The contaminants and impurities (Group 3) were discarded, while the samples of cementitious material (Group 1) and ceramic material (Group 2) were stored separately in plastic containers and called, respectively, Recycled Concrete Aggregate (RCA) and Recycled Masonry Aggregate (RMA).

Thus, henceforward in this study, it is considered that the Recycled Concrete Aggregate (RCA) sample is composed entirely of cement-based fragments and natural rocks; the Recycled Masonry Aggregate (RMA) sample is composed only of masonry elements such as ceramic debris, bricks, and roof tiles; and Mixed Recycled Aggregate (MRA) is the recycled aggregate as received from Reciclax recycling plant.

3.2.2. Pulverulent Content of Recycled Aggregates

The excess of pulverulent content impairs the adhesion between the mortar and the aggregates and increases water consumption, causing shrinkage and a decrease in the concrete strength. Thus, the lower the pulverulent content, the higher the aggregate quality.

The pulverulent content of coarse aggregates was obtained according to the Brazilian standard ABNT NBR NM 46:2003 [238], which establishes the method for determining the material finer than a 75 µm mesh sieve in the aggregate sample. During this procedure, clay particles and other materials are dispersed. However, the author would like to inform that this standard was replaced by ABNT NBR 16973:2021 [239], whose main differences from the old standard are: a change in the minimum mass of the test sample from 100g to 300g for aggregates with a maximum grain size equal to 2.36 mm; a change in the drying temperature of the sample from 110ºC to 105ºC; and, a suppression of the washing procedure using a wetting agent.

For this test, four samples of approximately 5 kg of each type of recycled aggregate (MRA, RCA, RMA) were cleaned with running water (as described in Section 3.2.1). Then, samples were oven-dried for approximately 24 hours at 105ºC, and the masses (M_i) were recorded. Then the samples were placed in a container and covered with water (**Figure 3-5**).

Figure 3-5. Mixed recycled aggregate samples during pulverulent content test.

The samples were shaken until the pulverulent material was in suspension, and then they were drained through a 75 µm mesh sieve. This process was repeated until the wash water was clear. The material retained on the sieve was oven-dried, and after 24 hours, the final mass was determined (M_f). The mixed recycled aggregate pulverulent content (< 75 µm) is calculated by equation **Eq. 3-1** [239]:

$$m\ (\%) = \frac{M_i - M_f}{M_i} \times 100 \qquad \textbf{Eq. 3-1}$$

Where:

m is the amount of material finer than the 75 µm mesh sieve (%);

M_i is the initial mass (kg);

M_f is the final mass (kg).

3.2.3. Grain-size Distribution of Coarse Aggregates

The grain size distribution curves of coarse aggregates were obtained according to the Brazilian standard ABNT NBR NM 248:2003 [240]. However, the author would like to inform that this standard was replaced by NBR 17054:2022 [241], which deals with the grain-size distribution of aggregates with a maximum size of up to 75 mm and presents an update of the normative references.

The grain size distribution aims to classify the aggregates by their respective sizes and measure the fractions corresponding to each size. The grain size composition is the characteristic of an aggregate of greater application in practice, mainly because the grain size distribution curve allows planning a better packing of aggregate grains, thereby reducing voids and improving the interface between aggregate and cement paste.

Table 3-2 shows the standard set of sieves used for grain-size distribution of coarse aggregates (NAT, MRA, RCA, RMA). After arranging the sieves in the correct order (the biggest mesh opening on top), samples were placed at the top of the sieve set, and sieving was carried out for 10 minutes. Then, the weight of the samples retained in each sieve was calculated. Samples weighted approximately 10 kg.

Table 3-2. The standard set of sieves used in the grain-size distribution analysis.

Coarse Aggregate
25 mm
19 mm
12.5 mm
9.5 mm
6.3 mm
4.75 mm
2.36 mm
1.18 mm

The grain-size distribution makes it possible to determine the maximum grain size of the aggregates, which is the mesh opening of the smallest sieve through which at least 95% of the material passes.

The grain-size distribution curves also provide the Uniformity Coefficient (C_u), which expresses the variety in particle sizes, and the Coefficient of Curvature (C_c), which measures the gradation of particles.

The Uniformity Coefficient (C_u) is the ratio of D60 to D10 (**Eq. 3-2**). When $C_u > 4$, the aggregate is classified as well-graded, whereas when $C_u < 4$, the aggregate is classified as poorly graded. When C_u is approximately equal to one, particles are all the same size. For well-graded aggregate, the Coefficient of Curvature (C_c), calculated by **Eq. 3-3**, must be more than one and less than three.

$$C_u = \frac{D_{60}}{D_{10}} \qquad \textbf{Eq. 3-2}$$

$$C_c = \frac{(D_{30})^2}{D_{10} \times D_{60}} \qquad \textbf{Eq. 3-3}$$

Where:

C_u is the uniformity coefficient;

C_c is the coefficient of curvature;

D60 is the size of the particle corresponding to 60% finer;

D30 is the size of the particle corresponding to 30% finer;

D10 is the size of the particle corresponding to 10% finer.

3.2.4. Shape Index of Coarse Aggregates

The shape index of each coarse aggregate sample was analyzed according to the Brazilian standard NBR 7809:2019 [242] and it is calculated as a relationship

between the aggregate average length and the average thickness. This index allows evaluating the quality of a coarse aggregate, considering that aggregates with rounded grains (optimal shape for crushed aggregates) will have a shape index close to 1. On the other hand, lamellar grains will present much higher values of shape index, with a limit of shape index equal to 3 being acceptable.

This test used samples of 200 grains of each type of coarse aggregate (NAT, MRA, RCA, RMA). The dimensions "C" (length) and "e" (thickness) of each grain were obtained using a digital caliper (**Figure 3-6**). The grain length "C" is the largest possible dimension to be measured and defines the length direction; meanwhile, the grain thickness "e" is the greatest possible distance between two planes parallel to the grain length direction. The shape index (I) is calculated by **Eq. 3-4** [242]:

$$I = \frac{C}{e} \qquad \textbf{Eq. 3-4}$$

Where:

I is the shape index;

C is the average length of 200 grains (mm);

e is the average thickness of 200 grains (mm).

Figure 3-6. Digital caliper used to measure the length and thickness of coarse aggregate grains.

3.2.5. Particle Densities, Water Absorption, and Apparent Porosity of Coarse Aggregates

The apparent particle density, the saturated surface-dry density, the oven-dry density, the water absorption, and the apparent porosity of coarse aggregates (NAT, MRA, RCA, RMA) were measured according to the Brazilian standard ABNT NBR 16917:2021 [243]. At first, the samples were immersed in water at room temperature for 24 h (**Figure 3-7**). Then samples were rolled in a large absorbent tissue until all visible water film was removed, and the saturated surface-dry mass was obtained (m_B) (**Figure 3-8**).

Figure 3-7. Samples immersed in water.

Figure 3-8. Aggregates being rolled in a large absorbent tissue.

After that, coarse aggregate samples were placed in a wire basket and immersed in the water at a temperature of 20 ± 5ºC with a cover of at least 50 mm above the top of the basket. After removing the entrapped air, the mass of saturated aggregate submerged in water was determined using a hydrostatic scale (m_C). It is important to notice that the scale was previously zeroed with the wire basket empty and immersed in water (**Figure 3-9**).

Figure 3-9. Saturated aggregate submerged in water and hydrostatic scale.

Finally, coarse aggregate samples were oven-dried at 105ºC for 24 h. After being cooled to room temperature for 3 h, the oven-dried mass was obtained (m_A). This procedure was repeated six times for 2 kg samples of each type of coarse aggregate (NAT, MRA, RCA, RMA).

The oven-dry density, the saturated surface-dry density, the apparent particle density, the water absorption, and the apparent porosity are calculated by **Eq. 3-5**, **Eq. 3-6**, **Eq. 3-7**, **Eq. 3-8**, and **Eq. 3-9**, respectively:

$$\rho_d = \frac{m_A}{m_B - m_C} \times 1000 \qquad \textbf{Eq. 3-5}$$

$$\rho_{ssd} = \frac{m_B}{m_B - m_C} \times 1000 \quad \textbf{Eq. 3-6}$$

$$\rho = \frac{m_A}{m_A - m_C} \times 1000 \quad \textbf{Eq. 3-7}$$

$$A = \frac{m_B - m_A}{m_A} \times 100 \quad \textbf{Eq. 3-8}$$

$$P = \frac{m_B - m_A}{m_A - m_C} \times 100 \quad \textbf{Eq. 3-9}$$

Where:

ρ is the apparent particle density (kg/m^3);

ρ_{ssd} is the saturated surface-dry density (kg/m^3);

ρ_d is the oven-dry density (kg/m^3);

A is the water absorption (%);

P is the apparent porosity (%);

m_A is the oven-dried mass (g);

m_B is the saturated surface-dry mass (g);

m_C is the mass of saturated aggregate submerged in water (g).

3.2.6. Bulk Density and Void Ratio of Coarse Aggregates

The bulk density of an aggregate is the ratio between its mass and volume without compacting, i.e., also considering the voids between the grains. It is used to convert mass into volume and vice versa. The bulk density and the void ratio of coarse aggregates (NAT, MRA, RCA, RMA) were measured according to the Brazilian standard ABNT NBR NM 16972:2021 [244].

Initially, the mass of the empty container was measured (m_c), and then the container was filled with water. The mass of the set (container + water), m_{cw}, was then obtained. The temperature of the water in the container was measured with a thermometer, and the specific mass of the water was obtained from Table 2 of the Brazilian standard ABNT NBR NM 16972:2021 [244]. The volume of the container (V) was obtained by dividing the mass of water needed to fill the container ($m_w = m_{cw} - m_c$) by its specific mass (ρ_w).

One-third of the container was filled, and then the layer of aggregate was compacted by 25 strokes of the compacting rod, evenly distributed over the entire

surface of the material. This procedure was repeated with another two layers of aggregate until the container was fulfilled.

For these tests, the aggregate sample should comprise approximately 150% of the material required to fill the container. Finally, the mass of the container filled with aggregate (m_T) was obtained. This procedure was repeated six times for each type of aggregate.

The bulk density (ρ_{ap}) and the void ratio (E_v) of coarse aggregates are calculated by **Eq. 3-10** and **Eq. 3-11,** respectively:

$$\rho_{ap} = \frac{m_T - m_c}{V} \quad \textbf{Eq. 3-10}$$

$$E_V = \frac{100 \times [(\rho \times \rho_w) - \rho_{ap}]}{\rho \times \rho_w} \quad \textbf{Eq. 3-11}$$

Where:

ρ_{ap} is the bulk density (kg/m^3);

m_T is the mass of the container fulfilled with aggregate (kg);

m_c is the mass of the empty container (kg);

V is the volume of the container (m^3);

E_v is the void ratio (%);

ρ is the apparent particle density, obtained in 3.2.5 (kg/m^3);

ρ_w is the specific mass of water (kg/m^3).

3.2.7. Water Absorption Curve of Coarse Aggregates

Samples of approximately 1 kg were oven-dried at 105ºC for 24 h (m_d) to determine the water absorption curve of coarse aggregates (NAT, MRA, RCA, RMA). Then, samples were placed in a wire basket and immersed in the water at a temperature of 20 ± 5ºC (m_0). The mass at each instant (m_N) was measured using a hydrostatic scale as described below:

- up to the first 15 minutes, one reading every minute;
- from 15-30 minutes, one reading every 5 minutes;
- from 30-60 minutes, one reading every 10 minutes;
- from 1-2 h, one reading every 15 minutes;
- from 2-8 h, one reading every 1 h;
- one last reading after 24 h.

The water absorption at each instant (A_N) is calculated by **Eq. 3-12**:

$$A_N = \left(\frac{m_N - m_0}{m_d - m_0}\right) \times 100 \qquad \textbf{Eq. 3-12}$$

Where:

A_N is the water absorption at each instant (%);

m_d is the mass of the oven-dried sample (g);

m_0 is the initial mass submerged in water, using a hydrostatic scale (g);

m_N is the mass at each moment, using a hydrostatic scale (g).

3.2.8. Crushing Value (ACV) of Coarse Aggregates

The British standard BS 812 Part 110:1990 [245] describes a method for determining the aggregate crushing value (ACV), which estimates the aggregate's strength to crushing under a gradually applied compressive load.

First, coarse aggregate samples of NAT, MRA, RCA, and RMA were sifted on sieves 9.5 mm and 12.5 mm to remove the oversize and undersized fractions. The resulting 12.5 to 9.5 mm fraction was divided into three samples of each type of coarse aggregate. Samples were oven-dried at 105ºC for 4 h and then cooled to room temperature. The initial mass (m_1) was measured.

The samples were placed in a steel cylinder container in three layers of approximately the same height, each layer subjected to 25 strokes. The steel cylinder had a 153 mm internal diameter and 125 mm internal depth. The metal plunger was placed carefully over the surface of the aggregate. The apparatus was placed on a servo-hydraulic MTS actuator and loaded at a uniform rate so that the required force of 400 kN was reached in 10 min ± 30 s (**Figure 3-10**). After crushing, the mass of the material passing the 2.36 mm sieve mesh was measured (m_2).

The aggregate crushing value (ACV) was calculated as a relationship between the mass of the material passing the sieve 2.36 mm after crushing (m_2) and the total mass (m_1) (**Eq. 3-13**). Thus, as lower the crushing value, the higher the strength to crushing under a gradually applied compressive load.

$$ACV = \frac{m_2}{m_1} \times 100 \qquad \textbf{Eq. 3-13}$$

Where:

ACV is the aggregate crushing value (%);

m_1 is the initial mass of the sample (g);

m_2 is the mass of the material passing the 2.36 mm sieve mesh (g).

(a) (b)

Figure 3-10. (a) Aggregate sample inside the metal container and (b) load application.

3.2.9. Experimental Packing Density

The experimental packing density developed by De Larrard [240] determines each aggregate's compaction degree. In the case of identical cubic particles and considering the packing of the grains one by one, the packing density would be the maximum possible ($\phi = 1$).

The mechanical compression and vibration test are used to determine the experimental packing density of coarse aggregates. For this test, a steel cylinder with a 153 mm internal diameter and a 125 mm internal depth, a plunger, and a baseplate were used (i.e., the same apparatus as in Section 3.2.8). The steel cylinder container was filled with a known amount (m; **Eq. 3-14**) of oven-dried aggregates and closed with the metal plunger. The apparatus was placed on a servo-hydraulic MTS actuator, and a compression of 10 kPa was applied on the top.

Then, the steel container was submitted to a vibrating table for 2 minutes. The final height of the aggregate sample (h_c) is calculated by subtracting the internal

depth of the container and the distance between the surface of the aggregate and the top of the cylinder, measured with a ruler (**Figure 3-11**).

The experimental packing density (ϕ) was calculated by **Eq. 3-14** [246]:

$$\phi = \frac{m}{A_e \times h_c \times \rho} \qquad \textbf{Eq. 3-14}$$

Where:

ϕ is the experimental packing density;

m is the mass of the aggregate sample (kg);

A_e is the area of the steel cylinder container (m^2);

h_c is the final height of the aggregate sample inside the cylinder (m);

ρ is the apparent particle density obtained in **Eq. 3-7** (kg/m^3).

Figure 3-11. Measurement of the distance between the surface of the aggregate and the top of the steel cylinder container.

In addition to the analysis of the total experimental packing density of the coarse aggregates, to obtain a more accurate result, the experimental packing density was also evaluated for different particle size classes: (i) class 1 corresponded to grains larger than 12.5 mm, (ii) class 2 corresponded to grains between 6.3 and 12.5 mm, and (iii) class 3 corresponded to particles smaller than 6.3 mm.

The coarse aggregate samples were sieved and separated into the size classes. Then, the test procedure described above was repeated for each class, obtaining the experimental packing density of each one.

3.3. Results and Discussions

All recycled aggregates (MRA, RCA, and RMA) presented a continuous grain-size distribution curve, which was very similar to each other and the natural aggregate (NAT) curve (**Figure 3-12**). Besides, the maximum size of the four types of aggregates was 19 mm. It can also be observed that the grain-size distribution curves of the recycled aggregates were located between zones 4.75/12.5 and 9.5/25, as defined by ABNT NBR 7211:2009 [247]. Similar results were presented by Tenório [248].

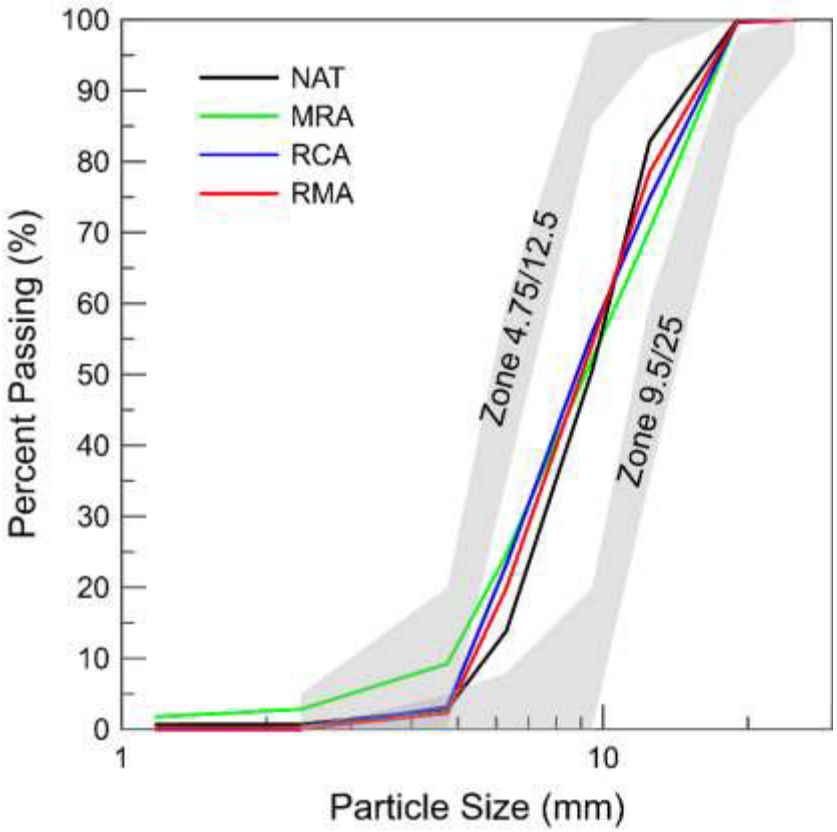

Figure 3-12. Grain-size distribution curves of recycled and natural coarse aggregates.

Moreover, the grain-size distribution curve of the MRA used in this study and produced in São Paulo (Brazil) was very similar to those curves obtained for recycled aggregates from several other places in Brazil [39], [123], [249], and from the United Kingdom [115] and India [250] (**Figure 3-13**).

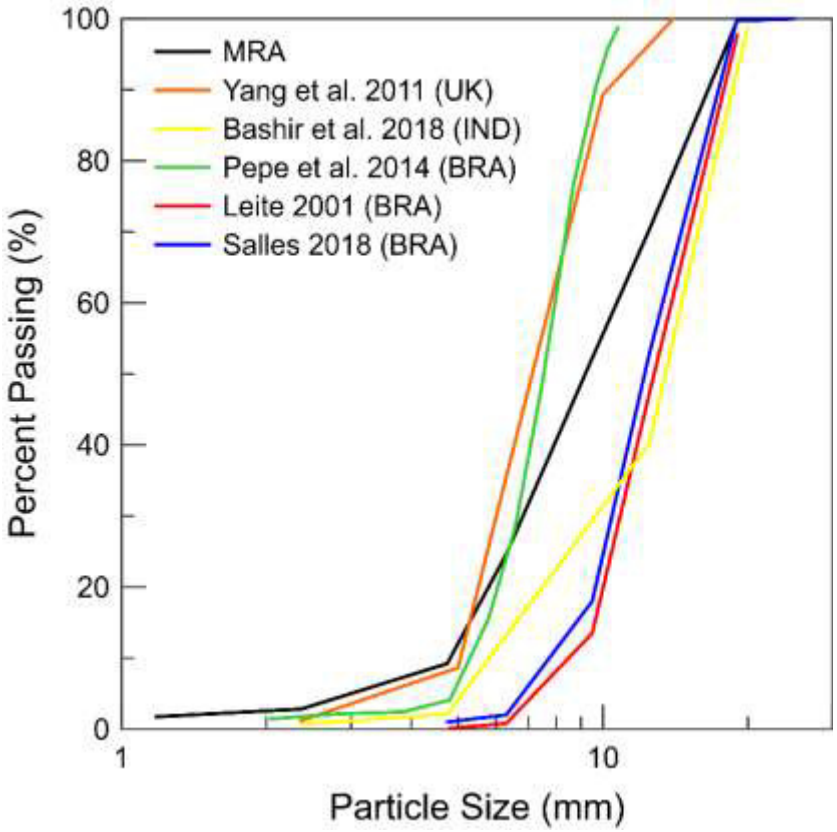

Figure 3-13. Grain-size distribution curves of recycled aggregates from different locations [39], [115], [123], [249], [250].

Table 3-3 shows the Uniformity Coefficient (C_u) and the Coefficient of Curvature (C_c) of coarse aggregates (NAT, MRA, RCA, RMA). It can be observed that coarse aggregates are classified as uniformly graded. It is also interesting to note that MRA has the highest value of C_u, which means that, among the coarse aggregates, it comprises the largest number of particles of different sizes.

Table 3-3. Uniformity Coefficient (Cu) and Coefficient of Curvature (Cc) of coarse aggregates (NAT, MRA, RCA, RMA).

	NAT	MRA	RCA	RMA
Uniformity Coefficient (Cu)	1.8	2.3	1.9	1.9
Coefficient of Curvature (Cc)	0.9	0.9	0.9	0.9

MRA presented 0.59 ± 0.31% of pulverulent material content (Table 3-4), while RCA and RMA presented 0.35 ± 0.17% and 0.74 ± 0.19%, respectively (**Table 3-5** and **Table 3-6**). All these values are under the limit established for the Brazilian standard ABNT NBR 15116:2021 [46], which limit the pulverulent content to 12% for aggregates protected from surface abrasion.

As expected, the Recycled Masonry Aggregate (RMA) presented the highest amount of pulverulent content since it is composed entirely of ceramic materials

such as bricks and roof tiles. Likewise, the Mixed Recycled Aggregate (MRA) showed an intermediate value of pulverulent content, with the highest standard deviation, as it is more heterogeneous than the others and is composed of ceramic and cementitious material.

Table 3-4. Pulverulent content of Mixed Recycled Aggregate (MRA).

Mixed Recycled Aggregate (MRA)	Sample 1	Sample 2	Sample 3	Sample 4
M_i (kg)	10.00	10.00	10.00	10.00
M_f (kg)	9.953	9.926	9.977	9.907
Pulverulent Content (< 75 µm) (%)	0.47	0.74	0.23	0.93

Table 3-5. Pulverulent content of Recycled Concrete Aggregate (RCA).

Recycled Concrete Aggregate (RCA)	Sample 1	Sample 2	Sample 3	Sample 4
M_i (kg)	5.015	5.006	5.026	5.082
M_f (kg)	4.998	4.995	5.013	5.052
Pulverulent Content (< 75 µm) (%)	0.34	0.21	0.25	0.59

Table 3-6. Pulverulent content of Recycled Masonry Aggregate (RMA).

Recycled Masonry Aggregate (RMA)	Sample 1	Sample 2	Sample 3	Sample 4
M_i (kg)	5.038	5.092	5.078	5.034
M_f (kg)	5.001	5.044	5.037	5.010
Pulverulent Content (< 75 µm) (%)	0.73	0.93	0.80	0.48

Regarding the shape index, the difference between the values obtained for RCA and RMA is consistent with the visual observation of each sample (**Figure 3-14**). While RCA is composed of more rounded grains, such as mortar pieces, RMA presents some flatter and elongated grains, such as tiles. It is also possible to visually observe that RCA has a much rougher surface than RMA.

Table 3-7. Shape index of recycled and natural aggregates.

	NAT	MRA	RCA	RMA
Average Length – C (mm)	19.43	20.90	19.67	20.54
Average Thickness – e (mm)	10.39	10.02	9.99	8.74
Shape Index - I	1.87	2.09	1.97	2.35

(a) (b)

Figure 3-14. (a) RCA and (b) RMA sample.

Table 3.7 shows that the shape index of MRA is intermediate between RCA and RMA, which is coherent once MRA is a mixture of the concrete and the masonry fractions (RCA and RMA, respectively). However, natural aggregate (NAT) is the most rounded one. Nevertheless, all values were within the limit established by the Brazilian standard NBR 7211:2009 [247].

RCA comprises a natural coarse aggregate with an adhered mortar characterized by micro-cracks generated during recycling and pores accessible to water. Thus, compared to the natural aggregate (NAT), this adhered mortar was responsible for an increase of 364% in the apparent porosity and 427% in the water absorption (**Table 3-8**). Equally, RCA presented a reduction of 12% in oven-dry density compared to the natural aggregate (NAT). The adhered mortar's influence on RCA characteristics was analyzed by Pepe et al. [149]. The authors observed that, after autogenous cleaning, water absorption of RCA was reduced by almost 50%, and the oven-dry density increased by almost 16%. Limbachiya, Leelawat, and Dhir [251] also investigated RCA with different amounts of adhered mortar, observing an increase in water absorption and a reduction in both oven-dry density and saturated surface-dry (SSD) density for RCA when the amount of attached cement paste increased.

Meanwhile, as ceramic materials are naturally more porous than natural rocks, RMA presented an apparent porosity 616% higher, a water absorption 845% higher, and an oven-dry density 24% lower than the natural aggregate (NAT).

Similar results were obtained for Cavalline and Weggel [97], using brick masonry as coarse recycled aggregate. In their study, water absorption increased from 0.34% for NAT to 12.2% for RMA, while apparent particle density reduced from 2840 kg/m^3 for NA to 2190 kg/m^3 for RMA (**Table 3-8**). Finally, as RCA was responsible for almost 90% of the composition of the MRA in this study (**Table 3-1**), the results obtained for both samples were very similar. MRA also exhibited a higher apparent porosity, higher water absorption, and lower density than the natural aggregate (NAT) (**Table 3-8**).

Table 3-8. Physical properties of recycled and natural aggregates.

	NAT	MRA	RCA	RMA
Apparent Particle Density – ρ (kg/m^3)	2653 ± 3	2626 ± 12	2631 ± 9	2497 ± 8
SSD Density – ρ_{SSD} (kg/m^3)	2601 ± 6	2350 ± 6	2396 ± 10	2164 ± 9
Oven-dry Density – ρ_d (kg/m^3)	2570 ± 10	2181 ± 14	2253 ± 13	1942 ± 12
Bulk Density - ρ_{ap} (kg/m^3)	1424 ± 4	1262 ± 3	1315 ± 5	1120 ± 7
Water Absorption – A (%)	1.21 ± 0.2	7.77 ± 0.47	6.38 ± 0.17	11.43 ± 0.23
Apparent Porosity – P (%)	3.10 ± 0.50	16.95 ± 0.91	14.38 ± 0.31	22.20 ± 0.32

Figure 3-15 shows a relationship between the oven-dry density and the apparent porosity, as well as between the water absorption and the apparent porosity. The increase in apparent porosity means an increase in the number of pores. Thus, while the oven-dry density decreases, the water absorption increases.

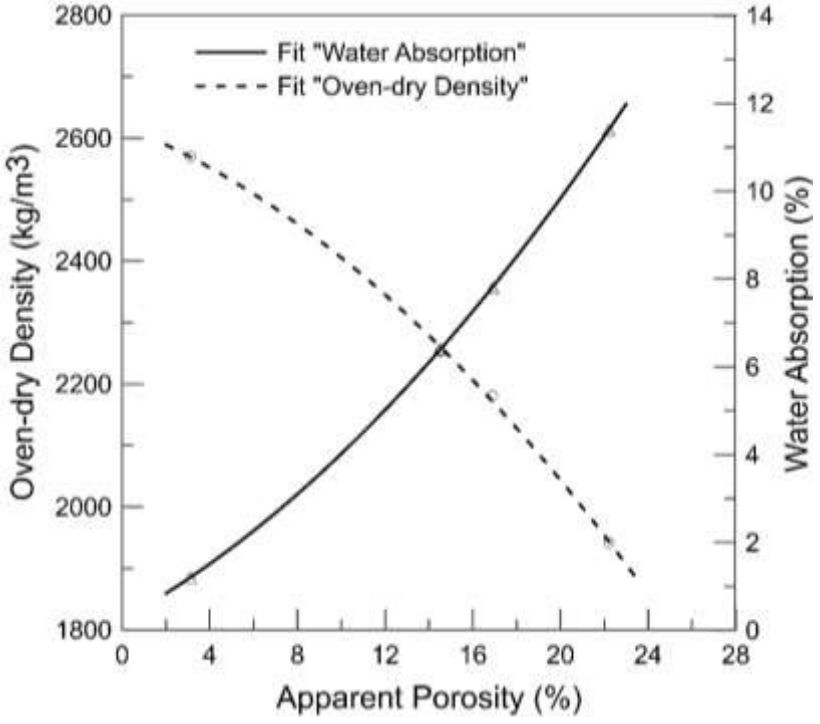

Figure 3-15. Oven-dry density and water absorption *versus* apparent porosity.

While the apparent porosity measures the total amount of void space accessible from the surface of the aggregate, the void ratio is the number of voids between the aggregates at a certain known volume. **Table 3-9** shows the aggregates' void ratio and experimental packing density.

It can be observed that the lower the void ratio, the greater the experimental packing density. However, regardless of the aggregate, the void ratio and experimental packing density results were very similar. This can be explained by the fact that all aggregates had the same maximum size (d = 19 mm) and similar values for shape indexes.

Table 3-9. Physical properties of recycled and natural aggregates.

	NAT	MRA	RCA	RMA
Void Ratio – E_v (%)	46.2 ± 0.2	51.8 ±0.1	50.4 ± 0.2	55.0 ± 0.3
Experimental Packing Density – ϕ	0.66 ± 0.01	0.54 ± 0.0	0.57 ± 0.01	0.50 ± 0.01

As mentioned, the experimental packing density was also evaluated for different particle size classes of coarse aggregates (class 1 - grains larger than 12.5 mm; class 2 - grains between 6.3 and 12.5 mm; and class 3 - grains smaller than 6.3 mm). **Table 3-10** presents the experimental packing density of each particle size class.

Table 3-10. Experimental packing density for different particle size classes of each coarse aggregate (NAT, MRA, RCA, and RMA).

Particle Size Classes		**Experimental Packing Density**			
		NAT	**MRA**	**RCA**	**RMA**
Class 1	**Φ > 12.5**	0.573	0.497	0.520	0.439
Class 2	**6.3 < Φ < 12.5**	0.560	0.491	0.483	0.436
Class 3	**Φ < 6.3**	0.595	0.431	0.510	0.423

Figure 3-16 and **Figure 3-17** show the 24 h and 15-minute water absorption curves for each coarse aggregate (NAT, MRA, RCA, and RMA). In the first few minutes, while the natural aggregate (NAT) presented a linear behavior, the recycled aggregates showed a higher absorption rate and reached a saturation plateau.

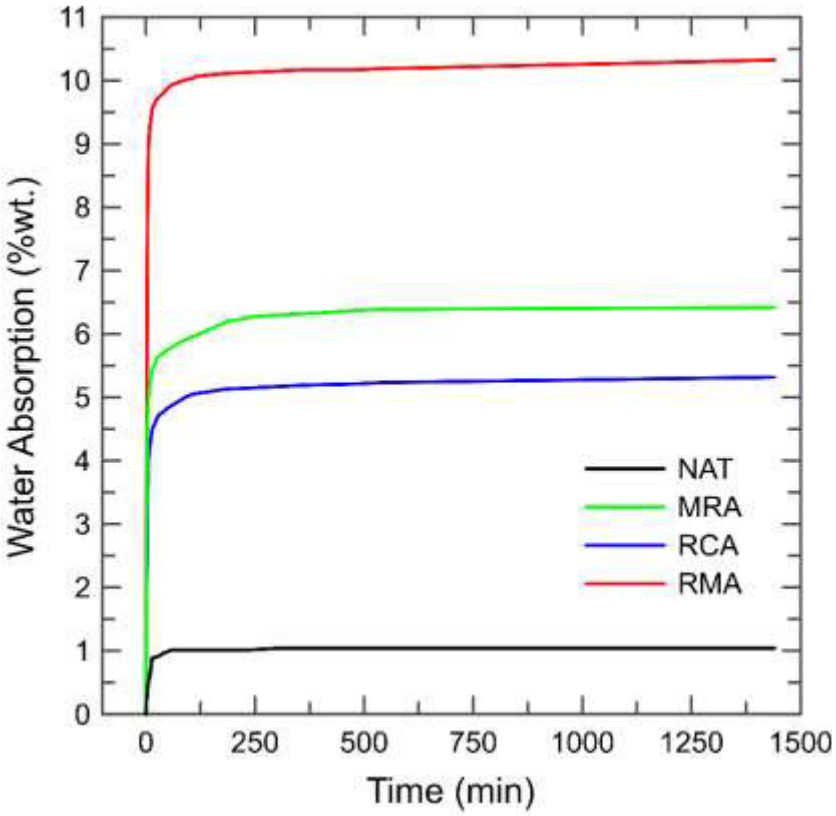

Figure 3-16. 24 h water absorption curve of the recycled and the natural aggregates.

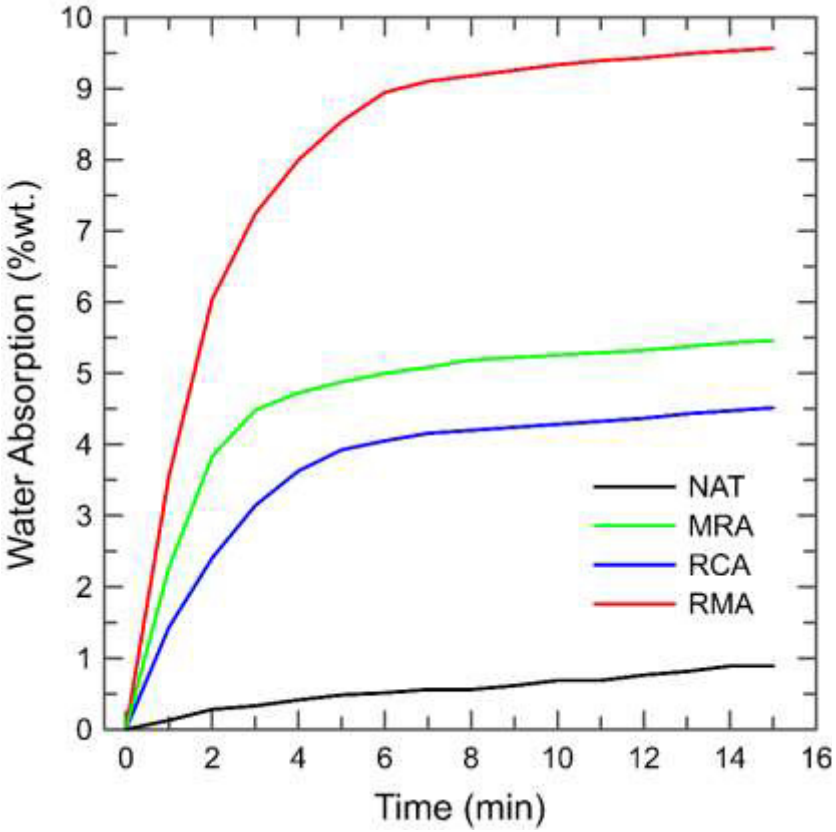

Figure 3-17. 15 min water absorption curve of the recycled and the natural aggregates.

In the first 10 minutes, the natural aggregate (NAT) reached 66% of its total water absorption, while RCA, MRA, and RMA reached 81%, 82%, and 90%, respectively. This behavior is related to the material's porosity: when the availability of pores is higher, the water absorption rate in the initial period is also higher. The maximum water absorption achieved for each aggregate was similar to the values in **Table 3-8**. Similar results were obtained by Salles [39]: more than 90% of the final water absorption occurred in the first five minutes of testing for the three types of recycled aggregate analyzed (MRA, RCA, and RMA).

Regarding the Aggregate Crushing Value (ACV) (**Table 3-11**), RMA presented a lower strength to gradually applied compressive load because of its porous and weak composition. Meanwhile, MRA and RCA presented a similar strength to gradually applied compressive load, which was approximately 15% higher than RMA and 8% lower than the natural aggregate (NAT). This reduction in the strength of MRA and RCA compared to NAT can be explained by the presence of the adhered mortar in the CDW concrete-based fragments: when the adhered mortar increased, the aggregate's strength decreased.

Table 3-11. Aggregate Crushing Value (ACV) of recycled and natural aggregates.

	NAT	MRA	RCA	RMA
ACV (%)	30.5 ± 0.2	33.4 ± 0.4	32.5 ± 0.5	38.9 ± 0.5

Duan and Poon [66] obtained similar results when analyzing the composition of three RCA samples, with different ratios of rock/concrete, by mass: 96%, 98%, and 99%. They observed that the RCA samples presented similar strength, with a variable reduction from 6% to 9% compared to a natural aggregate sample.

3.4. Conclusions

This chapter carried out an experimental investigation on the physical and mechanical properties of recycled coarse aggregates with different contents of ceramic debris. The four coarse aggregates (MRA, RCA, RMA, and NAT) presented continuous grain-size distribution curves, very similar and located within the usable zone as prescribed by Brazilian standard ABNT NBR 7211:2009 [247]. Also, regardless of the content of ceramic fragments, all three samples of recycled aggregates presented pulverulent content under the limit value established by the Brazilian standard ABNT NBR 15116:2021 [46].

Regarding the shape of the grains, although the values do not vary much, recycled concrete aggregate (RCA) is composed of more rounded grains and has a rougher surface, while recycled masonry aggregate (RMA) presents flatter and elongated grains. Mixed recycled aggregate (MRA) presented an intermediate shape index closer to the value obtained for the recycled concrete aggregate (RCA). As mentioned in the literature review, the more rounded the grains, the less the need for mixing water; meanwhile, aggregates with an angular shape offer higher adhesion to the mortar, leading to concretes with higher strength.

The increase in apparent porosity means an increase in the number of pores. Because of its higher porosity, the recycled aggregates (MRA, RCA, RMA) were less dense, less resistant, and absorbed more water than the natural aggregate (NAT). All recycled aggregates absorbed almost 90% of the total water after approximately 12 minutes. This must be considered when mixing the concrete since water absorption can reduce the water available for the cement hydration reaction. Besides that, the results obtained for the mixed recycled aggregate (MRA) were very similar to the results obtained for the recycled concrete aggregate (RCA).

Regarding water absorption, it was possible to verify that recycled aggregates (MRA, RCA, RMA) presented higher water absorption rates in the first minutes than the natural aggregate (NAT). Their higher porosity justifies this situation and must be considered when mixing the concrete. Lastly, as all four types of coarse aggregates presented comparable values for shape index and the same maximum size, they all showed very similar values of void ratio and, consequently, similar packing density.

From the discussions presented in this chapter, it can be concluded that when the recycled aggregate has a ceramic fraction lower than 15%, its physical and mechanical properties are not very different from those obtained for the recycled concrete aggregate, composed only of cement-based fragments. Thus, concrete made with recycled aggregate with a ceramic fraction lower than 15% is expected to present a similar behavior to concrete made with recycled concrete aggregate.

In addition, the non-necessity of separating the ceramic fraction decreases recycling costs, makes the recycling process more feasible, and increases market demand for this material. In this way, it would be interesting if the standards that restrict the use of recycled aggregate with ceramic fractions were reviewed to expand the possibilities of using this material.

4. Mix Design for Mixed Recycled Aggregate Concrete through the Compressible Packing Model (CPM)

4.1. Introduction

Since concrete is a heterogeneous material with complex behavior in fresh and hardened states, its mix design is challenging. It consists of determining the ideal proportion of the constituent materials to produce a technically adequate and economically viable mixture.

Brazil has no consensus on how the concrete mix design should be implemented. Because there are no specific regulatory guidelines on procedures and parameters, several researchers present their design methods developed by national research institutes or by adapting foreign standards [252], [253].

For example, the ABCP (Brazilian Association of Portland Cement) method was adapted from the ACI (American Concrete Institute) method. It is based on tables and graphics prepared from average values of experimental results, adequate for conventional concrete mix design.

As a second example, the IPT/EPUSP mix design method was developed by researchers from the Technological Research Institute of São Paulo (IPT) and the Polytechnic School of the University of São Paulo (EPUSP) and enshrined in the technical literature since the 1970s [254]. This method creates a design diagram, which is only valid for the same type and class of cement, mineral additives, and aggregates. Any modification of the initially selected parameters implies a new mix design. From this diagram – which schematically correlates the compressive strength, water/cement ratio, total dry aggregates/cement ratio, and cement consumption – it is possible to obtain concretes with distinct and well-defined properties in their hardened state. However, this method presents some limitations of application [252], such as:

- Compressive strength: 5 MPa ≤ fc ≤ 150 MPa;
- Water/cement ratio (w/c): 0.15 ≤ w/c ≤ 1.50;
- Slump: 0 mm ≤ slump ≤ self-compacting;
- Maximum size of coarse aggregate: 4.8 mm ≤ D_{max} ≤ 100 mm;

• Dry mortar content: 30% < α < 90%;

• Water/dry materials ratio (H): 5% < H < 12%;

• Concrete density: greater than 1500 kg/m³.

In this method, at first, an experimental adjustment of the proportions of the constituent materials of the concrete is made, aiming to determine the ideal mortar content. The study begins with the preliminary evaluation with a mix design of 1:5 (cement: total dry aggregates, by mass). Based on the information obtained from this mixture, two more are made, with mix designs defined as 1:3.5 and 1:6.5 [255]. The definition of an ideal mortar content is due to the problems caused by its lack or excess: the lack of mortar in the mixture results in porosity in the concrete or concreting failures, while its excess provides concrete with a better appearance, but with a higher cost per cubic meter and risk of cracking due to thermal and drying shrinkage. For the three concrete mixtures, manufactured specimens are subjected to wet curing and then tested at the established ages to determine their mechanical properties in the hardened state. The minimum amount of three concrete mixtures allows adjustment of the mix design correlation equations, enabling the construction of the mix design diagram, in which, by linear regression, any compressive strength can be achieved within the range studied for concrete mixes of the same family.

The current North American design procedures for proportioning conventional concrete - the ACI 211–1 Standard Practice for Selecting Proportions for Normal, Heavyweight, and Mass Concrete - offers a comprehensive approach for proportioning concrete of a maximum compressive strength of 40 MPa and a maximum slump of 180 mm. This method depends on the w/c ratio to achieve the required strength and the water content to obtain the desired slump. No special consideration is made to the quality of cement and aggregates or chemical admixtures (common in high-performance concrete) [256]. In summary, although the ACI mix design method applies to aggregate with a wide range of mineralogical and granulometric properties, it does not include any supplementary cementitious materials or additions, except for an air-entraining admixture. This method assumes that the maximum size of the coarse aggregate, the amount of mixing water, and the presence or absence of entrained air are the only parameters affecting slump, while the concrete compressive strength is affected only by the w/c ratio and the amount of entrained air.

In this method, after defining the water/cement ratio and the amount of mixing water, the mass proportions of the different constituent materials are transformed into volumetric fractions based on the relationship between the mass and volume of these materials (i.e., their specific gravity). To apply the ACI mix design method, it is necessary to know the fineness modulus of the fine aggregate, the dry-rodded unit weight of the coarse aggregate, the specific gravity of the aggregates, and the free moisture and absorption capacity of the aggregate, which are determined in the laboratory. This procedure assumes that the aggregate is well-graded and that the specific gravity of the cement is 3150 kg/m^3.

Although traditional mix design methods differ, they were all designed for the conventional strength concrete class. However, with the development of civil construction and structural engineering, sometimes special concretes are needed to meet the demands of works in which conventional concrete cannot be applied. This is also due to the evolution of the materials technology, mainly Portland cement, mineral additions, and chemical additives, which make it possible for concrete to achieve better physical and mechanical performances, in addition to other requirements such as the reduction of the cross-section of the structural elements, materials savings, and greater durability that extends the useful life of structures and, consequently, reduces maintenance costs.

Concrete is no longer a simple mixture of water, aggregates, and cement. It is becoming a complex mixture, made up of several granular materials that interact with each other. Thus, concrete's properties are becoming more difficult to predict theoretically, even though the use of computers facilitates complex calculations.

In this context, particle packing is widely applied in engineering areas that require a higher degree of technological development to produce high-quality materials. In civil construction, packing is necessary to obtain special concretes since the particle size distribution affects the packing density of the aggregate: the smaller the volume of voids to be filled with the cement paste, the higher the density of concrete [257], [258]. Therefore, modifying the concrete mix design formulation using the particle packing technique is an efficient way to produce concretes with higher durability and better mechanical performance, with reduced cement consumption [259].

The study of particle packing can be defined as the selection of the correct proportion between the materials, in addition to the definition of the adequate size

of the aggregates, so that the larger voids are filled by smaller particles, whose voids will be filled again with even smaller particles, and so on [260]. This concept aims to determine a particle size distribution that results in the highest packing density. The Particle Packing Method (PPM) is an optimization process to achieve an appropriate proportion of the aggregate mixture to attain minimum voids content.

In 1892, Féret published the first study on packing particles in concrete. Since then, packing models have been proposed to calculate the packing density of particles and thus optimize granular concrete mixes [261], [262]. Spherical particle packing models are presented through mathematical equations that prescribe how particles of different sizes interact geometrically. These models calculate the theoretical packing density of a given mixture based on the grain-size distribution.

The theoretical packing models can be categorized as continuous or discrete models. The continuous model assumes that all possible sizes of aggregates are present in the particle distribution system. On the other hand, discrete models assume that each particle size class contributes to the mixture of particles of various size classes to achieve the maximum possible density. These discrete models can be classified as binary, ternary, and multi-modal packing models.

The binary packing models consider blending two different-sized particles, where the smaller-sized particles fill up the voids between the larger-sized particles without disturbing the packing of the larger ones. Thus, the mixture voids can be minimized. However, these models are unsuitable for concrete mix, as the interaction effects are not accounted for since the theory is based on spherical-shaped particles. The concept of the binary packing model was extended to form a ternary mixture by adding the fine aggregate and simulating it as a binary packing model with the binary mixture of coarse and medium-sized aggregates [217].

In a multimodal packing model, Anderson and Dewar [263] proposed a method to calculate the void ratio for a particular combination of the aggregate mixture by considering the mean log size of each material (coarse aggregate, fine aggregate, and cementitious material) present in the mixture. Stovall et al. [264] proposed a multi-component mixture model (Linear Packing Model - LPM), where the packing density of a multi-grain mixture is represented as a function of the solid fractional volume of each size of grain present in the mixture. Then, by modifying the Linear Packing Model (LPM), De Larrard and collaborators of the *Laboratoire*

Central des Ponts et Chaussées (LCPC, Paris) [246] proposed the Compressible Packing Model (CPM).

The Compressible Packing Model (CPM) determines the packing of dry mixes for all materials used in concrete batching. Its main advantage is the possibility to define the desired properties at the fresh and hardened state of the resulting concrete through the intrinsic characteristics of each compound. The CPM considers that all the grains interact, influencing the resulting mixture.

4.2. Compressible Packing Model (CPM)

The Compressible Packing Model (CPM) is divided into two steps: 1) calculate the virtual packing, the largest possible packing for a given mixture; 2) experimentally obtain the actual packing based on the compactness of the grains. Then, correlations are established between the virtual and the real packing density through the compaction index (K).

The virtual packing density (γ) is the maximum compactness that a monodisperse granular mixture (particles of approximately the same size) can reach by stacking the grains one by one, without changing their original shape, in an infinite volume.

Another important definition is the dominant aggregate class. In binary mixtures (composed of two classes of grains of different sizes), when the larger grains dominate, the smaller particles fill part of the voids left by the larger particles without interfering with their accommodation (**Figure 4-1a)**. Maximum packing occurs when the smaller grains fill the voids left between the larger grains. However, when the smaller grains are the dominant class, they are packed in the porosity of the larger particles, as shown in **Figure 4-1b**.

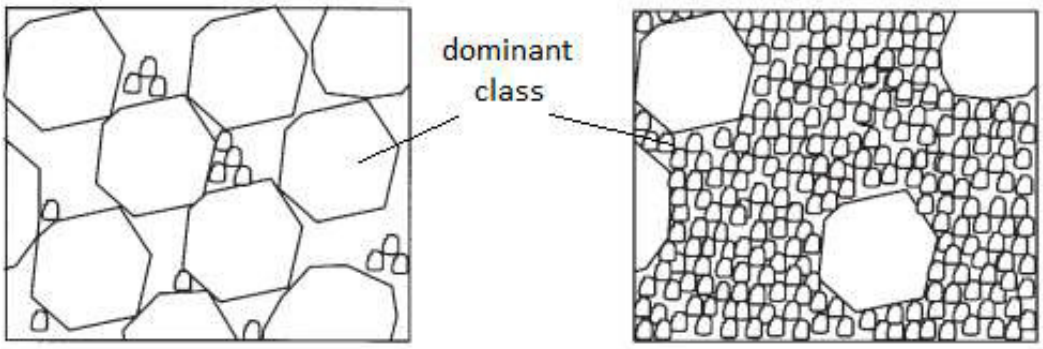

(a) (b)

Figure 4-1. Binary mixture without interaction: (a) coarse grains dominant; (b) fine grains dominant [246].

A binary mixture is said to be without interaction when the grain size of one class is much larger than the grain size of the other class ($d_1 \gg d_2$). When the sizes of the classes are relatively close, mixing is said to be interactional, and two effects can arise: the loosening effect and the wall effect. These two effects tend to decrease the mixture packing.

The loosening effect, which arises when the class of larger grains is dominant, occurs when the size of the voids left by the larger particles is smaller than the size of the smaller particles. Thus, the smaller grains move the larger grains away (**Figure 4-2**).

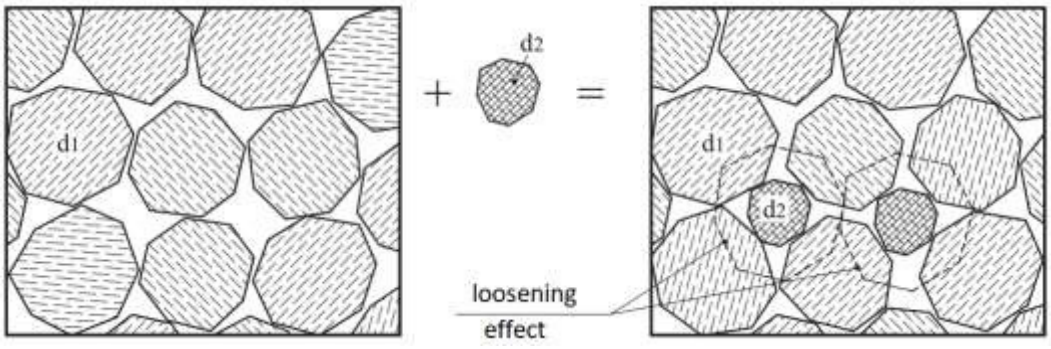

(a) (b)

Figure 4-2. Binary mixture with interaction: (a) undisturbed mixture; (b) loosening effect caused by smaller grains (d_2) on larger grains (d_1) [246].

The wall effect occurs in mixtures where the smaller grain class is dominant. In this case, a certain number of voids will appear on the contact surface between the two classes, caused by the significant difference in size between the particles so that the contact surface of the larger grain is practically flat (**Figure 4.3**).

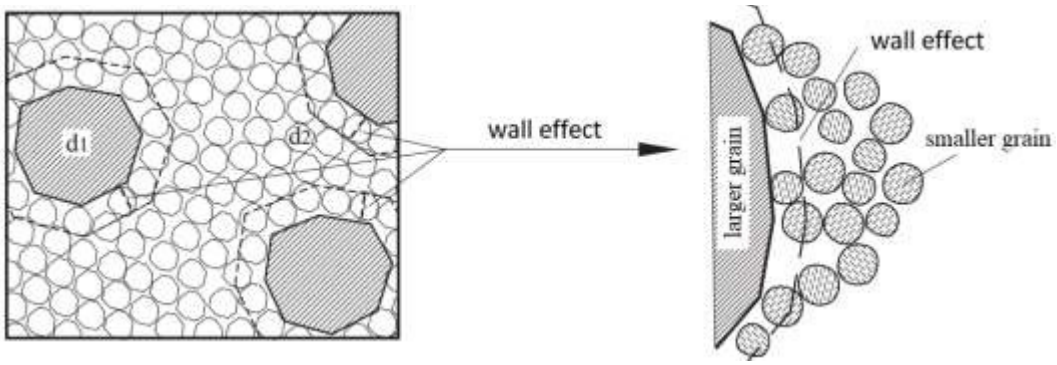

Figure 4-3. Binary mixture with interaction: wall effect exerted by the larger diameter grain on the smaller diameter grain [246].

It is important to observe that the virtual packing density (γ) occurs theoretically as if the grains were organized, one by one, to obtain the best possible arrangement. Thus, experimentally, the mixture packing obtained cannot be considered equal to the virtual packing density (γ) calculated by mathematical packing models.

The real packing density (ϕ) of a granular mixture depends, in addition to the particle size distribution, on the type of experimental packing protocol used. Thus, it is possible to correlate the virtual compactness to the real compactness through a parameter known as the compaction index (K). This index considers the energy associated with the experimental packing process, so the higher the index, the closer the real and the virtual packing. **Table 4-1** presents the compaction index (K) values for different packing processes obtained by de Larrard [246].

Table 4-1. Summary of compaction index (K) values for different packing processes.

Dry Packing Processes	Compaction Index (K)
Pouring	4.1
Sticking with a rod	4.5
Vibration	4.75
Vibration + Compaction 10 kPa	9

The virtual packing density (γ) of a given grain-size class "i" can be obtained experimentally through a test to determine the real packing density (ϕ) of the gran-size class with a certain packing process, with a known K index, through **Eq. 4-1**:

$$\gamma^{(i)} = \frac{1+K}{K}\phi_i \qquad \textbf{Eq. 4-1}$$

Where:

K is the compaction index;

$\gamma^{(i)}$ is the virtual packing density of a given grain-size class "i";

ϕ_i is the real packing density of a given grain-size class "i".

Thus, the real packing density (ϕ) of a polydisperse granular mixture is obtained by **Eq. 4-2**:

$$K = \sum_{i=1}^{n} \frac{y_i/\beta_i}{1/\phi - 1/\gamma_{(i)}} \qquad \textbf{Eq. 4-2}$$

Where:

K is the compaction index;

ϕ is the real packing density of the aggregate mixture;

n is the number of different aggregate sizes in the aggregate mixture;

β_i is the residual packing density of aggregate size "I," determined using dry-rodded unit weight testing, i.e., $\beta_i = \rho_{bulk}/\rho$ (ρ = apparent particle density);

y_i is the individual volume fraction of the aggregate size "i" in the mixture;

γ_i is the virtual packing density of the aggregate mixture considering aggregate size "i" as the dominant aggregate size.

In the Compressible Packing Model (CPM), the packing density of a granular mixture is governed by the aggregate particles' shape, surface texture, and size. Thus, to use this model, the packing density of each class size of aggregate used in the mixture should be experimentally measured.

4.2.1. Correlation between CPM and Concrete Strength

The matrix and inert aggregates' strength greatly influence concrete's compressive strength. The correlation between the 28-day compressive strength of sealed-cured cement paste and the Compressible Packing Model (CPM) is presented in **Eq.4-3** [246]:

$$f_{cp} = 13.4 R_{c28} \left(\frac{v_c}{v_c + v_w + v_a}\right)^{2.85} \qquad \textbf{Eq. 4-3}$$

Where:

f_{cp} is the strength of sealed-cured cement paste at 28 days (MPa);

R_{c28} is the strength of cement at 28 days (MPa);

v_c is the volume of cement (m^3);

v_w is the volume of water (m^3);

v_a is the volume of air (in m^3).

Considering that the volume and the aggregates' maximum dimension also influence the concrete's compressive strength, defining a parameter that measures these two effects is necessary. This parameter is called Maximum Paste Thickness (MPT) (**Figure 4-4**) and corresponds to the average distance between the aggregates immersed in the matrix (**Eq. 4-4**) [246]:

$$MPT = D\left(\sqrt[3]{\frac{g^*}{g}} - 1\right) \qquad \textbf{Eq. 4-4}$$

Where:

MPT is the maximum paste thickness (mm);

D is the maximum dimension of the aggregate (mm);

g is the volume of aggregates in a unit volume of concrete;

$g*$ is the packing density of the aggregates through the packing protocol corresponding to K=9.

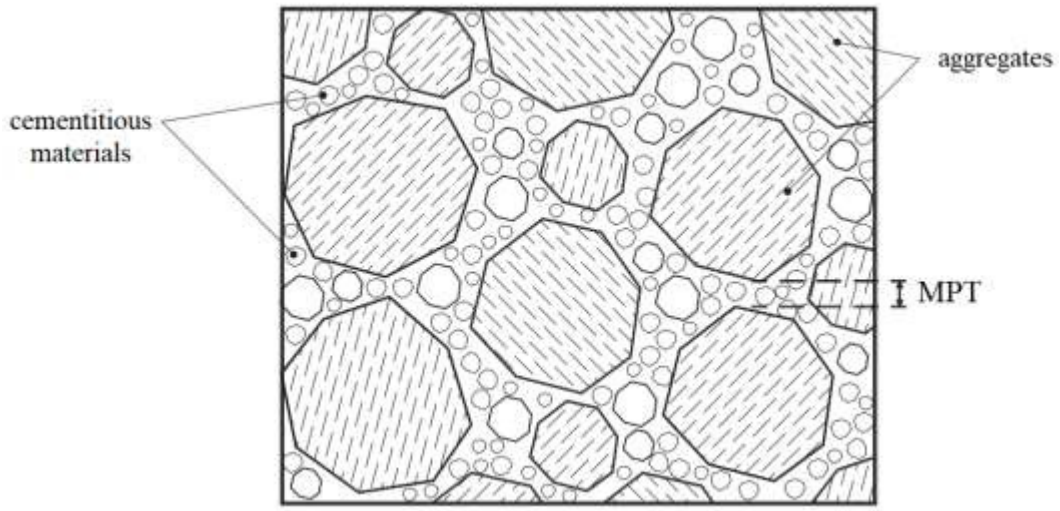

Figure 4-4. Maximum paste thickness in a dry granular mix [265].

According to De Larrard [246], it is possible to deduce the compressive strength of Portland cement concrete at 28 days, considering the cement paste strength, the cement concentration in the fresh paste, the Maximum Paste Thickness (MPT) effects, the bond between paste and aggregate, and the intrinsic strength of the aggregate (**Eq. 4-5** and **Eq. 4-6**):

$$f_{cm} = 13.4R_{c28}\left(\frac{v_c}{v_c+v_w+v_a}\right)^{2.85} \times MPT^{-0.13} \quad \textbf{Eq. 4-5}$$

$$f_c = \frac{p \cdot f_{cm}}{q \cdot f_{cm}+1} \quad \textbf{Eq. 4-6}$$

Where:

f_{cm} is the matrix strength at 28 days (MPa);

f_c is the concrete strength at 28 days (MPa);

p is the parameter related to the bond between paste and aggregate;

q is the parameter related to the intrinsic strength of the aggregate (MPa^{-1}).

The "p" and "q" parameters represent the influence of aggregates on the compressive strength of concrete through its adherence to the cement paste (expressed by "p") and its intrinsic strength (expressed by "q"). **Eq. 4-7** and **Eq. 4-8** present the mathematical formulation for defining "p" and "q" parameters, respectively. Based on the equations, the smaller the "q", the greater the intrinsic strength of the aggregate, and the greater the "p", the greater the bond between cement paste and aggregate.

$$p = \frac{1}{f_{cm}\left(\frac{1}{f_c} - \frac{1}{2.14 f_{cg}}\right)} \quad \textbf{Eq. 4-7}$$

$$q = \frac{p}{2.14 f_{cg}} \quad \textbf{Eq. 4-8}$$

Where:

f_{cg} is the intrinsic strength of the aggregate (MPa);

f_{cm} is the matrix strength at 28 days (MPa);

f_c is the concrete strength at 28 days (MPa);

p is the parameter related to the bond between paste and aggregate;

q is the parameter related to the intrinsic strength of the aggregate (MPa^{-1}).

4.3. Experimental Program

Mix design based on the Compressible Packing Model (CPM) can be performed with the software Bétonlab Pro 3, which allows the simulation of different materials mixtures to select the one that best meets the concrete's desired properties. This software relies on a raw materials database to estimate concrete

properties in fresh and hardened states. Therefore, this chapter presents the results of the concrete mix design, based on the Compressible Packing Model (CPM), through the software BétonLab Pro 3, developed by the *Institut français des sciences et technologies des transports, de l'aménagement et des réseaux* (IFSTTAR). Based on predetermined concrete mixtures, the compressive strength of concrete was estimated using the software BétonLab Pro 3. The theoretical results were then compared with the compressive strength values obtained experimentally, to verify the accuracy of the concrete mix design based on the Compressible Packing Model (CPM). In addition, the experimental values of tensile strength and modulus of elasticity were analyzed, comparing them with the theoretical values provided by the Brazilian standard ABNT NBR 6118:2014 [71].

4.3.1. Materials and Methods

In this section, two concrete strength classes were analyzed concerning compressive strength at 28 days using the software BétonLab Pro 3: concrete class of 30 MPa and 50 MPa. Henceforward, these two concrete strength classes will be called “C30” and “C50”.

Concrete class C30 was designed with 20%, 50%, and 100% mixed recycled coarse aggregate. The 20% content was chosen because this is generally the maximum amount of recycled coarse aggregate allowed by international standards for use in structural concrete, as observed in Section 2.7. The 100% content was adopted seeking a sustainable concrete regarding the use of coarse aggregate, i.e., without any natural aggregate. Finally, an intermediate content was also adopted, equivalent to 50%. For comparison, in the case of concrete with the highest strength class (C50), only the concrete made with 100% recycled aggregate was analyzed. For both concrete strength classes (C30 and C50), a reference concrete was fabricated with only natural coarse aggregate, i.e., 0% mixed recycled coarse aggregate.

Throughout this work, the mixed recycled coarse aggregate contents of 0%, 20%, 50%, and 100% will be referred to as “00”, “20”, “50” and “100”, respectively. For example, concrete C30-50 consists of a 30 MPa concrete strength class with 50% mixed recycled coarse aggregate. **Table 4-2** presents a summary of the nomenclatures used and the respective characteristics of each concrete.

Table 4-2. Summary of nomenclatures used for each concrete.

Nomenclature	Concrete Strength Class	% MRA
C30-00	C30	0%
C30-20	C30	20%
C30-50	C30	50%
C30-100	C30	100%
C50-00	C50	0%
C50-100	C50	100%

MRA = mixed recycled coarse aggregate

Figure 4-5 illustrates the experimental program, referring to the concrete mix design.

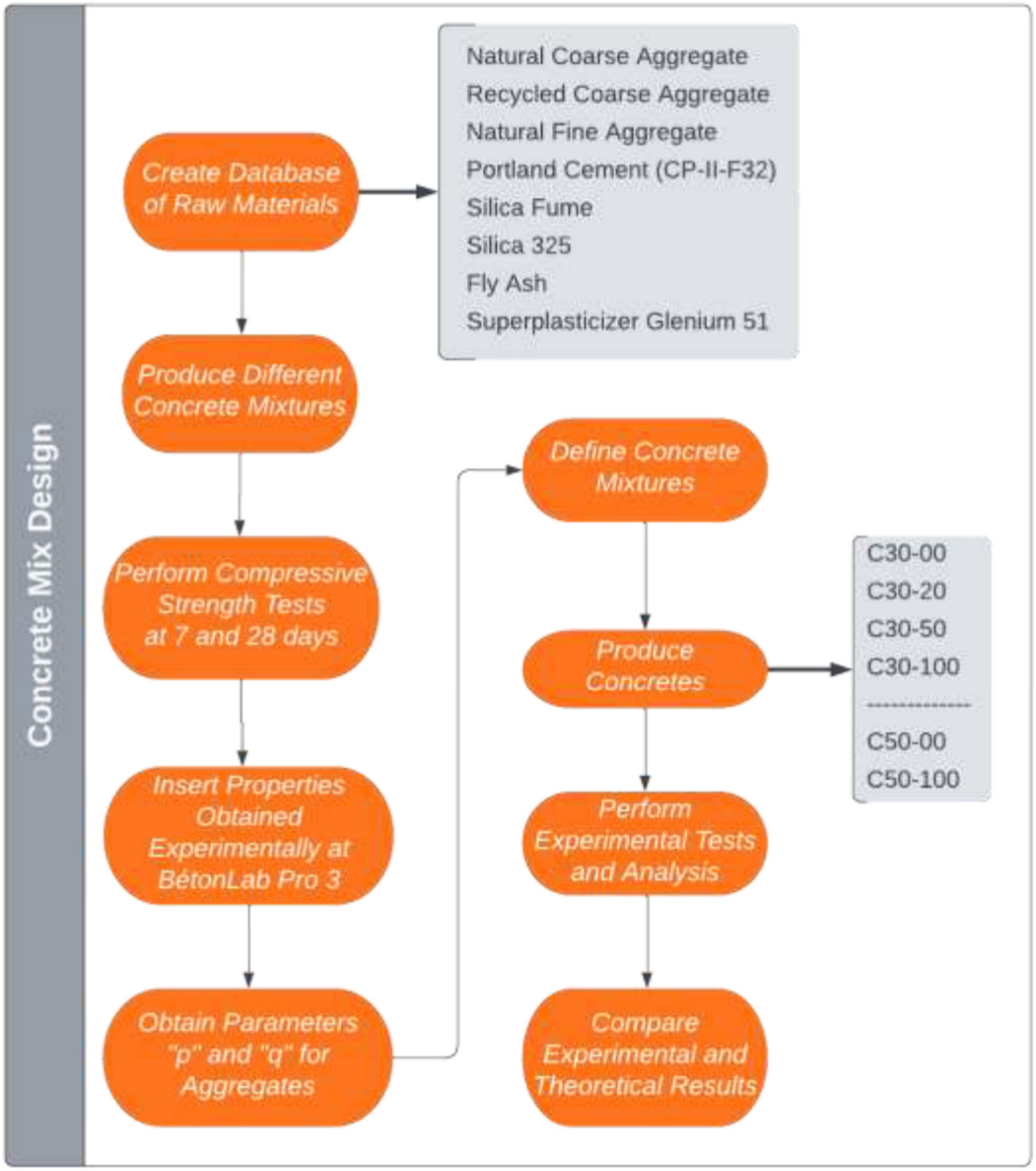

Figure 4-5. Experimental Program – Concrete mix design.

4.3.1.1. Portland Cement (CP-II-F32)

The cement used in this study was a Portland cement CP-II-F32, whose parameters met the conditions specified in Brazilian standard ABNT 16697:2018 [266]. It has a specific gravity of 2974 ± 9 kg/m^3, obtained through the Le Chatelier flask test, according to the Brazilian standard ABNT NBR 16605:2017 [267] (**Figure 4-6**).

(a) (b) (c)

Figure 4-6. Obtaining the specific gravity of Portland cement from the Le Chatelier flask test.

To apply the Compressible Packing Model (CPM), it is also essential to determine the experimental packing density of cement through a water demand test [246]. A planetary mixer with a capacity of 2 liters was required. Initially, a small amount of water was added to 350 g of cement, with the mixer on low speed for 1 minute. Subsequently, successive additions of water were made and maintained for 1 minute at high speed until the capillary state was observed, characterized by a homogeneous paste and no moisture on the wall of the mixer (**Figure 4-7**). From this point on, adding water to the mixing will cause the particles to move away, reducing compactness and increasing fluidity. The average test time was 10 minutes. Thus, it is possible to calculate the experimental packing density of Portland cement through **Eq. 4-9** [268]. The Portland cement CP-II-F32 used in this study has an experimental packing density (water demand) of 0.5406.

$$C = \frac{1}{1+\left(\delta \times \frac{m_a}{350}\right)} \quad \textbf{Eq. 4-9}$$

Where:

C is the experimental packing density of Portland cement;

δ is the specific gravity of Portland cement, obtained in 3.3.8 (g/cm^3);

m_a is the total mass of water added until the capillary state is observed (ml).

Figure 4-7. Capillary state, characterized by a homogeneous paste and no moisture on the mixer's wall.

4.3.1.2. Natural Fine Aggregate

In this study, the fine aggregate was a natural river quartz sand, with an oven-dry density of 2656 ± 67 kg/m^3 and water absorption of 4.38 ± 0.77%, according to the Brazilian standard NBR 16916:2021 [269].

The natural fine aggregate presented a well-graded continuous grain-size distribution curve located within the usable zone and close to the optimal zone [240] (**Figure 4-8**). It has a maximum size of 4.75 mm and a fineness modulus equal to 2.77. According to the Brazilian standard ABNT NBR 7211:2009 [247], the optimal zone for fineness modulus varies from 2.20 to 2.90.

As well as for the coarse aggregates in Section 3.2.9, for the application of the Compressible Packing Model (CPM), the experimental packing density [246] of fine aggregate was also evaluated for different particle size classes: i) class 1 -

grains larger than 1.18 mm; ii) class 2 - grains smaller than 1.18 mm. **Table 4-3** shows the experimental packing density of each particle size class.

Table 4-3. Experimental packing density for different particle size classes of natural quartz sand.

Particle size classes	Experimental packing density	
Class 1	**Φ ≥ 1.18 mm**	0.618
Class 2	**Φ < 1.18 mm**	0.586

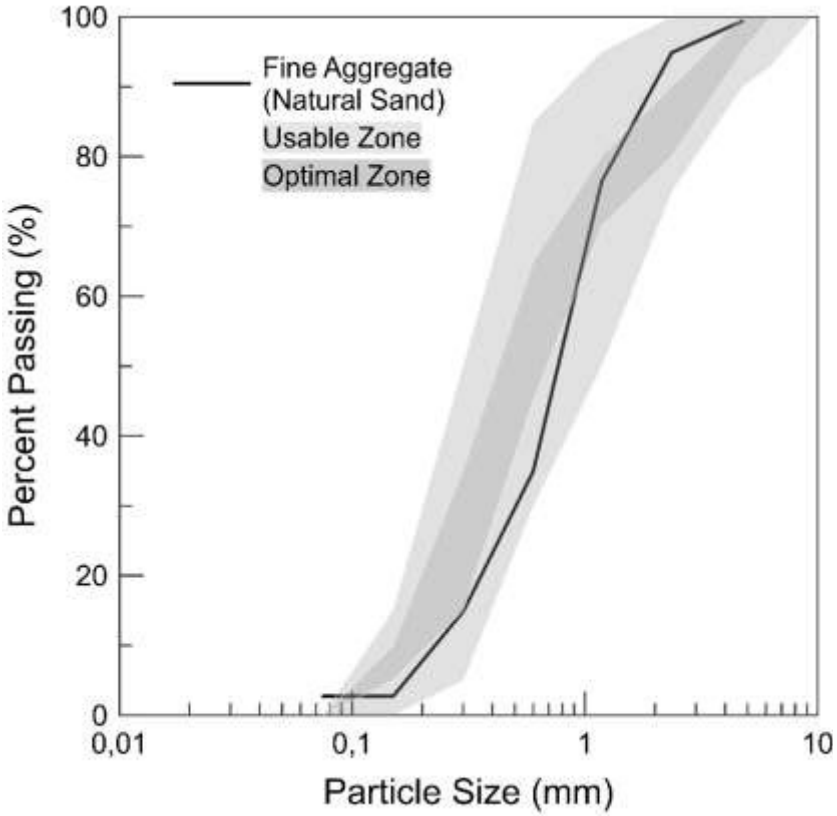

Figure 4-8. Fine aggregate (natural quartz sand) grain-size distribution curve.

The two specific fractions of the natural fine aggregate characterized above were used in the mix design presented in this study to obtain the high-strength concrete (C50). These fractions were named S1 and S2. **Table 4-4** shows the particle size of S1 and S2 and their oven-dry density, water absorption, and experimental packing density.

Table 4-4. Properties of fine aggregate fractions (S1 and S2) used for mix design of high-strength concrete (C50).

	Particle size	Oven-dry density (kg/m^3)	Water absorption (%)	Experimental packing density
S1	**150 μm < Φ < 0.85 mm**	2565.0	4.49	0.552
S2	**0.85 mm ≤ Φ < 4.75 mm**	2604.0	4.27	0.553

4.3.1.3. Natural and Mixed Recycled Coarse Aggregate

The coarse aggregates used in the concrete mix design in this chapter were the natural granitic coarse aggregate (NAT) and the mixed recycled coarse aggregate (MRA), whose physical and mechanical properties were presented in Chapter 3.

4.3.1.4. Mineral Additives

The mineral additives used in the concrete mix design were Fly Ash POZOFLY®, Silica Fume, and a quartz powder filler from the ceramic industry, named in this study as Silica 325 (**Table 4-5**, **Table 4-6,** and **Table 7**). These mineral additives had their granulometric compositions determined by granulometry laser with CILAS 1190 equipment at the Geotechnics and Environment Laboratory at PUC-Rio. **Figure 4-9** illustrates the grain-size distribution curves of mineral additives, as well as the Portland cement CP-II-F32 (described in Section 4.3.1.1).

Table 4-5. Properties of the Fly Ash POZOFLY®.

$SiO_2 + Al_2O_3 + Fe_2O_3$	> 70.0 %
SO_3	< 5.00 %
Moisture content	< 0.05 %
Ignition loss	< 2.00 %
Alkaline equivalent – Na_2O	< 1.50 %
Pozzolanic activity with cement at 28 days	> 75.0 %
Pozzolanic activity with lime at 7 days	> 6.00 MPa
Water requirement	< 110.0 %
Density	2.210 g/cm^3

Table 4-6. Properties of the Silica Fume.

SiO_2	94.69 %
Ignition loss	1.45 %
Moisture content	0.38 %
Alkaline equivalent – Na_2O_3	1.18 %
Density	0.600 g/cm^3

Table 4-7. Properties of the Silica 325.

SiO_2	99.50 %
AL2O3	0.14 %
Fe2O3	0.03 %
Na2O	0.03 %
K2O	0.02 %
Others	0.15 %
pH	8.40
Moisture content	0.20 %
Density	0.730 g/cm^3

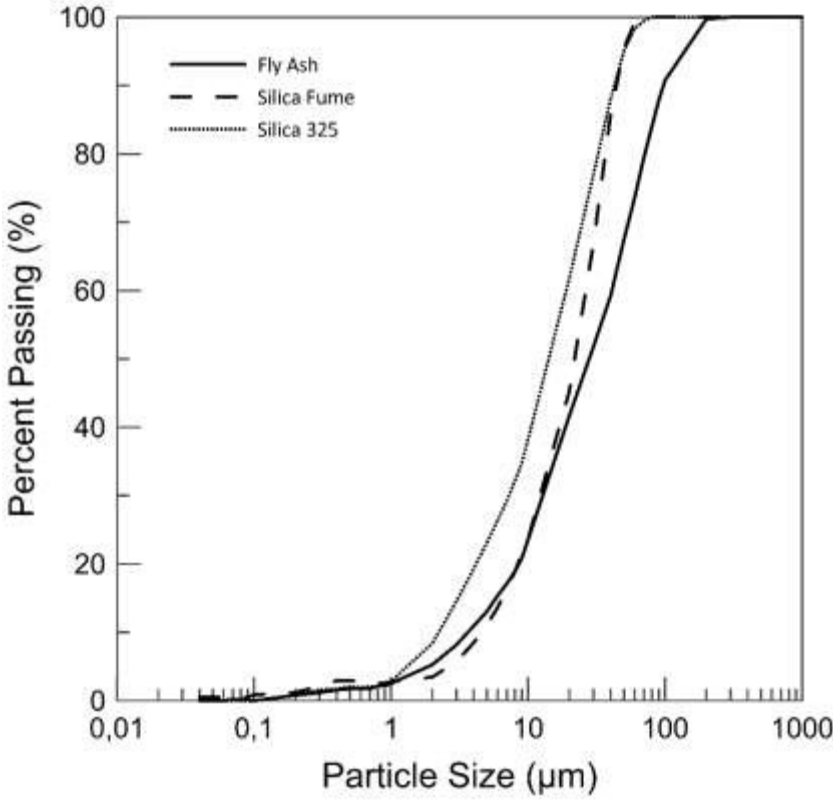

Figure 4-9. Grain-size distribution curves of mineral additives and Portland cement CP-II-F32.

4.3.1.5. Superplasticizer

Superplasticizer additive Glenium 51, produced by the company BASF, was used in the concrete mix design. It is based on a modified polycarboxylic ether chain that acts as a dispersant of the cementitious material, providing high water reduction and improving workability without changing the setting time. **Table 8** presents the superplasticizer additive's main properties, as provided by the manufacturer.

Table 4-8. Properties of the superplasticizer additive (www.basf.com.br).

Type	Polycarboxylic ether
Aspect	Opaque white liquid
pH	5 - 7
Density (g/cm^3)	1.067 – 1.107
Solid content (%)	28.5 – 31.5

A flow test was conducted using the Marsh funnel to evaluate the compatibility and determine the saturation point between the superplasticizer and Portland cement CP-II-F32. Samples were prepared with fixed amounts of cement and water, with a water/cement ratio of 0.35 and superplasticizer contents varying between 0.2% and 1.4% to the cement mass. Cement, water, and superplasticizer were mixed for 5 minutes in a planetary mixer, and then the paste was poured into the Marsh funnel with a diameter of 1 cm. **Figure 4-10** shows the saturation point of Glenium 51 superplasticizer with Portland cement CP-II-F32. Considering the mixing time of 5 minutes, it is possible to notice that the saturation point corresponds to the dosage of 1.0% of superplasticizer to the cement mass.

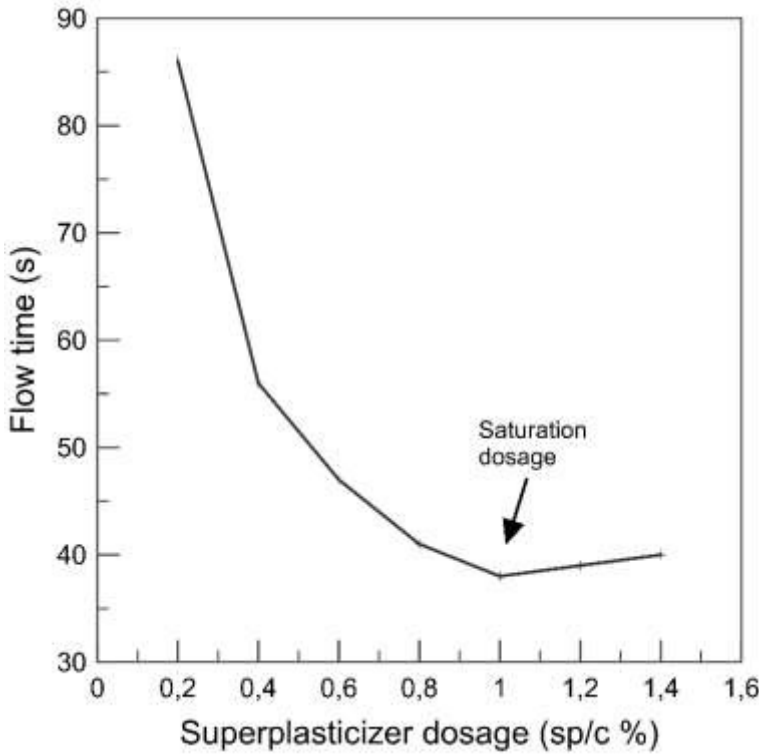

Figure 4-10. Variation of the flow time for various superplasticizer dosages.

4.3.2. Concrete Mix Design Using BétonLab Pro 3

4.3.2.1. Step 1 - Database creation

The first step of concrete optimization by BétonLab Pro 3 consisted of creating a database of raw materials (natural and recycled coarse aggregates, natural fine aggregate, cement, superplasticizer, silica fume, silica 325, and fly ash). The necessary test procedures to obtain these properties are presented in **Table 4-9** and **Table 4-10**.

Table 4-9. Coarse and fine aggregate test procedures required for BétonLab Pro 3 database.

Properties	Coarse Aggregate	Fine Aggregate
Density	NBR 16917:2021	NBR 16916:2021
Water Absorption	NBR 16917:2021	NBR 16916:2021
Grain-size Distribution	NBR NM 248:2003	NBR NM 248:2003
Experimental Packing density	Compression + Vibration	Compression + Vibration

Table 4-10. Cement, mineral additives, and superplasticizer test procedures required for BétonLab Pro 3 database.

Properties	Portland cement CP-II-F32	Silica Fume	Silica 325	Fly Ash	Superplasticizer
Density	NBR 16605:2017	Provided by manufacturer	Provided by manufacturer	Provided by manufacturer	Provided by manufacturer
Grain-size Distribution	Provided by manufacturer	Granulometry laser	Granulometry laser	Granulometry laser	-
Experimental Packing Density	Water demand	BétonLab database	BétonLab database	BétonLab database	-
Compressive Strength	Provided by manufacturer	-	-	-	-
Chemical Composition	Provided by manufacturer	-	-	-	-
Pozzolanic Coefficient	-	BétonLab database	-	BétonLab database	-
Solid Content	-	-	-	-	Provided by manufacturer
Saturation Amount	Marsh Cone Test	Provided by manufacturer	Provided by manufacturer	-	-

Grain size distribution, density, water absorption, and experimental packing density were computed for coarse and fine aggregates. In addition to the properties mentioned before for the aggregates, chemical composition, and strength at a certain age must be considered for Portland cement CP-II-F32, as well as the pozzolanic coefficient of Silica Fume and Fly Ash.

Water absorption is considered only for coarse and fine aggregates, and saturation amount is only for cement and mineral additives. Regarding the superplasticizer, solid content and density are computed.

For example, **Figure 4-11** shows part of the database created for the mixed recycled coarse aggregate (MRA). The database for natural coarse aggregate, natural fine aggregate (including fractions S1 and S2, as described in Section 3.2.9), Superplasticizer Glenium 51, Portland cement CP-II-F32, Silica Fume, Silica 325, and Fly Ash are presented in **Annex A**.

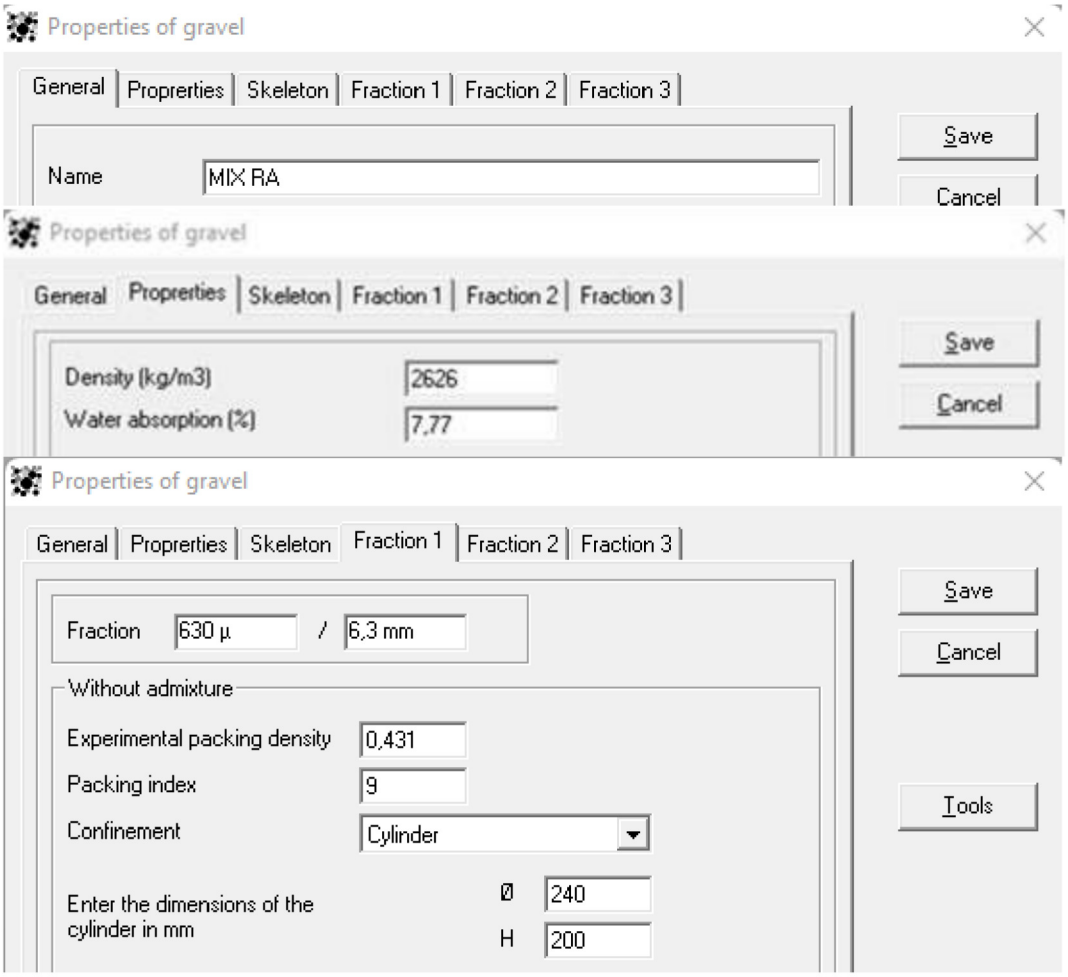

Figure 4-11. Database creation on Bétonlab Pro 3 for mixed recycled coarse aggregate (MRA).

4.3.2.2. Step 2 - Calibration of “p” and “q” parameters

The second step of concrete optimization by BétonLab Pro 3 consists of defining aggregates' “p” and “q” parameters. These parameters are calibrated through the compressive strength obtained experimentally for two concrete mixtures: one of high strength and another of low strength.

Mortars were produced with only natural sand, cement, and superplasticizer to calibrate fine aggregate's “p” and “q” parameters. As for coarse aggregates, concretes were produced with natural or mixed recycled coarse aggregate, natural sand, cement, and superplasticizer. The specimens of mortars and concretes were tested under compression at 7 and 28 days, and the compressive strength of each sample was inserted into the software BétonLab Pro 3. Thus, the software calculated each material's “p” and “q” parameters.

The high strength (HS) and low strength (LS) mixtures tested for calibration of the “p” and “q” parameters for natural coarse aggregate (NAT), mixed recycled coarse aggregate (MRA), and natural fine aggregate are presented in **Table 4-11**, **Table 4-12** and **Table 4-13**.

Table 4-11. Mixtures for calibration of the “p” and “q” parameters of NAT.

Materials (kg/m^3)	HS Mixture	LS Mixture
Portland Cement (CP-II-F32)	380	320
Natural Fine Aggregate	760	711
Natural Coarse Aggregate	1140	1066
Water	190	224
Superplasticizer Glenium 51	1.14	0.96

Table 4-12. Mixtures for calibration of the “p” and “q” parameters of MRA.

Materials (kg/m^3)	HS Mixture	LS Mixture
Portland Cement (CP-II-F32)	410	340
Natural Fine Aggregate	760	711
Recycled Coarse Aggregate	1140	1066
Water	205	238
Superplasticizer Glenium 51	1.23	1.02

Table 4-13. Mixtures for calibration of the “p” and “q” parameters of natural fine aggregate.

Materials (kg/m^3)	HS Mixture	LS Mixture
Portland Cement (CP-II-F32)	600	420
Natural Fine Aggregate	1360	1560
Water	240	294
Superplasticizer Glenium 51	1.08	1.26

As an example, **Figure 4-12** shows the software BétonLab Pro 3 output after calibration of the “p” and “q**”** parameters for mixed recycled coarse aggregate

(MRA). The parameters “p” and “q” obtained for natural coarse and fine aggregate are presented in **Annex B**.

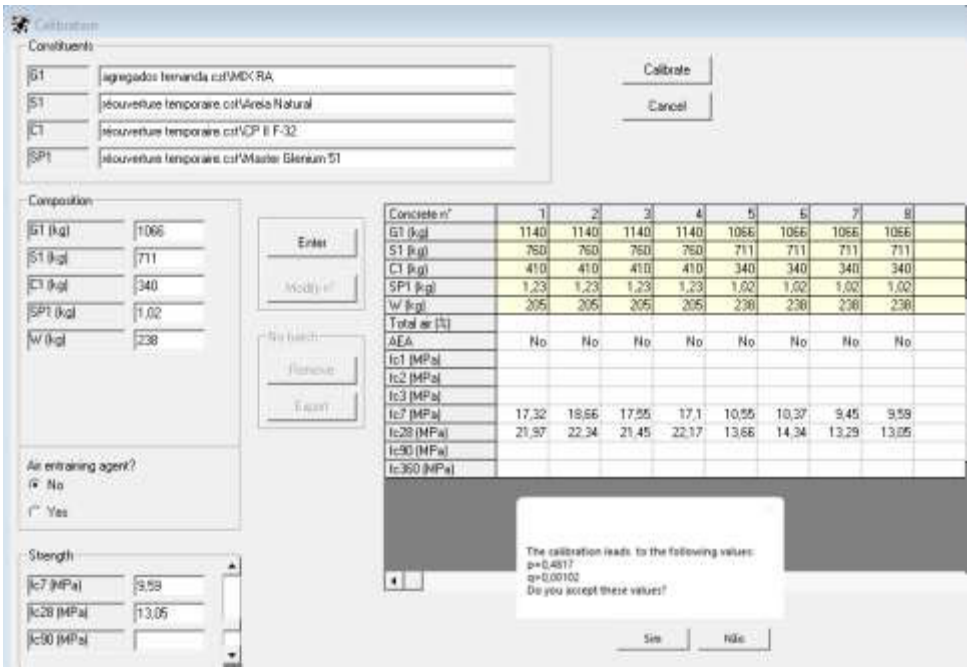

Figure 4-12. Calibration of “p” and “q” parameters on Bétonlab Pro 3 for the mixed recycled coarse aggregate (MRA).

4.3.2.3. Step 3 – Concrete mix design

Once the “p” and “q” parameters are obtained, the mix design simulations can be initiated. In this study, for concretes C30, cement consumption was kept constant at 360 kg, and a w/c ratio equal to 0.50 was adopted. Furthermore, the ratio between fine and coarse aggregates was kept constant at 40% of fine aggregates and 60% of coarse aggregates.

As for the C50 concrete, in addition to the cement consumption of 360 kg and the w/c ratio of 0.5, constant values of mineral additives were adopted: 70 kg of silica 325, 45 kg of silica fume, and 168 kg of fly ash. Lastly, the ratio between fine and coarse aggregates was kept constant at 58% of natural quartz sand fraction S1 (150 μm < Φ < 0.85 mm), 7% of natural quartz sand fraction S2 (0.85 mm ≤ Φ < 4.75 mm), and 35% of coarse aggregates.

Ultimately, for both groups C30 and C50, the natural aggregate was replaced by volume by the mixed recycled aggregate, considering the content of recycled aggregate to be obtained in each concrete mixture.

Table 4-14. Concrete mixtures for concrete class C30.

Material (kg/m^3)	C30-00	C30-20	C30-50	C30-100
Portland Cement (CP-II-F32)	360	360	360	360
Natural Coarse Aggregate (NAT)	1091	873	540	-
Mixed Recycled Coarse Aggregate (MRA)	-	216	546	1080
Natural Fine Aggregate ($\Phi \leq 4.75$mm)	728	728	728	728
Total Water	223	237	258	291
Free Water	180	180	180	180
Superplasticizer	1.1	1.1	1.1	2.2

Table 4-15. Concrete mixtures for concrete class C50.

Material (kg/m^3)	C50-00	C50-100
Portland Cement (CP-II-F32)	360	360
Silica 325	70	70
Silica Fume	45	45
Fly Ash	168	168
Natural Fine Aggregate S1 (150µm $< \Phi <$ 0.85mm)	830	830
Natural Fine Aggregate S2 (0.85mm $\leq \Phi <$ 4.75mm)	100	100
Natural Coarse Aggregate (NAT)	494	-
Mixed Recycled Coarse Aggregate (MRA)	-	489
Total Water	275	280
Free Water	180	180
Superplasticizer	45	50

Thus, through the software BétonLab Pro 3, it was possible to estimate the compressive strength of the concrete mixtures C30 and C50**.** As an example, the mix proportion for the reference concrete C30-00 is presented in **Figure 4-13.** The mix proportions for the concretes C30-20, C30-50, C30-100, C50-00, and C50-100 are presented in **Annex C**.

Concrete n°	3
G1 (kg/m3)	1090,6
S1 (kg/m3)	727,9
C1 (kg/m3)	360
SP1 (kg/m3)	1,1
W (kg/m3)	222,6
G1 (%)	60
S1 (%)	40
Saturation amount (%)	1,01
Superplasticizer content (%)	0,3
Eff water	180

fc1 (MPa)	11
fc2 (MPa)	16,1
fc3 (MPa)	18,9
fc7 (MPa)	23,8
fc28 (MPa)	27,9
fc90 (MPa)	31,2
fc360 (MPa)	35,2
Segregation index (confined)	0,943
Packing index of unconfined concrete	11,166
Packing index of confined concrete	11,166
Fines contribution K'f	2,703
Coarse gravel contribution K'gg	2,581
Packing of unconfined skeleton Ø°	0,7958
Aggregate packing g°	0,7371

Figure 4-13. Mix proportions for the reference concrete C30-00.

4.3.3. Mixing Process and Tests Methods

The mixing process was performed in a 30-liter planetary mixer (previously wet) for all concrete mixtures. For concrete strength class C30 (C30-00, C30-20, C30-50, and C30-100), the materials were mixed following the three steps:

1. Add all aggregates (natural fine aggregate and coarse aggregate – natural or recycled) and mix for 1 min;
2. Add the total amount of cement and 70% of the water and mix for 1 min;
3. Add the remaining water (30%) and the superplasticizer, and mix for 10 min.

For concrete class C50 (C50-00 and C50-100), the mixing procedure was conducted through the five steps below:

1. Add all aggregates (natural fine aggregate S1, natural fine aggregate S2, and coarse aggregate – natural or recycled) with 70% of the water and mix for 1 min;
2. Add all mineral additives (silica 325, silica fume, and fly ash) and mix for 1 min;
3. Add the total amount of cement and mix for 1 min;
4. Add the remaining water (30%) and the superplasticizer, and mix for 10 min.

4.3.3.1. Slump Cone Test

The slump cone test was carried out following the requirements of the Brazilian standard ABNT NBR 16889:2020 [270]. The test was performed using a steel mold with a cylindrical shape, with a 20 cm bottom diameter, a 10 cm top diameter, and a 30 cm height. A rectangular base plate and a compaction rod (circular steel section with a diameter of 16 mm and a length of 60 cm) were also used. Before testing, the whole apparatus was cleaned and dried.

After positioning the cylindrical mold on the base plate, the mold was filled with concrete in three layers of equal height. Each layer was compacted through 25 blows with the compacting rod. When the mold was filled with concrete, the top surface was flushed with the top opening of the mold. The mold was held firmly against its base during the entire operation through handles and footrests welded to the mold so that it could not move due to concrete leakage. Finally, the cylindrical mold was slowly lifted vertically, and the slump was measured.

4.3.3.2. Compressive Strength Test

The compressive strength was measured at 28 days using cylindrical specimens (ϕ = 100 mm and h = 200 mm), according to the Brazilian standard ABNT NBR 5739:2018 [271]. The mixing process was performed as described before. After 24 h, these specimens were demolded and taken to a humid chamber. After 28 days, before tests, they were flattened, avoiding irregular surfaces [272].

The compressive strength tests were performed at a loading rate of 0.35 MPa/s on a 500 kN servo-hydraulic MTS actuator. Two displacement transducers (LVDTs) were installed to measure the strain during loading, coupled to rings lightly attached to the specimens and 119 mm apart (gage length), as shown in **Figure 4-14**. The specific strain was calculated as the average of the relative strain measured by each of the LVDTs divided by the gage length.

The experimental results of compressive strength were used to verify the theoretical concrete mix design based on the Compressible Packing Model (CPM), by comparing the values obtained experimentally and those predicted by the software BétonLab Pro 3.

Figure 4-14. Compressive strength test performed on a 500 kN servo-hydraulic MTS actuator.

4.3.3.3. Tensile Strength Test

The tensile strength was indirectly measured through the diametral compression test proposed by the Brazilian researcher Lobo Carneiro in 1943. This test is known for its easy execution compared to the direct tensile strength test.

According to the Brazilian standard ABNT NBR 7222:2011 [273], the diametral compression test involves applying a compressive load along two generatrixes in the same diametrical plane of the cylindrical specimen (ϕ = 100 mm and h = 200 mm). The mixing process was performed as described before. After 24 h, the concrete specimens were demolded and taken to a humid chamber for 28 days [272].

For test execution, the cylindrical specimens were placed horizontally, supported by two wooden strips. The wooden strips were 3.5 mm tall and had a base of 15 mm. The load was applied continuously at 0.05 MPa/s until the specimen failed. The indirect tensile strength, obtained through the diametral compression test, is calculated by **Eq. 4-10**:

$$f_{ct,sp} = \frac{2 \cdot F}{\pi \cdot L \cdot d} \qquad \textbf{Eq. 4-10}$$

Where:

$f_{ct,sp}$ is the indirect tensile strength (MPa);

F is the maximum applied force (N);

L is the specimen length (mm);

D is the specimen diameter (mm).

According to the Brazilian standard ABNT NBR 6118:2014 [71], the direct tensile strength ($f_{ct,m}$) can be considered equal to 0.9 of the indirect tensile strength ($f_{ct,sp}$), obtained by the diametral compression test (**Eq. 4-11**):

$$f_{ct,m} = 0.9 \cdot f_{ct,sp} \quad \textbf{Eq. 4-11}$$

Also, the relationship between compressive strength (f_{ck}) and the direct tensile strength ($f_{ct,m}$) of concrete of strength class up to C50 is given by **Eq. 4-12**:

$$f_{ct,m} = 0.3 \cdot f_{ck}^{\frac{2}{3}} \quad \textbf{Eq. 4-12}$$

Thus, the correlation between the indirect tensile strength ($f_{ct,sp}$) and the compressive strength (f_{ck}) can be obtained by **Eq. 4-13**:

$$f_{ct,sp} = \frac{\left(0.3 \cdot f_{ck}^{\frac{2}{3}}\right)}{0.9} \quad \textbf{Eq. 4-13}$$

Where:

$f_{ct,sp}$ is the indirect tensile strength (MPa);

f_{ck} is the compressive strength (MPa).

4.4. Results and Discussions

Regarding the consistency of fresh concrete, the reference concrete C30-00 presented a slump value equal to 75 mm. As the content of mixed recycled aggregate increased, there was a reduction in the slump value. Concrete with 20%, 50%, and 100% mixed recycled aggregate showed reductions in the slump value of 15%, 31%, and 35%, respectively. This reduction in workability can be explained by the higher water absorption of the mixed recycled aggregate compared to the natural aggregate, causing a reduction in the available mixing water. Specifically for concrete with 100% mixed recycled aggregate (C30-100), the higher amount of superplasticizer in the mixture reduced the negative impact on the workability of

the higher water absorption. Thus, the slump result was similar to the sample with 50% mixed recycled aggregate. **Figure 4-15** shows the concrete C30-50 in the fresh concrete and its slump result.

(a) (b)

(c)

Figure 4-15. Fresh concrete (a and b) and slump result (c) for concrete C30-50.

Concerning the properties of concrete in the hardened state, **Table 4-16** and **Figure 4-16** present the results obtained in the compressive strength test and the tensile strength test for concretes C30 (C30-00, C30-20, C30-50, and C30-100). As the content of mixed recycled aggregate increases, it is possible to observe a slight reduction in compressive strength, modulus of elasticity, and indirect tensile strength of concrete. Compared to the reference concrete (C30-00), concrete C30 made with 100% mixed recycled aggregate (C30-100) presented a reduction of 10% in compressive strength, 12% in modulus of elasticity, and 3% in indirect tensile strength.

Table 4-16. Experimental maximum compressive strength, maximum strain, modulus of elasticity, and indirect tensile strength of concrete mixtures C30.

	C30-00	**C30-20**	**C30-50**	**C30-100**
f_c (MPa)	28.2 ± 1.9	27.3 ± 1.8	25.8 ± 0.8	25.4 ± 0.4
ε (μm/m)	2028.1 ± 75.1	2189.4 ± 117.1	2349.2 ± 105.7	2316.6 ± 179.1
E (GPa)	30.1 ± 0.8	28.6 ± 0.9	26.9 ± 0.8	26.4 ± 0.4
$f_{ct,sp}$ (MPa)	3.34 ± 0.25	3.17 ± 0.12	3.20 ± 0.08	3.24 ± 0.05

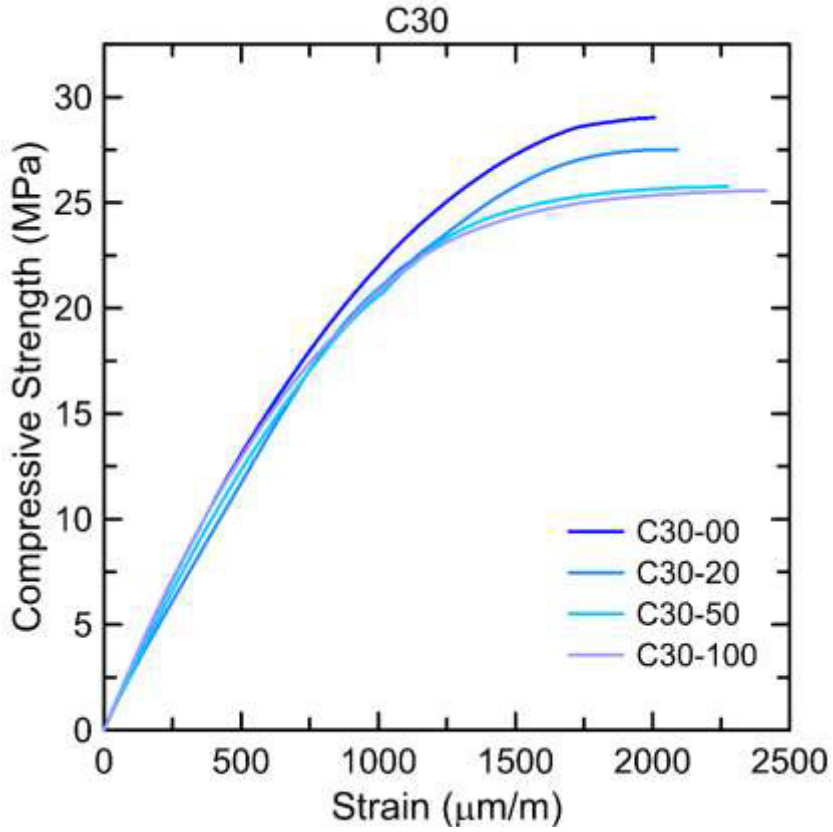

Figure 4-16. Compressive stress-strain curves of concrete mixtures C30.

Figure 4-17 shows the concrete C30 samples after the diametral compression test, which was used to obtain the indirect tensile strength. In a visual analysis, it is possible to observe that there is no relevant difference in terms of porosity between the samples.

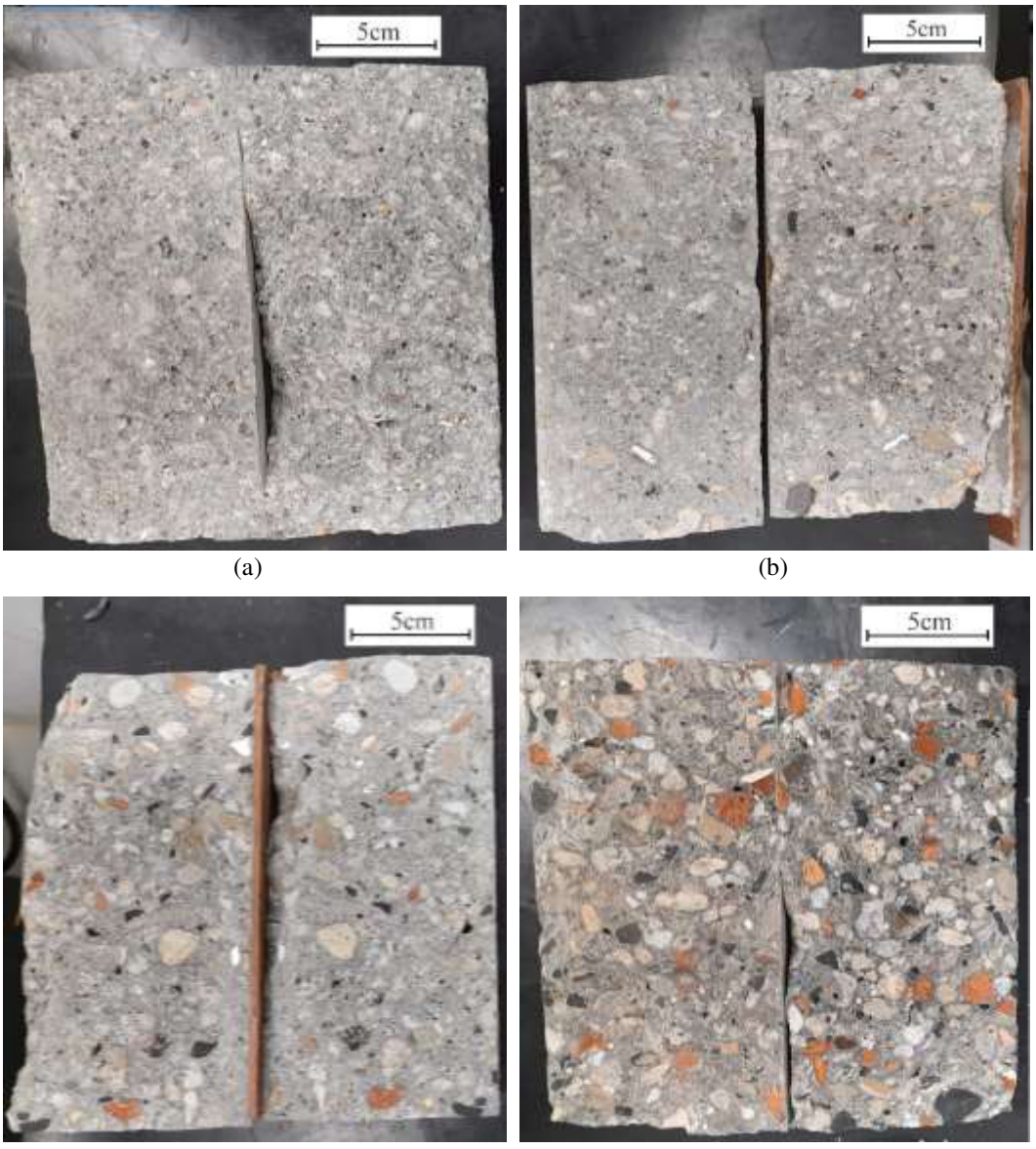

(a) (b)

(c) (d)

Figure 4-17. Samples of (a) C30-00, (b) C30-20, (c) C30-50, and (d) C30-100 after the diametral compression test.

The work developed by Ferreira [274] using samples made with the same mix designs C30-00 and C30-50 applied in this study (including the same natural and mixed recycled coarse aggregates) showed a slight difference between samples regarding the pore volume. The author conducted an x-ray microtomography analysis at PUC-Rio using a Zeiss-XRadia 510 Versa X-ray microtomography with a minimum spatial resolution of 0.7 µm. **Table 4-17** and **Figure 4-18** show the results obtained by Ferreira [274].

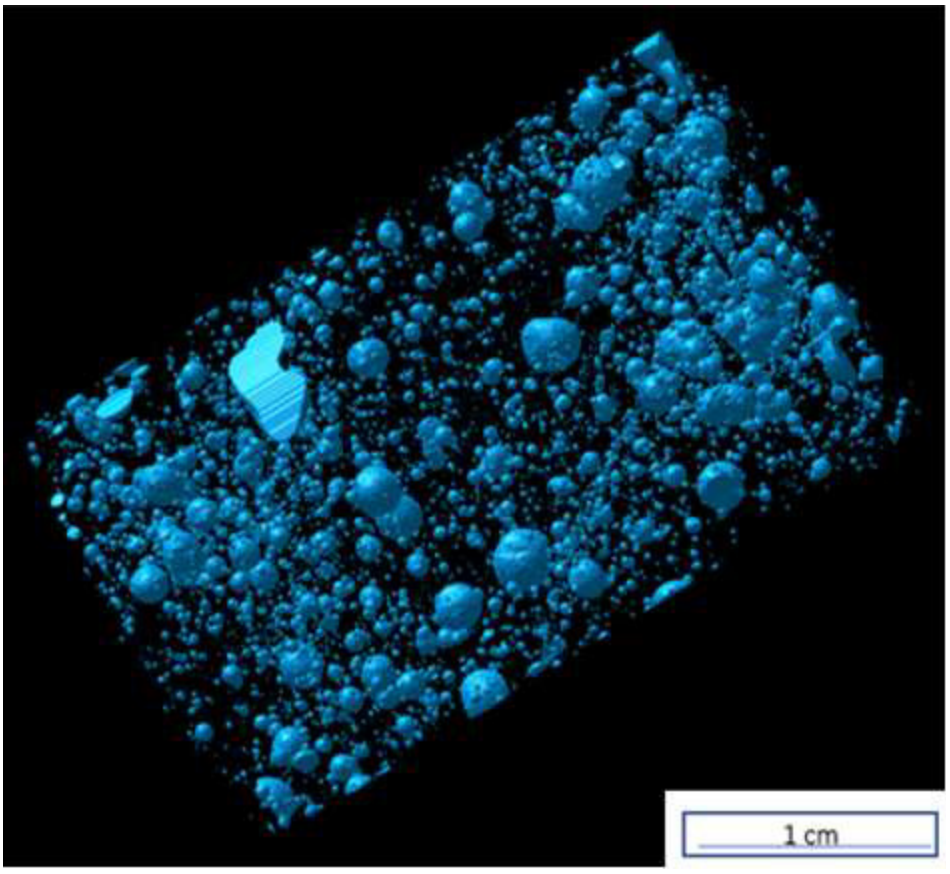

(a)

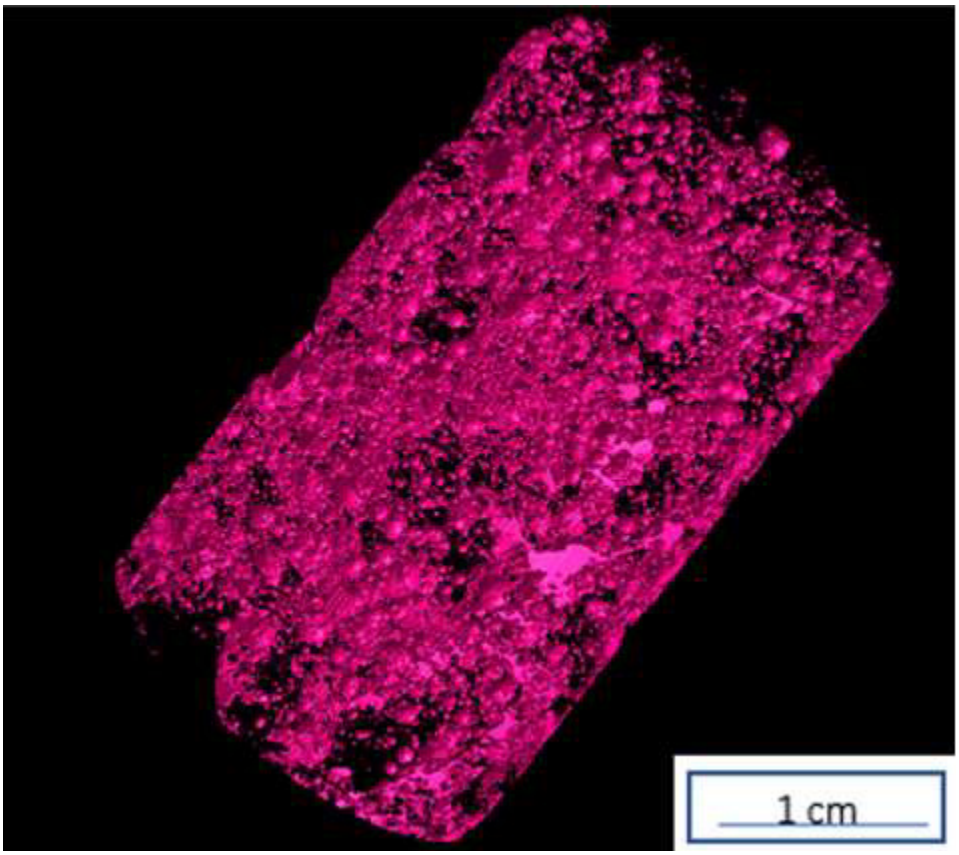

(b)

Figure 4-18. The pore volume of (a) C30-00 and (b) C30-50 samples [274].

Table 4-17. The total pore and mass volume of C30-00 and C30-50 samples [274].

	Total Pore Volume (%)	**Mass Volume (%)**
C30-00	2.82 ± 0.35	97.18 ± 0.35
C30-50	4.38 ± 0.60	95.62 ± 0.60

Porosity is a parameter directly associated with the concrete quality: the higher the porosity (volume of voids), the lower the concrete strength. Thus, based on the available data by Ferreira [274], it can be said that the replacement of natural aggregate by mixed recycled aggregate does not generate a relevant negative impact in terms of the material's porosity.

Table 4-18 and **Figure 4-19** present the results obtained in the compressive and tensile strength tests for concretes C50 (C50-00 and C50-100). For concrete strength class C50, the impact of the complete replacement of natural aggregate with mixed recycled aggregate was more pronounced. For concrete made with 100% mixed recycled aggregate (C50-100), the compressive strength, modulus of elasticity, and indirect tensile strength were reduced by 26%, 22%, and 21%, respectively, when compared to the reference concrete (C50-00). Both groups, C30 and C50, presented stress-strain curves with similar behavior (**Figure 4-16** and **Figure 4-19**, respectively).

Table 4-18. Experimental maximum compressive strength, maximum strain, modulus of elasticity, and indirect tensile strength of concrete mixtures C50.

	C50-00	**C50-100**
f_c (MPa)	51.6 ± 1.4	38.4 ± 2.7
ε (μm/m)	3357.4 ± 111.1	2606.8 ± 191.8
E (GPa)	41.2 ± 3.5	32.3 ± 1.5
$f_{ct,sp}$ (MPa)	4.75 ± 0.15	3.73 ± 0.18

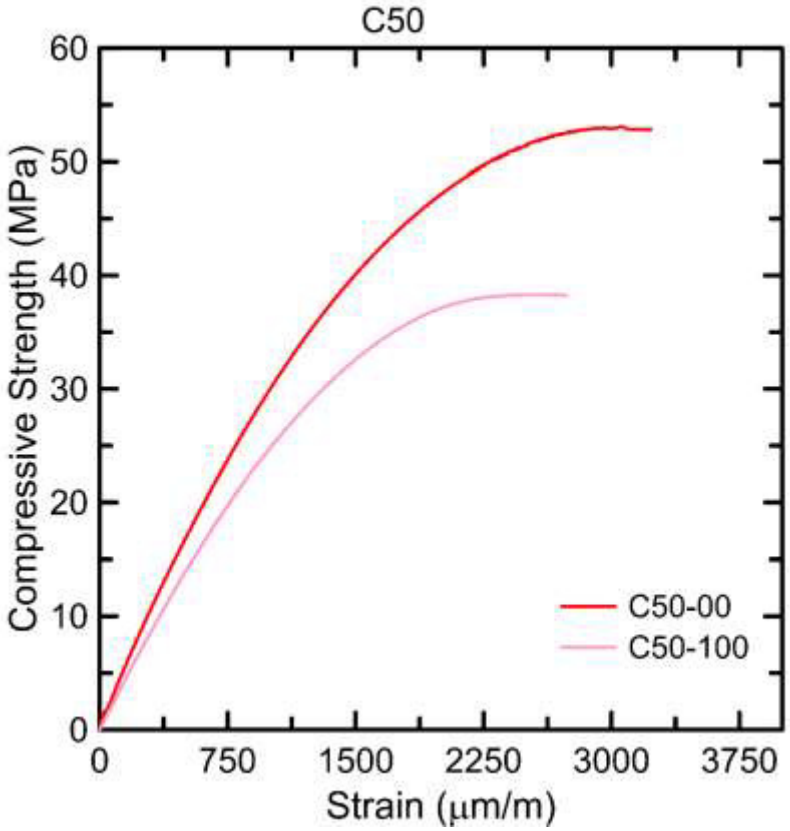

Figure 4-19. Compressive stress-strain curves of concrete mixtures C50.

Furthermore, as seen in **Table 4-19,** the experimental results of compressive strength showed a high correlation with the values predicted by the Compressible Packing Model (CPM) through the software BétonLab Pro 3. For the reference concrete C30-00 and concrete made with 20% mixed recycled aggregate (C30-20), the ratio between the theoretical value and the experimental value of compressive strength was approximately 1, reducing to 0.95 and 0.94 for concretes made with 50% and 100% mixed recycled aggregate (C30-50 and C30-100), respectively. As for concrete strength class C50, the ratio between the theoretical and experimental compressive strength values was approximately 0.92 for reference concrete (C50-00) and concrete made with 100% mixed recycled aggregate (C50-100).

Table 4-19. Correlation between experimental and theoretical compressive strength of concrete.

	C30-00	**C30-20**	**C30-50**	**C30-100**	**C50-00**	**C50-100**
f_c (MPa) – Experimental	28.2	27.3	25.8	25.4	51.6	38.4
f_c (MPa) – Theoretical	27.9	27.2	24.5	24.0	48.1	35.9
Ratio (theoretical /experimental)	0.99	1.00	0.95	0.94	0.93	0.93

Table 4-19 shows that this correlation is more accurate for concrete strength class C30 than for concrete strength class C50, regardless of the amount of mixed

recycled aggregate. This variation may be associated with the properties of the mineral additives (fly ash, silica 325, and silica fume) provided by the manufacturers or obtained directly from the BétonLab database. In other words, some properties considered in the mix design of C50 concretes using the software BétonLab may differ from the real values of the materials used, which may have impacted the accuracy of the software prediction for these concretes.

Nevertheless, the ratio above 90% between theoretical and experimental values for all samples demonstrates that, with the aid of the software BétonLab Pro, the Compressible Packing Model (CPM) can be successfully applied for the mix design of concrete made with mixed recycled aggregate up to strength class C50.

Regarding the indirect tensile strength ($f_{ct,sp}$), it was possible to calculate the theoretical value using the experimental concrete compressive strength (f_c). When comparing this theoretical value with the experimental results, the ratio was above 0.90 for all concrete samples, regardless of the concrete strength class and the content of mixed recycled aggregate (**Table 4-20**). Therefore, in the case of tensile strength, there is no need to propose any adjustments in the theoretical formulation of the Brazilian standard ABNT NBR 6118:2014 [71] for concretes made with mixed recycled aggregate.

Table 4-20. Correlation between concrete's experimental and theoretical tensile strength.

	C30-00	**C30-20**	**C30-50**	**C30-100**	**C50-00**	**C50-100**
$f_{ct,sp}$ (MPa) – Experimental	3.31	3.17	3.20	3.21	4.75	3.73
$f_{ct,sp}$ (MPa) – Theoretical	3.09	3.02	2.91	2.88	4.62	3.80
Ratio (theoretical /experimental)	0.94	0.95	0.91	0.90	0.97	1.02

The Brazilian standard ABNT NBR 6118:2014 [71] also presents a theoretical formulation for obtaining the modulus of elasticity of concrete between C20 and C50 as a function of its compressive strength (f_{ck}) (**Eq. 4-14**):

$$E_{ci} = \alpha_E \cdot 5600\sqrt{f_{ck}} \qquad \textbf{Eq. 4-14}$$

Where:

E_{ci} is the modulus of elasticity (MPa);

f_{ck} is the compressive strength (MPa);

α_E is a constant that varies according to the type of coarse aggregate:

α_E = 1.2 to basalt and diabase

α_E = 1.0 to granite and gneiss

α_E = 0.9 to limestone

α_E = 0.7 to sandstone

As seen above, the Brazilian standard ABNT NBR 6118:2014 [71] does not prescribe the constant α_E when using recycled aggregate as coarse aggregate in concrete. Thus, to obtain the α_E for the mixed recycled aggregate used in this study, a graph was initially made with the experimental values of the modulus of elasticity and the compressive strength for concretes made with 20%, 50%, and 100% of mixed recycled aggregate (**Figure 4-20**).

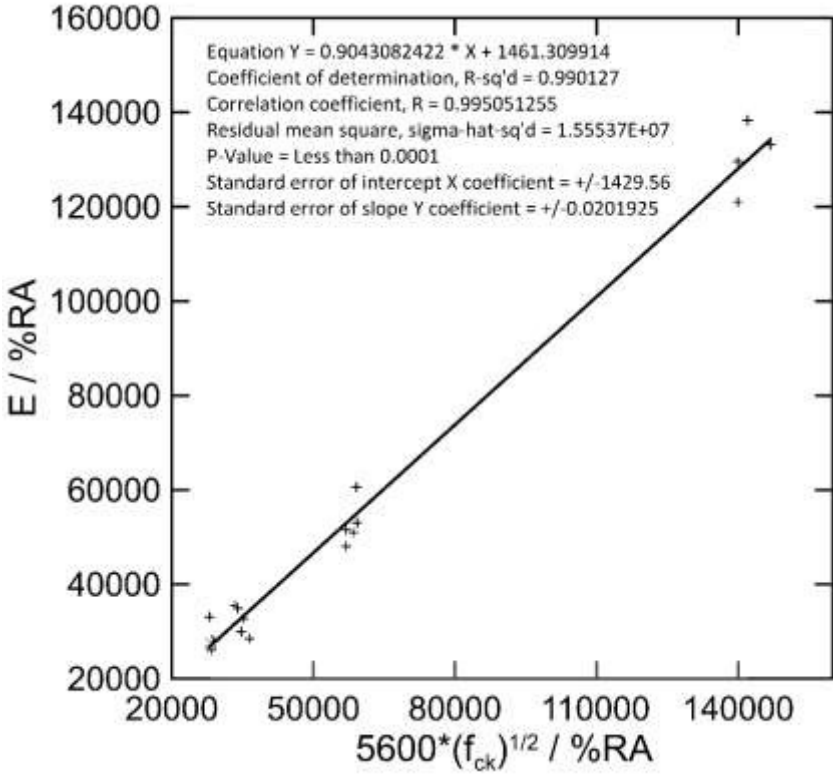

Figure 4-20. Correlation between experimental modulus of elasticity of concretes with 100% recycled aggregate and respective theoretical values.

Based on the fit curve, the following **Eq. 4-15** was obtained:

$$\frac{E_{ci}}{RA_c} = 0.9 \cdot \frac{(5600\sqrt{f_{ck}})}{RA_c} + 1461$$

$$E_{ci} = 5040\sqrt{f_{ck}} + 1461 \cdot RA_c \qquad \textbf{Eq. 4-15}$$

Where:

RA_c is the recycled aggregate content (20% = 0.2; 50% = 0.5; 100% = 1);

E_{ci} is the modulus of elasticity (MPa);

f_{ck} is the compressive strength (MPa).

Table 4-21 shows the correlation between the experimental and theoretical modulus of elasticity of concrete mixtures C30 and C50. For concretes made with mixed recycled aggregate (C30-20, C30-50, C30-100, C50-100), the proposed **Eq. 4-15** was applied. For reference concretes C30-00 and C50-100, **Eq. 4-14** was used, considering α_E value equal to one since the natural aggregate is granitic.

Table 4-21. Correlation between the experimental and theoretical modulus of elasticity of concrete mixtures C30 and C50.

	C30-00	**C30-20**	**C30-50**	**C30-100**	**C50-00**	**C50-100**
E_{ci} (GPa) – Experimental	30.1	28.6	26.9	26.4	41.2	32.3
E_{ci} (GPa) – Theoretical	29.7	26.6	26.3	26.9	40.2	26.9
Ratio (theoretical /experimental)	0.99	0.93	0.98	1.02	0.98	0.83

The results show a high correspondence between theoretical and experimental values, especially for concrete strength class C30. Thus, based on the experimental data available in this study, it can be concluded that **Eq. 4-15** can be successfully used for calculating the modulus of elasticity of concrete made with mixed recycled aggregate up to strength class C50.

4.5. Conclusions

In this chapter, a study was carried out on the mix design of concretes with two different strength classes (C30 and C50) manufactured with mixed recycled aggregate through the Compressible Packing Model (CPM) using the software BetónLab Pro 3.

It can be concluded that the quality of the materials characterization tests is directly related to the accuracy of the materials database to be developed in the software BétonLab Pro 3. Also, the greater the quantity of high and low-strength concrete mixtures to be tested under compression, the more accurate the calibration of aggregates' “p” and “q” parameters.

During the mixing process, the required water was split into two parts (70% and 30%), the smallest fraction added only in the final step, together with the superplasticizer. Since the recycled aggregate presents a higher water absorption, this procedure guarantees a greater proportion of free water, making the mixture

more homogeneous. Regarding the consistency of fresh concrete, as the content of mixed recycled aggregate increased, there was a reduction in workability because of the higher water absorption of the mixed recycled aggregate compared to the natural aggregate causing a reduction in the available mixing water. Therefore, the use of superplasticizers can reduce this negative impact.

In a visual analysis, no relevant difference was observed in porosity between the concrete samples, regardless of the content of mixed recycled aggregate. Using x-ray microtomography analysis, only a slight increase in pore volume and in the percentage of connected pores was observed by Ferreira [274] when 50% of natural aggregate was replaced with mixed recycled aggregate.

Regarding the compressive strength, for concrete strength class C30, as the content of recycled aggregate increases, there is only a slight reduction in the compressive strength and the modulus of elasticity and a small increase in the maximum strain. Although this difference becomes more pronounced for the higher strength class (C50), the stress-strain curves of all concrete mixtures presented a similar behavior, and it is possible to declare that even the replacement of 100% of the natural aggregate with mixed recycled aggregate with a ceramic fraction lower than 15% did not cause a significant impact on the concrete compressive strength.

The ratio between the theoretical and experimental compressive strength values was above 0.91 for all concretes. Thus, based on the available data in this study, it can be said that the Compressible Packing Model (CPM) can be successfully applied for the mixture proportioning of concrete made with mixed recycled aggregate for both strength classes C30 and C50.

Regarding the tensile strength, for all concrete strength classes and mixed recycled aggregate content, the experimental values showed a correlation above 90% compared with the theoretical value, calculated through the formulation of the Brazilian standard ABNT NBR 6118:2014 [71]. In such a way, there is no need to propose any adjustments in this theoretical formulation when using mixed recycled aggregate in the concrete.

Lastly, using the experimental results, it was possible to propose a theoretical formulation to correlate the modulus of elasticity with the compressive strength and the mixed recycled aggregate content in concrete, thus adapting the existing formulation in the Brazilian standard ABNT NBR 6118:2014 [71], which consider only concrete manufactured with natural aggregates of different types.

5. Flexural Behavior of Short Reinforced Concrete Beams Made with Mixed Recycled Aggregate

5.1. Introduction

One of the oldest publications on recycled aggregates in reinforced concrete beams was published in 1988 in Japan [275]. After that, many researches have been carried out to evaluate the structural performance of concrete manufactured with recycled concrete aggregate [53]–[66].

In general, it can be said that the bending behavior of beams is not significantly affected by the replacement of natural aggregates with recycled concrete aggregates (with no ceramic fragments) [56], [58], [61]–[64]. When compared to conventional concrete beams, beams made with recycled concrete aggregate present similar yielding and ultimate moments and a lower cracking moment [56], [58], [59]. Pradhan et al. [55] remarked that cracking load is affected by the lower tensile strength of concrete made with recycled aggregate while incorporating recycled concrete aggregates less influences the ultimate load. Regarding cracking, some authors observed that crack spacing decreases as the content of recycled concrete aggregates increases [53], [55], [58], [59]. Besides that, there is no consensus concerning the crack width: in some studies, the crack width increases with the increase in the content of recycled concrete aggregates [53], [54], [63]. Meanwhile, in other research, no relevant discrepancy was observed [57], [58]. The divergence in some results can be explained by the different research methodologies and materials used in each study since there are different ways to obtain and select the recycled aggregate from construction and demolition waste.

On the other hand, although some researchers have shown that mixed recycled aggregate can generate high-quality concrete ([23], [34], [35], [67]–[70]), the use of mixed recycled aggregate in the design of structural concrete is usually not addressed in concrete codes and standards, due primarily to the gaps in scientific-technical understanding of performance attributable to a paucity of research and the great heterogeneity of the mixed recycled aggregate. In Brazilian,

for example, the use in structural concrete of recycled aggregate with any ceramic fraction is not allowed. Consequently, mixed recycled aggregate is widely used as a pavement base and raw material for non-structural concrete, limiting valorization opportunities.

Therefore, to help provide grounds for including this type of aggregate in the existing standards, fueling the recycling of construction and demolition waste, this chapter seeks to comprehend the flexural behavior of short reinforced concrete beams manufactured with mixed recycled aggregate when subjected to short-term loading. For this, will be used a mixed recycled aggregate with approximately 13% of ceramic fragments. This recycled aggregate was received directly from a Brazilian recycling plant, located in Ribeirão Preto, São Paulo.

5.2. Experimental Program

Initially, beams were produced with concretes of strength classes C30, with 0%, 20%, 50%, and 100% of mixed recycled aggregate, as presented in Chapter 4. These beams were designed according to the Brazilian standard ABNT NBR 6118:2014 [71], considering a ductile failure, which means that reinforcement yields before concrete failure. Henceforward, these four beams will be called C30-00-D, C30-20-D, C30-50-D, and C30-100-D ("D" being a reference to “ductile failure”).

After that, to understand the impact of concrete strength on the structural performance, two other beams were produced, using the same reinforced section as before but using concrete with strength class C50. These beams were produced with 0% and 100% of mixed recycled aggregate, as presented in Chapter 4, and from now on, they will be called C50-00-D and C50-100-D, respectively.

Subsequently, two other beams, with 0% and 100% mixed recycled aggregate, were designed using concrete strength classes C30, but this time with an over-reinforced section to present a brittle failure (characterized by the crushing of concrete before the rebar yields). Thus, throughout this work, these two beams will be referred to as C30-00-B and C30-100-B, in reference to brittle failure (“B”).

A pull-out test was also conducted to investigate the bond behavior between the steel rebar and the different concretes (C30-00, C30-20, C30-50, C30-100, C50-

00, and C50-100). The purpose of this test was to complement the understanding of the four-point bending test results (performed for the six beams described above).

Finally, to investigate the applicability of the Brazilian standard ABNT NBR 6118:2014 [71] to beams made with mixed recycled aggregate, the experimental results were compared to the theoretical equations, mainly concerning the cracking moment and crack opening.

Figure 5-1 illustrates the experimental program related to the flexural behavior of reinforced concrete beams made with mixed recycled aggregate.

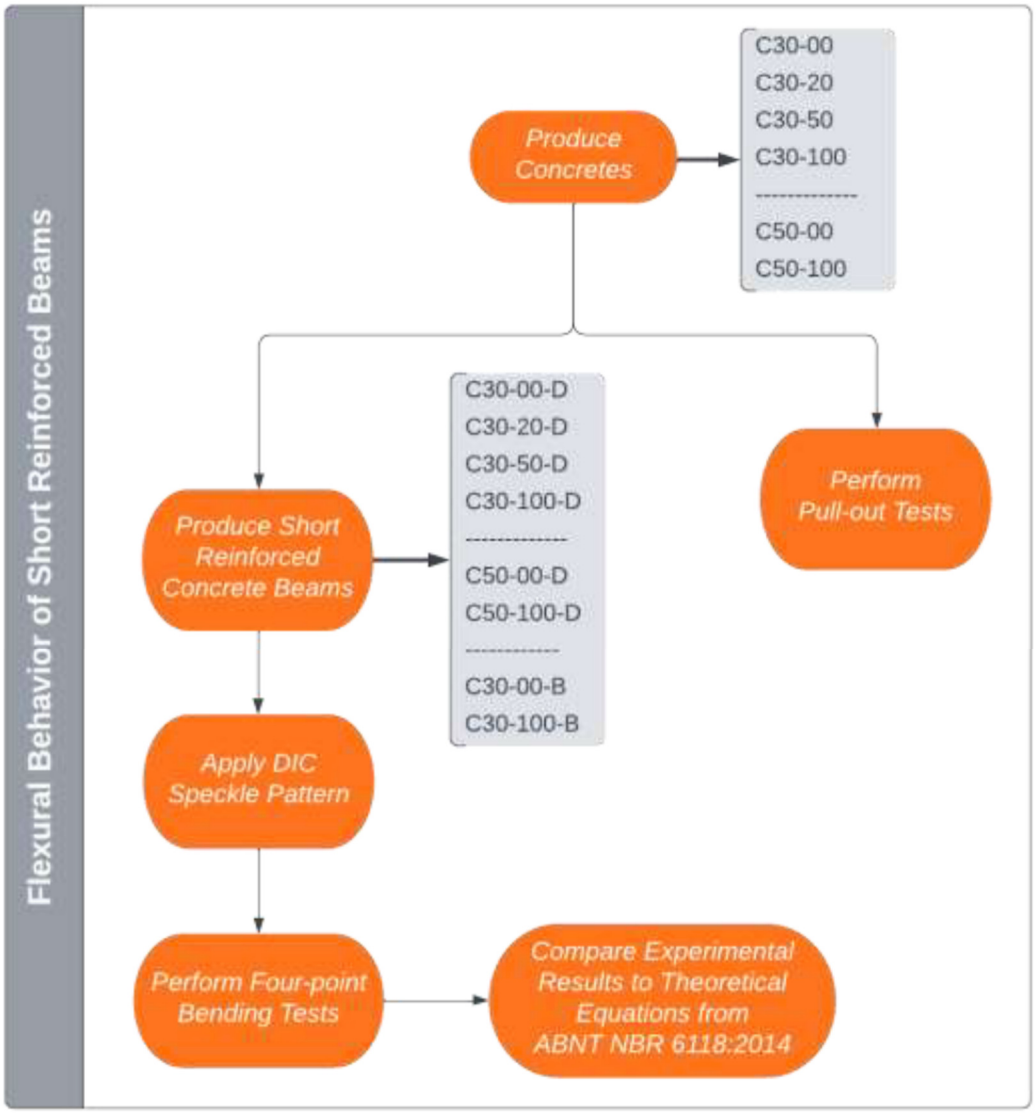

Figure 5-1. Experimental Program – Flexural behavior of short reinforced concrete beams made with mixed recycled aggregate**.**

5.2.1. Four-point Bending Test

The flexural performance was evaluated through a four-point bending test of simply supported beams with a rectangular cross-section of 120 x 150 mm (width x height) and 1200 mm in length. This test generates a constant bending moment at the beam's midspan, where maximum strains, moments, and deflections occur.

A 500 kN servo-hydraulic MTS actuator mounted in a steel test frame was used to apply the load to a metallic frame. A hinge was positioned between the actuator and the metallic frame to avoid any uneven load applied by the actuator. The metallic frame distributed the applied load to two rollers positioned in the central third of the beams, generating a region of constant bending moment.

Digital Image Correlation (DIC) technique was used to understand the crack evolution process better. A speckle pattern was created on the surface of the beams in the Area of Interest (AOI) located between the load application points. Tiny black dots (made with spray paint) were randomly applied over a white background to create this pattern. For all beams, pictures for the DIC technique were taken each 10s using a CANON camera.

The load was applied for all beams using a displacement control method with a 1.0 mm/min rate. The deflection was measured by three LVDTs, placed at the beam's midspan and towards each load application point to confirm the experimental data registered by the midspan displacement transducer. A strain gauge was placed in the mid-length of each flexural reinforcement bar to register the steel strains. Also, the concrete beams' upper and bottom faces were instrumented with strain gauges to measure the midspan concrete strains.

Beams designed for ductile failure (C30-00-D, C30-20-D, C30-50-D, C30-100-D, C50-00-D, and C50-100-D) were positioned on rollers located 50 mm from the beam edges, with freedom of horizontal movement, resulting in a clear span of 1100 mm, a flexural span of 370 mm, and two symmetrical shear spans of 365 mm. The flexural reinforcement was made with two 8 mm ribbed steel bars (reinforcement ratio of 0.5%) CA-50 with a yield strength of 500 MPa [276]. All beams were reinforced with sufficient transversal reinforcement to prevent shear failure (stirrups of 6.3 mm every 15 cm, except for the central span) (**Figura 5-2**).

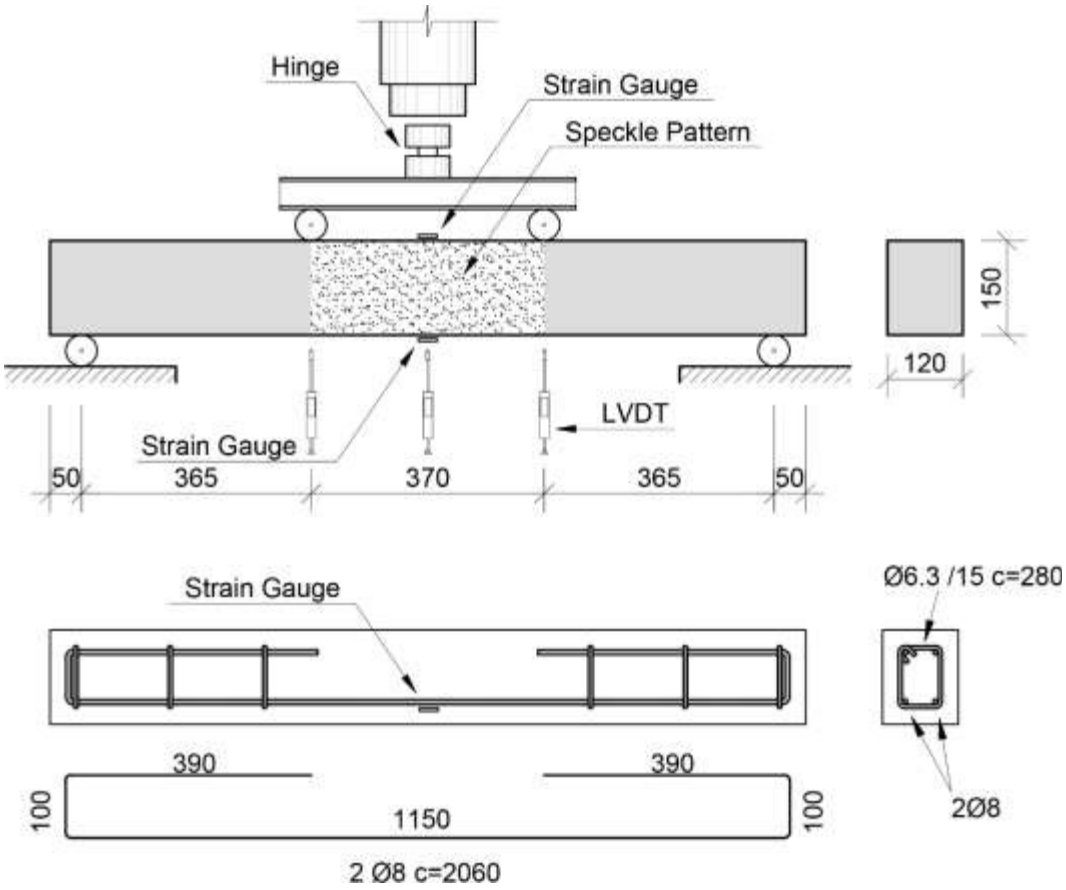

Figure 5-2. Setup and reinforcement of beams designed for ductile failure (in mm).

Figure 5-3 shows the setup and the reinforcement of beams designed for brittle failure (C30-00-B and C30-100-B). These beams were positioned on rollers located 100 mm from the beam edges, with freedom of horizontal movement to avoid shear failure. Thus, the clear span was 1000 mm, the flexural span was 340 mm, and the two symmetrical shear spans were 330 mm. To ensure the beams had a brittle failure, the flexural reinforcement was made with two 16 mm ribbed steel bars (reinforcement ratio of 2.2%) CA-50 with a yield strength of 500 MPa [276]. The region of the supports was reinforced with stirrups of 6.3 mm every 7.5 cm, except for the central span, to prevent shear failure. Compression longitudinal bars of 6.3 mm favored the distribution of stirrups.

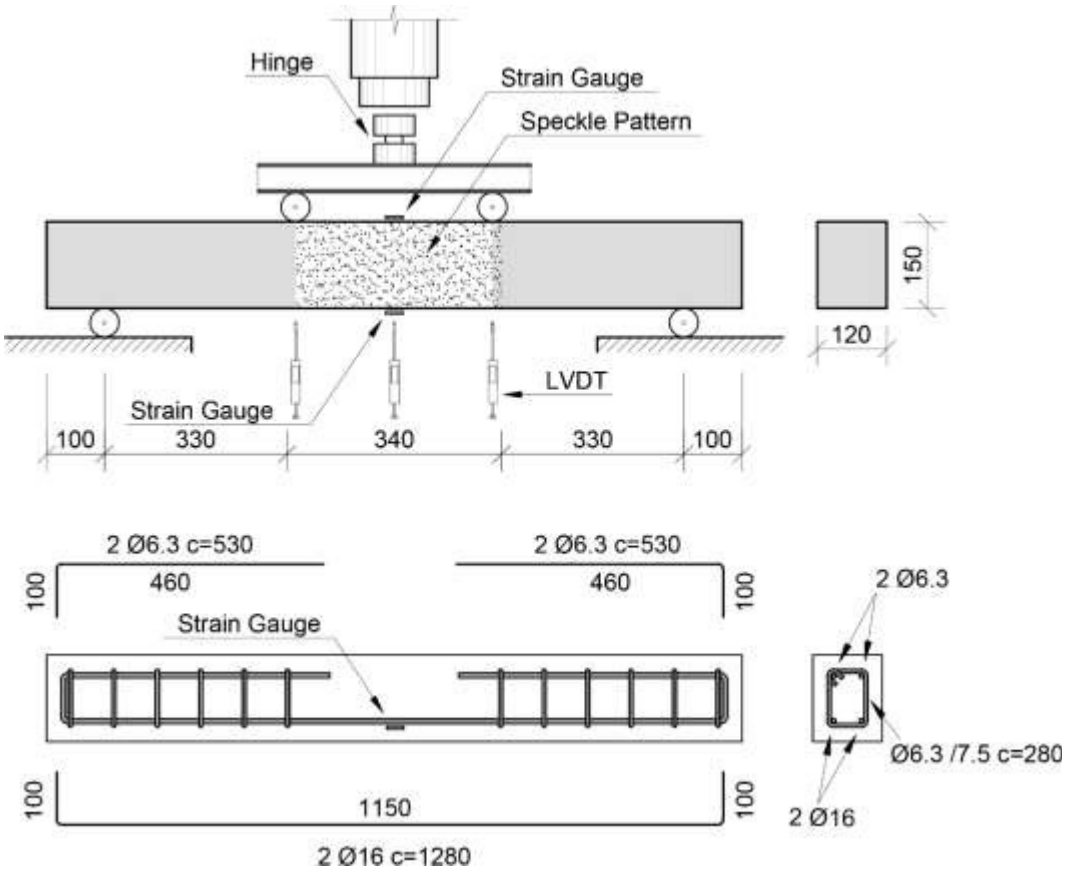

Figure 5-3. Setup and reinforcement of beams designed for brittle failure (in mm).

The wooden formworks were manufactured in 30 mm naval plywood. They all underwent a dimensional inspection before each concreting, resulting in elements varying ± 2 mm in their dimensions. Before pouring the concrete, plastic reinforcement spacers were positioned to ensure a 25 mm concrete cover, the formworks were positioned on a leveled base, and a release agent was applied.

Concrete was poured directly onto the formworks with a metallic ladle, varying the placement points. For every third of the volume of concrete placed, a manual concrete vibrator was used to avoid trapping air on the internal surfaces. For beams C30-00-B and C30-100-B, because of the over-reinforcement, a concrete vibrating table was necessary. After pouring the concrete, a screeding tool was used to flatten the wet concrete. **Figure 5-4** shows the reinforcement of beam C30-00-D positioned at the wooden formworks and the beams C30-00-D, C30-20-D, and C30-50-D after concrete pouring. The stripping of formwork was carried out after the first day of age, followed by wet curing for 28 days.

Figure 5-4. Reinforcement positioned at wooden formwork and beams after concrete pouring.

The mixing process was performed in a 30-liter planetary mixer. The beams were demolded 24h later and taken to a humid chamber. After 28 days of curing, the beams were kept for 24 hours in a dry place so that it was possible to apply the DIC speckle pattern. The four-point bending tests were carried out 30 days after molding.

Figure 5-5 shows a beam positioned for the four-point bending test, while **Figure 5-6** presents the LVDTs and the base painting for monitoring by a digital image correlation system (DIC).

Figure 5-5. Beam positioned for the four-point bending test.

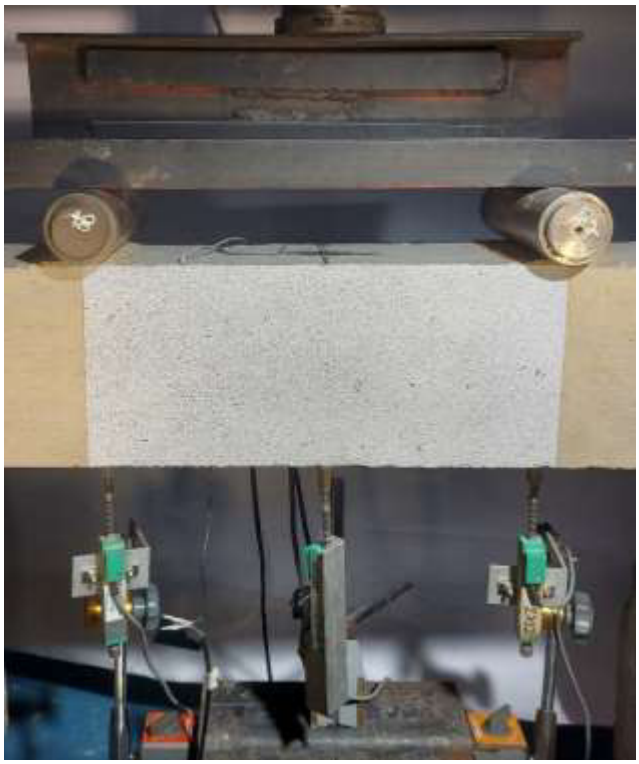

Figure 5-6. Detail of the LVDTs and speckle pattern for DIC.

5.2.1. Pull-out Test

The pull-out tests were performed using a setup adapted from RILEM recommendations [277]. For this investigation, ϕ8 mm ribbed steel bars CA-50 were used. The steel bars were rust-free. The molds measured 150 x 150 x 150 mm, and an embedment length of 10ϕ (i.e., 80 mm) was adopted.

A 30-liter planetary mixer was used to manufacture six specimens for each designed concrete. The specimens were cast with the steel rebar in a horizontal position to simulate the situation of end rebar anchorage in concrete beams. All the specimens were demolded a day after pouring and transferred to a humid chamber for 28 days.

For the pull-out test, a 500 kN servo-hydraulic MTS actuator was used. The specimens were placed in a cage, attached to the actuator's superior claw by its upper end. The specimen rebar was anchored to the actuator's inferior claw. Two 10 mm LVDTs were used: one measured the displacement between the specimen and the cage, while the other recorded the displacement of the free end of the steel bar embedded in the concrete (i.e., the slip between the steel rebar and the concrete). Under different loading levels, the relative displacement between the steel rebar and the concrete was computed by the difference between the two LVDTs. The test was

performed under a machine displacement control rate of 0.5 mm/min until reaching 10 mm slip. **Figure 5-7** and **Figure 5-8** show the setup for the pull-out test and test photos, respectively.

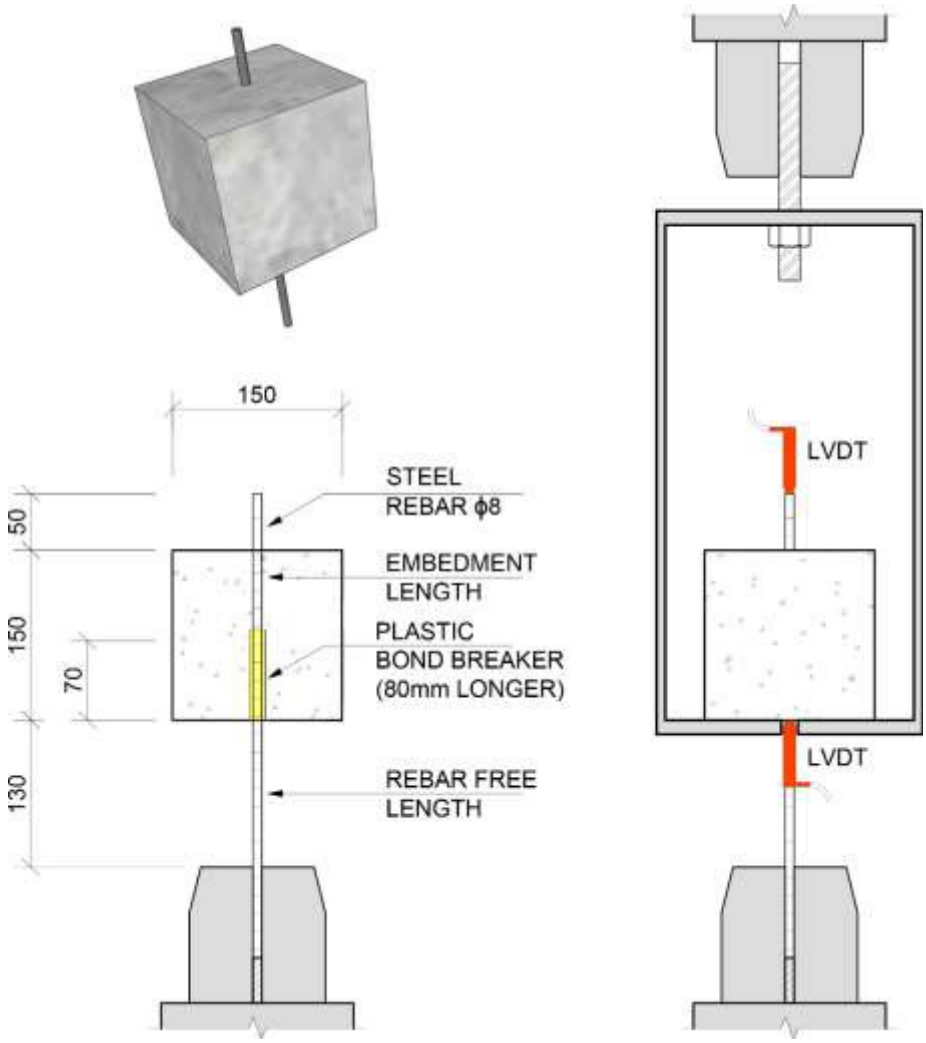

Figure 5-7. Pull-out test setup and specimens' details (in mm).

Figure 5-8. Pull-out test photos.

When ribbed bars are used, the ribs provide a mechanical interlock that allows the development of greater bond stress after overcoming the chemical adhesion. This mechanical interlock provides bearing force against the face of the bar ribs.

The bond stress-slip diagram can be divided into five stages (**Figure 5-9**). There is a short non-slip straight line section at the initial loading stage, mainly due to the chemical adhesion and friction between the steel bar and the concrete (stage 1). When the loading increases, the chemical adhesion between the rebar and concrete fail, and the rebar and concrete produce a relatively slight slip (stage 2). As the load increases, radial splits appear around the rebar due to the radial pressure exerted by the rebar ribs (stage 3). When the ultimate bond stress (τ_f) is reached, the shear-cut slip along the rib diameter occurs. Then, the bond stress decreases quickly, and the slip amount increases rapidly (stage 4). When the slip amount reaches a certain value, the concrete between the ribs is completely cut-off. At this time, the bond stress did not keep decreasing; from this point, the residual bonding stress (τ_f) is only provided by the friction between the steel bar and the surrounding concrete (stage 5).

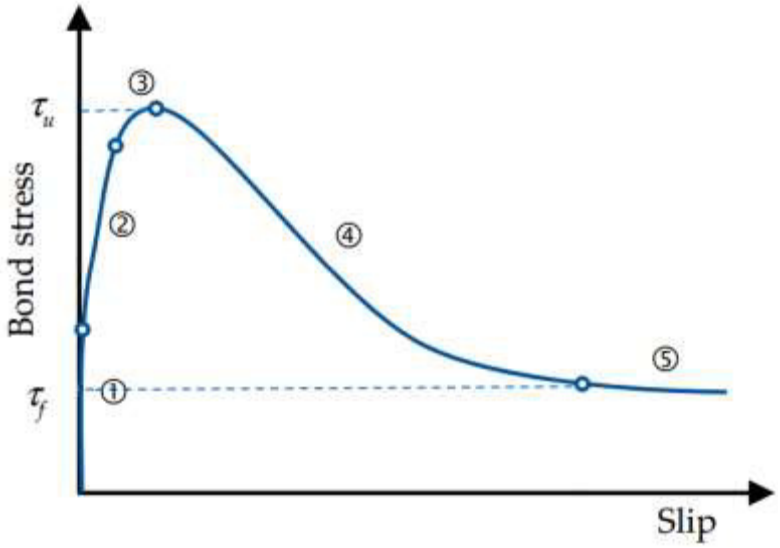

Figure 5-9. Typical bond stress-slip diagram considering ribbed steel bars (adapted from [278]).

The bond stress in the pull-out test can be considered constant along the length of the steel bar embedded in the concrete. The bond stress (τ) is obtained by dividing the applied load by the nominal anchorage surface (**Eq. 5-1**):

$$\tau = \frac{P}{\pi \cdot \emptyset \cdot l_b} \qquad \textbf{Eq. 5-1}$$

Where:

τ is the bond stress (MPa);

P is the applied load (N);

l_b is the embedment length (mm);

$\emptyset$ is the rebar diameter (mm).

5.3. Results and Discussions

Figure 5-10 and **Figure 5-11** show the diagrams of the moment–midspan deflection of the C30-00-D, C30-20-D, C30-50-D, C30-100-D, C50-00-D, and C50-100-D concrete beams, all of them designed for ductile failure.

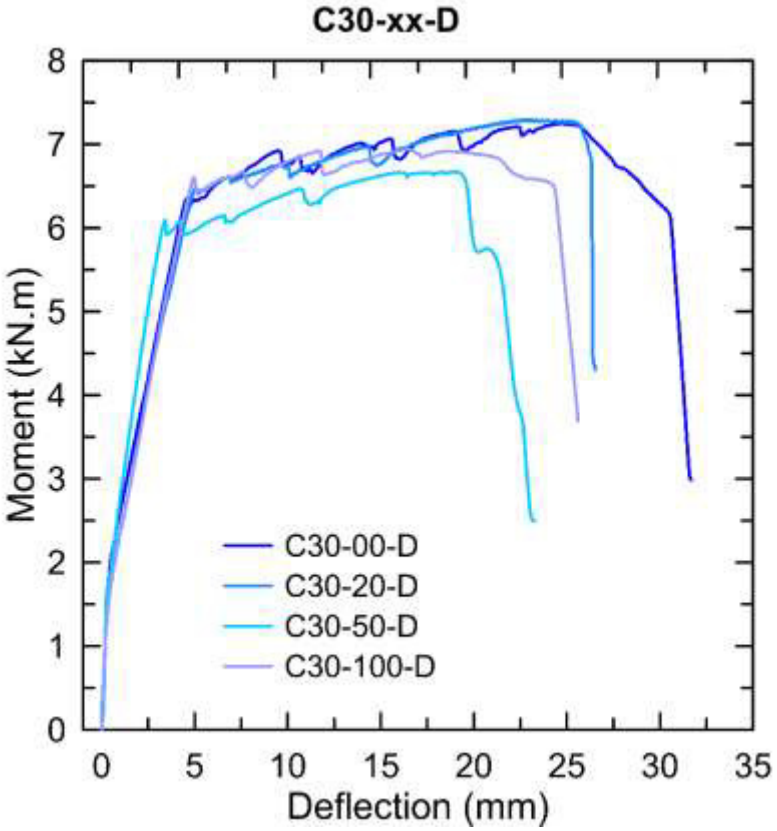

Figure 5-10. Moment–deflection at midspan of beams made with concrete strength class C30 designed for ductile failure (C30-00-D, C30-20-D, C30-50-D, and C30-100-D). X

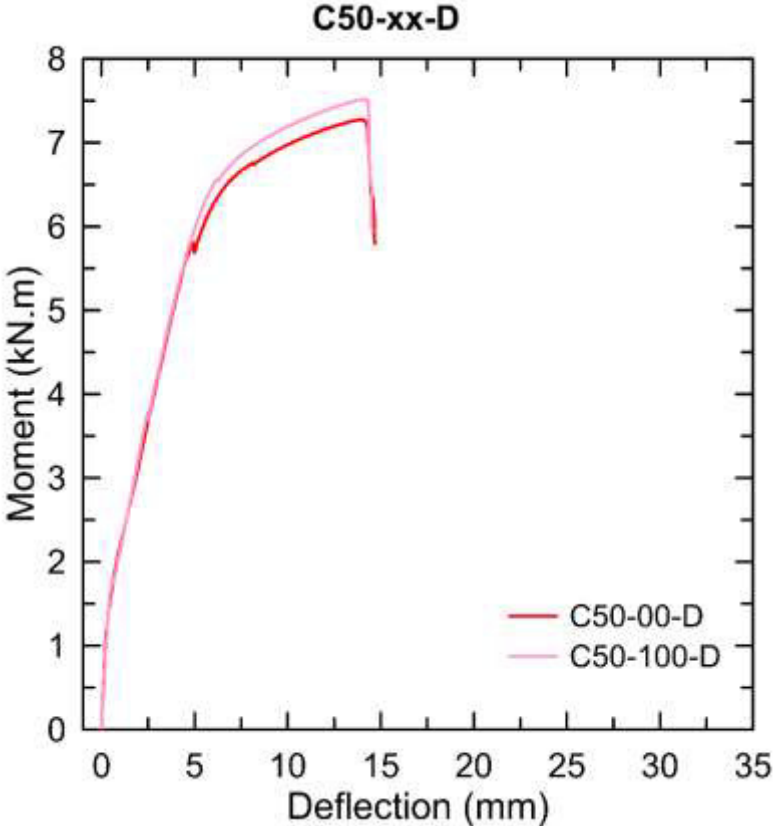

Figure 5-11. Moment–deflection at midspan of beams made with concrete strength class C50 designed for ductile failure (C50-00-D and C50-100-D).

Overall, a similar trend was observed for recycled and conventional concretes. All specimens showed nearly linear behavior before and after cracking until the onset of the yielding of the reinforcement bar. From that point, the specimens showed nonlinear behavior until culminating in their failure. All concrete beams failed in flexure due to the yielding of the longitudinal steel and the subsequent concrete crushing in the compression zone.

At first, by analyzing the moment–deflection diagrams (**Figure 5-10** and **Figure 5-11**), it is possible to observe that the behavior of all beams before cracking is practically the same. That is, it can be said that the initial uncracked stiffness of the beams is not affected by the concrete's content of mixed recycled aggregate.

For each specimen, the bending moments were calculated using the load registered at the midspan of the beam, where the maximum value occurs. **Table 5-1** presents the cracking moment (M_{cr}), yielding moment (M_{yiel}), and ultimate moment (M_{ult}) of beams designed for ductile failure (C30-00-D, C30-20-D, C30-50-D, C30-100-D, C50-00-D, and C50-100-D), as well as the moment related to the maximum deflection under serviceability conditions, named as $M_{l/250}$ [71]. Since the clear span of these beams was 1100 mm, $M_{l/250}$ corresponds to a deflection of 4.4 mm at the midspan. Considering this deflection value, the bending moments related to the maximum deflection under serviceability conditions $M_{l/250}$ were obtained directly from the moment-deflection diagrams (**Figure 5-10** and **Figure 5-11**). Accordingly, the cracking deflection (δ_{cr}), yielding deflection (δ_{yiel}), and ultimate deflection (δ_{ult}) were also presented in **Table 5-1**.

Table 5-1. Bending moments and deflections for beams designed for ductile failure.

	C30-00-D	**C30-20-D**	**C30-50-D**	**C30-100-D**	**C50-00-D**	**C50-100-D**
M_{cr} (kN.m)	1.97	1.68	1.63	1.60	2.70	2.63
$M_{l/250}$ (kN.m)	6.24	5.98	5.95	6.12	5.45	5.53
M_{yiel} (kN.m)	6.29	6.42	6.03	6.54	5.73	6.35
M_{ult} (kN.m)	7.25	7.30	6.67	6.94	7.27	7.51
δ_{cr} (mm)	0.47	0.36	0.28	0.43	1.54	1.45
δ_{yiel} (mm)	4.46	4.92	3.32	4.85	4.97	5.67
δ_{ult} (mm)	24.78	22.90	18.93	16.32	14.00	13.99
δ_{ult} / δ_{yiel}	5.56	4.65	5.71	3.36	2.82	2.47

Reductions of 15%, 17%, and 19% in cracking moments have been detected for C30-20-D, C30-50-D, and C30-100-D, respectively, compared to reference

beam C30-00-D. These reductions are consistent with the lower tensile strength of recycled concretes, which leads to an earlier cracking than conventional concretes.

Regarding the beams made with concrete of a higher concrete strength class (C50), the cracking moments are greater than those of recycled concrete beams C30. That is, C50 beams take longer to crack, which is consistent with the higher tensile strength of this concrete. In addition, it can also be noted that the reduction in the cracking moment between the reference beam C50-00-D and the beam made with 100% mixed recycled aggregate C50-100-D is only 6%. Thus, considering the cracking moment of the beams, the higher the strength class of concrete, the lower the impact of replacing natural aggregate with mixed recycled aggregate.

Regarding bending moment for maximum deflection under serviceability conditions ($M_{l/250}$), the variations between concrete with different amounts of mixed recycled aggregate can be considered negligible regardless of concrete strength class. That is, the complete replacement of the natural aggregate by the mixed recycled aggregate did not negatively impact the bending moment for maximum deflection under the serviceability conditions of the beams. Considering the previous analysis, it can be said that the serviceability characteristics of the beams were not significantly affected by the content of mixed recycled aggregate.

Furthermore, the difference in ductility ($\delta_{ult}/\delta_{yiel}$) can be considered negligible between reference beam C30-00-D and beams with up to 50% mixed recycled aggregate (C30-20-D and C30-50-D). The reduction in ductility is more clearly observed when the mixed recycled aggregate content is 100%, regardless of the concrete strength class (**Table 5-1**).

It is also possible to verify that there is essentially no difference between the ultimate moments (M_{ult}) and yielding moments (M_{yiel}) obtained for the reference beam and the recycled concrete beams, regardless of the strength class of the concrete and the content of mixed recycled aggregate (**Table 5-1** and **Figure 5-12**).

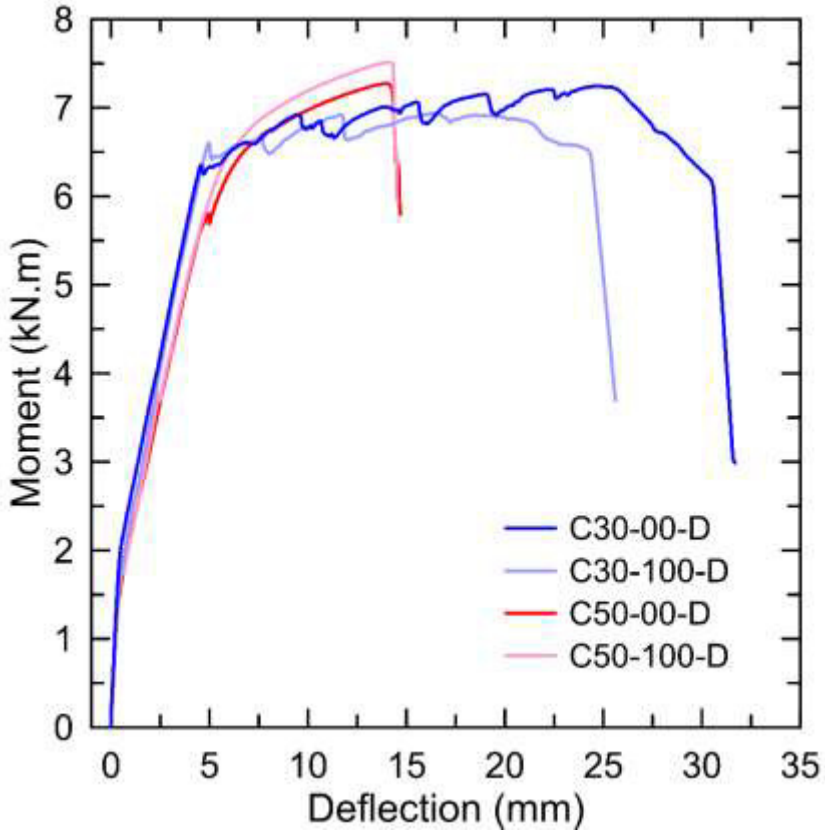

Figure 5-12. Comparison between the diagrams of the moment–midspan deflection of beams with 0% and 100% mixed recycled aggregate and concrete strength classes C30 and C50.

Considering that customary service conditions occur after cracking, the performance of the cracked cross-section was analyzed at 50% of the ultimate load. The strain diagrams of the cross-section after cracking were obtained using the experimental strains registered at the upper and bottom faces of the concrete beams and the average strain registered by the strain gauges placed in the midspan of each flexural reinforcement bar (**Figure 5-13**). According to the Bernoulli hypothesis for bending beams, these diagrams were drawn based on the assumption that plane sections remain plane after loading.

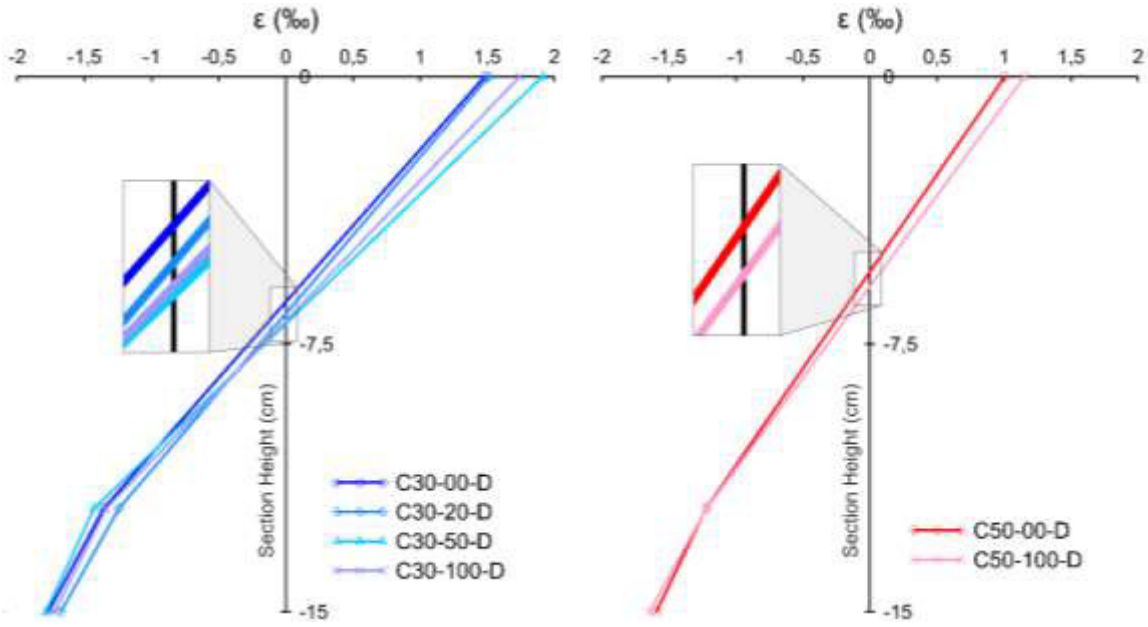

Figure 5-13. Strain diagrams in the mid-span section at 50% of ultimate load.

The distribution of strains across the mid-span section can be considered linear for all beams, proving the Bernoulli hypothesis. Small differences were observed between beams regarding the depth of the compression zone. For beams made with concrete strength class C30, the depth of the compression zone ranged from 6.3 to 6.9 cm, while for beams made with concrete strength class C50, it varied from 5.4 cm to 5.9 cm. Despite these small differences, regardless of the concrete strength class, the depth of the compression zone increases as the content of mixed recycled aggregate increases. This difference can be attributed to the lower modulus of elasticity of recycled concrete (especially noticeable with high replacement percentages), which leads to greater deformations at the compression zone of the beam, and, consequently, to an increase in depth of the compression zone.

Figure 5-14 presents the load-deflection relationship along the beams at different loading stages. The three LVDTs on the beam's bottom face measured the deflection levels. For all beams, constant load values of 10kN, 20kN, and 30kN were analyzed, as well as loads equivalent to the respective reinforcement yielding and ultimate load.

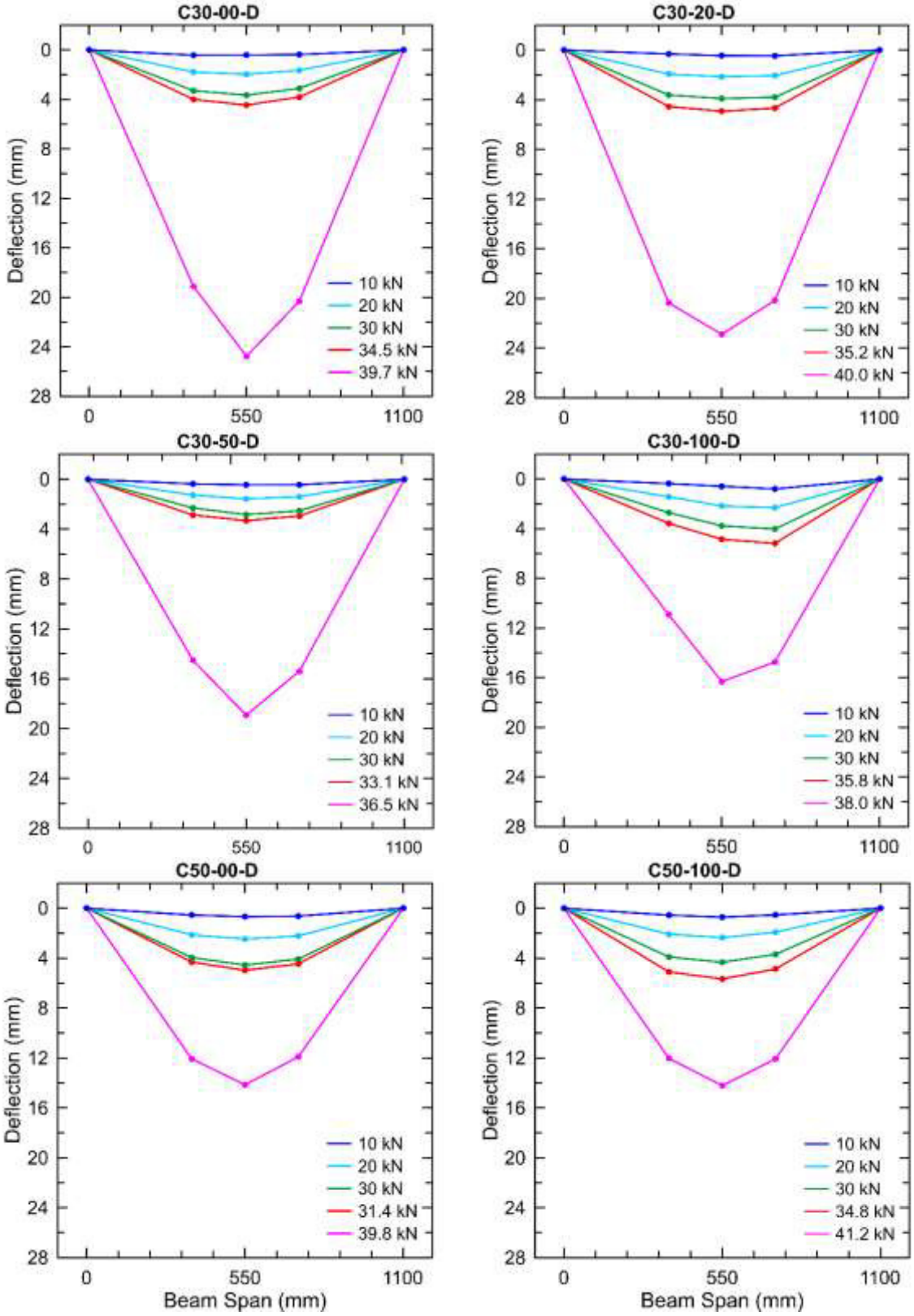

Figure 5-14. Load-deflection for beams C30-xx-D and C50-xx-D at different load stages.

At 10 kN, with already cracked concrete, all beams presented a linear behavior and very similar values of deflections, despite de content of mixed recycled aggregate and the concrete strength class. For concrete strength class C50,

almost no difference was observed between the deflections obtained for the beams, regardless of the applied load. For concrete strength class C30, deflections of all beams are similar up to the reinforcement yielding load. However, because of the higher deformability of mixed recycled concrete (due to its lower modulus of elasticity), mixed recycled concrete beams were expected to present higher deflections than conventional concrete beams. To further understand these tendencies, beams with a higher reinforcement ratio were produced, seeking a brittle failure governed by the concrete.

Figure 5-15 shows the moment–midspan deflection diagrams obtained for the beams C30-00-B and C30-100-B. Meanwhile, **Table 5-2** presents the cracking moments (M_{cr}), ultimate moments (M_{ult}), bending moments related to the maximum deflection under serviceability conditions ($M_{l/250}$), cracking deflections (δ_{cr}), and ultimate deflections (δ_{ult}). For these beams C30-00-B and C30-100-B, since the clear span was 1000 mm, the bending moment related to the maximum deflection under serviceability conditions ($M_{l/250}$) corresponds to a deflection of 4.0 mm at the midspan.

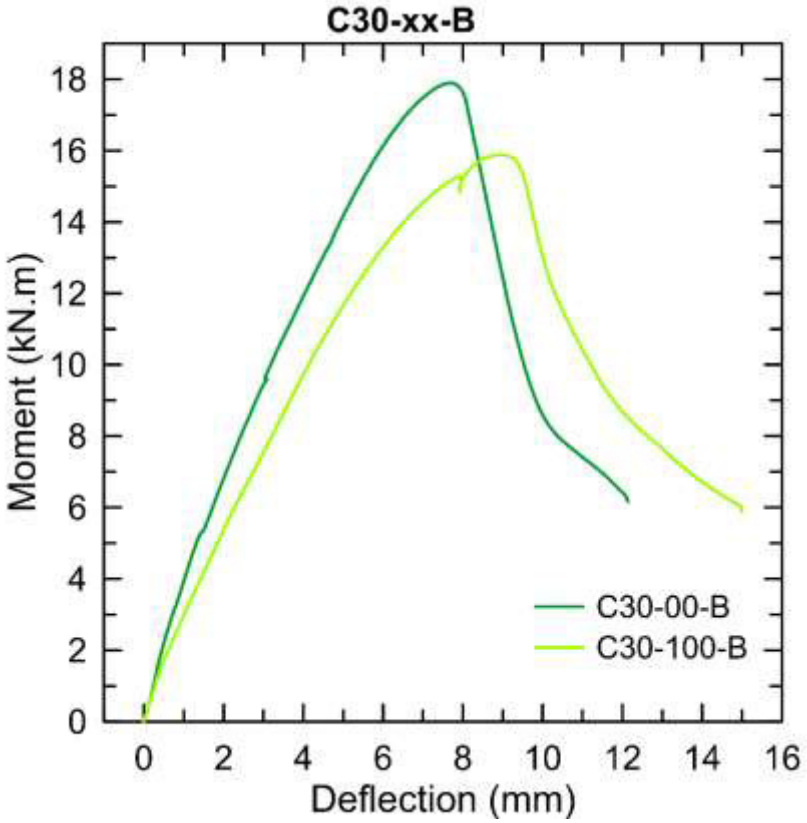

Figure 5-15. Moment–deflection at midspan of beams made with concrete strength class C30 designed for brittle failure (C30-00-B and C30-100-B).

Table 5-2. Bending moments and deflections at midspan for beams designed for brittle failure.

	C30-00-B	C30-100-B
M_{cr} (kN.m)	2.29	1.94
$M_{l/250}$ (kN.m)	11.92	9.72
M_{ult} (kN.m)	17.90	15.88
δ_{cr} (mm)	0.59	0.63
δ_{ult} (mm)	7.67	8.92

Figure 5-16 shows the moment-rebar strain obtained for all beams in this study. For each beam, the rebar strain was calculated from the average of the values obtained for the strain gauge placed in the midspan of each flexural reinforcement bar. The diagram shows that the reinforcement does not yield for beams C30-00-B and C30-100-B, unlike what happens for the other beams. This confirms that these over-reinforced beams C30-00-B and C30-100-B failed in compression without reinforcement yielding, confirming the brittle failure for which they were designed.

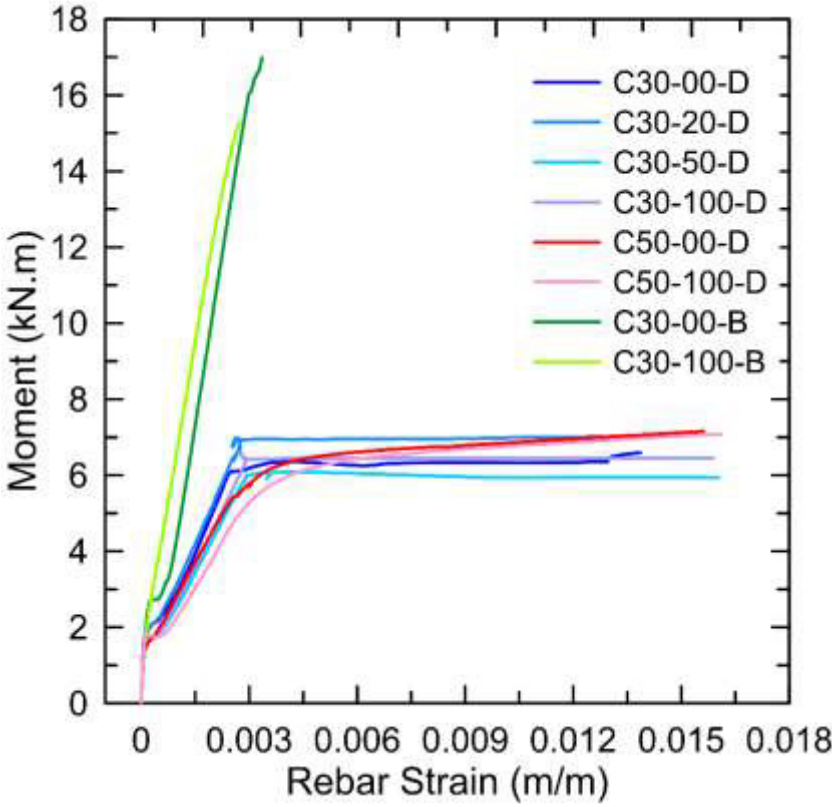

Figure 5-16. Moment–rebar strain diagram.

As for beams designed for ductile failure, in the case of beams designed for brittle failure, it is also possible to observe in **Table 5-2** an earlier cracking for the mixed recycled aggregate beam (C30-100-B) when compared to the reference beam (C30-00-B). For the beam with 100% mixed recycled aggregate C30-100-B, the

cracking moment (M_{cr}) was reduced by 15% compared to the reference beam C30-00-B.

Regarding bending moments related to the maximum deflection under serviceability conditions ($M_{l/250}$) and ultimate moments (M_{ult}), reductions of 18% and 11% are observed, respectively, between the 100% mixed recycled aggregate beam (C30-100-B) and the reference beam (C30-00-B) (**Table 5-2**).

Figure 5-17 presents the load-deflection relationship along the beams C30-00-B and C30-100-B at different loading stages. The three LVDTs on the beam's bottom face measured the deflection levels. For all beams, constant load values of 10kN, 20kN, and 30kN were analyzed, as well as the load equivalent to the respective ultimate load. Even at lower loading stages, it is possible to observe that the beam made with 100% of mixed recycled aggregate presents higher deflections than the reference beam.

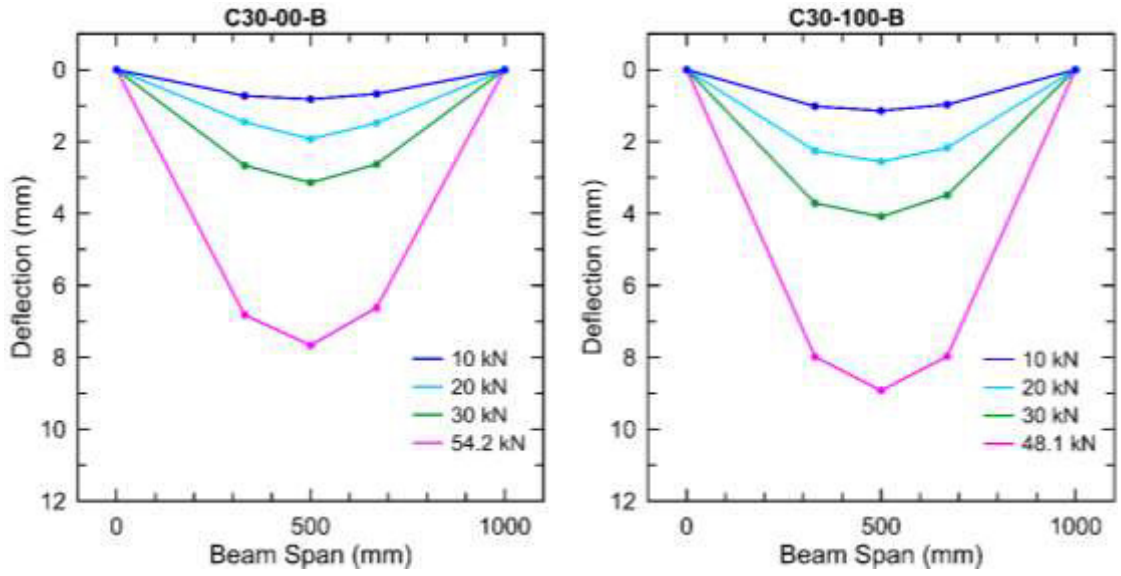

Figure 5-17. Load-deflection relationship along the beams C30-00-B and C30-100-B at different load stages.

These more accentuated differences in bending moments and deflections found between the beams C30-00-B and C30-100-B can be explained by the fact that these beams are over-reinforced, i.e., they were designed to present a brittle failure, characterized by the crushing of concrete before the rebar yields. Since concrete produced with 100% mixed recycled aggregate has lower compressive strength, lower modulus of elasticity, and lower tensile strength, it is natural that beams produced with this concrete and over-reinforced (i.e., designed for brittle failure) present lower bending moments and higher deflections when compared to

the beam produced with conventional concrete. Thus, it can be said that in the case of the beams designed for brittle failure, since the concrete governs flexural behavior, the replacement of the natural aggregate by the mixed recycled aggregate causes a greater impact.

Also, when comparing beams produced with the same type of concrete (same concrete strength class and same content of mixed recycled aggregate), the ultimate moment (M_{ult}) increases considerably as the reinforcement ratio increases. The ultimate moment of beam C30-00-B is 147% higher than beam C30-00-D. Between beams with 100% mixed recycled aggregate, there was an increase of 129% for the ultimate moment of beam C30-100-B compared to beam C30-100-D. Likewise, when comparing beams produced with the same type of concrete, there is a large reduction in ultimate deflection (δ_{ult}) as the reinforcement ratio increases. Beam C30-00-B presents an ultimate deflection 69% lower than beam C30-00-D, while beam C30-100-B presents an ultimate deflection 45% lower than beam C30-100-D.

On the other hand, for the same type of concrete, using a higher reinforcement ratio leads to scarce differences in deflection at serviceability. Considering 50% of the ultimate load, the deflection of beams designed for brittle failure is less than 20% lower than beams designed for ductile failure. Thus, in agreement with Ignjatovic et at. [63], the results show that the analysis of deflections at serviceability in a concrete beam cannot be related only to material properties (i.e., modulus of elasticity) in a straightforward manner. For a more accurate analysis, other factors should be considered, such as the reinforcement ratio and the combined effect of the different elements that can influence the concrete deflections (reinforcement ratio, concrete cover, modulus of elasticity of concrete, and modulus of elasticity of reinforcement steel).

The most significant difference between beams C30-00-B and C30-100-D was the scale of concrete damage at failure. With the increase in the content of mixed recycled aggregate, the failure surface's size and the concrete destruction level increased (**Figure 5-18**). The explanation is found in mixed recycled aggregate concrete's much more complicated microscopic structure than conventional concrete. Considering only the cementitious fraction of the mixed recycled aggregate, as explained in Section 2.4.2.1, there is an old ITZ between the natural aggregate and the old adhered mortar, which is very porous and has pre-

existing cracks. Also, the ceramic fragments of the mixed recycled aggregate have lower strength than the natural aggregate present in conventional concrete. These characteristics probably cause higher concrete destruction of the mixed recycled aggregate concrete beam at failure than the beam made with only natural aggregates.

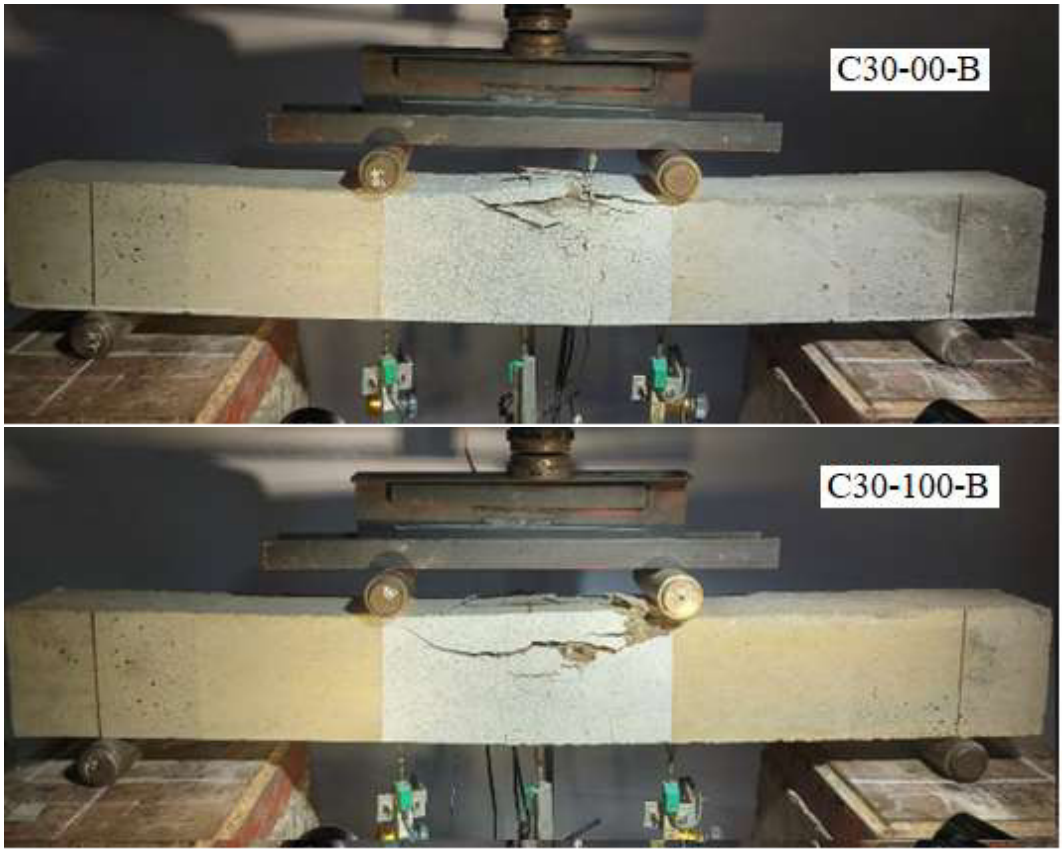

Figure 5-18. Beams C30-00-B and C30-100-B at failure.

As mentioned in Section 5.2, the Digital Image Correlation (DIC) technique was also used to understand the beams' crack evolution during the four-point bending test. **Figure 5-19** to **Figure 5-24** show the crack pattern of beams at two different loading levels: at 50% of the ultimate moment and ultimate moment, respectively.

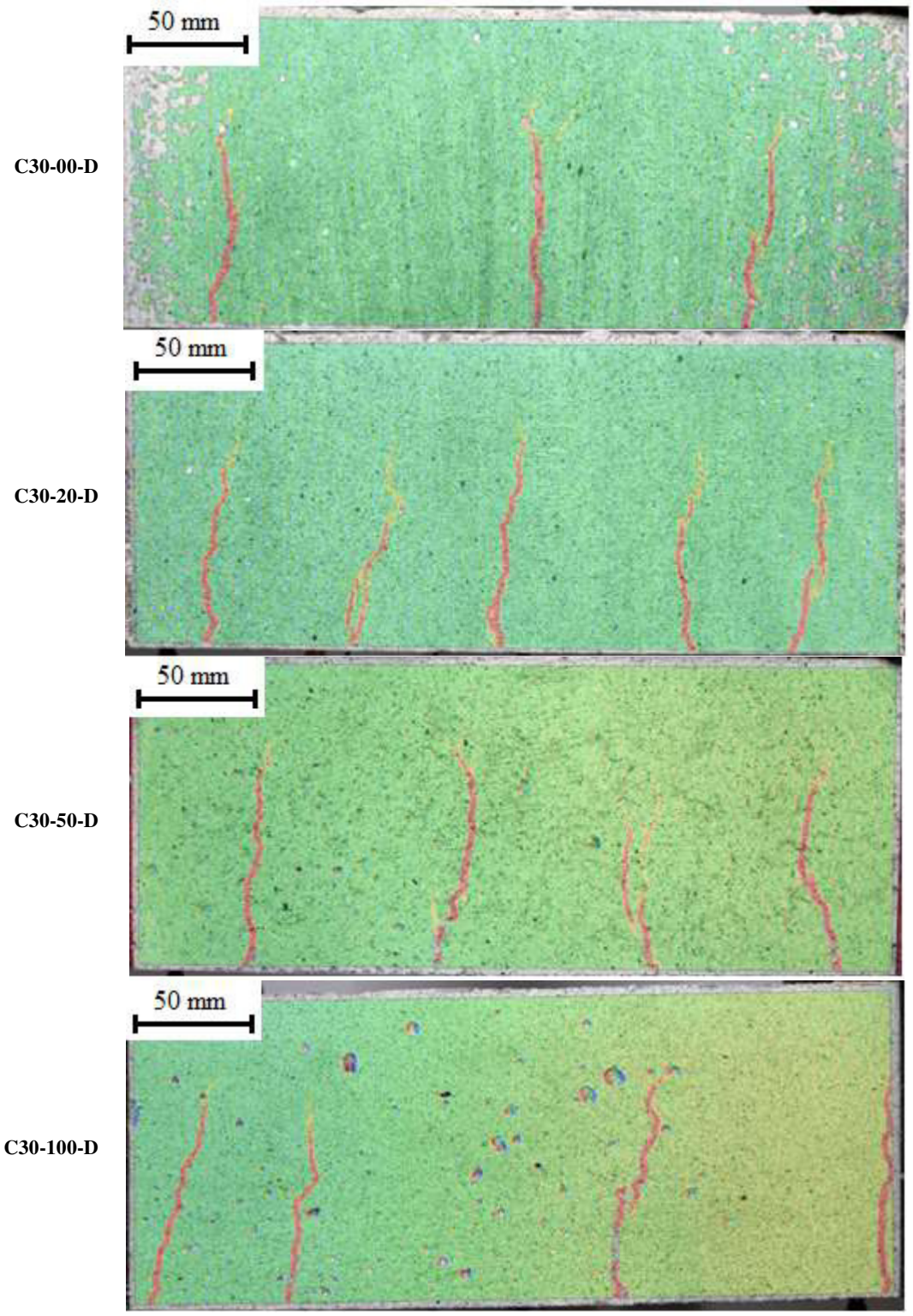

Figure 5-19. Crack distribution at the beams C30-xx-D at 50% of the ultimate moment.

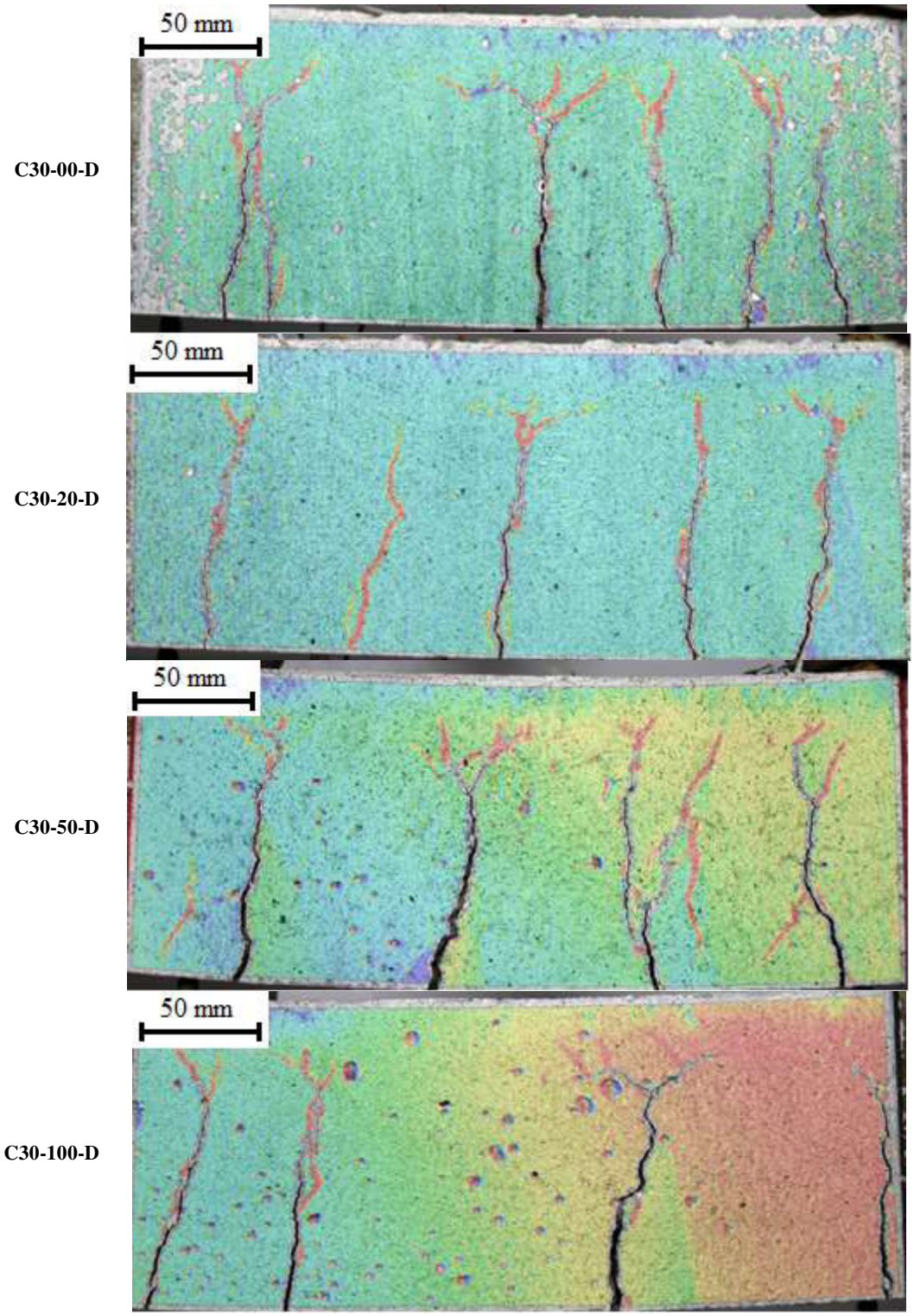

Figure 5-20. Crack distribution at the beams C30-xx-D at the ultimate moment.

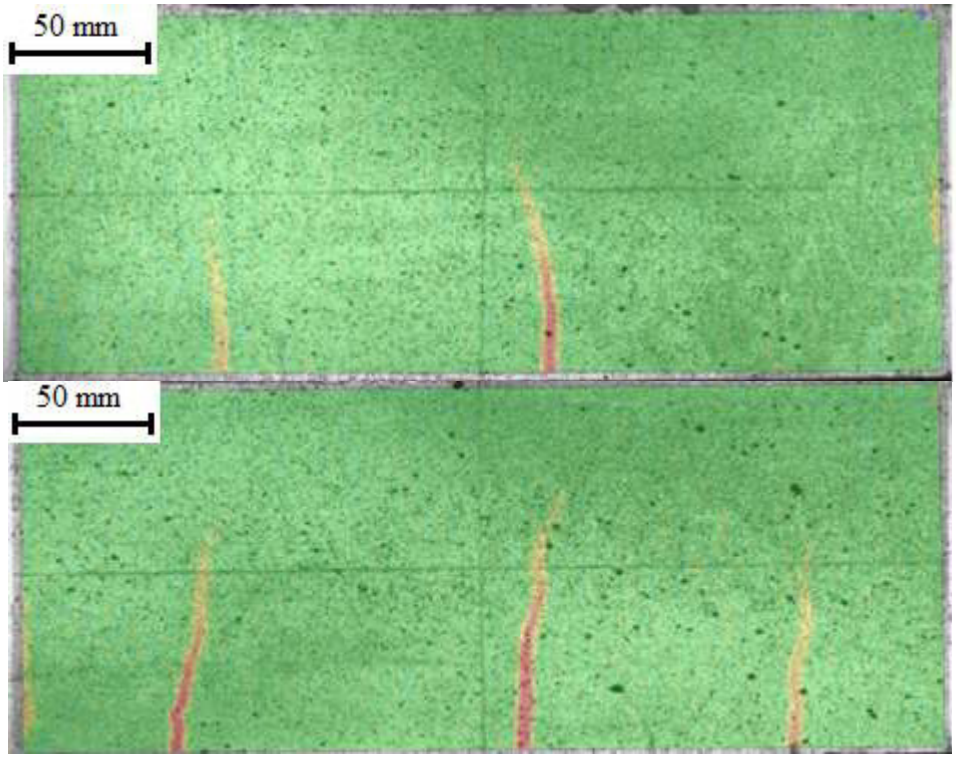

Figure 5-21. Crack distribution at the beams C50-xx-D at 50% of the ultimate moment.

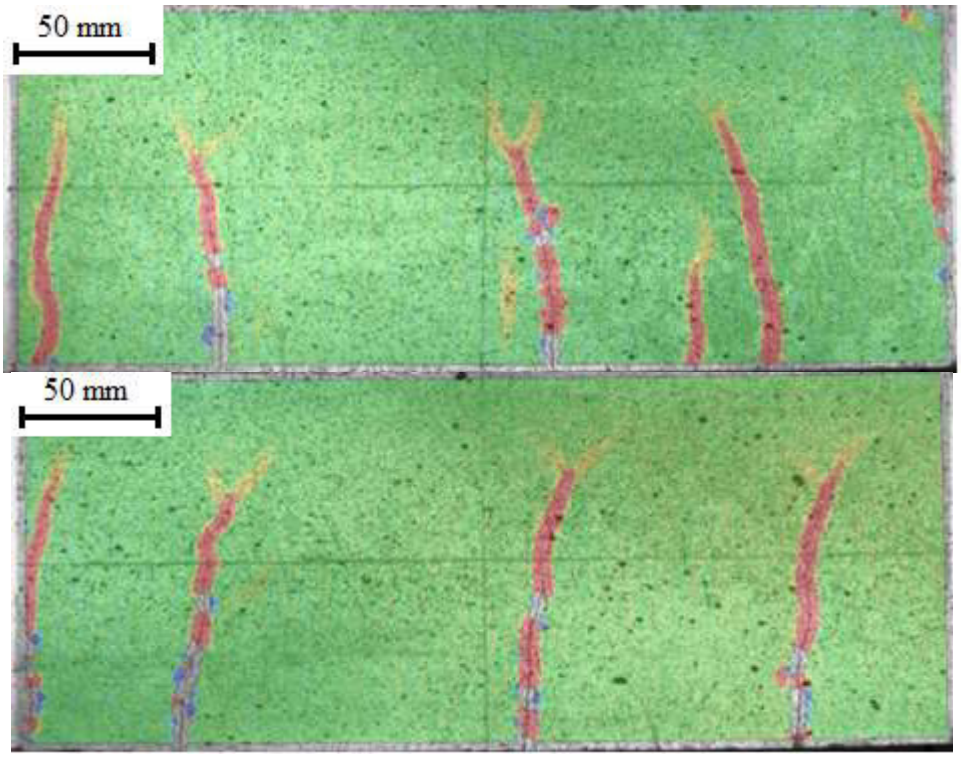

Figure 5-22. Crack distribution at the beams C50-xx-D at the ultimate moment.

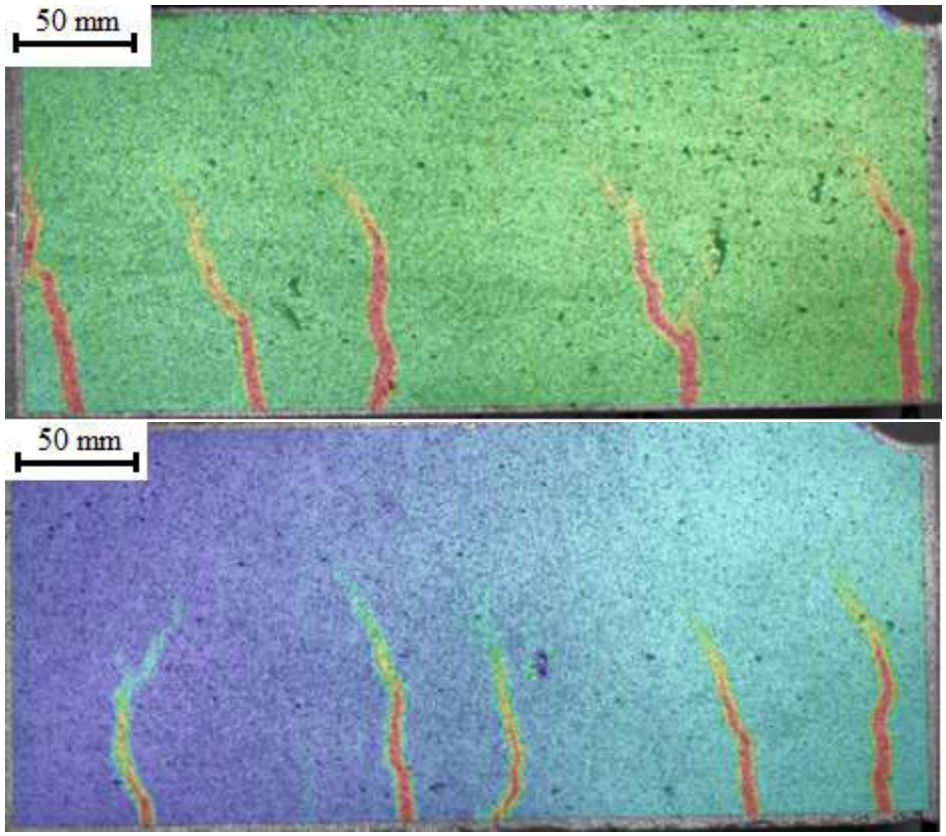

Figure 5-23. Crack distribution at the beams C30-xx-B at 50% of the ultimate moment.

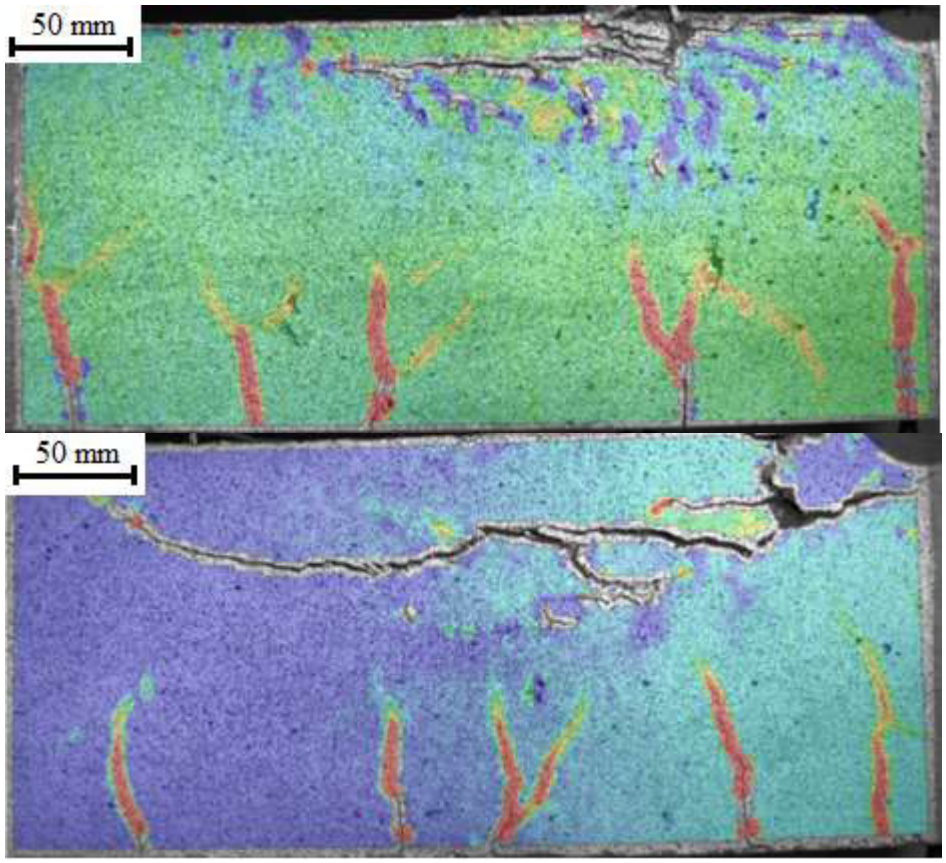

Figure 5-24. Crack distribution at the beams C30-xx-B at the ultimate moment.

The crack development of all concrete beams began with the appearance of flexural cracks at the middle section. For beams designed for ductile failure (C30-00-D, C30-20-D-, C30-50-D, C30-100-D, C50-00-D, and C50-100-D), cracks grew vertically until the beams failed. Meanwhile, for beams designed for brittle failure (C30-00-B and C30-100-B), cracks grow only half of the beam height in the final loading stage. At the ultimate moment, the concrete failure is observed.

In addition, for the same load application, the number of cracks does not vary substantially as the content of mixed recycled aggregate increases. Thus, in general, through visual analysis, it is possible to say that the development of cracking is not significantly affected by the replacement of natural aggregate by mixed recycled aggregate.

Figure 5-25 presents the moment-average crack opening diagram until the ultimate moment, while **Figure 5-26** shows a magnification of this same diagram to allow a better observation of the crack opening of each beam.

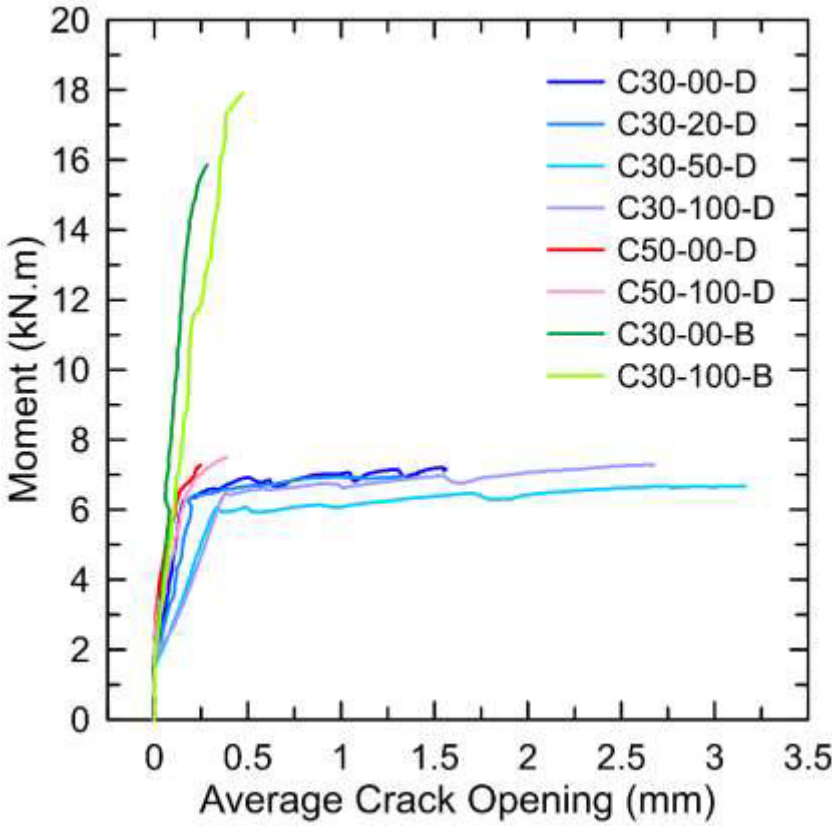

Figure 5-25. Moment-average crack opening diagram until the ultimate moment.

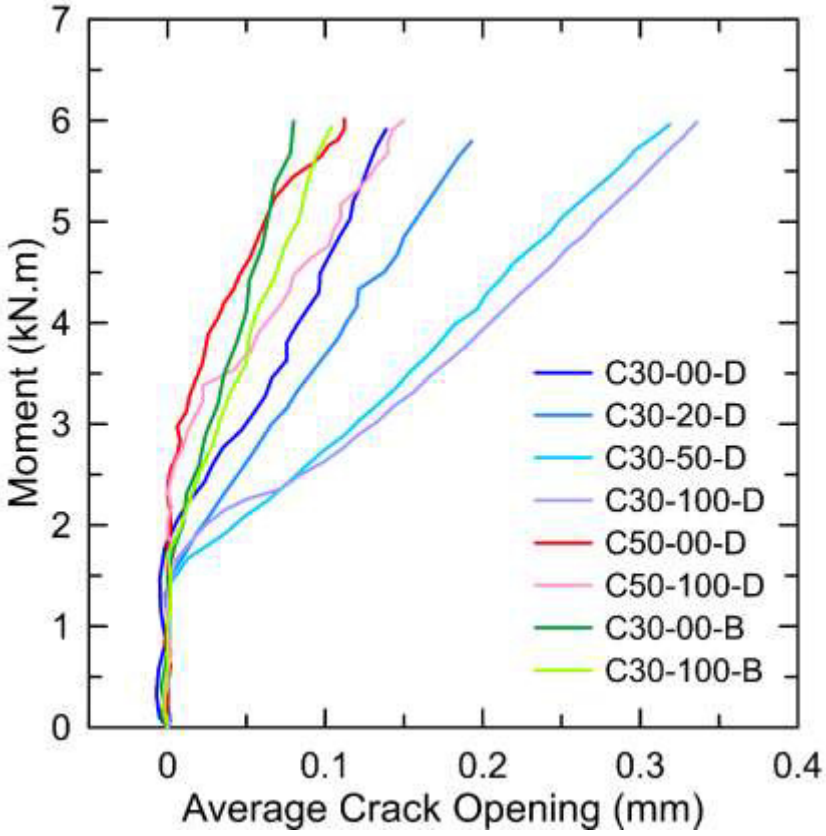

Figure 5-26. Magnification of moment-average crack opening diagram.

When the beams are over-reinforced (group B), the average crack opening practically does not vary with the increased content of mixed recycled aggregate. In addition, the over-reinforced beams (group C30-B) present smaller crack openings than those with the same concrete strength class and a lower reinforcement ratio (group C30-D). Because of their higher reinforcement ratio, the over-reinforced beams (group C30-B) have a higher strength on their face subjected to tensile, consequently less deflection, and thus smaller crack openings.

The variation in the crack openings with increasing content of mixed recycled aggregate is remarkable for the beams designed for ductile failure (groups C30-D and C50-D). As the content of mixed recycled aggregate increases, crack opening also increases. Cement-based recycled aggregates have a layer of residual mortar adhered to the original aggregate, which is usually a weak interface in the recycled aggregate composition, constituting an easier path for crack propagation. Thus, the crack tends to break the aggregate instead of going around the aggregate. In the case of mixed recycled aggregates, there are also ceramic fragments, which are more fragile and break as the cracks open. This may lead to a reduction in the contribution

of the aggregate interlock, which essentially depends on the points of contact between the faces of the crack [279].

In addition, the increase in the crack opening is more substantial for beams C30. Concrete C50 (even when made with 100% mixed recycled aggregate) has greater tensile splitting strength, greater modulus of elasticity, and greater stiffness than concrete C30. Therefore, the beams C50 present smaller crack openings than the beams C30.

Another characteristic that may affect the crack opening in beams produced with mixed recycled aggregate is the bond strength between the concrete and the reinforcement steel. The knowledge of bond strength is also essential to determine the necessary anchorage length when designing reinforced concrete structures. When bond strength decreases, anchorage length must be increased to the same extent, and vice versa.

Figure 5-27 shows the bond stress-slip diagram for concretes C30-00, C30-20, C30-50, C30-100, C50-00, and C50-100. The general shape of the bond stress-slip diagrams is similar, regardless of the concrete strength class and the mixed recycled aggregate content. At first, a linear behavior is observed, and a perfect bond between the rebar and the concrete can be assumed. The slip rate increases as the load increases, and the curve becomes distinctly nonlinear until it reaches the ultimate bond stress load. At the descending stage, the load declines rapidly, and the slip increases. In this study, as previously explained, the tests were stopped when the MTS displacement reached 10mm.

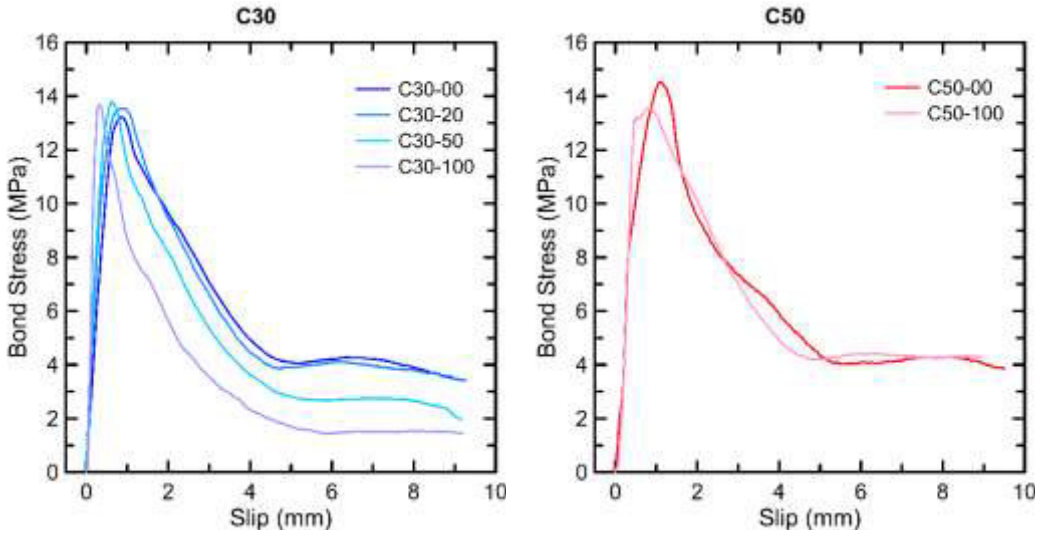

(a) (b)

Figure 5-27. Bond strength-slip diagram for concretes a) C30 and b) C50.

Table 5-3 shows the experimental maximum bond strength ($\tau_{b,max}$) and residual bonding stress (τ_f) and their respective slips for concretes C30 and C50.

Table 5-3. Maximum ($\tau_{b,max}$) and residual bond strength (τ_f) for concrete C30 and C50.

	C30-00	**C30-20**	**C30-50**	**C30-100**	**C50-00**	**C50-100**
$\tau_{b,max}$ **(MPa)**	13.23	13.55	13.80	13.76	14.53	13.57
τ_f **(MPa)**	4.10	4.01	2.73	1.51	4.15	4.21

It can be seen that the maximum bond strength ($\tau_{b,max}$) between the concrete and the rebar is hardly affected by the replacement of natural aggregate by mixed recycled aggregate in the concrete, regardless of the concrete strength class.

In addition, all concretes presented a residual plateau, referring to residual bonding stress (τ_f). For concrete strength class C30, it is possible to observe a reduction in the residual bonding stress (τ_f) as the content of mixed recycled aggregate increases. Since the residual bonding stress is provided by the friction between the steel rebar and the surrounding concrete, the use of mixed recycled aggregate may cause an impact on the friction between the concrete and the rebar.

For concretes with a higher strength class (C50), this impact in the residual bonding stress (τ_f) is not observed. As seen in Chapter 4, the concretes C50 include mineral additives in their mix design, such as fly ash and silica, which are finer than Portland cement and generate other hydration products. The positive effects of using these materials, such as reduced porosity and increased strength of the concrete matrix, may somehow outweigh the negative effect of using mixed recycled aggregate.

5.3.1. Comparative Analysis with the Brazilian Design Code

Although the structural application of concrete with recycled aggregate is practiced in some countries, as observed in **Table 2-4**, the international standards only establish prerequisites on the physical properties of recycled aggregates and criteria to produce these concretes, such as maximum percentage of replacement of natural aggregate by recycled aggregate and range of compressive strength values. Once these requirements are met, the design of concrete elements made with mixed recycled aggregate is carried out following the prescriptions established for conventional concrete elements. Thus, to investigate the applicability of the Brazilian standard ABNT NBR 6118:2014 [71] to beams made with mixed recycled

aggregate, the experimental results from the current study were compared to the theoretical equations.

Aiming to corroborate the experimental tests, an analytical model for the bending capacity of reinforced concrete beams was used to predict the moment-curvature by an iterative calculation using the software Maple. This model considers the following hypotheses: i) Bernoulli's principle for plane sections; ii) the concrete and reinforcement acting together, i.e., perfect adhesion between concrete and reinforcement; iii) the concrete and reinforcement stress can be calculated by the stress-strain curves.

The behavior of the concrete was described according to the Brazilian standard ABNT NBR 6118:2014 [71] (**Eq. 5-2** and **Eq. 5-3),** which considers the nonlinear behavior of the material:

$$\sigma_c = f_c\left[1-\left(1-\frac{\varepsilon_c}{\varepsilon_{c2}}\right)^2\right] \qquad \text{for } 0 < \varepsilon_c < 2‰ \qquad \textbf{Eq. 5-2}$$

$$\sigma_c = f_c \qquad \text{for } 2‰ < \varepsilon_c < 3.5‰ \qquad \textbf{Eq. 5-3}$$

For each beam, depending on the concrete (C30 or C50), the values obtained experimentally for modulus of elasticity, compressive strength, and tensile strength were used, as shown in Chapter 4.

For the steel rebars, an elastic-linear behavior was assumed until their ultimate strength. The ultimate strength was considered as 500 MPa and the modulus of elasticity was equal to 210 GPa.

Figure 5-28 presents a diagram for the reinforced concrete's stress-strain relationship based on the forces' equilibrium. For each curvature, the equilibrium of forces creates a moment.

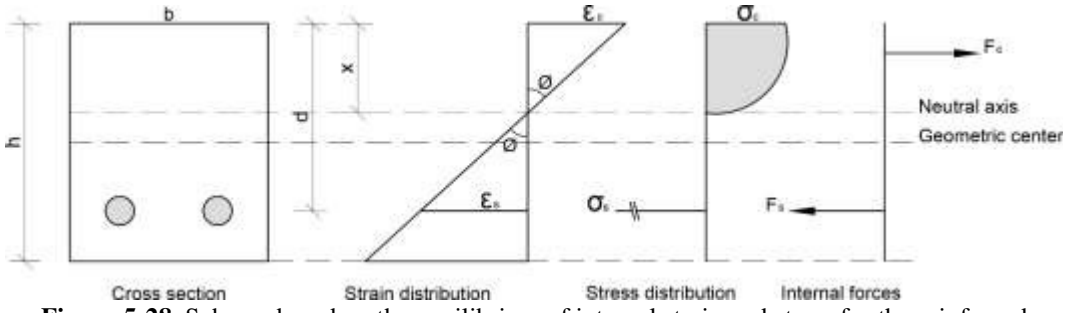

Figure 5-28. Scheme based on the equilibrium of internal strain and stress for the reinforced concrete.

The forces and moments equilibrium were used to determine the neutral line position up to the ultimate strain limit of the materials. The force interactions were determinate by the stress-strain diagram integrating. The analytical model of the section was calculated by the following **Eq. 5-4** and **Eq. 5-5**:

$$\sum F = 0: \qquad -[\int \sigma_c b d_x] + \sigma_s A_s = 0 \qquad \textbf{Eq. 5-4}$$

$$\sum M = 0: \qquad -[\int \sigma_c b x d_x] + \sigma_s A_s (h - d) = 0 \qquad \textbf{Eq. 5-5}$$

From the model interactions, the moment-curvature vectors were determined for each position of the neutral line, and then the analytical curves were predicted.

For purposes of comparison with the theoretical results, the experimental moment-curvature diagrams were also defined. The experimental curvatures were calculated using the average of the strains recorded by the gauges placed at the midspan of each one of the longitudinal reinforcement bars and assuming the Bernoulli-Euler hypothesis, which admits a linear strain distribution over the cross-section.

Figure 5-29, **Figure 5-30**, and **Figure 5-31** show the experimental and theoretical moment-curvature diagrams for each group of beams (C30-xx-D, C50-xx-D, and C30-xx-B, respectively).

During the initial load application (linear elastic behavior), both theoretical and experimental curves presented similar stiffness for all concrete beams. However, after the concrete cracking, the theoretical curves presented a sudden drop that did not appear in the experimental curves. This occurs because, in the theoretical model, there is an abrupt transition from one stage to another, while this transition occurs gradually with the appearance of several cracks along the beam. Nevertheless, theoretical and experimental moment-curvature diagrams exhibit similar behavior during the yielding growth curve.

Lastly, for beams C30-xx-D and C50-xx-D, both theoretical and experimental moment-curvature diagrams present a similar trend for the horizontal yield plateau. This does not occur for the C30-xx-B group of beams since their failure occurs due to concrete compression before the steel yielding.

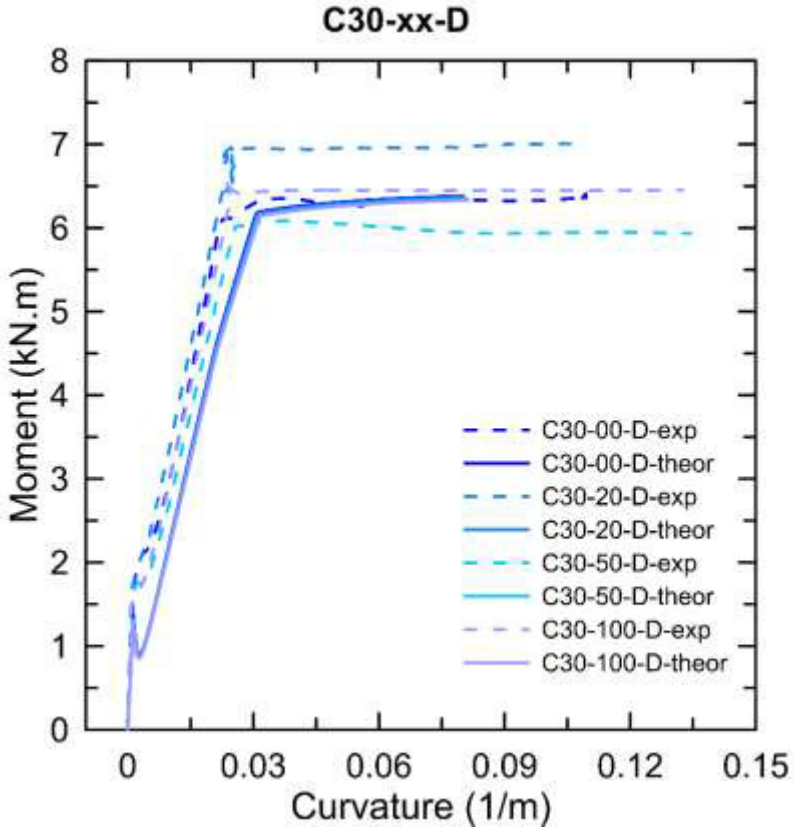

Figure 5-29. Theoretical and experimental moment-curvature diagrams for C30-xx-D beams.

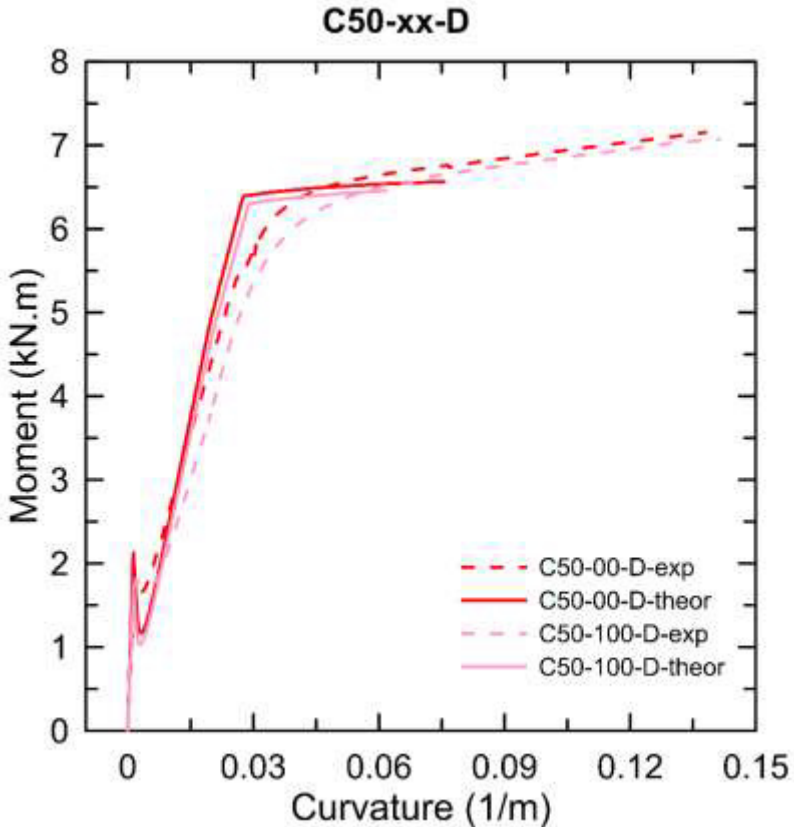

Figure 5-30. Theoretical and experimental moment-curvature diagrams for C50-xx-D beams.

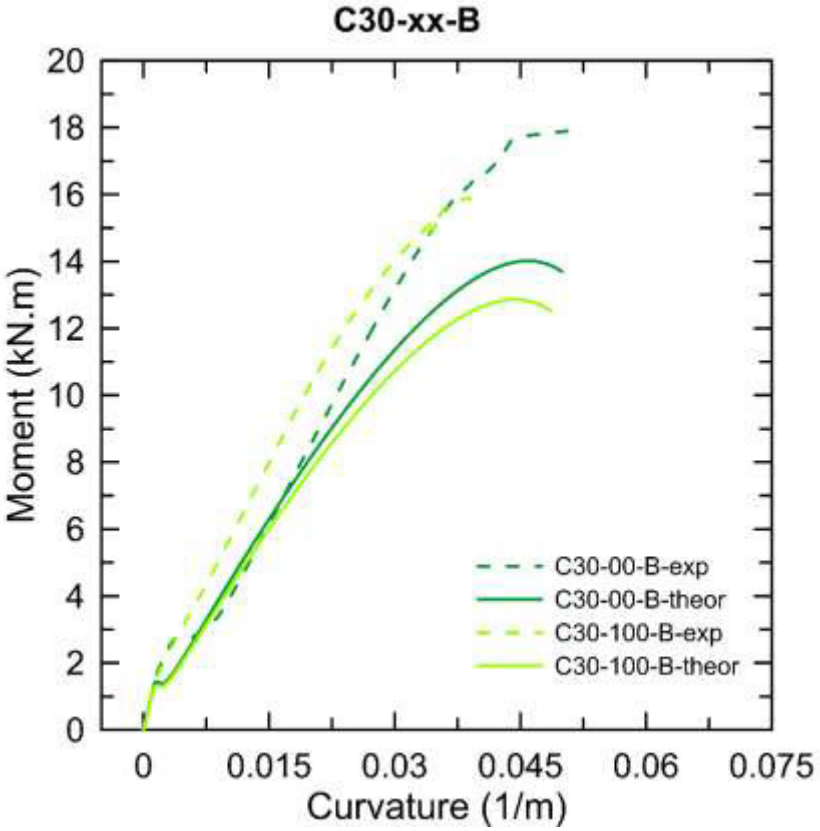

Figure 5-31. Theoretical and experimental moment-curvature diagrams for C30-xx-B beams.

For the two groups of beams made with concrete of strength class C30 (designed for ductile or brittle flexural failure) – C30-xx-D and C30-xx-B –, it is also possible to observe that the theoretical results are more conservative than the experimental results, showing that the formulation of the Brazilian standard ABNT NBR 6118:2014 [71] is in favor of safety. As for the beam made with concrete of strength class C50, the moments obtained experimentally are slightly lower during the yielding growth curve than the theoretical results. This indicates that, when designing beams with higher-strength concrete containing mixed recycled aggregate, more attention should be paid to strength requirements for flexural design.

The theoretical cracking moment for each group of beams (C30-xx-D, C50-xx-D, and C30-xx-B) was also calculated based on the formulations of the Brazilian standard ABNT NBR 6118:2014 [71] (**Eq. 5-6**):

$$M_r = \frac{\alpha f_{ct} I_c}{y_t} \qquad \textbf{Eq. 5-6}$$

Where:

M_r is the cracking moment (kN.cm);

α is equal to 1.5 for a rectangular section;

f_{ct} is the direct tensile strength of the concrete, according to item 8.2.5 of the ABNT NBR 6118:2014 [71] (kN/cm^2);

I_c is the moment of inertia of the concrete section (cm^4);

y_t is the distance from the center of gravity of the section to the most stressed fiber (cm). For a rectangular section, y_t is equal to half the height of the beam.

The theoretical crack opening was also calculated according to Section 17.3.3.2 of the Brazilian standard ABNT NBR 6118:2014 [71]. The characteristic crack opening (w_k) is the smaller value between those obtained by the following two equations (**Eq. 5-7** and **Eq. 5-8**):

$$w_k = \frac{\phi_i}{12{,}5 \cdot \eta_1} \cdot \frac{\sigma_{si}}{E_{si}} \cdot \frac{3\sigma_{si}}{f_{ctm}} \qquad \textbf{Eq. 5-7}$$

$$w_k = \frac{\phi_i}{12{,}5 \cdot \eta_1} \cdot \frac{\sigma_{si}}{E_{si}} \cdot \left(\frac{4}{\rho_{cri}} + 45\right) \qquad \textbf{Eq. 5-8}$$

Where:

A_{cri} is the area of the boundary region protected by bar ϕ_i (cm^2);

ϕ_i is the diameter of the bar (cm);

E_{si} is the modulus of elasticity of the steel rebar with diameter ϕi (kN/cm^2);

ρ_{ri} is the reinforcement ratio concerning A_{cri};

σ_{si} is the tensile stress at the center of gravity of the considered steel reinforcement, calculated in stage II (kN/cm^2);

f_{ct} is the direct tensile strength of the concrete, according to Section 8.2.5 of the ABNT NBR 6118:2014 [71];

η_1 is 2.25 for ribbed steel bars, according to Section 9.3.2.1 of the ABNT NBR 6118:2014 [71].

Knowing these theoretical values, it was possible to calculate the "experimental value/theoretical value" ratios to assess the approximation degree of Brazilian standard code expressions regarding the cracking moment and the crack opening (**Table 5-4**).

Table 5-4. Correlation between the experimental and the theoretical values of the cracking moment and crack opening.

Beam	$M_{cr,exp}$ / $M_{cr,ABNT}$	w_{exp} / w_{ABNT}
C30-00-D	1.50	1.12
C30-20-D	1.31	1.61
C30-50-D	1.32	1.15
C30-100-D	1.31	0.68
C50-00-D	1.37	0.73
C50-100-D	1.63	0.63
C30-00-B	1.74	2.23
C30-100-B	1.58	1.31

Regarding cracking moment and based on the results obtained with the experimental data available in this study, it is possible to observe that the ratios between experimental and theoretical results are always greater than 1, indicating that the formulation of the Brazilian standard ABNT NBR 6118:2014 [71] is in favor of safety even when high levels of mixed recycled aggregate are used. In addition, it is also possible to observe a certain tendency in the ratios obtained for the different beams. Thus, this means that the cracking moment of mixed recycled concrete beams can be calculated using the above-mentioned Brazilian standard without any modification to the presented equation.

On the other hand, regarding the crack opening, there is no clear tendency in the ratios obtained for the different beams. In some cases, the ratio between experimental and theoretical values is less than 1, showing that the crack opening was greater than predicted. Thus, given the results of this research, it can be said that it is necessary to adjust the expressions of the Brazilian standard ABNT NBR 6118:2014 [71] for the calculation of crack opening of beams made with mixed recycled aggregate. This adjustment in the equation should probably be made considering the recycled aggregate content and also an aspect related to its strength, such as the aggregate crushing value.

Although the experimental data on crack opening available in this research are not sufficient to establish a proposal to correct the equation, at this moment, in the case of beams produced with mixed recycled aggregate, it is recommended that its use in areas with potentially aggressive environments must be carefully evaluated, since the behavior of these elements in terms of the crack opening is not clear.

5.4. Conclusions

This chapter analyzed the flexural behavior of reinforced concrete beams made with mixed recycled aggregate. The short beams were made with different concrete strength classes, reinforcement ratios, and mixed recycled aggregate content (0%, 20%, 50%, and 100%). The experimental results and discussion lead to the following conclusions:

- When the beams are designed for ductile failure (reinforcement yields before concrete failure), the moment-deflection diagrams show the same trend for the same concrete strength class, regardless of the content of mixed recycled aggregate. The initial uncracked stiffness of the beams was not affected by the content of mixed recycled aggregate in the concrete;
- However, the lower tensile strength of mixed recycled aggregate concretes leads to an earlier cracking for mixed recycled aggregate beams than the reference beam. This situation can be observed equally for beams designed for ductile or brittle failure;
- Beams made with concrete strength class C50 take longer to crack when compared to beams made with concrete C30. This is consistent with the higher tensile strength of concretes C50. Additionally, the cracking moment variation between the reference beam and 100% mixed recycled aggregate beam is smaller for concrete with strength class C50 when compared to concrete C30. Thus, regarding the cracking moment, the higher the strength class of concrete, the lower the impact of replacing natural aggregate with mixed recycled aggregate;
- When beams are designed for ductile failure (reinforcement yields before concrete failure), the replacement of the natural aggregate by the mixed recycled aggregate does not negatively impact the bending moment for maximum deflection under the serviceability conditions of the beams, regardless of the content of mixed recycled aggregate and concrete strength class. Also, no relevant difference in ductility ($\delta_{ult}/\delta_{yiel}$) was found between beams up to 50% mixed recycled aggregate and concrete strength class C30;
- Linear strain distribution over the height of the cross-section proves that the Bernoulli hypothesis is valid for beams made with mixed recycled aggregate, regardless of the replacement ratio of mixed recycled aggregate. Regardless of the concrete strength class, the depth of the compression zone increases as the

content of mixed recycled aggregate increases, which can be attributed to the lower modulus of elasticity of mixed recycled concrete, which leads to greater deformations at the compression zone;

- When the beams are designed for brittle failure (crushing of concrete before the rebar yields), the beam produced with 100% of mixed recycled aggregate presented lower bending moments and higher ultimate deflections compared to the beam produced with conventional concrete. In these cases, the bending behavior is governed by the concrete and, therefore, the replacement of the natural aggregate by the mixed recycled aggregate causes a greater impact;
- For beams produced with the same type of concrete (same strength class and same content of mixed recycled aggregate), as the reinforcement ratio increases, there is a considerable increase in the ultimate moment and a decrease in ultimate deflection;
- Regarding service deflections, no substantial difference was observed for beams made with mixed recycled aggregate concrete compared to conventional concrete beams, regardless of the concrete strength class. Furthermore, for the same type of concrete, using high amounts of reinforcement steel also leads to scarce differences in service deflections. Thus, the analysis of deflections at serviceability in a concrete beam cannot be directly related to material properties (i.e., modulus of elasticity) straightforwardly;
- For over-reinforced concrete beams, the size of the failure surface and the level of concrete destruction at failure were substantially affected by the amount of mixed recycled aggregate in the concrete. When the beam is produced with 100% mixed recycled aggregate concrete, the size of the failure surface and the level of the concrete destruction increases, because of the highly porous old ITZ, with pre-existing cracks;
- Through visual analysis, it is possible to say that the development of cracking was not significantly affected by the replacement of natural aggregate with mixed recycled aggregate;
- When the beams are over-reinforced, the average crack opening practically does not vary with the increased content of mixed recycled aggregate. In addition, the over-reinforced beams present smaller crack openings than beams made with the same concrete strength class and a lower reinforcement ratio. The higher

reinforcement ratio causes a higher strength and less deflection on the beams' face subjected to tensile, and thus smaller crack openings;

- The variation in the crack openings with increasing content of mixed recycled aggregate is remarkable for the beams designed for ductile failure: as the content of mixed recycled aggregate increases, crack opening also increases. The layer of residual mortar on cement-based recycled aggregates constitutes an easier path for crack propagation. Also, the ceramic fragments of the mixed recycled aggregates are more fragile and break as the cracks open. This may reduce the contribution of the aggregate interlock, which essentially depends on the points of contact between the faces of the crack;
- In addition, this increase in the crack opening is more substantial for beams C30 because concrete C30 has smaller tensile splitting strength, smaller modulus of elasticity, and smaller stiffness than concrete C50;
- Regarding bond strength, the general shape of the bond stress-slip diagrams is similar, regardless of the concrete strength class and mixed recycled aggregate content. The maximum bond strength between the concrete and the rebar is hardly affected by the content of mixed recycled aggregate in the concrete;
- A residual plateau, referring to residual bonding stress, was also observed for all concrete (C30 and C50). However, for concrete strength class C30, the residual bonding stress reduced as the content of mixed recycled aggregate increased. Thus, it can be said that for concrete strength class C30, the use of mixed recycled aggregate may cause an impact on the friction between the concrete and the rebar. This reduction was not notable for concrete strength class C50 probably because of the presence of mineral additives, which generate different hydration products, reducing porosity and increasing concrete strength;
- The cracking moment of mixed recycled concrete beams can be calculated using the Brazilian standard ABNT NBR 6118:2014 [71] equation without any modification. On the other hand, regarding the crack opening, no clear tendency was observed in the ratios between experimental and theoretical values. Thus, given the results of this research, it is necessary to adjust the expressions of the aforementioned Brazilian standard to calculate the crack opening of beams made with mixed recycled aggregate. This adjustment in the equation should probably consider not only the content of mixed recycled aggregate but also some aspect related to its strength, such as the aggregate crushing value;

- For beams made with mixed recycled concrete of strength class C30, the theoretical results of moment-curvature based on the Brazilian standard ABNT NBR 6118:2014 [71] are more conservative than the experimental results. However, more attention should be paid to flexural design strength requirements when designing beams with higher-strength mixed recycled aggregate concrete.

Considering the experimental data available in this research, comparing load-deflection behavior, crack pattern, and bond strength of reference beams and beams made with concrete with up to 100% of mixed recycled aggregate with up to 15% of ceramic fragments, the flexural behavior of mixed recycled aggregate beams is satisfactory. Special attention should be given to the use of beams made with mixed recycled aggregate concrete in potentially aggressive environments since the behavior of these elements in terms of the crack opening is unclear.

6. General Conclusions

Recycling construction and demolition waste (CDW) to generate recycled aggregate is challenging due to the heterogeneity of the waste material. CDW comprises various materials, such as concrete, ceramic fragments, metals, plastics, and wood, which often require different recycling processes. The recycled aggregate's quality can vary depending on the waste material's origin and composition, affecting the resulting concrete's mechanical properties and durability.

International standards limit the use of recycled aggregate in structural concrete depending on the desired concrete strength class and the characteristics of the recycled aggregate. The Brazilian standard NBR 15116:2021 [47] limits recycled aggregates in structural concrete to 20% recycled concrete aggregate, regardless of strength class. In Brazil, any content of ceramic fragments makes the use of recycled aggregate in structural concrete unfeasible. Thus, the difficulty in recycling lies in the need to separate and classify each material before processing it, which is a time-consuming and costly task.

Improving the recycling and reuse of CDW is crucial to reduce waste disposal and conserving natural resources. To achieve this goal, it is necessary to promote using recycled materials in the construction industry. A better comprehension of the structural behavior of elements made with recycled aggregate with a certain content of ceramic fragments, so-called mixed recycled aggregate, would make the recycling process more feasible, decrease recycling costs, and increase market demand for this material.

Thus, in the present work, three stages were developed. First, an investigation was carried out on the physical and mechanical properties of recycled coarse aggregates with different amounts of ceramic fragments, comparing them with a natural coarse aggregate. Then, the mix design of different concretes was carried out based on the principles of the Compressible Packing Model, using the software Bétonlab Pro 3. The third and final step consisted of using different content of mixed recycled aggregate on short reinforced concrete beams and analyzing its

flexural behavior, in addition to analyzing the bond strength between the concrete and the steel rebar based on the pull-out test.

By examining the experimental results available in the first stage of this study, it was possible to observe that the four coarse aggregates (MRA, RCA, RMA, and NAT) presented very similar grain-size distribution curves and pulverulent content under the limit value established by the Brazilian standard ABNT NBR 15116:2021 [46]. Regarding the shape index, although the values do not vary much, as the content of ceramic fragments increases, the recycled aggregates become more flattened and elongated.

All three types of recycled aggregate studied were less dense, less resistant, more porous, and absorbed more water than the natural aggregate. However, the mixed recycled aggregate (with 13.2% ceramic fraction) presented similar results to the recycled concrete aggregate. Lastly, as all four coarse aggregates presented comparable values for shape index and the same maximum size, they all showed similar values of void ratio and, consequently, similar packing density. Thus, from the discussions presented in the first stage of this study, it was possible to conclude that when the recycled aggregate has a ceramic fraction lower than 15%, its physical and mechanical properties are not very different from those obtained for the recycled concrete aggregate, composed only of cement-based fragments.

Regarding mix design, traditional methods are usually designed for the conventional concrete strength class. However, with the development of civil construction and structural engineering, sometimes special concretes are needed, made up of several granular materials that interact. Thus, due to the complexity of this material, mix design methods based on particle packing are becoming more frequent since the particle size distribution of the aggregates affects the packing density of the concrete, which is directly related to the concrete's strength. Therefore, modifying the concrete mix design formulation using the particle packing technique can efficiently produce concretes with higher durability and better mechanical performance with reduced cement consumption.

The experimental results of compressive strength presented in the second stage of this study showed a high correlation (above 90%) with the theoretical values predicted by the Compressible Packing Model (CPM) through the software BétonLab Pro 3. Thus, based on the available data in this study, it can be said that

the Compressible Packing Model can be successfully applied for the mix design of concrete up to strength class C50 and made with mixed recycled aggregate.

It was also possible to observe that all concrete mixtures' compressive stress-strain curves presented a similar behavior, regardless of the amount of mixed recycled aggregate. Furthermore, even replacing 100% of the natural aggregate with mixed recycled aggregate did not cause a significant impact on the concrete workability, compressive strength, and tensile strength.

Regarding the formulation proposed by the Brazilian standard ABNT NBR 6118:2014 [54] to predict the tensile strength of concrete, the available data in this study showed that there is no need to make any adjustments to predict the tensile strength for concretes made with mixed recycled aggregate with a ceramic fraction up to 15%. Regarding the modulus of elasticity, a theoretical formulation was proposed to correlate the modulus of elasticity with the compressive strength and the mixed recycled aggregate content in concrete, thus adapting the existing formulation in the Brazilian standard ABNT NBR 6118:2014 [54], which consider only concrete manufactured with natural aggregates of different types.

When analyzing the flexural behavior of reinforced concrete beams made with mixed recycled aggregate, it was possible to observe that when the beams are designed for ductile failure (reinforcement yields before concrete failure), the moment-deflection diagrams trend are very similar, regardless of the content of mixed recycled aggregate. Also, the replacement of the natural aggregate by the mixed recycled aggregate does not negatively impact the bending moment for maximum deflection under the serviceability conditions of the beams.

When the beams are designed for brittle failure (crushing of concrete before the rebar yields), as the concrete governs bending behavior, the replacement of the natural aggregate by the mixed recycled aggregate causes a greater impact. For these over-reinforced concrete beams, the size of the failure surface and the level of concrete destruction at failure were substantially affected by the amount of mixed recycled aggregate in the concrete, because of the highly porous old ITZ, with pre-existing cracks.

Regarding cracking, the lower tensile strength of mixed recycled aggregate concretes leads to an earlier cracking for mixed recycled aggregate beams. However, through visual analysis, based on the available data in this study, it is

possible to declare that the development of cracking was not significantly affected by replacing natural aggregate with mixed recycled aggregate.

Using the DIC technic, the crack openings were calculated. It was noticed that as the content of mixed recycled aggregate increases, crack opening also increases. The layer of residual mortar can explain this on cement-based recycled aggregates, which constitutes an easier path for crack propagation. Also, the ceramic fragments of the mixed recycled aggregates are more fragile and break as the cracks open, reducing the contribution of the aggregate interlock.

Regarding bond strength, the general shape of the bond stress-slip diagrams was similar, regardless of the concrete strength class and mixed recycled aggregate content. The maximum bond strength between the concrete and the rebar was hardly affected by the content of mixed recycled aggregate in the concrete. However, for concrete strength class C30, the residual bonding stress (i.e., friction between the concrete and the rebar) reduced as the content of mixed recycled aggregate increased. This reduction was not notable for concrete strength class C50, probably because the mineral additives generate different hydration products, reducing porosity and increasing concrete strength.

Based on the available data in this study, it was observed that the Brazilian standard ABNT NBR 6118:2014 [54] could be used to forecast the cracking moment of beams made with mixed recycled aggregate concrete with up to 15% of ceramic fragments. On the other hand, regarding the crack opening, given the results of this research, it is necessary to adjust the expressions of the aforementioned Brazilian standard. This adjustment should probably consider the content of mixed recycled aggregate and some aspect related to its strength, such as the aggregate crushing value.

As a final remark, the prescriptions for bending behavior of the Brazilian standard ABNT NBR 6118:2014 [54] were reasonably close to the experimental results obtained in this research for beams made with concrete of strength class C30. This indicates that the existing analytical model for conventional reinforced concrete beams can also be applied to beams made with mixed recycled aggregate concrete with up to 15% of ceramic fragments. However, more attention should be paid to flexural design strength requirements when designing beams with higher-strength mixed recycled aggregate concrete. It is also necessary to have special attention when using beams made with mixed recycled aggregate concrete in

potentially aggressive environments since the behavior of these elements in terms of the crack opening is unclear.

Ultimately, a conclusion from the available data in this study is that mixed recycled aggregate (with up to 15% of ceramic fragments) may be suitable to produce quality concrete to be used by the construction sector in structural concretes, expanding the possibilities of using this material and, consequently, collaborating to reduce the environmental impact caused by the construction sector.

7. Suggestions for Future Research

Further research is certainly needed to develop a wide database that will allow researchers to state the design procedure of mixed recycled concrete beams with the same reliability as conventional ones. Thus, to complement the conclusions obtained in this study, it is suggested:

- Evaluate the physical and mechanical behavior of mixed recycled aggregates with up to 30% ceramic fragments and their impact on structural elements;
- Evaluate the flexural performance of beams made with mixed recycled aggregate with a higher length (for example, above 3 m);
- Examine the behavior of beams made with mixed recycled aggregate when subjected to shear;
- Determine expressions for predicting the crack opening in mixed recycled aggregate concrete beams, evaluating not only the replacement content of the aggregate but also some aspect related to its strength, such as the aggregate crushing value;
- Investigate the applicability of international standards, such as ACI and Eurocode, to beams made with mixed recycled aggregate, comparing the experimental results to the theoretical formulations.

8. Published Articles

The following articles were published based on the results of this doctoral thesis:

"Recycled aggregates from construction and demolition waste towards an application on structural concrete: a review."
Article published on April 1st, 2022
Journal of Building Engineering, vol. 52, p.104452 -
https://doi.org/10.1016/j.jobe.2022.104452

"Properties of recycled aggregates from different composition and its influence on concrete strength"
Article published on July 5th, 2021
Rev. IBRACON Estrut. Mater., vol. 14, no. 6, e14605, 2021
https://doi.org/10.1590/S1983-41952021000600005

References

[1] L. Huang, G. Krigsvoll, F. Johansen, Y. Liu, and X. Zhang, "Carbon emission of global construction sector," *Renewable and Sustainable Energy Reviews*, vol. 81, no. June 2017, pp. 1906–1916, 2018, doi: 10.1016/j.rser.2017.06.001.

[2] S. Lutter, S. Giljum, and B. Gözet, "Raw Materials Profile for Non-metallic minerals - construction dominant," *https://www.materialflows.net/visualisation-centre/raw-material-profiles/*, 2019.

[3] ANEPAC, "Anuário ANEPAC," 2013.

[4] ISWA, *ISWA REPORT ISWA at a Glance*. International Solid Waste Association, Viena, AUT, 2015.

[5] USEPA, "Advancing sustainable materials management: 2014 Fact Sheet Assessing Trends in Material Generation, Recycling, Composting, Combustion with Energy Recovery and Landfilling in the United States," *United States Environmental Protection Agency, Office of Land and Emergency Management, Washington, DC 20460*, no. November, p. 22, 2016, doi: EPA530F-18-004.

[6] B. Huang, X. Wang, H. Kua, Y. Geng, R. Bleischwitz, and J. Ren, "Construction and demolition waste management in China through the 3R principle," *Resour Conserv Recycl*, vol. 129, no. September 2017, pp. 36–44, 2018, doi: 10.1016/j.resconrec.2017.09.029.

[7] European Environment Agency, "EU as a Recycling Society -- Present recycling levels of Municipal Waste and Construction & Demolition Waste in the EU," 2009. [Online]. Available: http://scp.eionet.europa.eu/publications/wp2009_2/wp/WP2009_2

[8] ABRELPE, "Panorama dos Resíduos Sólidos no Brasil - 2021," 2021.

[9] USEPA, "Industrial and Construction and Demolition (C&D) Landfills." https://www.epa.gov/landfills/industrial-and-construction-and-demolition-cd-landfills (accessed Apr. 03, 2018).

[10] European Parliament and Council, *Commission Decision of 3 May 2000 replacing Decision 94/3/EC establishing a list of wastes pursuant to Article 1(a) of Council Directive 75/442/EEC on waste*. 2000. [Online]. Available: https://eur-lex.europa.eu/legal-content/EN/TXT/?uri=CELEX:32000D0532

[11] Ccanz, "Best Practice Guide for the use of Recycled Aggregates in New Concrete," 2011.

[12] Deloitte, "Construction and Demolition Waste management in France," 2015. http://ec.europa.eu/environment/waste/studies/deliverables/CDW_France_Factsheet_Final.pdf (accessed Apr. 03, 2018).

[13] U.S. Green Building Council, "LEED v4 for BUILDING DESIGN AND CONSTRUCTION," 2018. [Online]. Available: http://www.usgbc.org/sites/default/files/LEED v4 BDC_04.05.16_current.pdf

[14] R. Movassaghi, "Durability of Reinforced Concrete Incorporating Recycled Concrete as Aggregate (RCA)," University of Waterloo, 2006.

[15] S. Böhmer *et al.*, "Aggregates Case Study: Final Report referring to contract n° 150787-2007 F1SC-AT," 2008. [Online]. Available: http://www.sarmaproject.eu/uploads/media/JRC_Aggregates_FinalRep_UBA_080331.pdf

[16] A. Coelho and J. de Brito, "Economic viability analysis of a construction and demolition waste recycling plant in Portugal - Part I: Location, materials, technology and economic analysis," *J Clean Prod*, vol. 39, pp. 338–352, 2013, doi: 10.1016/j.jclepro.2012.08.024.

[17] ABRELPE, "Estimativas dos Custos para Viabilizar a Universalização da Destinação Adequada de Resíduos Sólidos no Brasil," 2015.

[18] S. C. Angulo, L. S. Oliveira, and L. Machado, "Pesquisa Setorial ABRECON 2020: a Reciclagem de Resíduos de Construção e Demolição no Brasil," Universidade de São Paulo. Escola Politécnica, Jun. 2022. doi: 10.11606/9786589190103.

[19] S. Kosmatka, B. Kerkhoff, and W. Paranese, *Design and Control of Concrete Mixtures*, 14th ed. Portland Cement Association, 2008.

[20] ABRECON, *Relatório Pesquisa Setorial 2017/2018*. Associação Brasileira para Recicilagem de Resíduos da Construção Civil e Demolição, BRA, 2018, p. 75. doi: 10.1017/CBO9781107415324.004.

[21] E. Vázquez, Ed., *Progress of Recycling in the Built Environment - Final Report of the RILEM Technical Committee 217-PRE*. Springer Netherlands, 2013. doi: 10.1007/978-94-007-4908-5.

[22] G. Bai, C. Zhu, C. Liu, and B. Liu, "An evaluation of the recycled aggregate characteristics and the recycled aggregate concrete mechanical properties," *Constr Build Mater*, vol. 240, p. 117978, 2020, doi: 10.1016/j.conbuildmat.2019.117978.

[23] M. Bravo, J. De Brito, J. Pontes, and L. Evangelista, "Mechanical performance of concrete made with aggregates from construction and demolition waste recycling plants," *J Clean Prod*, vol. 99, pp. 59–74, 2015, doi: 10.1016/j.jclepro.2015.03.012.

[24] V. Corinaldesi, "Mechanical and elastic behaviour of concretes made of recycled-concrete coarse aggregates," *Constr Build Mater*, vol. 24, pp. 1616–1620, 2010, doi: 10.1016/j.conbuildmat.2010.02.031.

[25] M. Etxeberria, E. Vázquez, A. Marí, and M. Barra, "Influence of amount of recycled coarse aggregates and production process on properties of recycled aggregate concrete," *Cem Concr Res*, vol. 37, no. 5, pp. 735–742, 2007, doi: 10.1016/j.cemconres.2007.02.002.

[26] V. W. Y. Tam, D. Kotrayothar, and J. Xiao, "Long-term deformation behaviour of recycled aggregate concrete," *Constr Build Mater*, vol. 100, pp. 262–272, 2015, doi: 10.1016/j.conbuildmat.2015.10.013.

[27] C. Thomas, J. Setién, J. A. Polanco, P. Alaejos, and M. Sánchez De Juan, "Durability of recycled aggregate concrete," *Constr Build Mater*, vol. 40, pp. 1054–1065, 2013, doi: 10.1016/j.conbuildmat.2012.11.106.

[28] M. Etxeberria, A. R. Marí, and E. Vázquez, "Recycled aggregate concrete as structural material," *Materials and Structures/Materiaux*

et Constructions, vol. 40, no. 5, pp. 529–541, 2007, doi: 10.1617/s11527-006-9161-5.

[29] X. Li, "Recycling and reuse of waste concrete in China. Part II. Structural behaviour of recycled aggregate concrete and engineering applications," *Resour Conserv Recycl*, vol. 53, pp. 107–112, 2009, doi: 10.1016/j.resconrec.2008.11.005.

[30] N. Mohamad, H. Khalifa, A. A. Abdul Samad, P. Mendis, and W. I. Goh, "Structural performance of recycled aggregate in CSP slab subjected to flexure load," *Constr Build Mater*, vol. 115, pp. 669–680, 2016, doi: 10.1016/j.conbuildmat.2016.04.086.

[31] H. Zhang and Y. Zhao, "Performance of Recycled Aggregate Concrete in a Real Project," *Advances in Structural Engineering*, vol. 17, no. 6, pp. 895–906, 2014, doi: 10.1260/1369-4332.17.6.895.

[32] J. R. Jiménez, J. Ayuso, A. P. Galvín, M. López, and F. Agrela, "Use of mixed recycled aggregates with a low embodied energy from non-selected CDW in unpaved rural roads," *Constr Build Mater*, vol. 34, pp. 34–43, 2012, doi: 10.1016/j.conbuildmat.2012.02.042.

[33] F. D. C. Leite, R. D. S. Motta, K. L. Vasconcelos, and L. Bernucci, "Laboratory evaluation of recycled construction and demolition waste for pavements," *Constr Build Mater*, vol. 25, no. 6, pp. 2972–2979, 2011, doi: 10.1016/j.conbuildmat.2010.11.105.

[34] I. Martínez-Lage, F. Martínez-Abella, C. Vázquez-Herrero, and J. L. Pérez-Ordóñez., "Properties of plain concrete made with mixed recycled coarse aggregate," *Constr Build Mater*, vol. 37, pp. 171–176, 2012, doi: 10.1016/j.conbuildmat.2012.07.045.

[35] B. Mas *et al.*, "Concrete with mixed recycled aggregates: Influence of the type of cement," *Constr Build Mater*, vol. 34, pp. 430–441, 2012, doi: 10.1016/j.conbuildmat.2012.02.092.

[36] J. Tavira, J. R. Jiménez, J. Ayuso, M. J. Sierra, and E. F. Ledesma, "Functional and structural parameters of a paved road section constructed with mixed recycled aggregates from non-selected construction and demolition waste with excavation soil," *Constr Build Mater*, vol. 164, pp. 57–69, 2018, doi: 10.1016/j.conbuildmat.2017.12.195.

[37] I. Vegas, J. A. Ibañez, A. Lisbona, A. Sáez De Cortazar, and M. Frías, "Pre-normative research on the use of mixed recycled aggregates in unbound road sections," *Constr Build Mater*, vol. 25, pp. 2674–2682, 2011, doi: 10.1016/j.conbuildmat.2010.12.018.

[38] J. Yang, Q. Du, and Y. Bao, "Concrete with recycled concrete aggregate and crushed clay bricks," *Constr Build Mater*, vol. 25, no. 4, pp. 1935–1945, 2011, doi: 10.1016/j.conbuildmat.2010.11.063.

[39] P. V. Salles, "Avaliação mecânica e de durabilidade de concretos fabricados com resíduos de construção e demolição," Dissertação de Mestrado. Centro Federal de Educação Tecnológica de Minas Gerais, Belo Horizonte, MG, Brasil, 2018.

[40] BSI, *BS 8500-2 - Concrete – Complementary British Standard to BS EN 206 – Part 2: Specification for constituent materials and concrete*. BSI, London, UK., 2015, p. 48.

[41] EHE, *EHE-08 - Instrucción de Hormigón Estructural*. Ministerio de Fomento S.G.T. Centro de Publicaciones, ESP., 2008, pp. 258–266.

[42] LNEC, *E 471-2009 - Guia para utilização de agregados reciclados grossos em betões de ligantes hidráulicos*. Laboratório Nacional de Engenharia Civil. Ministério das Obras Públicas , Transportes e Comunicações, Lisboa, PRT, 2009, p. 8.

[43] DIN, *EN 12620 - Aggregates for concrete*. Deutsches Institut Fur Normung, 2003.

[44] Italian Ministry of Infrastructure and Transport, *NTC 2008 – Italian Building Code. D.M. 14/01/2008*. Ministero delle Infrastrutture, ITA, 2008, p. 4428. doi: 10.1515/9783110247190.153.

[45] CSIRO, *HB 155 - Guide to the use of recycled concrete and masonry materials*. Australia: Commonwealth Scientific and Industrial Research Organisation (CSIRO), 2002, p. 80.

[46] ABNT, *NBR 15116 - Agregados reciclados de resíduos sólidos da construção civil - Utilização em pavimentação e preparo de concreto sem função estrutural - Requisitos*. 2021.

[47] Y. Kasai, K. D. Ravindra, A. H. Neil, and C. L. Mukesh, "Barriers to the reuse of construction by-products and the use of recycled

aggregate in concrete in Japan," *Sustainable Construction: Use of Recycled Concrete Aggregate*, 2015.

[48] C. Medina, W. Zhu, T. Howind, M. Frías, and M. I. De Sánchez Rojas, "Effect of the constituents (asphalt, clay materials, floating particles and fines) of construction and demolition waste on the properties of recycled concretes," *Constr Build Mater*, vol. 79, pp. 22–33, 2015, doi: 10.1016/j.conbuildmat.2014.12.070.

[49] M. Quattrone, S. C. Angulo, and V. M. John, "Energy and CO2 from high performance recycled aggregate production," *Resour Conserv Recycl*, vol. 90, pp. 21–33, 2014, doi: 10.1016/j.resconrec.2014.06.003.

[50] R. V. Silva, J. de Brito, and R. K. Dhir, "Availability and processing of recycled aggregates within the construction and demolition supply chain: A review," *J Clean Prod*, vol. 143, pp. 598–614, 2017, doi: 10.1016/j.jclepro.2016.12.070.

[51] K. Hu, Y. Chen, F. Naz, C. Zeng, and S. Cao, "Separation studies of concrete and brick from construction and demolition waste," *Waste Management*, vol. 85, pp. 396–404, 2019, doi: 10.1016/j.wasman.2019.01.007.

[52] I. Vegas, K. Broos, P. Nielsen, O. Lambertz, and A. Lisbona, "Upgrading the quality of mixed recycled aggregates from construction and demolition waste by using near-infrared sorting technology," *Constr Build Mater*, vol. 75, pp. 121–128, 2015, doi: 10.1016/j.conbuildmat.2014.09.109.

[53] Fathifazl G, Razaqpur A. G., Burkan Isgor O., Abbas A, Ournier B, and Foo S, "Flexural Performance of Steel-Reinforced Recycled Concrete Beams," *ACI Struct J*, vol. 106, no. 6, pp. 858–867, 2009.

[54] T. H. K. Kang, W. Kim, Y. K. Kwak, and S. G. Hong, "Flexural testing of reinforced concrete beams with recycled concrete aggregates," *ACI Struct J*, vol. 111, no. 3, pp. 607–616, 2014, doi: 10.14359/51686622.

[55] S. Pradhan, S. Kumar, and S. V. Barai, "Performance of reinforced recycled aggregate concrete beams in flexure: experimental and critical comparative analysis," *Materials and Structures/Materiaux et*

Constructions, vol. 51, no. 3, pp. 1–17, 2018, doi: 10.1617/s11527-018-1185-0.

[56] S. Zhao and C. Sun, "Experimental study of the recycled aggregate concrete beam flexural performance," *Applied Mechanics and Materials*, vol. 368–370, no. 1, pp. 1074–1079, 2013, doi: 10.4028/www.scientific.net/AMM.368-370.1074.

[57] W. Bai and B. Sun, "Experimental study on flexural behavior of recycled coarse aggregate concrete beam," *Applied Mechanics and Materials*, vol. 29–32, pp. 543–548, 2010, doi: 10.4028/www.scientific.net/AMM.29-32.543.

[58] S. Seara-Paz, B. González-Fonteboa, F. Martínez-Abella, and J. Eiras-López, "Flexural performance of reinforced concrete beams made with recycled concrete coarse aggregate," *Eng Struct*, vol. 156, pp. 32–45, Feb. 2018, doi: 10.1016/j.engstruct.2017.11.015.

[59] M. Arezoumandi, A. Smith, J. S. Volz, and K. H. Khayat, "An experimental study on flexural strength of reinforced concrete beams with 100% recycled concrete aggregate," *Eng Struct*, vol. 88, pp. 154–162, 2015, doi: 10.1016/j.engstruct.2015.01.043.

[60] R. Sato, I. Maruyama, T. Sogabe, and M. Sogo, "Flexural behavior of reinforced recycled concrete beams," *Journal of Advanced Concrete Technology*, vol. 5, no. 1, pp. 43–61, 2007, doi: 10.3151/jact.5.43.

[61] W. C. Choi, H. do Yun, and S. W. Kim, "Flexural performance of reinforced recycled aggregate concrete beams," *Magazine of Concrete Research*, vol. 64, no. 9, pp. 837–848, 2012, doi: 10.1680/macr.11.00018.

[62] A. B. Ajdukiewicz and A. T. Kliszczewicz, "Comparative Tests of Beams and Columns Made of Recycled Aggregate Concrete and Natural Aggregate Concrete," *Journal of Advanced Concrete Technology*, vol. 5, no. 2, pp. 259–273, 2007, doi: 10.3151/jact.5.259.

[63] I. S. Ignjatović, S. B. Marinković, Z. M. Mišković, and A. R. Savić, "Flexural behavior of reinforced recycled aggregate concrete beams under short-term loading," *Materials and Structures/Materiaux et Constructions*, vol. 46, no. 6, pp. 1045–1059, 2013, doi: 10.1617/s11527-012-9952-9.

[64] A. M. Knaack and Y. C. Kurama, "Behavior of Reinforced Concrete Beams with Recycled Concrete Coarse Aggregates," *Journal of Structural Engineering*, vol. 141, no. 3, 2015, doi: 10.1061/(asce)st.1943-541x.0001118.

[65] B. S. Hamad, A. H. Dawi, A. Daou, and G. R. Chehab, "Studies of the effect of recycled aggregates on flexural, shear, and bond splitting beam structural behavior," *Case Studies in Construction Materials*, vol. 9, Dec. 2018, doi: 10.1016/j.cscm.2018.e00186.

[66] W. C. Choi and H. D. Yun, "Long-term deflection and flexural behavior of reinforced concrete beams with recycled aggregate," *Mater Des*, vol. 51, pp. 742–750, 2013, doi: 10.1016/j.matdes.2013.04.044.

[67] B. Cantero, I. F. Sáez del Bosque, A. Matías, and C. Medina, "Statistically significant effects of mixed recycled aggregate on the physical-mechanical properties of structural concretes," *Constr Build Mater*, vol. 185, pp. 93–101, 2018, doi: 10.1016/j.conbuildmat.2018.07.060.

[68] C. Medina, W. Zhu, T. Howind, M. I. Sánchez De Rojas, and M. Frías, "Influence of mixed recycled aggregate on the physical-mechanical properties of recycled concrete," *J Clean Prod*, vol. 68, pp. 216–225, 2014, doi: 10.1016/j.jclepro.2014.01.002.

[69] I. F. Sáez del Bosque, W. Zhu, T. Howind, A. Matías, M. I. Sánchez de Rojas, and C. Medina, "Properties of interfacial transition zones (ITZs) in concrete containing recycled mixed aggregate," *Cem Concr Compos*, vol. 81, pp. 25–34, 2017, doi: 10.1016/j.cemconcomp.2017.04.011.

[70] T. Meng, H. Wei, X. Yang, B. Zhang, Y. Zhang, and C. Zhang, "Effect of mixed recycled aggregate on the mechanical strength and microstructure of concrete under different water cement ratios," *Materials*, vol. 14, no. 10, May 2021, doi: 10.3390/ma14102631.

[71] ABNT, *NBR 6118 - Projeto de estruturas de concreto - Procedimento*. Associação Brasileira de Normas Técnicas, BRA., 2014.

[72] A. E. B. Cabral, V. Schalch, D. C. C. D. Molin, and J. L. D. Ribeiro, "Mechanical properties modeling of recycled aggregate concrete,"

Constr Build Mater, vol. 24, no. 4, pp. 421–430, 2010, doi: 10.1016/j.conbuildmat.2009.10.011.

[73] CONAMA, "RESOLUÇÃO nº 307, de 5 de julho de 2002. Publicada no DOU n.136, de 17 de julho de 2002," pp. 95–96, 2002.

[74] United States Environmental Protection Agency, "Sustainable Management of Construction and Demolition Materials." https://www.epa.gov/smm/sustainable-management-construction-and-demolition-materials (accessed Apr. 04, 2018).

[75] R. V. Silva, J. De Brito, and R. K. Dhir, "Properties and composition of recycled aggregates from construction and demolition waste suitable for concrete production," *Constr Build Mater*, vol. 65, pp. 201–217, 2014, doi: 10.1016/j.conbuildmat.2014.04.117.

[76] S. B. Park, B. C. Lee, and J. H. Kim, "Studies on mechanical properties of concrete containing waste glass aggregate," *Cem Concr Res*, vol. 34, no. 12, pp. 2181–2189, 2004, doi: 10.1016/j.cemconres.2004.02.006.

[77] Z. Z. Ismail and E. A. AL-Hashmi, "Recycling of waste glass as a partial replacement for fine aggregate in concrete," *Waste Management*, vol. 29, no. 2, pp. 655–659, 2009, doi: 10.1016/j.wasman.2008.08.012.

[78] S. C. Kou and C. S. Poon, "Properties of self-compacting concrete prepared with recycled glass aggregate," *Cem Concr Compos*, vol. 31, no. 2, pp. 107–113, 2009, doi: 10.1016/j.cemconcomp.2008.12.002.

[79] Y. W. Choi, D. J. Moon, J. S. Chung, and S. K. Cho, "Effects of waste PET bottles aggregate on the properties of concrete," *Cem Concr Res*, vol. 35, no. 4, pp. 776–781, 2005, doi: 10.1016/j.cemconres.2004.05.014.

[80] R. Siddique, J. Khatib, and I. Kaur, "Use of recycled plastic in concrete: A review," *Waste Management*, vol. 28, no. 10, pp. 1835–1852, 2008, doi: 10.1016/j.wasman.2007.09.011.

[81] C. Albano, N. Camacho, M. Hernández, A. Matheus, and A. Gutiérrez, "Influence of content and particle size of waste pet bottles on concrete behavior at different w/c ratios," *Waste Management*, vol. 29, no. 10, pp. 2707–2716, 2009, doi: 10.1016/j.wasman.2009.05.007.

[82] R. V. Silva, J. De Brito, and R. K. Dhir, "Performance of cementitious renderings and masonry mortars containing recycled aggregates from construction and demolition wastes," *Constr Build Mater*, vol. 105, pp. 400–415, 2016, doi: 10.1016/j.conbuildmat.2015.12.171.

[83] Z. H. Duan and C. S. Poon, "Properties of recycled aggregate concrete made with recycled aggregates with different amounts of old adhered mortars," *Mater Des*, vol. 58, pp. 19–29, 2014, doi: 10.1016/j.matdes.2014.01.044.

[84] S. Nagataki, A. Gokce, T. Saeki, and M. Hisada, "Assessment of recycling process induced damage sensitivity of recycled concrete aggregates," *Cem Concr Res*, vol. 34, no. 6, pp. 965–971, 2004, doi: 10.1016/j.cemconres.2003.11.008.

[85] C. Shi, Y. Li, J. Zhang, W. Li, L. Chong, and Z. Xie, "Performance enhancement of recycled concrete aggregate - A review," *J Clean Prod*, vol. 112, pp. 466–472, 2016, doi: 10.1016/j.jclepro.2015.08.057.

[86] M. Behera, S. K. Bhattacharyya, A. K. Minocha, R. Deoliya, and S. Maiti, "Recycled aggregate from C&D waste & its use in concrete - A breakthrough towards sustainability in construction sector: A review," *Constr Build Mater*, vol. 68, pp. 501–516, 2014, doi: 10.1016/j.conbuildmat.2014.07.003.

[87] D. Matias, J. De Brito, A. Rosa, and D. Pedro, "Mechanical properties of concrete produced with recycled coarse aggregates - Influence of the use of superplasticizers," *Constr Build Mater*, vol. 44, pp. 101–109, 2013, doi: 10.1016/j.conbuildmat.2013.03.011.

[88] E. Mulder, T. P. R. de Jong, and L. Feenstra, "Closed Cycle Construction: An integrated process for the separation and reuse of C&D waste," *Waste Management*, vol. 27, no. 10, pp. 1408–1415, 2007, doi: 10.1016/j.wasman.2007.03.013.

[89] H. Shima, H. Tateyashiki, R. Matsuhashi, and Y. Yoshida, "An Advanced Concrete Recycling Technology and its Applicability Assessment through Input-Output Analysis," *Journal of Advanced Concrete Technology*, vol. 3, no. 1, pp. 53–67, 2005, doi: 10.3151/jact.3.53.

[90] A. Akbarnezhad, K. C. G. Ong, M. H. Zhang, C. T. Tam, and T. W. J. Foo, "Microwave-assisted beneficiation of recycled concrete aggregates," *Constr Build Mater*, vol. 25, no. 8, pp. 3469–3479, 2011, doi: 10.1016/j.conbuildmat.2011.03.038.

[91] K. Bru, S. Touzé, F. Bourgeois, N. Lippiatt, and Y. Ménard, "Assessment of a microwave-assisted recycling process for the recovery of high-quality aggregates from concrete waste," *Int J Miner Process*, vol. 126, pp. 90–98, 2014, doi: 10.1016/j.minpro.2013.11.009.

[92] M. S. de Juan and P. A. Gutiérrez, "Study on the influence of attached mortar content on the properties of recycled concrete aggregate," *Constr Build Mater*, vol. 23, no. 2, pp. 872–877, 2009, doi: 10.1016/j.conbuildmat.2008.04.012.

[93] M. Pepe, R. D. Toledo Filho, E. A. B. Koenders, and E. Martinelli, "Alternative processing procedures for recycled aggregates in structural concrete," *Constr Build Mater*, vol. 69, pp. 124–132, 2014, doi: 10.1016/j.conbuildmat.2014.06.084.

[94] A. K. Padmini, K. Ramamurthy, and M. S. Mathews, "Influence of parent concrete on the properties of recycled aggregate concrete," *Constr Build Mater*, vol. 23, no. 2, pp. 829–836, 2009, doi: 10.1016/j.conbuildmat.2008.03.006.

[95] C. S. Poon, Z. H. Shui, L. Lam, H. Fok, and S. C. Kou, "Influence of moisture states of natural and recycled aggregates on the slump and compressive strength of concrete," *Cem Concr Res*, vol. 34, no. 1, pp. 31–36, 2004, doi: 10.1016/S0008-8846(03)00186-8.

[96] K. K. Sagoe-Crentsil, T. Brown, and A. H. Taylor, "Performance of concrete made with commercially produced coarse recycled concrete aggregate," *Cem Concr Res*, vol. 31, no. 5, pp. 707–712, 2001, doi: 10.1016/S0008-8846(00)00476-2.

[97] T. L. Cavalline and D. C. Weggel, "Recycled brick masonry aggregate concrete:Use of brick masonry from construction and demolition waste as recycled aggregate in concrete," *Structural Survey*, vol. 31, no. 3, pp. 160–180, 2013, doi: 10.1108/SS-09-2012-0029.

[98] A. S. Brand, J. R. Roesler, and A. Salas, “Initial moisture and mixing effects on higher quality recycled coarse aggregate concrete,” *Constr Build Mater*, vol. 79, pp. 83–89, Mar. 2015, doi: 10.1016/j.conbuildmat.2015.01.047.

[99] P. K. Mehta and P. J. M. Monteiro, *Concrete: microstructure, properties, and materials*. 2006. doi: 10.1036/0071462899.

[100] J. Xiao, W. Li, Z. Sun, D. A. Lange, and S. P. Shah, “Properties of interfacial transition zones in recycled aggregate concrete tested by nanoindentation,” *Cem Concr Compos*, vol. 37, no. 1, pp. 276–292, 2013, doi: 10.1016/j.cemconcomp.2013.01.006.

[101] N. Kisku, H. Joshi, M. Ansari, S. K. Panda, S. Nayak, and S. C. Dutta, “A critical review and assessment for usage of recycled aggregate as sustainable construction material,” *Constr Build Mater*, vol. 131, pp. 721–740, 2017, doi: 10.1016/j.conbuildmat.2016.11.029.

[102] G. C. Lee and H. B. Choi, “Study on interfacial transition zone properties of recycled aggregate by micro-hardness test,” *Constr Build Mater*, vol. 40, pp. 455–460, 2013, doi: 10.1016/j.conbuildmat.2012.09.114.

[103] Q. Liu, J. Xiao, and Z. Sun, “Experimental study on the failure mechanism of recycled concrete,” *Cem Concr Res*, vol. 41, pp. 1050–1057, 2011, doi: 10.1016/j.cemconres.2011.06.007.

[104] D. S. Seo and H. B. Choi, “Effects of the old cement mortar attached to the recycled aggregate surface on the bond characteristics between aggregate and cement mortar,” *Constr Build Mater*, vol. 59, pp. 72–77, 2014, doi: 10.1016/j.conbuildmat.2014.02.047.

[105] D. A. Lange, H. M. Jennings, and S. P. Shah, “Image analysis techniques for characterization of pore structure of cement-based materials,” *Cem Concr Res*, vol. 24, no. 5, pp. 841–853, 1994, doi: 10.1016/0008-8846(94)90004-3.

[106] A. B. Abell, K. L. Willis, and D. A. Lange, “Mercury Intrusion Porosimetry and Image Analysis of Cement-Based Materials,” *J Colloid Interface Sci*, vol. 211, no. 1, pp. 39–44, Mar. 1999, doi: 10.1006/JCIS.1998.5986.

[107] J. M. V. Gómez-Soberón, "Porosity of recycled concrete with substitution of recycled concrete aggregate: An experimental study," *Cem Concr Res*, vol. 32, pp. 1301–1311, 2002, doi: 10.1016/S0008-8846(02)00795-0.

[108] H. Zhang, Y. Wang, D. E. Lehman, Y. Geng, and K. Kuder, "Time-dependent drying shrinkage model for concrete with coarse and fine recycled aggregate," *Cem Concr Compos*, vol. 105, no. May 2019, p. 103426, 2020, doi: 10.1016/j.cemconcomp.2019.103426.

[109] G. Andreu and E. Miren, "Experimental analysis of properties of high performance recycled aggregate concrete," *Constr Build Mater*, vol. 52, pp. 227–235, 2014, doi: 10.1016/j.conbuildmat.2013.11.054.

[110] H. Guo *et al.*, "Durability of recycled aggregate concrete – A review," *Cem Concr Compos*, vol. 89, pp. 251–259, 2018, doi: 10.1016/j.cemconcomp.2018.03.008.

[111] F. de A. Salgado and F. de A. Silva, "Properties of recycled aggregates from different composition and its influence on concrete strength," *Revista IBRACON de Estruturas e Materiais*, vol. 14, no. 6, 2021, doi: 10.1590/s1983-41952021000600005.

[112] W. H. Kwan, M. Ramli, K. J. Kam, and M. Z. Sulieman, "Influence of the amount of recycled coarse aggregate in concrete design and durability properties," *Constr Build Mater*, vol. 26, no. 1, pp. 565–573, 2012, doi: 10.1016/j.conbuildmat.2011.06.059.

[113] H. B. Le and Q. B. Bui, "Recycled aggregate concretes – A state-of-the-art from the microstructure to the structural performance," *Constr Build Mater*, vol. 257, 2020, doi: 10.1016/j.conbuildmat.2020.119522.

[114] H. Mefteh, O. Kebaïli, H. Oucief, L. Berredjem, and N. Arabi, "Influence of moisture conditioning of recycled aggregates on the properties of fresh and hardened concrete," *J Clean Prod*, vol. 54, pp. 282–288, 2013, doi: 10.1016/j.jclepro.2013.05.009.

[115] J. Yang, Q. Du, and Y. Bao, "Concrete with recycled concrete aggregate and crushed clay bricks," *Constr Build Mater*, vol. 25, no. 4, pp. 1935–1945, 2011, doi: 10.1016/j.conbuildmat.2010.11.063.

[116] J. De Brito, J. Ferreira, J. Pacheco, D. Soares, and M. Guerreiro, "Structural, material, mechanical and durability properties and behaviour of recycled aggregates concrete," *Journal of Building Engineering*, vol. 6, pp. 1–16, 2016, doi: 10.1016/j.jobe.2016.02.003.

[117] M. Arezoumandi, A. R. Steele, and J. S. Volz, "Evaluation of the Bond Strengths Between Concrete and Reinforcement as a Function of Recycled Concrete Aggregate Replacement Level," *Structures*, vol. 16, pp. 73–81, 2018, doi: 10.1016/j.istruc.2018.08.012.

[118] M. Etxeberria, E. Vázquez, and A. Marí, "Microstructure analysis of hardened recycled aggregate concrete," *Magazine of Concrete Research*, vol. 58, no. 10, pp. 683–690, 2006, doi: 10.1680/macr.2006.58.10.683.

[119] B. S. Hamad, A. H. Dawi, A. Daou, and G. R. Chehab, "Studies of the effect of recycled aggregates on flexural, shear, and bond splitting beam structural behavior," *Case Studies in Construction Materials*, vol. 9, no. 2018, p. e00186, 2018, doi: 10.1016/j.cscm.2018.e00186.

[120] C. S. Poon, Z. H. Shui, and L. Lam, "Effect of microstructure of ITZ on compressive strength of concrete prepared with recycled aggregates," *Constr Build Mater*, vol. 18, no. 6, pp. 461–468, 2004, doi: 10.1016/j.conbuildmat.2004.03.005.

[121] S. W. Tabsh and A. S. Abdelfatah, "Influence of recycled concrete aggregates on strength properties of concrete," *Constr Build Mater*, vol. 23, no. 2, pp. 1163–1167, 2009, doi: 10.1016/j.conbuildmat.2008.06.007.

[122] M. B. De Oliveira and E. Vazquez, "The influence of retained moisture in aggregates from recycling on the properties of new hardened concrete," *Waste Management*, vol. 16, no. 1–3, pp. 113–117, 1996, doi: 10.1016/S0956-053X(96)00033-5.

[123] M. Pepe, R. D. Toledo Filho, E. A. B. Koenders, and E. Martinelli, "Alternative processing procedures for recycled aggregates in structural concrete," *Constr Build Mater*, vol. 69, pp. 124–132, 2014, doi: 10.1016/j.conbuildmat.2014.06.084.

[124] H. Dilbas, M. Şimşek, and Ö. Çakir, "An investigation on mechanical and physical properties of recycled aggregate concrete (RAC) with

and without silica fume," *Constr Build Mater*, vol. 61, no. March 2006, pp. 50–59, 2014, doi: 10.1016/j.conbuildmat.2014.02.057.

[125] S. Ismail and M. Ramli, "Mechanical strength and drying shrinkage properties of concrete containing treated coarse recycled concrete aggregates," *Constr Build Mater*, vol. 68, pp. 726–739, 2014, doi: 10.1016/j.conbuildmat.2014.06.058.

[126] S. C. Kou and C. S. Poon, "Long-term mechanical and durability properties of recycled aggregate concrete prepared with the incorporation of fly ash," *Cem Concr Compos*, vol. 37, no. 1, pp. 12–19, 2013, doi: 10.1016/j.cemconcomp.2012.12.011.

[127] J. Xiao, J. Li, and C. Zhang, "Mechanical properties of recycled aggregate concrete under uniaxial loading," *Cem Concr Res*, vol. 35, no. 6, pp. 1187–1194, 2005, doi: 10.1016/j.cemconres.2004.09.020.

[128] N. K. Bairagi, K. Ravande, and V. K. Pareek, "Behaviour of concrete with different proportions of natural and recycled aggregates," *Resour Conserv Recycl*, vol. 9, no. 1–2, pp. 109–126, 1993, doi: 10.1016/0921-3449(93)90036-F.

[129] D. Xuan, B. Zhan, and C. S. Poon, "Assessment of mechanical properties of concrete incorporating carbonated recycled concrete aggregates," *Cem Concr Compos*, vol. 65, pp. 67–74, 2016, doi: 10.1016/j.cemconcomp.2015.10.018.

[130] S. M. S. Kazmi, M. J. Munir, Y. F. Wu, I. Patnaikuni, Y. Zhou, and F. Xing, "Effect of recycled aggregate treatment techniques on the durability of concrete: A comparative evaluation," *Constr Build Mater*, vol. 264, p. 120284, 2020, doi: 10.1016/j.conbuildmat.2020.120284.

[131] N. K. Bui, T. Satomi, and H. Takahashi, "Improvement of mechanical properties of recycled aggregate concrete basing on a new combination method between recycled aggregate and natural aggregate," *Constr Build Mater*, vol. 148, pp. 376–385, 2017, doi: 10.1016/j.conbuildmat.2017.05.084.

[132] S. Kou and C. Poon, "Mechanical properties of 5-year-old concrete prepared with recycled aggregates obtained from three different

sources," *Magazine of Concrete Research*, vol. 60, no. 1, pp. 57–64, 2008, doi: 10.1680/macr.2007.00052.

[133] J. de Brito, J. Ferreira, J. Pacheco, D. Soares, and M. Guerreiro, "Structural, material, mechanical and durability properties and behaviour of recycled aggregates concrete," *Journal of Building Engineering*, vol. 6, pp. 1–16, 2016, doi: 10.1016/j.jobe.2016.02.003.

[134] M. B. Leite and P. J. M. Monteiro, "Microstructural analysis of recycled concrete using X-ray microtomography," *Cem Concr Res*, vol. 81, pp. 38–48, 2016, doi: 10.1016/j.cemconres.2015.11.010.

[135] I. Martínez-Lage, P. Vázquez-Burgo, and M. Velay-Lizancos, "Sustainability evaluation of concretes with mixed recycled aggregate based on holistic approach: Technical, economic and environmental analysis," *Waste Management*, vol. 104, pp. 9–19, 2020, doi: 10.1016/j.wasman.2019.12.044.

[136] K. N. Rahal and Y. T. Alrefaei, "Shear strength of recycled aggregate concrete beams containing stirrups," *Constr Build Mater*, vol. 191, pp. 866–876, 2018, doi: 10.1016/j.conbuildmat.2018.10.023.

[137] S. Pradhan, S. Kumar, and S. V. Barai, "Shear performance of recycled aggregate concrete beams: An insight for design aspects," *Constr Build Mater*, vol. 178, pp. 593–611, 2018, doi: 10.1016/j.conbuildmat.2018.05.022.

[138] F. Al Mahmoud, R. Boissiere, C. Mercier, and A. Khelil, "Shear behavior of reinforced concrete beams made from recycled coarse and fine aggregates," *Structures*, vol. 25, no. October 2019, pp. 660–669, 2020, doi: 10.1016/j.istruc.2020.03.015.

[139] C. S. Poon and D. Chan, "The use of recycled aggregate in concrete in Hong Kong," *Resour Conserv Recycl*, vol. 50, no. 3, pp. 293–305, 2007, doi: 10.1016/j.resconrec.2006.06.005.

[140] L. Butler, J. S. West, and S. L. Tighe, "The effect of recycled concrete aggregate properties on the bond strength between RCA concrete and steel reinforcement," *Cem Concr Res*, vol. 41, no. 10, pp. 1037–1049, 2011, doi: 10.1016/j.cemconres.2011.06.004.

[141] D. Talamona and K. Hai Tan, "Properties of recycled aggregate concrete for sustainable urban built environment," *J Sustain Cem*

Based Mater, vol. 1, no. 4, pp. 202–210, 2012, doi: 10.1080/21650373.2012.754571.

[142] M. T. Khan, I. Jahan, and K. M. Amanat, "Splitting tensile strength of natural aggregates, recycled aggregates and brick chips concrete," *Proceedings of Institution of Civil Engineers: Construction Materials*, vol. 173, no. 2, pp. 79–88, 2020, doi: 10.1680/jcoma.18.00049.

[143] N. K. Bui, T. Satomi, and H. Takahashi, "Recycling woven plastic sack waste and PET bottle waste as fiber in recycled aggregate concrete: An experimental study," *Waste Management*, vol. 78, pp. 79–93, 2018, doi: 10.1016/j.wasman.2018.05.035.

[144] M. Limbachiya, M. S. Meddah, and Y. Ouchagour, "Use of recycled concrete aggregate in fly-ash concrete," *Constr Build Mater*, vol. 27, no. 1, pp. 439–449, 2012, doi: 10.1016/j.conbuildmat.2011.07.023.

[145] S. C. Kou, C. S. Poon, and M. Etxeberria, "Influence of recycled aggregates on long term mechanical properties and pore size distribution of concrete," *Cem Concr Compos*, vol. 33, no. 2, pp. 286–291, 2011, doi: 10.1016/j.cemconcomp.2010.10.003.

[146] M. Ahmadi, S. Farzin, A. Hassani, and M. Motamedi, "Mechanical properties of the concrete containing recycled fibers and aggregates," *Constr Build Mater*, vol. 144, pp. 392–398, 2017, doi: 10.1016/j.conbuildmat.2017.03.215.

[147] S. Moallemi Pour and M. Shahria Alam, "Investigation of Compressive Bond Behavior of Steel Rebar Embedded in Concrete With Partial Recycled Aggregate Replacement," *Structures*, vol. 7, pp. 153–164, 2016, doi: 10.1016/j.istruc.2016.06.010.

[148] N. Fonseca, J. De Brito, and L. Evangelista, "The influence of curing conditions on the mechanical performance of concrete made with recycled concrete waste," *Cem Concr Compos*, vol. 33, no. 6, pp. 637–643, 2011, doi: 10.1016/j.cemconcomp.2011.04.002.

[149] M. Pepe, R. D. Toledo Filho, E. A. B. Koenders, and E. Martinelli, "A novel mix design methodology for Recycled Aggregate Concrete," *Constr Build Mater*, vol. 122, pp. 362–372, 2016, doi: 10.1016/j.conbuildmat.2016.06.061.

[150] H. R. Chaboki, M. Ghalehnovi, A. Karimipour, J. de Brito, and M. Khatibinia, "Shear behaviour of concrete beams with recycled aggregate and steel fibres," *Constr Build Mater*, vol. 204, pp. 809–827, 2019, doi: 10.1016/j.conbuildmat.2019.01.130.

[151] B. Mas, A. Cladera, T. Del Olmo, and F. Pitarch, "Influence of the amount of mixed recycled aggregates on the properties of concrete for non-structural use," *Constr Build Mater*, vol. 27, no. 1, pp. 612–622, 2012, doi: 10.1016/j.conbuildmat.2011.06.073.

[152] K. H. Younis and K. Pilakoutas, "Strength prediction model and methods for improving recycled aggregate concrete," *Constr Build Mater*, vol. 49, pp. 688–701, 2013, doi: 10.1016/j.conbuildmat.2013.09.003.

[153] M. Malešev, V. Radonjanin, and S. Marinković, "Recycled concrete as aggregate for structural concrete production," *Sustainability*, vol. 2, no. 5, pp. 1204–1225, 2010, doi: 10.3390/su2051204.

[154] A. M. Wagih, H. Z. El-Karmoty, M. Ebid, and S. H. Okba, "Recycled construction and demolition concrete waste as aggregate for structural concrete," *HBRC Journal*, vol. 9, no. 3, pp. 193–200, 2013, doi: 10.1016/j.hbrcj.2013.08.007.

[155] S. C. Kou and C. S. Poon, "Enhancing the durability properties of concrete prepared with coarse recycled aggregate," *Constr Build Mater*, vol. 35, pp. 69–76, 2012, doi: 10.1016/j.conbuildmat.2012.02.032.

[156] K. Islam, J. Rahman, K. Sakil, M. Rezaul, and A. H. M. Muntasir, "Flexural response of fiber reinforced concrete beams with waste tires rubber and recycled aggregate," *J Clean Prod*, vol. 278, p. 123842, 2021, doi: 10.1016/j.jclepro.2020.123842.

[157] R. Ali and R. Hamid, "Workability and Compressive Strength of Recycled Concrete Waste Aggregate Concrete," *Applied Mechanics and Materials*, vol. 754–755, pp. 417–420, 2015, doi: 10.4028/www.scientific.net/AMM.754-755.417.

[158] V. V. W. Y. Tam, X. F. X. Gao, and C. C. M. Tam, "Microstructural analysis of recycled aggregate concrete produced from two-stage

mixing approach," *Cem Concr Res*, vol. 35, no. 6, pp. 1195–1203, 2005, doi: 10.1016/j.cemconres.2004.10.025.

[159] K. Kim, M. Shin, and S. Cha, "Combined effects of recycled aggregate and fly ash towards concrete sustainability," *Constr Build Mater*, vol. 48, pp. 499–507, 2013, doi: 10.1016/j.conbuildmat.2013.07.014.

[160] V. W. Y. Tam, A. Butera, and K. N. Le, "Carbon-conditioned recycled aggregate in concrete production," *J Clean Prod*, vol. 133, pp. 672–680, 2016, doi: 10.1016/j.jclepro.2016.06.007.

[161] A. Katz, "Treatments for the Improvement of Recycled Aggregate," *Journal of Materials in Civil Engineering*, vol. 16, no. 6, pp. 597–603, 2004, doi: 10.1061/(ASCE)0899-1561(2004)16:6(597).

[162] A. Abd Elhakam, A. E. Mohamed, and E. Awad, "Influence of self-healing, mixing method and adding silica fume on mechanical properties of recycled aggregates concrete," *Constr Build Mater*, vol. 35, pp. 421–427, 2012, doi: 10.1016/j.conbuildmat.2012.04.013.

[163] M. Pepe, E. A. B. Koenders, C. Faella, and E. Martinelli, "Structural concrete made with recycled aggregates: Hydration process and compressive strength models," *Mech Res Commun*, vol. 58, pp. 139–145, 2014, doi: 10.1016/j.mechrescom.2014.02.001.

[164] V. Corinaldesi, "Structural concrete prepared with coarse recycled concrete aggregate: From investigation to design," *Advances in Civil Engineering*, vol. 2011, pp. 1–7, 2011, doi: 10.1155/2011/283984.

[165] E. E. Etman, H. M. Afefy, A. T. Baraghith, and S. A. Khedr, "Improving the shear performance of reinforced concrete beams made of recycled coarse aggregate," *Constr Build Mater*, vol. 185, pp. 310–324, 2018, doi: 10.1016/j.conbuildmat.2018.07.065.

[166] S. C. Kou and C. S. Poon, "Properties of concrete prepared with PVA-impregnated recycled concrete aggregates," *Cem Concr Compos*, vol. 32, no. 8, pp. 649–654, 2010, doi: 10.1016/j.cemconcomp.2010.05.003.

[167] J. Amorim, P. Roberto, L. Lima, M. Batista, R. Dias, and T. Filho, "Cement & Concrete Composites Compressive stress – strain behavior of steel fiber reinforced-recycled aggregate concrete," *Cem*

Concr Compos, vol. 46, pp. 65–72, 2014, doi: 10.1016/j.cemconcomp.2013.11.006.

[168] P. S. Lovato, "Verificação dos parâmetros de controle de agregados reciclados de resíduos de construção e demolição para utilização em concreto," Dissertação de Mestrado, Universidade Federal do Rio Grande do Sul (UFRGS), 2007.

[169] R. S. Ravindrarajah and C. Tam, "Properties of concrete made with crushed concrete as coarse aggregate," *Magazine of Concrete Research*, 1985, doi: 10.1680/macr.1985.37.130.29.

[170] V. W. Y. Tam and C. M. Tam, "Assessment of durability of recycled aggregate concrete produced by two-stage mixing approach," *J Mater Sci*, vol. 42, no. 10, pp. 3592–3602, 2007, doi: 10.1007/s10853-006-0379-y.

[171] V. W. Y. Tam and C. M. Tam, "Diversifying two-stage mixing approach (TSMA) for recycled aggregate concrete: TSMAsand TSMAsc," *Constr Build Mater*, vol. 22, no. 10, pp. 2068–2077, 2008, doi: 10.1016/j.conbuildmat.2007.07.024.

[172] V. W.-Y. Tam, X.-F. Gao, and C. M. Tam, "Comparing performance of modified two-stage mixing approach for producing recycled aggregate concrete," *Magazine of Concrete Research*, vol. 58, no. 7, pp. 477–484, 2006, doi: 10.1680/macr.2006.58.7.477.

[173] S. Ismail and M. Ramli, "Engineering properties of treated recycled concrete aggregate (RCA) for structural applications," *Constr Build Mater*, vol. 44, pp. 464–476, 2013, doi: 10.1016/j.conbuildmat.2013.03.014.

[174] V. W. Y. Tam, C. M. Tam, and K. N. Le, "Removal of cement mortar remains from recycled aggregate using pre-soaking approaches," *Resour Conserv Recycl*, vol. 50, no. 1, pp. 82–101, 2007, doi: 10.1016/j.resconrec.2006.05.012.

[175] P. Saravanakumar, K. Abhiram, and B. Manoj, "Properties of treated recycled aggregates and its influence on concrete strength characteristics," *Constr Build Mater*, vol. 111, pp. 611–617, 2016, doi: 10.1016/j.conbuildmat.2016.02.064.

[176] L. Wang, J. Wang, X. Qian, P. Chen, Y. Xu, and J. Guo, "An environmentally friendly method to improve the quality of recycled concrete aggregates," *Constr Build Mater*, vol. 144, pp. 432–441, 2017, doi: 10.1016/j.conbuildmat.2017.03.191.

[177] V. Spaeth and A. Djerbi Tegguer, "Improvement of recycled concrete aggregate properties by polymer treatments," *International Journal of Sustainable Built Environment*, vol. 2, no. 2, pp. 143–152, 2013, doi: 10.1016/j.ijsbe.2014.03.003.

[178] V. Spaeth and J. P. Lecomte, "Hydration Process and Microstructure Development of Integral Water Repellent Cement Based Materials," *5th International Conference on Water Repellent Treatment of Building Materials*, vol. 254, pp. 245–254, 2008.

[179] F. H. Wittmann, Y. Xian, T. Zhao, F. Beltzung, and S. Giessler, "Drying and Shrinkage of Integral Water Repellent Concrete," vol. 12, no. March, pp. 229–242, 2006.

[180] M. Tsujino, T. Noguchi, M. Tamura, M. Kanematsu, and I. Maruyama, "Application of Conventionally Recycled Coarse Aggregate to Concrete Structure by Surface Modification Treatment," *Journal of Advanced Concrete Technology*, vol. 5, no. 1, pp. 13–25, 2007, doi: 10.3151/jact.5.13.

[181] W. Zhao, T. , Wittmann, F.H., Jiang, R., Li, "Application of Silane-based Compounds for the Production of Application of Silane-based Compounds for the Production of Integral Water Repellent Concrete." HVI, 6th International Conference on WR Treatment of Building Materials, pp. 137e144, 2011.

[182] Y. G. Zhu, S. C. Kou, C. S. Poon, J. G. Dai, and Q. Y. Li, "Influence of silane-based water repellent on the durability properties of recycled aggregate concrete," *Cem Concr Compos*, vol. 35, no. 1, pp. 32–38, 2013, doi: 10.1016/j.cemconcomp.2012.08.008.

[183] R. V. Silva, J. de Brito, R. Neves, and R. Dhir, "Prediction of Chloride Ion Penetration of Recycled Aggregate Concrete," *Materials Research*, vol. 18, no. 2, pp. 427–440, 2015, doi: 10.1590/1516-1439.000214.

[184] J. Wang, B. Vandevyvere, S. Vanhessche, J. Schoon, N. Boon, and N. De Belie, "Microbial carbonate precipitation for the improvement of quality of recycled aggregates," *J Clean Prod*, vol. 156, pp. 355–366, 2017, doi: 10.1016/j.jclepro.2017.04.051.

[185] F. Hammes and W. Verstraete, "Key roles of pH and calcium metabolism in microbial carbonate precipitation," *Rev Environ Sci Biotechnol*, vol. 1, no. 1, pp. 3–7, 2002, doi: 10.1023/A:1015135629155.

[186] A. M. Grabiec, J. Klama, D. Zawal, and D. Krupa, "Modification of recycled concrete aggregate by calcium carbonate biodeposition," *Constr Build Mater*, vol. 34, pp. 145–150, 2012, doi: 10.1016/j.conbuildmat.2012.02.027.

[187] J. Qiu, D. Q. S. Tng, and E. H. Yang, "Surface treatment of recycled concrete aggregates through microbial carbonate precipitation," *Constr Build Mater*, vol. 57, pp. 144–150, 2014, doi: 10.1016/j.conbuildmat.2014.01.085.

[188] M. Thiery, P. Dangla, P. Belin, G. Habert, and N. Roussel, "Carbonation kinetics of a bed of recycled concrete aggregates: A laboratory study on model materials," *Cem Concr Res*, vol. 46, pp. 50–65, 2013, doi: 10.1016/j.cemconres.2013.01.005.

[189] J. Zhang *et al.*, "Performance Enhancement of Recycled Concrete Aggregates through Carbonation," vol. 27, no. 5, 2015, doi: 10.1061/(ASCE)MT.1943-5533.0001296.

[190] J. Zhang, C. Shi, Y. Li, X. Pan, C. S. Poon, and Z. Xie, "Influence of carbonated recycled concrete aggregate on properties of cement mortar," *Constr Build Mater*, vol. 98, pp. 1–7, 2015, doi: 10.1016/j.conbuildmat.2015.08.087.

[191] S. C. Kou, B. J. Zhan, and C. S. Poon, "Use of a CO2 curing step to improve the properties of concrete prepared with recycled aggregates," *Cem Concr Compos*, vol. 45, pp. 22–28, 2014, doi: 10.1016/j.cemconcomp.2013.09.008.

[192] B. Zhan, C. S. Poon, Q. Liu, S. Kou, and C. Shi, "Experimental study on CO2 curing for enhancement of recycled aggregate properties,"

Constr Build Mater, vol. 67, pp. 3–7, 2014, doi: 10.1016/j.conbuildmat.2013.09.008.

[193] D. Kong, T. Lei, J. Zheng, C. Ma, J. Jiang, and J. Jiang, "Effect and mechanism of surface-coating pozzalanics materials around aggregate on properties and ITZ microstructure of recycled aggregate concrete," *Constr Build Mater*, vol. 24, no. 5, pp. 701–708, 2010, doi: 10.1016/j.conbuildmat.2009.10.038.

[194] V. S. Babu, A. K. Mullick, K. K. Jain, and P. K. Singh, "Strength and durability characteristics of high-strength concrete with recycled aggregate-influence of processing," *J Sustain Cem Based Mater*, vol. 4, no. 1, pp. 54–71, 2014, doi: 10.1080/21650373.2014.976777.

[195] R. V. Silva, J. De Brito, R. Neves, and R. Dhir, "Prediction of chloride ion penetration of recycled aggregate concrete," *Materials Research*, vol. 18, no. 2, pp. 427–440, 2015, doi: 10.1590/1516-1439.000214.

[196] S. C. Kou, C. S. Poon, and F. Agrela, "Comparisons of natural and recycled aggregate concretes prepared with the addition of different mineral admixtures," *Cem Concr Compos*, vol. 33, no. 8, pp. 788–795, 2011, doi: 10.1016/j.cemconcomp.2011.05.009.

[197] M. Limbachiya, M. Meddah, and Y. Ouchagour, "Performance of portland silica fume cement concrete produced with recycled concrete aggregate," *ACI Mater J*, vol. 109, no. 1, pp. 91–100, 2012.

[198] L. P. Singh, S. R. Karade, S. K. Bhattacharyya, M. M. Yousuf, and S. Ahalawat, "Beneficial role of nanosilica in cement based materials - A review," *Constr Build Mater*, vol. 47, pp. 1069–1077, 2013, doi: 10.1016/j.conbuildmat.2013.05.052.

[199] C. Lima, A. Caggiano, C. Faella, E. Martinelli, M. Pepe, and R. Realfonzo, "Physical properties and mechanical behaviour of concrete made with recycled aggregates and fly ash," *Constr Build Mater*, vol. 47, pp. 547–559, 2013, doi: 10.1016/j.conbuildmat.2013.04.051.

[200] R. Somna, C. Jaturapitakkul, P. Rattanachu, and W. Chalee, "Effect of ground bagasse ash on mechanical and durability properties of recycled aggregate concrete," *Mater Des*, vol. 36, pp. 597–603, 2012, doi: 10.1016/j.matdes.2011.11.065.

[201] R. Somna, C. Jaturapitakkul, and A. M. Amde, "Effect of ground fly ash and ground bagasse ash on the durability of recycled aggregate concrete," *Cem Concr Compos*, vol. 34, no. 7, pp. 848–854, 2012, doi: 10.1016/j.cemconcomp.2012.03.003.

[202] R. Kurda, J. de Brito, and J. D. Silvestre, "Influence of recycled aggregates and high contents of fly ash on concrete fresh properties," *Cem Concr Compos*, vol. 84, no. 2017, pp. 198–213, 2017, doi: 10.1016/j.cemconcomp.2017.09.009.

[203] W. Tangchirapat, R. Buranasing, and C. Jaturapitakkul, "Use of High Fineness of Fly Ash to Improve Properties of Recycled Aggregate Concrete," *Journal of Materials in Civil Engineering*, vol. 22, no. 6, pp. 565–571, 2010, doi: 10.1061/(ASCE)MT.1943-5533.0000054.

[204] V. W. Y. Tam, C. M. Tam, and Y. Wang, "Optimization on proportion for recycled aggregate in concrete using two-stage mixing approach," *Constr Build Mater*, vol. 21, no. 10, pp. 1928–1939, Oct. 2007, doi: 10.1016/j.conbuildmat.2006.05.040.

[205] J. Moreno Juez, B. Cazacliu, A. Cothenet, R. Artoni, and N. Roquet, "Recycled concrete aggregate attrition during mixing new concrete," *Constr Build Mater*, vol. 116, pp. 299–309, Jul. 2016, doi: 10.1016/j.conbuildmat.2016.04.131.

[206] E. A. B. Koenders, M. Pepe, and E. Martinelli, "Compressive strength and hydration processes of concrete with recycled aggregates," *Cem Concr Res*, vol. 56, pp. 203–212, Feb. 2014, doi: 10.1016/j.cemconres.2013.11.012.

[207] ACI, *ACI 555R-01 - Removal and Reuse of Hardened Concrete*. 2001.

[208] M. Amario, C. S. Rangel, M. Pepe, and R. D. Toledo Filho, "Optimization of normal and high strength recycled aggregate concrete mixtures by using packing model," *Cem Concr Compos*, vol. 84, pp. 83–92, 2017, doi: 10.1016/j.cemconcomp.2017.08.016.

[209] N. K. Bairagi, H. S. Vidyadhara, M. Tech, and K. Ravande, "Mix design procedure for recycled aggregate concrete," 1990.

[210] I. B. Topçu and S. Şengel, "Properties of concretes produced with waste concrete aggregate," *Cem Concr Res*, vol. 34, no. 8, pp. 1307–1312, Aug. 2004, doi: 10.1016/j.cemconres.2003.12.019.

[211] G. Fathifazl, A. Abbas, A. G. Razaqpur, O. B. Isgor, B. Fournier, and S. Foo, "New Mixture Proportioning Method for Concrete Made with Coarse Recycled Concrete Aggregate", doi: 10.1061/ASCE0899-1561200921:10601.

[212] P. K. Gupta, Z. A. Khaudhair, and A. K. Ahuja, "A new method for proportioning recycled concrete," *Structural Concrete*, vol. 17, no. 4, pp. 677–687, Dec. 2016, doi: 10.1002/suco.201400076.

[213] N. Deshpande, S. Londhe, and S. Kulkarni, "Modeling compressive strength of recycled aggregate concrete by Artificial Neural Network, Model Tree and Non-linear Regression," *International Journal of Sustainable Built Environment*, vol. 3, no. 2, pp. 187–198, 2014, doi: 10.1016/j.ijsbe.2014.12.002.

[214] M. Pepe, "A Conceptual Model for Designing Recycled Aggregate Concrete for Structural Applications," Springer International Publishing Switzerland, 2015, pp. 7–16. doi: 10.1007/978-3-319-26473-8_2.

[215] S. Kumar and M. Santhanam, "Particle packing theories and their application in concrete mixture proportioning: A review," 2003.

[216] R. Jones, L. Zheng, and M. Newlands, "Comparison of particle packing models for proportioning concrete constituents for minimum voids ratio," *Mater Struct*, vol. 35, no. February 2016, pp. 301–309, 2002, doi: 10.1007/BF02482136.

[217] S. Pradhan, S. Kumar, and S. v Barai, "Recycled aggregate concrete : Particle Packing Method (PPM) of mix design approach," *Constr Build Mater*, vol. 152, pp. 269–284, 2017, doi: 10.1016/j.conbuildmat.2017.06.171.

[218] M. G. Winter, "A conceptual framework for the recycling of aggregates and other wastes," *Municipal Engineer*, vol. 151, no. 3, pp. 177–187, 2002, doi: 10.1680/muen.151.3.177.38887.

[219] RILEM, *Final report of the RILEM Technical Committee 217-PRE*. Springer Netherlands, 2013. doi: 10.1007/978-94-007-4908-5.

[220] V. W. Y. Tam, M. Soomro, and A. C. J. Evangelista, "A review of recycled aggregate in concrete applications (2000–2017)," *Constr*

Build Mater, vol. 172, pp. 272–292, 2018, doi: 10.1016/j.conbuildmat.2018.03.240.

[221] DIN, *DIN 4226-100 Aggregates for concrete and mortar - Part 100 : Recycled aggregates*. Deutsches Institut Fur Normung, 2002.

[222] Royal Netherlands Standardization Institute, *NEN 5905 - Aggregates for concrete - Materials with a density of at least 2000 kg/m^3*. 1997.

[223] RILEM, *TC 121-DRG Guidance for Demolition and Reuse of Concrete and Masonry - Specifications for Concrete with Recycled Aggregates*, vol. 27. 1994, pp. 557–559. doi: 10.1007/BF02473217.

[224] Japan Society of Civil Engineers, *New Standards on Recycled Aggregates and Molten-Slag in Japan*. [Accessed 03 May 2021]. Available from Internet: www.jsce.or.jp/committee/concrete/e/newsletter/newsletter08/Recycled%20Aggregates%20and%20Molten-Slag.pdf.

[225] X. Li, "Recycling and reuse of waste concrete in China. Part I. Material behaviour of recycled aggregate concrete," *Resour Conserv Recycl*, vol. 53, no. 1–2, pp. 36–44, 2008, doi: 10.1016/j.resconrec.2008.09.006.

[226] L. J. Butler, J. S. West, and S. L. Tighe, "Bond of Reinforcement in Concrete Incorporating Recycled Concrete Aggregates," *Journal of Structural Engineering*, vol. 141, no. 3, Mar. 2015, doi: 10.1061/(asce)st.1943-541x.0000928.

[227] S. Seara-Paz, B. González-Fonteboa, J. Eiras-López, and M. F. Herrador, "Bond behavior between steel reinforcement and recycled concrete," *Materials and Structures/Materiaux et Constructions*, vol. 47, no. 1–2, pp. 323–334, Jan. 2014, doi: 10.1617/s11527-013-0063-z.

[228] F. al Mahmoud, R. Boissiere, C. Mercier, and A. Khelil, "Shear behavior of reinforced concrete beams made from recycled coarse and fine aggregates," *Structures*, vol. 25, pp. 660–669, Jun. 2020, doi: 10.1016/j.istruc.2020.03.015.

[229] T. U. Mohammed, K. H. Shikdar, and M. A. Awal, "Shear strength of RC beam made with recycled brick aggregate," *Eng Struct*, vol. 189, pp. 497–508, Jun. 2019, doi: 10.1016/j.engstruct.2019.03.093.

[230] K. N. Rahal and Y. T. Alrefaei, "Shear strength of recycled aggregate concrete beams containing stirrups," *Constr Build Mater*, vol. 191, pp. 866–876, Dec. 2018, doi: 10.1016/j.conbuildmat.2018.10.023.

[231] S. Pradhan, S. Kumar, and S. v. Barai, "Shear performance of recycled aggregate concrete beams: An insight for design aspects," *Constr Build Mater*, vol. 178, pp. 593–611, Jul. 2018, doi: 10.1016/j.conbuildmat.2018.05.022.

[232] E. E. Etman, H. M. Afefy, A. T. Baraghith, and S. A. Khedr, "Improving the shear performance of reinforced concrete beams made of recycled coarse aggregate," *Constr Build Mater*, vol. 185, pp. 310–324, Oct. 2018, doi: 10.1016/j.conbuildmat.2018.07.065.

[233] M. Arezoumandi, A. Smith, J. S. Volz, and K. H. Khayat, "An experimental study on shear strength of reinforced concrete beams with 100% recycled concrete aggregate," *Constr Build Mater*, vol. 53, pp. 612–620, Feb. 2014, doi: 10.1016/j.conbuildmat.2013.12.019.

[234] G. Wardeh, E. Ghorbel, and B. Fouré, "Poutres soumises à l'effort tranchant," in *Le béton recyclé*, F. Larrard and H. Colina, Eds., Marne-la-Vallée: Ifsttar, 2018, pp. 459–473.

[235] N. Tošić, S. Marinković, and I. Ignjatović, "A database on flexural and shear strength of reinforced recycled aggregate concrete beams and comparison to Eurocode 2 predictions," *Constr Build Mater*, vol. 127, pp. 932–944, Nov. 2016, doi: 10.1016/j.conbuildmat.2016.10.058.

[236] J. N. Pacheco, J. de Brito, C. Chastre, and L. Evangelista, "Uncertainty of shear resistance models: Influence of recycled concrete aggregate on beams with and without shear reinforcement," *Eng Struct*, vol. 204, Feb. 2020, doi: 10.1016/j.engstruct.2019.109905.

[237] K. E.-G. Hassan, J. M. Reid, and M. S. Al-Kuwari, "Recycled aggregates in structural concrete – a Qatar case study," *Proceedings of the Institution of Civil Engineers - Construction Materials*, vol. 169, no. 2, pp. 72–82, 2016, doi: 10.1680/coma.15.00017.

[238] ABNT, *NBR NM 46 - Agregados - Determinação do material fino que passa através da peneira 75 um, por lavagem*. Associação Brasileira de Normas Técnicas, BRA., 2003.

[239] ABNT, *NBR 16973 - Agregados - Determinação do material fino que passa pela peneira de 75 μm por lavagem*. 2021.

[240] ABNT, *NBR NM 248 - Agregados - Determinação da composição granulométrica*. Associação Brasileira de Normas Técnicas, BRA., 2003.

[241] ABNT, *NBR 17054 - Agregados - Determinação da composição granulométrica - Método de ensaio*. 2022.

[242] ABNT, *NBR 7809 - Agregado graúdo - Determinação do índice de forma pelo método do paquímetro - Método de ensaio*. Associação Brasileira de Normas Técnicas, BRA., 2019.

[243] ABNT, *NBR 16917 - Agregado Graúdo - Determinação da densidade e absorção da água*. 2021. [Online]. Available: www.abnt.org.br

[244] ABNT, *NBR 16972 - Agregados - Determinação da massa unitária e do índice de vazios*. 2021.

[245] BSI, *BS 812 Part 110 - Aggregate Crushing Value*. BSI, London, UK, 1990.

[246] F. de. Larrard, *Concrete mixture proportioning: A scientific approach*. E & FN Spon, New Fetter Lane, London, UK, 1999. doi: 10.1017/CBO9781107415324.004.

[247] ABNT, *NBR 7211 - Agregado para concreto - Especificação*. Associação Brasileira de Normas Técnicas, BRA., 2009.

[248] J. J. L. Tenório, "Avaliação De Propriedades Do Concreto Produzido com Agregados Reciclados de Resíduos de Construção e Demolição Visando Aplicações Estruturais," Dissertação de Mestrado. Universidade Federal de Alagoas, 2007.

[249] M. B. Leite, "Avaliação de propriedades mecânicas de concretos produzidos com agregados reciclados de resíduos de construção e demolição," Universidade Federal do Rio Grande do Sul, Porto Alegre, Brasil, 2001. doi: 000292768.

[250] A. Bashir, G. Chhavi, A. M.A., and A. S.I., "Comparison of Properties of Coarse Aggregate Obtained from Recycled Concrete with that of

Conventional Coarse Aggregates," *European Journal of Advances in Engineering and Technology*, vol. 5, no. 8, pp. 628-637., 2018, doi: 10.13140/RG.2.2.35863.83361.

[251] M. C. Limbachiya, T. Leelawat, and R. K. Dhir, "Use of recycled concrete aggregate in high-strength concrete," *Mater Struct*, vol. 33, no. 9, pp. 574–580, 2000, doi: 10.1007/BF02480538.

[252] P. Helene and B. F. Tutikian, "Dosagem dos Concretos de Cimento Portland," in *Concreto: Ciência e Tecnologia*, Ipsis, Ed., São Paulo, 2011, pp. 415–452.

[253] B. de Oliveira, L. Ricci, A. M. Pereira, and J. L. Akasaki, "Estudo de Dosagens Visando Obter Concretos para Obras de Pequeno Porte," *Fórum Ambiental da Alta Paulista*, vol. 13, pp. 182–194, 2017.

[254] R. S. A. ALENCAR, "Dosagem do concreto autoadensável: produção de pré-fabricados," Universidade de São Paulo, São Paulo, 2008.

[255] P. R. L. ; Helene and P. Terzian, *Manual de Dosagem e Controle do Concreto*. São Paulo: SENAI, 1992. [Online]. Available: www.docsity.com

[256] P. C. Aïtcin, "High-performance mix design methods," in *High-Performance Concrete*, E & FN SPON, 1998.

[257] A. K. H. Kwan, P. L. Ng, and K. Y. Huen, "Effects of fines content on packing density of fine aggregate in concrete," *Constr Build Mater*, vol. 61, pp. 270–277, Jun. 2014, doi: 10.1016/j.conbuildmat.2014.03.022.

[258] M. Noël, L. Sanchez, and G. Fathifazl, "Recent Advances in Sustainable Concrete for Structural Applications," *Sustainable Construction Materials & Technologies*, vol. 4, pp. 1–10, 2016.

[259] B. L. DAMINELI, R. G. PILEGGI, and V. M. JOHN, "Influence of packing and dispersion of particles on the cement content of concretes," *Revista IBRACON de Estruturas e Materiais*, vol. 10, no. 5, pp. 998–1024, Sep. 2017, doi: 10.1590/s1983-41952017000500004.

[260] I. R. OLIVEIRA, A. R. STUDART, and PILEGGI, "Dispersão e Empacotamento de Partículas: Princípios e Aplicações em Processamento Cerâmico," *Fazendo Arte Editorial*, 2000.

[261] F. de Larrard and T. Sedran, “Mixture-proportioning of high-performance concrete,” *Cem Concr Res*, vol. 32, no. 11, pp. 1699–1704, 2002.

[262] W. Aiqin, Z. Chengzhi, and Z. Ningsheng, “Study of the influence of the particle size distribution on the properties of cement,” *Cem Concr Res*, vol. 27, no. 5, pp. 685–695, 1997.

[263] J. D. Dewar and R. (Robert) Anderson, *Manual of ready-mixed concrete*. Blackie Academic & Professional, 2003.

[264] T. Stovall, F. de Larrard, and M. Buil, “Linear packing density model of grain mixtures,” *Powder Technol*, vol. 48, no. 1, pp. 1–12, 1986, doi: 10.1016/0032-5910(86)80058-4.

[265] S. Formagini, “DOSAGEM CIENTÍFICA E CARACTERIZAÇÃO MECÂNICA DE CONCRETOS DE ALTÍSSIMO DESEMPENHO,” UFRJ, 2005.

[266] ABNT, *NBR 16697 - Cimento Portland - Requisitos*. Associação Brasileira de Normas Técnicas, BRA., 2018.

[267] ABNT, *NBR 16605 - Cimento Portland e outros materiais em pó - Determinação da massa específica*. 2017.

[268] M. Amario, “Dosagem científica de concretos estruturais contendo agregado de resíduo de concreto (ARC),” *Dissertação COPPE UFRJ*, p. 213, 2015.

[269] ABNT, *NBR 16916 - Agregado miúdo -Determinação da densidade e da absorção de água*. 2021. [Online]. Available: www.abnt.org.br

[270] ABNT, *NBR 16889 - Concreto - Determinação Da Consistência Pelo Abatimento Do Tronco de Cone*. Associação Brasileira de Normas Técnicas, BRA., 2020.

[271] ABNT, *NBR 5739 - Concreto - Ensaio de compressão de corpos de prova cilíndricos*. 2018. [Online]. Available: www.abnt.org.br

[272] ABNT, *NBR 5738 - Concreto - Procedimentos para moldagem e cura de corpos de prova*. 2015.

[273] ABNT, *NBR 7222 - Concreto e argamassa - Determinação da resistência à tração por compressão diametral de corpos de prova cilíndricos*. 2011.

[274] I. C. A. Ferreira, "Caracterização microestrutural 2D e 3D de concreto com agregados reciclados de construção e demolição," PUC-Rio, Rio de Janeiro, 2022.

[275] Mukai T and Kikuchi M, "Properties of reinforced concrete beams containing recycled aggregate, demolition and reuse of concrete and masonry," in *Vol. 2, Reuse of Demolition Waste, Proceedings of the Second International RILEM Symposium*, 1988, pp. 670–679.

[276] ABNT, *NBR 7480 - Aço destinado às armaduras para estruturas de concreto armado - Requisitos*. 2022. [Online]. Available: www.abnt.org.br

[277] RILEM, *Technical Recommendations for the Testing and Use of Construction Materials*. 1994. doi: 10.1201/9781482271362.

[278] C. W. Tang and C. K. Cheng, "Modeling local bond stress-slip relationships of reinforcing bars embedded in concrete with different strengths," *Materials*, vol. 13, no. 17, Sep. 2020, doi: 10.3390/MA13173701.

[279] J. Xiao, H. Xie, and Z. Yang, "Shear transfer across a crack in recycled aggregate concrete," *Cem Concr Res*, vol. 42, no. 5, pp. 700–709, May 2012, doi: 10.1016/j.cemconres.2012.02.006.

Annex A – BétonLab Pro 3 - Database

A.1. Natural Coarse Aggregate (NAT)

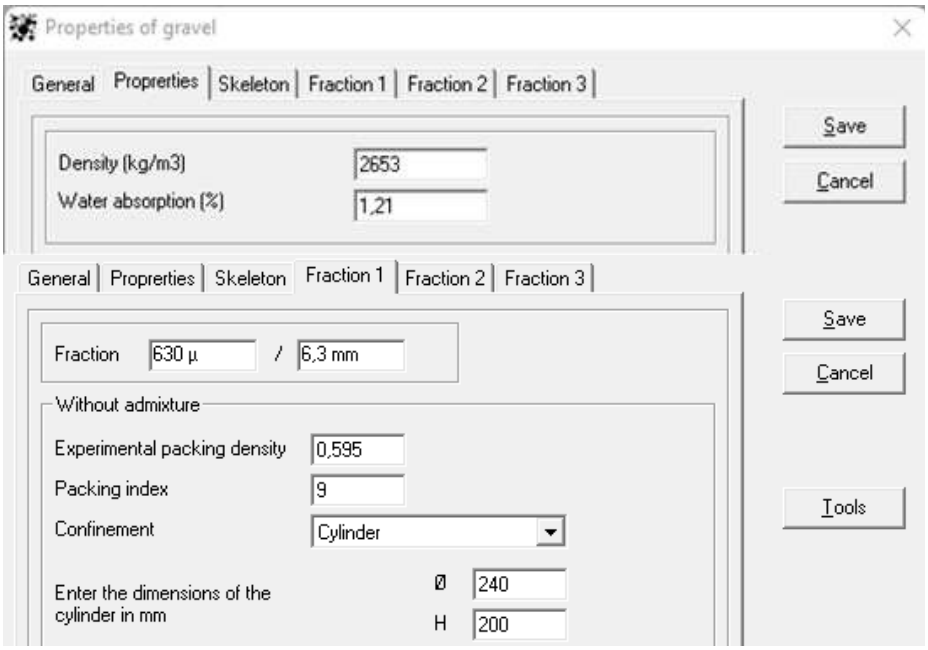

Figure A-0-1. Database creation on Bétonlab Pro 3 for natural coarse aggregate.

A.2. Natural Fine Aggregate

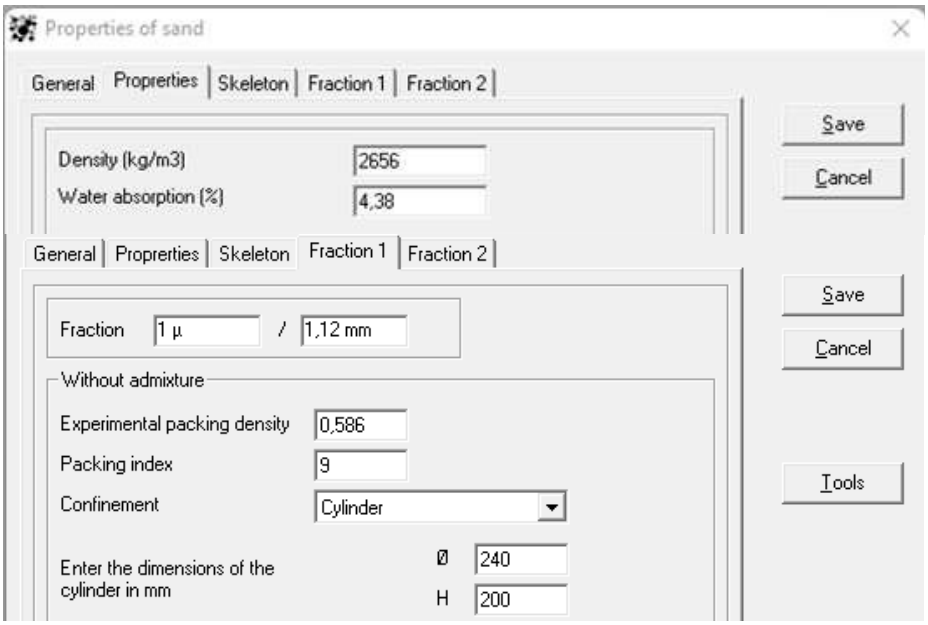

Figure A-0-2. Database creation on Bétonlab Pro 3 for natural fine aggregate (sand).

A.3. Natural Fine Aggregate – Fraction S1 - 150 µm < Φ < 0.85 mm

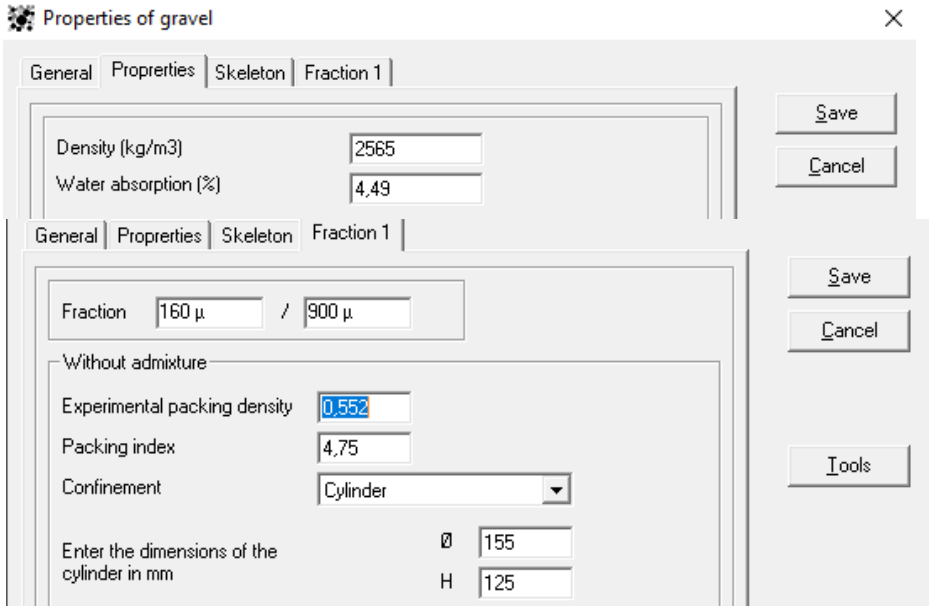

Figure A-0-3. Database creation on Bétonlab Pro 3 for natural fine aggregate (sand) - fraction S1 - 150 µm < Φ < 0.85 mm.

A.4. Natural Fine Aggregate – Fraction S2 - 0.85 mm < Φ < 4.75 mm

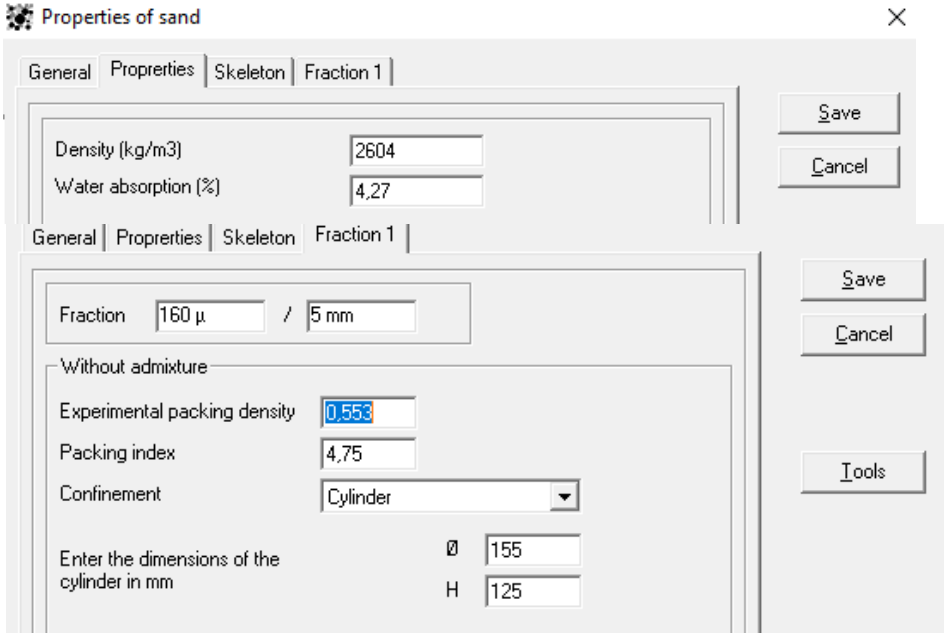

Figure A-0-4. Database creation on Bétonlab Pro 3 for natural fine aggregate (sand) - fraction S2 - 0.85 mm < Φ < 4.75 mm.

A.5. Portand cement CP-II-F32

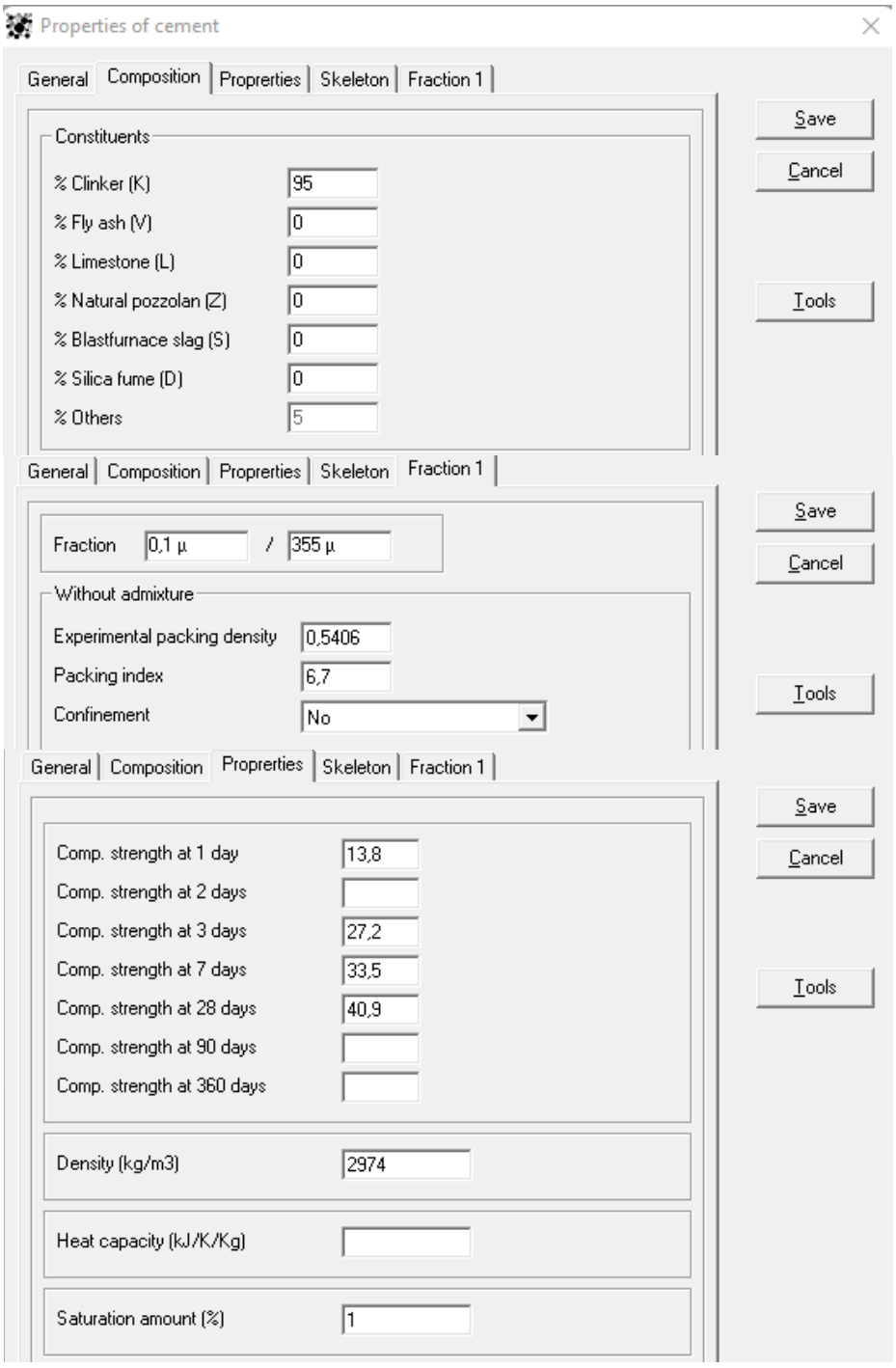

Figure A-0-5. Database creation on Bétonlab Pro 3 for cement CPII-F32.

A.6. Silica Fume

Figure A-6. Database creation on Bétonlab Pro 3 for Silica Fume.

A.7. Fly Ash

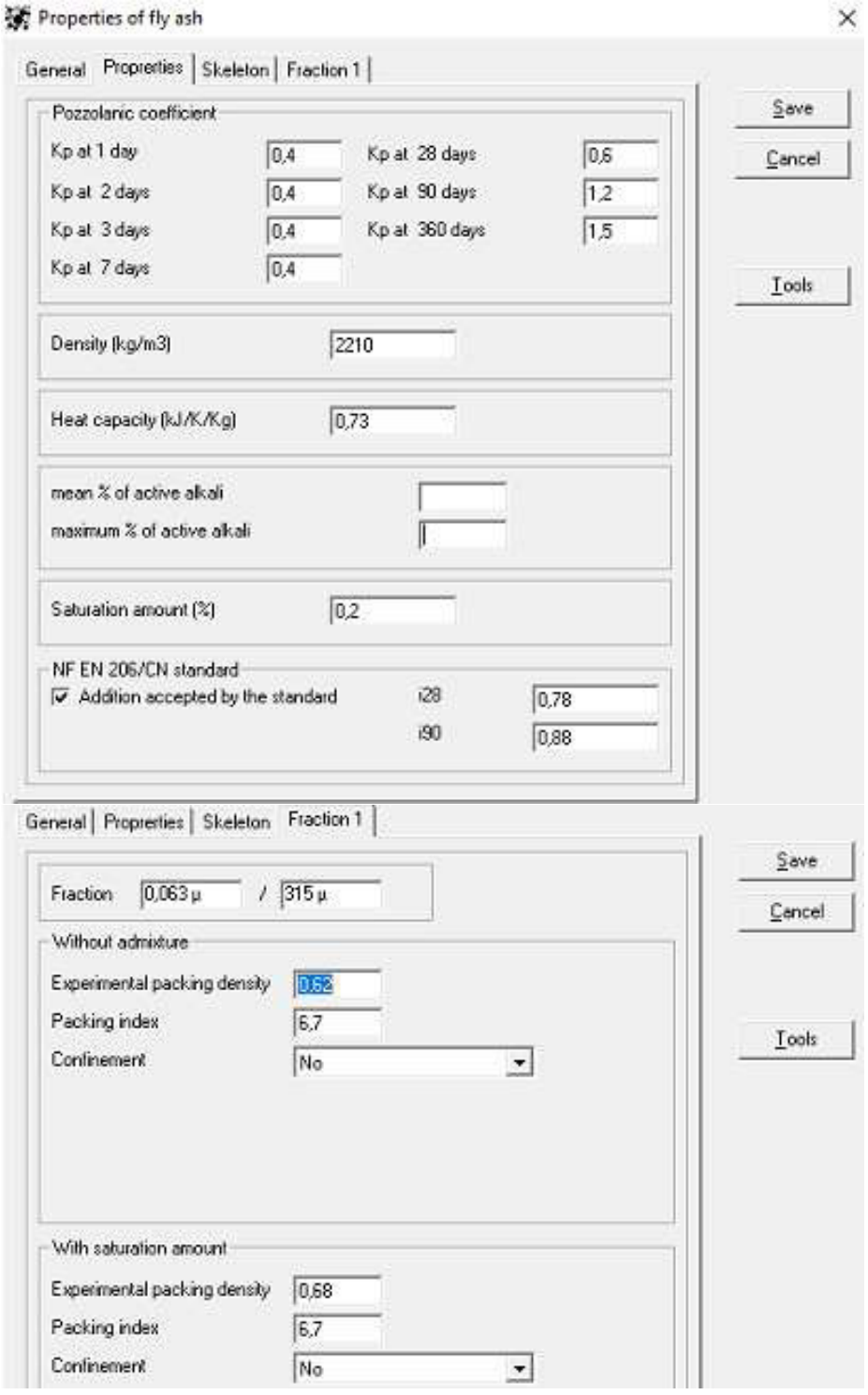

Figure A-7. Database creation on Bétonlab Pro 3 for Fly Ash.

A.8. Silica 325

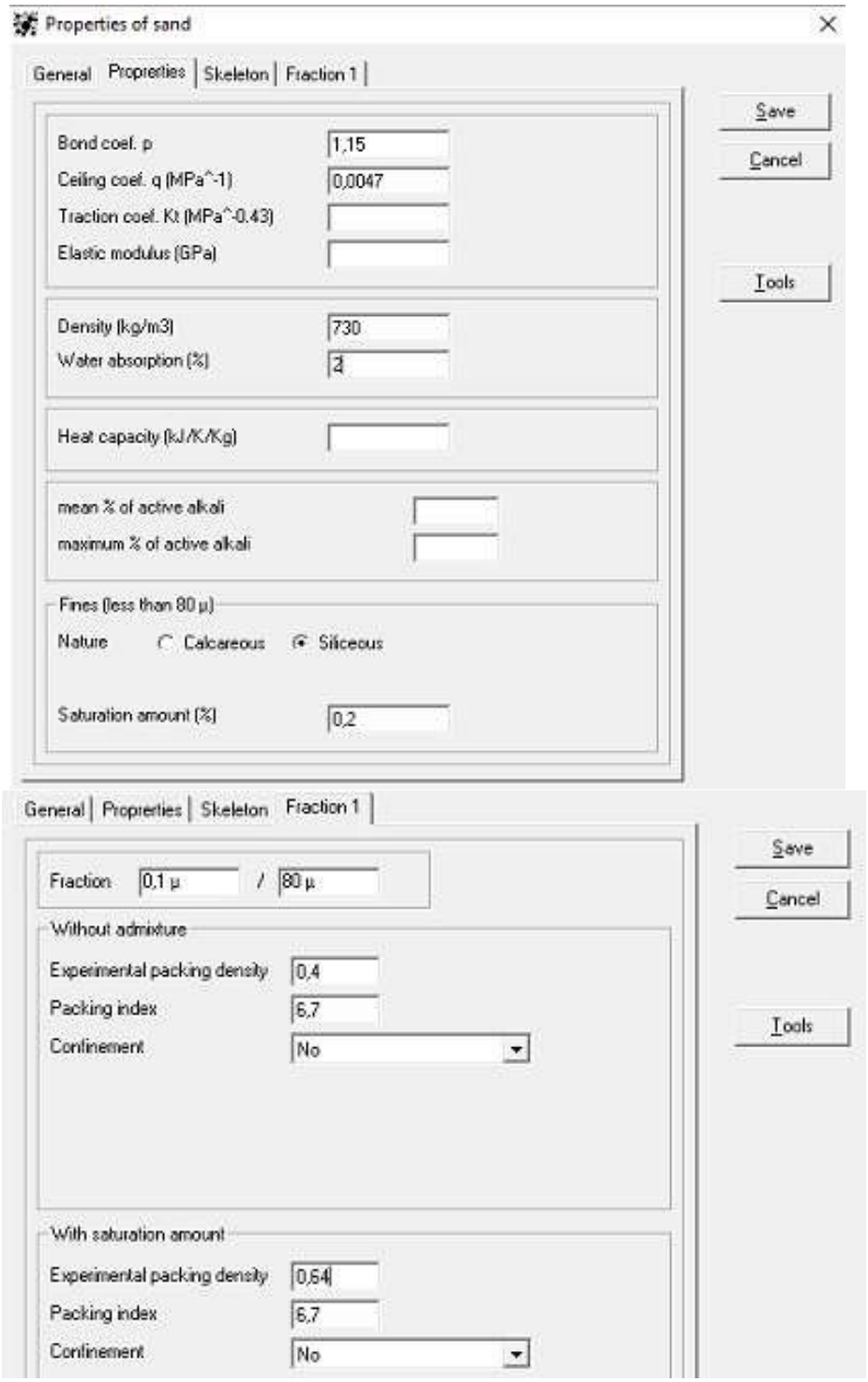

Figure A-8. Database creation on Bétonlab Pro 3 for Silica 325.

A.9. Superplasticizer

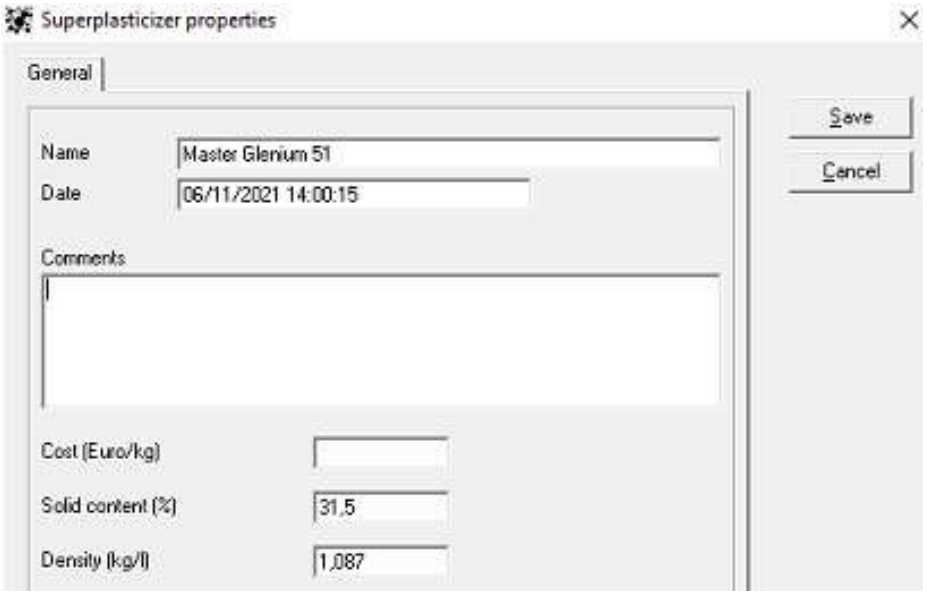

Figure A-9. Database creation on Bétonlab Pro 3 for superplasticizer Master Glenium 51.

Annex B – BétonLab Pro 3 - Calibration of parameters “p” and “q”

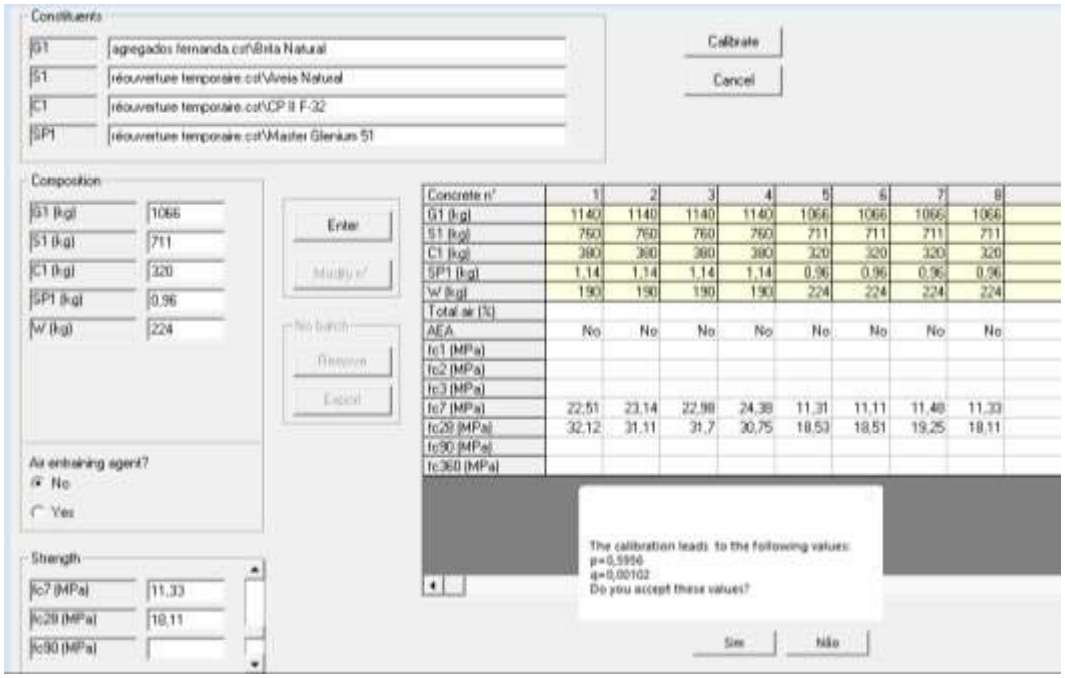

Figure B-0-1. Calibration of “p” and “q” parameters for the natural coarse aggregate (NAT).

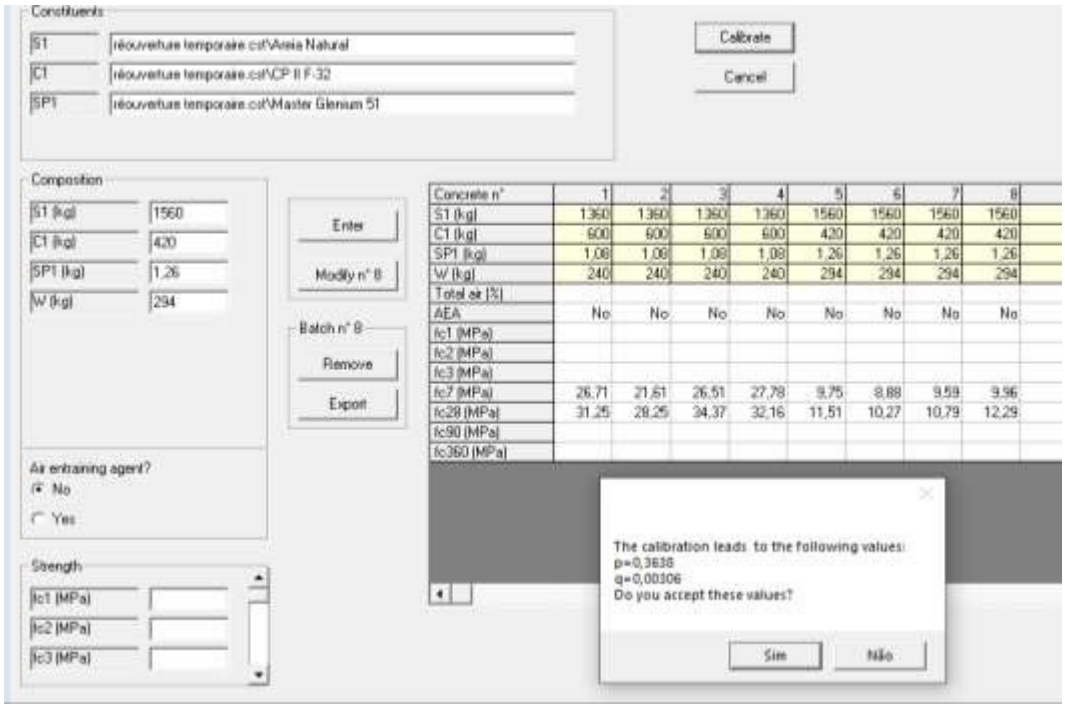

Figure B-0-2. Calibration of “p” and “q” parameters for natural fine aggregate.

Annex C – BétonLab Pro 3 - Mix Proportions

Concrete n°	1
G1 (kg/m3)	872,7
G2 (kg/m3)	216
S1 (kg/m3)	728,1
C1 (kg/m3)	360
SP1 (kg/m3)	1,1
W (kg/m3)	236,7
G1 (%)	48
G2 (%)	12
S1 (%)	40
Saturation amount (%)	1,01
Superplasticizer content (%)	0,3
Eff water	180
fc1 (MPa)	10,8
fc2 (MPa)	15,7
fc3 (MPa)	18,5
fc7 (MPa)	23,3
fc28 (MPa)	27,2
fc90 (MPa)	30,5
fc360 (MPa)	34,4
Segregation index (confined)	0,945
Packing index of unconfined concrete	11,976
Packing index of confined concrete	11,976
Fines contribution K'i	2,711
Coarse gravel contribution K'gg	2,601
Packing of unconfined skeleton Ø*	0,789
Aggregate packing g*	0,7273

Figure C-0-1. Mix proportions for concrete C30-20.

Concrete n°	1
G1 (kg/m3)	540
G2 (kg/m3)	545,5
S1 (kg/m3)	728,2
C1 (kg/m3)	360
SP1 (kg/m3)	1,1
W (kg/m3)	257,9
G1 (%)	30
G2 (%)	30
S1 (%)	40
Saturation amount (%)	1,01
Superplasticizer content (%)	0,3
Eff water	180
fc1 (MPa)	10
fc2 (MPa)	14,4
fc3 (MPa)	16,9
fc7 (MPa)	21,1
fc28 (MPa)	24,5
fc90 (MPa)	27,4
fc360 (MPa)	30,6
Segregation index (confined)	0,945
Packing index of unconfined concrete	13,497
Packing index of confined concrete	13,497
Fines contribution K'i	2,724
Coarse gravel contribution K'gg	2,887
Packing of unconfined skeleton Ø*	0,7781
Aggregate packing g*	0,712

Figure C-0-2. Mix proportions for concrete C30-50.

Concrete n°	1
G1 (kg/m3)	1080,1
S1 (kg/m3)	728,3
C1 (kg/m3)	360
SP1 (kg/m3)	2,2
W (kg/m3)	290,8
G1 (%)	60
S1 (%)	40
Saturation amount (%)	1,01
Superplasticizer content (%)	0,6
Eff water	180

fc1 (MPa)	9,8
fc2 (MPa)	14,2
fc3 (MPa)	16,6
fc7 (MPa)	20,7
fc28 (MPa)	24
fc90 (MPa)	26,8
fc360 (MPa)	30
Segregation index (confined)	0,945
Packing index of unconfined concrete	17,546
Packing index of confined concrete	17,546
Fines contribution K'f	2,75
Coarse gravel contribution K'gg	2,867
Packing of unconfined skeleton Ø*	0,758
Aggregate packing g*	0,6852

Figure C-0-3. Mix proportions for concrete C30-100.

Concrete n°	1
G1 (kg/m3)	493,8
G2 (kg/m3)	829,9
S1 (kg/m3)	99,6
C1 (kg/m3)	360
FA1 (kg/m3)	168
SF1 (kg/m3)	70
SF2 (kg/m3)	45
SP1 (kg/m3)	70
W (kg/m3)	274,57
G1 (%)	35
G2 (%)	58
S1 (%)	7
Saturation amount (%)	2,37
Superplasticizer content (%)	13
Eff water	180

fc1 (MPa)	8,6
fc2 (MPa)	13,7
fc3 (MPa)	17,6
fc7 (MPa)	32,3
fc28 (MPa)	48,1
fc90 (MPa)	50,7
fc360 (MPa)	53,3
Segregation index (confined)	0,966
Packing index of unconfined concrete	16,792
Packing index of confined concrete	16,792
Fines contribution K'f	14,353
Coarse gravel contribution K'gg	0,365
Packing of unconfined skeleton Ø*	0,7632
Aggregate packing g*	0,7039

Figure C-0-4. Mix proportions for the reference concrete C50-00.

Concrete n°	1
G1 (kg/m3)	488,7
G2 (kg/m3)	829,9
S1 (kg/m3)	99,6
C1 (kg/m3)	360
FA1 (kg/m3)	168
SF1 (kg/m3)	70
SF2 (kg/m3)	45
SP1 (kg/m3)	75
W (kg/m3)	281,17
G1 (%)	35
G2 (%)	58
S1 (%)	7
Saturation amount (%)	2,37
Superplasticizer content (%)	14
Eff water	180

fc1 (MPa)	8,3
fc2 (MPa)	13,1
fc3 (MPa)	17,1
fc7 (MPa)	24
fc28 (MPa)	35,9
fc90 (MPa)	38,1
fc360 (MPa)	40,3
Segregation index (confined)	0,935
Packing index of unconfined concrete	53,371
Packing index of confined concrete	53,371
Fines contribution K'f	15,136
Coarse gravel contribution K'gg	0,592
Packing of unconfined skeleton Ø*	0,7226
Aggregate packing g*	0,6947

Figure C-0-5. Mix proportions for concrete C50-100.